

Functional genomics analysis of the effects of co-inhibition of the malarial S-adenosylmethionine decarboxylase/ornithine decarboxylase

by

Anna Catharina van Brummelen

Submitted in partial fulfilment of the requirements for the degree
Philosophiae Doctor

in the Faculty of Natural and Agricultural Sciences
Department of Biochemistry
University of Pretoria
Pretoria
South Africa

SUPERVISOR: Dr. Lyn-Marie Birkholtz
Department of Biochemistry, University of Pretoria, South Africa

CO-SUPERVISOR: Prof. Abraham I Louw
Department of Biochemistry, University of Pretoria, South Africa

CO-SUPERVISOR: Prof. Manuel Llinás
Department of Molecular Biology, Princeton University, USA

October 2008

DECLARATION:

I, Anna Catharina van Brummelen declare that the thesis/dissertation, which I hereby submit for the degree *Philosophiae Doctor* at the University of Pretoria, is my own work and has not previously been submitted by me for a degree at this or any other tertiary institution.

SIGNATURE:.....

DATE:



UNIVERSITEIT VAN PRETORIA
UNIVERSITY OF PRETORIA
YUNIBESITHI YA PRETORIA

Soli Deo gloria

ACKNOWLEDGEMENTS

The completion of this dissertation was made possible by the following people whom I would like to thank with all my heart:

My supervisor, Dr. Lyn-Marie Birkholtz, for your guidance, encouragement, support and faith in me.

Prof. Braam Louw, for your support, guidance and for giving me the opportunity to enrol for a PhD in Biochemistry.

Prof. Manuel Llinás, for the opportunity to do research in your laboratory, for stimulating discussions and long distance guidance via email.

Staff from the University of Pretoria, specifically Jaco de Ridder, Loveness Dzikiti, Fourie Joubert, Nicky Olivier and Sandra van Wyngaardt. Thank you for all your kindness and support, as well as assistance with experimental work and data analyses.

Fellow students and friends from the University of Pretoria, specifically Pieter Burger, Katherine Clark, Jandeli Niemand, Shaun Reeksting, Christiaan Stutzer, Gordon Wells and Marni Williams. It was pleasure to get to know all of you. Thank you for everything!

CSIR staff, specifically Bridget Crampton and Stoyan Stoychev, for your help with analyses.

Fellow students, technicians and friends from Princeton University, specifically Ilsa Leon, Kellen Olszewski and Daniel Wilinski. Thank you for making me feel welcome, also for teaching me to do microarrays and all your hard work with the metabolomics.

My husband, Roy van Brummelen, for all the times we had to go to the lab in the middle of the night, your unconditional love and support.

My parents, Johannes and Adéle Retief and my family. Thank you for all your love, continuous support, endless prayers and encouragement all my life.

SUMMARY

Polyamines are ubiquitous components of all living cells and their depletion usually causes growth arrest or cytostasis, a strategy employed for treatment of West-African trypanosomiasis. In the malaria parasite, *Plasmodium falciparum*, polyamine biosynthesis is regulated by the uniquely bifunctional protein, S-adenosylmethionine decarboxylase/ornithine decarboxylase (PfAdoMetDC/ODC). The unique nature of this protein could provide a selective mechanism for antimalarial treatment.

To validate polyamine depletion and specifically PfAdoMetDC/ODC, as drug target for antimalarial therapeutic intervention, polyamine biosynthesis was completely restrained via the inhibition of both catalytic sites of PfAdoMetDC/ODC with DFMO and MDL73811. The physiological effects during the resulting cytostasis were studied with a comprehensive functional genomics approach. The study was preceded by various assays to determine the treatment dosage that would result in complete cytostasis, without non-specific chemical cytotoxicity. The results obtained revealed that the cytostatic mechanism with growth arrest of the treated parasites and normal progression of the untreated controls require special consideration for basic comparisons of response in terms of the assay methodology used and data analysis. This is particularly important when studying a multistage organism such as *P. falciparum*, which constantly develops and change during the intraerythrocytic developmental cycle, such that growth arrest compared to normal progression would result in significant differences merely due to stage. This critical principle was kept in mind throughout the investigation and was applied to the relative quantification of RNA, proteins and metabolites via a relative time zero approach as opposed to the standard parallel time point comparison.

Three independent functional genomics investigations, namely transcriptomics, proteomics and metabolomics were conducted, in which highly synchronised 3D7 parasite cultures were treated during the schizont stage and parasites were sampled during a time course at three time points (just before and during cytostasis). Transcriptome analysis revealed the occurrence of a generalised transcriptional arrest just prior to the growth arrest. To our knowledge this is the first time that transcriptional arrest as the preceding mechanism of cytostasis due to polyamine depletion, was demonstrated. However, despite the transcriptional arrest, the abundance of 538 transcripts was differentially affected and included three perturbation-specific compensatory transcriptional responses: the increased abundance of the transcripts for lysine decarboxylase and ornithine aminotransferase (OAT) and the decreased abundance of that for S-adenosylmethionine synthetase (AdoMet synthetase). Pearson correlations indicated more subtle effects of the perturbation on the proteome and even more so on the metabolome where homeostasis was generally maintained, except downstream to the enzymatic blockade at PfAdoMetDC/ODC. The perturbation-specific compensatory roles of OAT in the

regulation of ornithine and AdoMet synthetase in the regulation of AdoMet were confirmed on both the protein and metabolite levels, confirming their biological relevance.

The results provide evidence that *P. falciparum* respond to alleviate the detrimental effects of polyamine depletion via the regulation of its transcriptome and subsequently the proteome and metabolome, which supports a role for transcriptional control in the regulation of polyamine and methionine metabolism within the parasite. The study concludes that polyamines are essential molecules for parasite survival and that PfAdoMetDC/ODC is a valid target for antimalarial drug development.

TABLE OF CONTENTS

| | |
|----------------------------|------|
| ACKNOWLEDGEMENTS | i |
| SUMMARY | ii |
| TABLE OF CONTENTS | iv |
| LIST OF EQUATIONS | ix |
| LIST OF FIGURES..... | x |
| LIST OF TABLES..... | xii |
| LIST OF ABBREVIATIONS..... | xiii |

CHAPTER 1

| | | |
|--------|--|----|
| 1.1 | HISTORY OF MALARIA | 1 |
| 1.2 | MALARIA AS GLOBAL HEALTH PROBLEM..... | 1 |
| 1.3 | THE PARASITE'S LIFE CYCLE..... | 3 |
| 1.4 | HUMAN MALARIA SPECIES..... | 5 |
| 1.5 | THE PATHOGENESIS AND CLINICAL PRESENTATION OF MALARIA..... | 6 |
| 1.6 | ANTIMALARIAL VACCINES..... | 8 |
| 1.7 | ANTIMALARIAL THERAPEUTICS | 9 |
| 1.7.1 | Quinoline and related antimalarials | 10 |
| 1.7.2 | Artemisinin and derivatives | 12 |
| 1.7.3 | Antifolates | 13 |
| 1.8 | ANTIMALARIAL DRUG TARGETS..... | 14 |
| 1.9 | POLYAMINE METABOLISM..... | 15 |
| 1.9.1 | The biological importance of polyamines | 15 |
| 1.9.2 | The biosynthesis of polyamines | 16 |
| 1.10 | MOLECULAR ASPECTS OF MALARIA | 19 |
| 1.10.1 | Sequenced <i>Plasmodium</i> genome data | 19 |
| 1.10.2 | <i>Plasmodium</i> transcriptome data | 21 |
| 1.10.3 | The <i>P. falciparum</i> proteome and interactome | 23 |
| 1.10.4 | The <i>P. falciparum</i> metabolome | 24 |
| 1.10.5 | Gene regulation in <i>P. falciparum</i> | 25 |
| 1.10.6 | Manipulation of the <i>Plasmodium</i> genome | 26 |
| 1.11 | FUNCTIONAL GENOMICS FOR DRUG DISCOVERY AND TARGET VALIDATION | 26 |

| | | |
|------|--------------------------|----|
| 1.12 | RESEARCH OBJECTIVES..... | 27 |
| | Papers: | 28 |
| | Conference proceedings: | 29 |

CHAPTER 2

| | | |
|-----------|--|----|
| 2.1 | INTRODUCTION | 30 |
| 2.1.1 | Polyamine biosynthesis inhibitors | 30 |
| 2.1.2 | Antimalarial drug sensitivity methods | 32 |
| 2.2 | MATERIALS AND METHODS | 34 |
| 2.2.1 | <i>In vitro</i> cultivation of asexual <i>P. falciparum</i> cultures | 34 |
| 2.2.2 | Sorbitol synchronisation of growth stage | 35 |
| 2.2.3 | Parasite growth and drug sensitivity assays | 36 |
| 2.2.3.1 | Drug treatment and plate storage until analysis | 36 |
| 2.2.3.2 | Indirect parasitaemia quantitation assays | 37 |
| 2.2.3.2.1 | Lactate dehydrogenase (Malstat) assay | 37 |
| 2.2.3.2.2 | Histidine-rich protein II (HRPII) ELISA | 38 |
| 2.2.3.3 | Direct parasitaemia quantitation assays | 39 |
| 2.2.3.3.1 | FACS analysis | 39 |
| 2.2.3.4 | Concentration-response curves | 39 |
| 2.2.3.5 | Propidium iodide (PI) membrane integrity assay | 40 |
| 2.3 | RESULTS | 41 |
| 2.3.1 | Validation of signal to inoculum linearity | 41 |
| 2.3.2 | Concentration-response curves and IC ₅₀ s | 44 |
| 2.3.3 | DFMO and MDL73811 interaction during PfAdoMetDC/ODC co-inhibition | 49 |
| 2.3.4 | PI membrane integrity assay of PfAdoMetDC/ODC co-inhibition | 49 |
| 2.4 | DISCUSSION..... | 50 |

CHAPTER 3

| | | |
|---------|---|----|
| 3.1 | INTRODUCTION | 54 |
| 3.1.1 | Transcriptional profiling of perturbed <i>P. falciparum</i> compared to other organisms | 54 |
| 3.1.2 | Transcriptomics methodologies, experimental design and data analysis | 55 |
| 3.2 | MATERIALS AND METHODS | 59 |
| 3.2.1 | Ensuring the correct treatment dosage for the transcriptomics investigation | 59 |
| 3.2.1.1 | Growth morphology studies | 59 |
| 3.2.1.2 | Radio-labelled substrate assays | 59 |

| | |
|--|-----|
| 3.2.2 Drug treatment for the transcriptomics investigation | 60 |
| 3.2.3 RNA isolation | 60 |
| 3.2.4 cDNA synthesis | 61 |
| 3.2.5 Oligonucleotide array spotting and slide post-processing | 62 |
| 3.2.6 Cy dye cDNA labelling | 63 |
| 3.2.7 Oligonucleotide array hybridisation, washing and scanning | 63 |
| 3.2.8 Data analysis | 64 |
| 3.2.8.1 Exploratory data analysis | 64 |
| 3.2.8.2 Differential transcript abundance analysis | 64 |
| 3.2.8.2.1 Linear models for microarray data (LIMMA) analysis | 64 |
| 3.2.8.2.2 EDGE time course analysis | 65 |
| 3.2.8.3 Additional data analysis | 65 |
| 3.2.9 Real-time PCR validation of differential transcript abundance data | 66 |
| 3.3 RESULTS | 66 |
| 3.3.1 Ensuring the correct treatment dosage for the functional genomics investigations | 66 |
| 3.3.2 Transcriptomics sampling, RNA isolation and cDNA synthesis | 68 |
| 3.3.3 Oligonucleotide microarray analysis | 70 |
| 3.3.4 Exploratory data analysis | 71 |
| 3.3.4.1 Hierarchical clustering of data with those of other perturbations | 71 |
| 3.3.4.2 Hierarchical clustering of data related to polyamine and methionine metabolism | 75 |
| 3.3.4.3 Phase-ordering and correlation calculations | 75 |
| 3.3.5 Differential transcript abundance analysis | 77 |
| 3.3.5.1 Data normalisation | 77 |
| 3.3.5.2 LIMMA data analysis | 80 |
| 3.3.5.3 EDGE time course analysis | 84 |
| 3.3.6 GO assignment of differentially affected transcripts | 84 |
| 3.3.7 Finding adjacently located genes with differentially affected transcripts | 85 |
| 3.3.8 PfAdoMetDC/ODC-interactome data comparisons | 87 |
| 3.3.9 Real-time PCR validation of differential transcript abundance data | 89 |
| 3.4 DISCUSSION..... | 92 |
| 3.5 RAW DATA AND SUPPLEMENTARY WEBSITE..... | 100 |

CHAPTER 4

| | |
|---|-----|
| 4.1 INTRODUCTION | 101 |
| 4.1.1 Evidence of post-transcriptional regulation in <i>P. falciparum</i> | 101 |

| | | |
|-----------|--|-----|
| 4.1.2 | Integrative biology from <i>Plasmodium</i> functional genomics data | 102 |
| 4.1.3 | Proteomics methodologies | 103 |
| 4.1.4 | Metabolomics methodologies | 105 |
| 4.2 | MATERIALS AND METHODS | 106 |
| 4.2.1 | Proteomics | 106 |
| 4.2.1.1 | Protein extraction and quantitation | 107 |
| 4.2.1.2 | Iso-electric focussing (IEF) | 107 |
| 4.2.1.3 | Two-dimensional polyacrylamide gel electrophoresis (2D-GE) | 108 |
| 4.2.1.4 | Gel scanning and data analysis | 108 |
| 4.2.1.5 | Spot excision, destaining and trypsin digestion for protein identification | 109 |
| 4.2.2 | Metabolomics | 110 |
| 4.2.2.1 | Metabolite extraction and polyamine derivatisation | 110 |
| 4.2.2.2 | LC-MS/MS metabolite analysis | 111 |
| 4.2.2.3 | Metabolomics data analysis | 111 |
| 4.2.3 | Decarboxylase activity assays | 112 |
| 4.2.3.1 | LDC induction in <i>E. coli</i> as assay positive control | 112 |
| 4.2.4 | Methylation status determination | 113 |
| 4.2.4.1 | CpG island analysis of the differential transcript abundance list | 113 |
| 4.2.4.2 | Global methylation assays | 113 |
| 4.2.4.2.1 | gDNA isolation | 113 |
| 4.2.4.2.2 | Methylation negative and positive controls | 113 |
| 4.2.4.2.3 | Restriction-enzyme digestion to assess gDNA methylation | 114 |
| 4.2.4.2.4 | South-Western immunoblotting | 114 |
| 4.3 | RESULTS | 115 |
| 4.3.1 | Proteomics analysis of PfAdoMetDC/ODC co-inhibited <i>P. falciparum</i> | 115 |
| 4.3.1.1 | Differential protein abundance analysis and protein identification | 117 |
| 4.3.1.2 | Perturbation-specific compensatory mechanisms confirmed in the proteome | 121 |
| 4.3.2 | Metabolomics analysis of PfAdoMetDC/ODC co-inhibited <i>P. falciparum</i> | 122 |
| 4.3.2.1 | Perturbation-specific compensatory mechanisms confirmed in the metabolome | 123 |
| 4.3.3 | Compensatory LDC induction during polyamine depletion investigated further | 127 |
| 4.3.5 | gDNA Methylation status investigation | 128 |
| 4.3.5.1 | CpG island analysis of the differential transcript abundance list | 128 |
| 4.3.4.2 | Global methylation assays | 128 |
| 4.3.4.2.1 | Methylation-sensitive restriction endonucleases | 129 |
| 4.3.4.2.2 | South-Western immunoblotting | 129 |
| 4.4 | DISCUSSION..... | 130 |

CHAPTER 5

CONCLUDING DISCUSSION..... 136

REFERENCES 142

APPENDIX A

APPENDIX B

APPENDIX C

APPENDIX D

APPENDIX E

LIST OF EQUATIONS

| Equation no. | Title of Equation | Page no. |
|--------------|---|----------|
| 2.1 | Percentage response | 37 |
| 2.2 | Concentration-response curve four-parameter logistic equation | 40 |
| 3.1 | Gene expression log ₂ -ratio | 57 |
| 3.2 | Enzyme total activity..... | 60 |
| 3.3 | Fluorescent dye labelling efficiency | 63 |
| 4.1 | Iso-electric focussing volt hours (constant)..... | 108 |
| 4.2 | Iso-electric focussing volt hours (gradient) | 108 |

LIST OF FIGURES

| Figure no. | Title of Figure | Page no. |
|------------|---|----------|
| 1.1 | Malaria geographical distribution and chloroquine resistance | 2 |
| 1.2 | Giemsa-stained thin smears depicting the life cycle of 3D7 <i>P. falciparum</i> | 4 |
| 1.3 | Currently used antimalarial drugs..... | 11 |
| 1.4 | Chemical structures of the natural polyamines | 15 |
| 1.5 | Polyamine metabolism in mammalian cells..... | 16 |
| 1.6 | Polyamine metabolism in <i>Plasmodium</i> | 18 |
| 1.7 | Composite diagram of polyamine levels and biosynthetic enzyme transcript levels..... | 18 |
| 1.8 | The 48 h IDC transcriptomes of 3D7, Dd2 and HBR <i>P. falciparum</i> | 22 |
| 1.9 | The proposed experimental layout for the application of transcriptome and proteome analysis to drug-challenged malaria parasites | 27 |
| 2.1 | Chemical structures of DFMO, MDL73811, MAOBA and MAOEA..... | 31 |
| 2.2. | Sigmoidal concentration-response curve used by GraphPad Prism 4.0 software to calculate the median inhibitory concentration (IC ₅₀)..... | 40 |
| 2.3 | HRPII ELISA optimisation | 42 |
| 2.4 | LDH assay validation | 42 |
| 2.5 | FACS versus microscopy..... | 43 |
| 2.6 | Typical FACS images..... | 44 |
| 2.7 | Concentration-response curves of chloroquine..... | 44 |
| 2.8 | Concentration-response curves of cytostatic compounds | 45 |
| 2.9 | Parasite stage-specific levels of HRPII and LDH activity..... | 47 |
| 2.10 | Transcript levels of LDH and three histidine-rich proteins during the IDC | 48 |
| 2.11 | Concentration-response curves of MDL73811, DFMO and the combination | 49 |
| 2.12 | Giemsa-stained thin smears of chicken erythrocytes and 3D7 <i>P. falciparum</i> -infected human erythrocytes | 50 |
| 3.1 | Six designs of microarray time course experiments | 57 |
| 3.2 | Giemsa-stained thin smears of untreated <i>P. falciparum</i> and cultures treated with 5 mM DFMO, 5 μM MDL73811 or the combination..... | 67 |
| 3.3 | Total activity of AdoMetDC and ODC based on the release of ¹⁴ CO ₂ | 68 |
| 3.4 | Transcriptomics sampling times | 69 |
| 3.5 | The total RNA yield and denaturing agarose/formaldehyde electrophoresis..... | 69 |
| 3.6 | Typical 70-mer oligonucleotide spotted arrays..... | 70 |
| 3.7 | Hierarchical data clustering between genes of the PfAdoMetDC/ODC co-inhibition data | 72 |
| 3.8 | Hierarchical data clustering between arrays of the PfAdoMetDC/ODC co-inhibition data and the Llinás perturbation data..... | 73 |
| 3.9 | A tight cluster containing several polyamine pathway transcripts..... | 74 |
| 3.10 | “Biphasic” segregation of the expression/peak abundance of polyamine and methionine metabolism transcripts | 75 |
| 3.11 | Phaseogram depicting the transcriptional profiles of untreated versus PfAdoMetDC/ODC co-inhibition data and Pearson correlation between the PfAdoMetDC/ODC co-inhibition data | 76 |
| 3.12 | Red and green background images of a typical array (111_TAt33) | 78 |
| 3.13 | MA-plots from a typical array (125_UTBt33) before and after data transformation. | 79 |
| 3.14 | Print-tip boxplots from a typical array (116_TBt25) before and after data transformation | 79 |
| 3.15 | Boxplots of log ₂ -ratios (M) and intensities (A) across all arrays post-normalisation. | 80 |
| 3.16 | Red/Green density plots of all the arrays before and after data transformation | 80 |
| 3.17 | Transcript profiles of PfAdoMetDC/ODC, lysine decarboxylase and ornithine aminotransferase | 8 |



| | | |
|------|--|-----|
| | 3 | |
| 3.18 | EDGE output in the form of a histogram | 84 |
| 3.19 | Functional classification of transcripts with increased and decreased differential abundance | 85 |
| 3.20 | Eleven gene cluster from chromosome 10 | 86 |
| 3.21 | The relative constant transcription profile of the putative cyclophilin (PFE0505w) in the PfAdoMetDC/ODC co-inhibition data and in the IDC transcriptome | 89 |
| 3.22 | A real-time PCR plot obtained for a five-part cDNA dilution series of the putative cyclophilin | 90 |
| 3.23 | Melting curve analysis of the amplification product of cyclophilin | 90 |
| 3.24 | A standard curve of the putative cyclophilin (PFE0505w) | 91 |
| 3.25 | Polyamine and methionine metabolism (differentially affected transcripts indicated) | 95 |
| 4.1 | The master image and actual images of the three best 2D-GE technical replicates used for analysis of UT _{t1} versus T _{t1} , T _{t2} and T _{t3} | 116 |
| 4.2. | A typical gel (UTt1_84404) indicating the 41 spots with differential abundance | 117 |
| 4.3 | MALDI-Q-TOF MS/MS protein identification of LDH as an example | 119 |
| 4.4 | A typical gel (UTt1_84404) with an enlarged view of AdoMet synthetase and OAT over the time course. | 121 |
| 4.5 | Metabolite profiles compared to relative t ₀ of putrescine, spermidine, 5-methylthioinosine, ornithine and AdoMet | 124 |
| 4.6 | Metabolite profiles of treated parasites directly compared to the parallel untreated controls for putrescine, spermidine, 5-methylthioinosine, ornithine and AdoMet | 126 |
| 4.7 | Lack of measurable LDC activity of untreated and DFMO/MDL73811-treated parasite lysates after incubation with L-[14C]-lysine. | 127 |
| 4.8 | Gel electrophoresis of digested and undigested gDNA to assess methylation after PfAdoMetDC/ODC co-inhibition. | 129 |
| 4.9 | South-Western blot of 5mC in <i>P. falciparum</i> gDNA | 130 |
| 4.10 | Polyamine and methionine metabolism (differentially affected transcripts, proteins and metabolites indicated) | 133 |

LIST OF TABLES

| Table no. | Title of Table | Page no. |
|-----------|---|----------|
| 1.1 | Antimalarial therapeutics and combinations | 10 |
| 2.1 | IC ₅₀ values obtained with three different drug sensitivity assays | 46 |
| 2.2 | PI assay and FACS analysis of PfAdoMetDC/ODC co-inhibited <i>P. falciparum</i> | 50 |
| 3.1 | Real-time PCR primer information | 66 |
| 3.2 | Pearson correlation within the PfAdoMetDC/ODC co-inhibition transcript data | 77 |
| 3.3 | Biological functions of a subset of the transcripts differentially affected according to LIMMA as a result of PfAdoMetDC/ODC co-inhibition | 81 |
| 3.4 | Adjacent gene clusters with decreased abundance transcripts | 86 |
| 3.5 | IDC mRNA expression profiles of the eleven gene cluster from chromosome 10 | 87 |
| 3.6 | Interactome data comparisons | 88 |
| 3.7 | Microarray data validation with real-time PCR..... | 92 |
| 4.1 | Iso-electric focussing step-and-hold programme | 108 |
| 4.2 | Correlation of the 2D-GE data across replicates groups | 115 |
| 4.3 | Identification and characterisation of a subset of proteins with differential abundance..... | 120 |
| 4.4 | Pearson correlation of the metabolite data | 122 |
| 4.5 | Metabolites with differential abundance (i.e. fold changes of more than 2 in either direction) in treated and untreated samples (relative to comparison)..... | 123 |
| 4.6 | Metabolites with differential abundance (i.e. fold changes of more than 2 in either direction) after PfAdoMetDC/ODC co-inhibition (parallel time point comparison)..... | 125 |
| 4.7 | Geecee-count analysis of the genes encoding the 538 differentially affected transcripts | 128 |

ABBREVIATIONS

| | |
|--------------------|---|
| ¹ H-NMR | Proton nuclear magnetic resonance |
| 2D | Two-dimensional |
| 2D-DIGE | Two-dimensional difference gel electrophoresis |
| 2D-GE | Two-dimensional gel electrophoresis |
| 2D-NMR | Two-dimensional nuclear magnetic resonance |
| 2D-PAGE | Two-dimensional polyacrylamide gel electrophoresis |
| 5mC | 5-Methyl-2-deoxycytosine |
| 5mC(P) | 5-Methylcytidine |
| 6mA | 6-Methyl-2-deoxyadenine |
| A | Adenosine or average signal intensities (MA plot) |
| AcN | Acetonitrile |
| AdoHcy | S-adenosylhomocysteine |
| AdoMet | S-adenosylmethionine |
| AdoMet synthetase | S-adenosylmethionine synthetase |
| AdoMetDC | S-adenosylmethionine decarboxylase |
| AMA1 | Apical membrane antigen 1 |
| APAD | 3-acetyl pyridine adenine dinucleotide |
| ApiAP2 | Apicomplexan Apetala2 |
| ATP | Adenosine triphosphate |
| BC | Before Christ |
| bp | Base pair |
| BSA | Bovine serum albumin |
| C | Cytidine |
| CD36 | Cluster determinant 36 |
| CHAPS | 3-[(3-cholamidopropyl)dimethylammonio]-1-propanesulfonate |
| CO | Carbon monoxide |
| CpG | Cytosine Guanine dinucleotide with connecting phosphodiester bond |
| CPM | Counts per minute |
| CSA | Chondroitin sulphate A |
| C _t | Cycle threshold of the real-time amplification curve |
| Cys | Cysteine |
| DALY | Disability adjusted life years |
| dATP | Deoxyadenosine triphosphate |
| DAVID | Database for annotation, visualization and integrated discovery |
| dCTP | Deoxycytidine triphosphate |
| dcAdoMet | Decarboxylated S-adenosylmethionine |
| DDT | Dichlorodiphenyltrichloroethane |
| DELI | Double-site enzyme-linked LDH immunodetection |
| DEPC | Diethyl pyrocarbonate |
| DFMO | DL-a-difluoromethylornithine |
| dGTP | Deoxyguanosine triphosphate |
| DHFR | Dihydrofolate reductase |



| | |
|------------------|---|
| DHFR/TS | Dihydrofolate reductase/thymidylate synthase |
| DHPS | Dihydroopteroate synthase |
| DHPS/PPPK | Dihydroopteroate synthase/dihydroxymethylpterin pyrophosphokinase |
| DIGE | Difference gel electrophoresis |
| DNA | Deoxyribonucleic acid |
| dNTP | Deoxynucleotide triphosphates |
| DPM | Disintegrations per minute |
| DTT | Dithiothreitol |
| dTTP | Deoxythymidine triphosphate |
| dUTP | Deoxyuridine triphosphate |
| EDTA | Ethylenediamine tetra-acetic acid |
| ELISA | Enzyme-linked immunosorbent assay |
| ESI | Electrospray ionization |
| EtOH | Ethanol |
| FACS | Fluorescence activated cell sorting |
| F-MES | Modified Falkow (medium) |
| FTICR | Fourier transform ion cyclotron resonance |
| G | Guanosine |
| GABA | Gamma-aminobutyrate or 4-aminobutyrate |
| gDNA | Genomic DNA |
| gff | General feature format |
| GO | Gene ontology |
| hpi | Hours post-invasion |
| HPLC | High-performance liquid chromatography |
| HRP | Histidine-rich proteins |
| hrp ^a | Horseradish peroxidase |
| hrp-conjugate | Anti-mouse horseradish peroxidase-conjugated secondary antibody |
| HRPII | Histidine- and alanine-rich protein 2 |
| IC ₅₀ | Median inhibitory concentration |
| ICAT | Isotope-coded affinity tags |
| IDC | Intraerythrocytic developmental cycle |
| IEF | Iso-electric focusing |
| IFN | Interferons |
| IL | Interleukin |
| IPG | Immobilized pH gradient |
| iTRAQ | Isobaric tags for relative and absolute quantitation |
| KEGG | Kyoto Encyclopedia of Genes and Genomes |
| LB | Luria-Bertani (broth) |
| LC | Liquid chromatography |
| LC-ESI/MS | Liquid chromatography/electron spray ionization mass spectrometry |
| LDC | Lysine decarboxylase |
| LDH | Lactate dehydrogenase |
| LIMMA | Linear models for microarray data (software) |
| LOWESS | Locally weighted scatterplot smoothing |



| | |
|--------------------|--|
| M | Log ₂ -ratios of transcript abundance |
| m/z | Mass/charge ratio |
| MALDI | Matrix assisted laser desorption/ionization |
| MAOBA | 5'-Deoxy-5'-[N-methyl]-N-[2-(aminooxy)buthyl]amino]adenosine |
| MAOEA | 5'-Deoxy-5'-[N-methyl]-N-[2-(aminooxy)ethyl]amino]adenosine |
| MDL73811 | 5'-{[(Z)-4-amino-2-butenyl]methylamino}-5'-deoxyadenosine |
| MDR1 | Multidrug-resistance type 1 protein |
| MeOH | Methanol |
| MIAME | Minimum information about a microarray experiment |
| MOPS | 3-(N-morpholino)propanesulfonic acid |
| MPMP | Malaria Parasite Metabolic Pathways |
| Mr | Molecular weight |
| mRNA | Messenger RNA |
| mRNP | Messenger ribonucleoprotein complexes |
| MS | Mass spectrometer/spectrometry |
| MS/MS | Tandem mass spectrometry |
| MSP1 | Merozoite surface protein 1 |
| MSRE | Methylation-sensitive restriction endonucleases |
| MudPIT | Multidimensional protein identification technology |
| | |
| NBT | Nitroblue tetrazolium |
| NMR | Nuclear magnetic resonance |
| NO | Nitric oxide |
| | |
| OAT | Ornithine aminotransferase |
| OAT _{met} | Methylated ornithine amino transferase DNA |
| ODC | Ornithine decarboxylase |
| ORF | Open reading frame |
| | |
| PBS | Phosphate buffered saline |
| PCR | Polymerase chain reaction |
| pdx1 | Pyridoxal-5'-phosphate synthase |
| PES | Phenazine ethosulphate |
| PEXEL | <i>Plasmodium</i> export element |
| PfAdoMetDC/ODC | <i>P. falciparum</i> S-adenosylmethionine decarboxylase/ornithine decarboxylase |
| PfCRT | <i>P. falciparum</i> chloroquine-resistance transporter |
| PfEMP1 | Erythrocyte membrane protein 1 |
| PI | Propidium iodide |
| pl | Iso-electric point |
| PlasmoDB | <i>Plasmodium</i> database |
| PLP | Pyridoxal-5'-phosphate |
| PLS | Partial Least Squares |
| PMF | Peptide mass fingerprint/fingerprinting |
| PMT | Photon multiplier tube (fluorescent scanners) |
| ppm | Parts per million |
| PUMAdb | Princeton University Microarray database |
| | |
| Q | Quadropole |
| Q-TOF | Quadropole-time-of-flight mass spectrometer/spectrometry |
| | |
| r | Pearson correlation |
| R | Correlation coefficient of the regression line of data plotted on the same graph |



| | |
|---------------|---|
| <i>Rifin</i> | Repetitive interspersed family (genes) |
| RNA | Ribonucleic acid |
| rRNA | Ribosomal RNA |
| SAGE | Serial analysis of gene expression |
| SDS | Sodium-dodecylsulphate |
| SERCA | Sarcoplasmic reticulum calcium-dependent ATPase |
| SRM | Single reaction monitoring (mass spectrometry) |
| SSC | Saline sodium citrate |
| SSP | Standard spot numbers |
| <i>Stevor</i> | Subtelomeric variable open reading frame (genes) |
| T | Thymidine or treated (sample) |
| t_0 | Time zero |
| t_1 | Time point 1 |
| t_2 | Time point 2 |
| t_3 | Time point 3 |
| TAE | 40 mM Tris, 20 mM glacial acetic acid, 1 mM EDTA (buffer) |
| T_m | Melting temperature |
| TNF | Tumour necrosis factor |
| TOF | Time-of-flight |
| tRNA | Transfer RNA |
| U | Units |
| UT | Untreated (sample) |
| UV | Ultraviolet |
| V | Volts |
| <i>var</i> | Variant (genes) |
| Vh | Volt hours |
| VTS | Vacuolar transport signal |
| WHO | World Health Organisation |

a. HRP is the customary abbreviation for horseradish peroxidase, but to distinguish from the abbreviated histidine rich protein, lowercase characters (hrp) were used.

CHAPTER 1

LITERATURE REVIEW

1.1 HISTORY OF MALARIA

Symptoms and characteristics of malaria have been documented in historical writings from ancient times [1], such as the Ebers Papyrus from 1570 before Christ (B.C.) [2] and the Chinese medical book Nei Ching (2700 B.C.) [3]. These records mentioned splenomegaly, periodical fevers and headaches. The prevalence of the disease in early civilizations was confirmed with modern methods, which detected malaria antigens in the skin and lungs of Egyptian mummies dating back to 3200 and 1304 B.C. [2]. In the Roman Republic (200 B.C.) the disease was prominent in the marshes of the Roman Campagna region and temples were dedicated to the goddess Febris, pictured with a prominent belly and swollen veins, in ancient Rome [3]. The condition was eventually known as Roman fever and gave rise to the Italian word mal'aria meaning "bad air", regarded as the cause of the disease at the time [1].

In 1880, Laveran (1845-1922) examined the blood of a soldier in Algeria suffering from intermittent fever and noticed crescent-shaped bodies within red blood cells. He subsequently realised that the bodies were alive and named them *Oscillaria malariae*. He could detect these life forms in 148 blood specimens from malaria patients, but not in those of controls [4]. Laveran reported his findings, but Italian scientists that also observed the motile parasites within erythrocytes subsequently named them *Plasmodium malariae* without considering Laveran's reports [1]. However, 26 years later in 1906, Laveran received a Nobel prize for discovering the causative agent of malaria [5]. Seventeen years after Laveran's discovery (1897), Ronald Ross (1857-1932) demonstrated that the dapple-winged, brown *Anopheles* mosquito transmits malaria [6]. In 1898 he postulated that human malaria goes through the same developmental stages as bird malaria [7, 8]. He received a Nobel prize for his work in 1902 [5].

Almost 60 years after the erythrocytic stages of malaria were discovered (1948), the tissue stages of primate and human malaria parasites were detected in the livers of rhesus monkeys infected with *P. cynomolgi* sporozoites by Shortt, Garnham and colleagues at the Ross Institute in London. Shortt and colleagues later also described the complete life cycle of *Plasmodium falciparum* [9].

1.2 MALARIA AS GLOBAL HEALTH PROBLEM

Most of Europe and the United States were cleared from malaria in the first half of the twentieth century by changed land use and vector control. A global malaria eradication programme was initiated in the 1950s and

1960s after the development of the insecticide dichlorodiphenyltrichloroethane (DDT), and was successful in countries of the former Soviet Union, Sri Lanka and India. However, due to the costs of the programme and problems such as the resistance of communities to repeated spraying of their homes and the emergence of resistance to the insecticide, global eradication was not achieved. Unfortunately, the failure of the programme and elimination of the disease from the western world (Europe and North America) led to a loss of interest in malaria for ~25 years (1970 - 1996), with regard to drug and insecticide development. The development of resistance of *P. falciparum* to the only affordable antimalarials, chloroquine and sulphadoxine/pyrimethamine, worsened the situation and the morbidity and mortality due to malaria increased [10]. Antimalarial drug resistance is "the ability of a parasite strain to survive and/or multiply despite the administration and absorption of a drug given in doses equal to or higher than those usually recommended, but within the limits of tolerance of the subject" [11]. The varying response of individual parasites to the available antimalarial drugs has been one of the major limiting factors in the prophylaxis and treatment of malaria [12].

Accurate estimation of the extent of the morbidity and mortality caused by malaria is difficult [13], but the current consensus is that there are annually about 500 million clinical cases of malaria, 2-3 million severe attacks and 1 million deaths, which equal in the order or 3000 deaths a day [13]. These numbers are probably an underestimation in view of the weakness of reporting systems for infectious diseases in Africa, where the majority of these cases are concentrated due to the presence of the *A. gambiae* mosquito in this region [10, 13, 14]. Most deaths occur in sub-Saharan Africa where children and pregnant women are affected worst. It is estimated that a child dies from malaria every 40 s on this continent [15]. The worldwide distribution of malaria and chloroquine resistance is shown in Fig. 1.1.

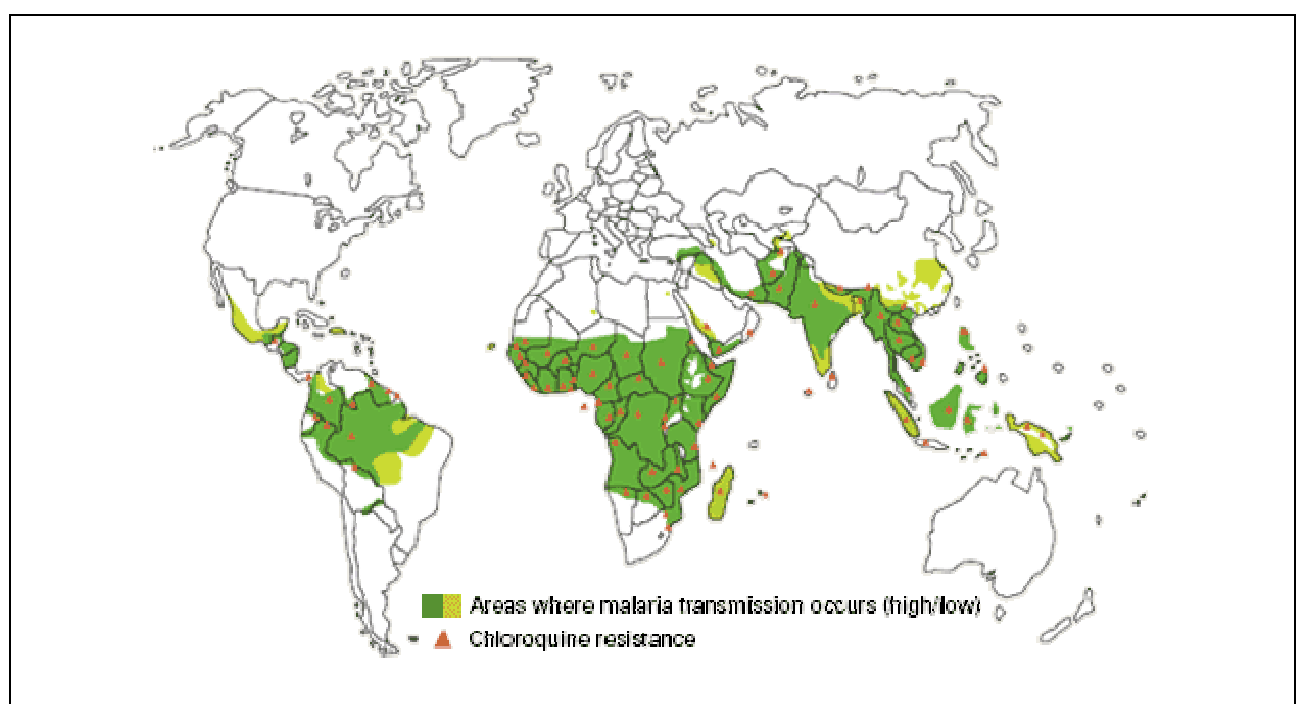


Fig. 1.1 Malaria geographical distribution and chloroquine resistance (WHO/UNICEF, World Malaria Report 2005, Geneva).

The potential influence of global warming on the transmission of malaria due to the changed habitat of the vectors is currently under debate [16-18]. Initial reports expressed the fear that the increased temperature in the 1980s and 1990s in areas of high altitude such as the East African highlands, where *P. falciparum* transmission was previously limited by low temperature, caused the increased number of cases witnessed in these areas in recent years [16, 19]. The rise in the numbers was subsequently attributed to factors other than meteorological patterns since a direct correlation could not be demonstrated [16], but fears still exist that climate change may result in the emergence of vector-borne diseases such as malaria, leishmaniasis, West Nile fever etc. in Europe and North America where these diseases are not endemic [18, 19].

The implications of malaria extend far beyond the morbidity and mortality of the disease. The economic effect on the affected communities is immense and it is estimated that the yearly gross national product of countries with endemic malaria is 2% less than in countries with similar backgrounds where the disease does not occur and that malaria costs Africa about US\$12 billion every year [13]. As a result, there is an unmistakable correlation between malaria and poverty. Poverty is concentrated in the tropical and subtropical areas, which closely coincides with the distribution of malaria transmission [20]. Adults in endemic areas generally develop partial immunity, but young children, especially at the pre-school stage, bear a considerable burden. School-age children also suffer symptoms resulting in reduced school attendance and loss of productivity and evidence suggests that the disease can impair intellectual development, with cerebral malaria potentially resulting in permanent developmental abnormalities [13]. The global burden of disease can be calculated by using a standard unit of health measurement, namely disability adjusted life years (DALYs). By using this single measure for morbidity, disability and mortality, the costs and the effects of intervention strategies to reduce the disease burden can be compared across diseases and debilitating risks, e.g. malaria resulted in 46 million DALYs compared to 84 million due to AIDS and 39 million due to road traffic accidents in 2002 [21]. The natural selection of malaria-protective genetic polymorphisms such as glucose-6-phosphate dehydrogenase deficiency and sickle cell disease, despite the reduced life expectancy resulting from homozygous inheritance of the latter, illustrates the enormous burden on communities living with malaria on a daily basis [20, 22].

1.3 THE PARASITE'S LIFE CYCLE

All malaria parasites are obligate intracellular protozoa of the genus *Plasmodium* with a complex life cycle consisting of sexual reproduction (sporogonic phase) in invertebrates, e.g. mosquitoes, and asexual reproduction (schizogonic phase) in vertebrates, e.g. mammals, birds and reptiles [23, 24].

Malaria is transmitted to humans by the intravenous inoculation of sporozoites by the bite of an infected female *Anopheline* mosquito (in Africa mainly *A. gambiae*), but in rare cases transmission occurs through exposure to

infected blood products or congenitally [25]. The sporozoites invade hepatocytes and transform, multiply and develop into tissue schizonts. This asymptomatic, pre- or exoerythrocytic stage lasts for ca. 7 to 30 days, depending on the *Plasmodium* species [25]. The tissue schizonts rupture and release thousands of merozoites into the bloodstream that invade erythrocytes, initiating the intraerythrocytic developmental cycle (IDC, Fig. 1.2). In *P. falciparum* and *P. malariae* infections, no parasites remain in the liver but with *P. vivax* and *P. ovale*, tissue parasites (hypnozoites) persist and can produce relapses months to years after the primary infection. Once the parasites enter the IDC they cannot invade tissues, therefore malaria contracted by transfusion does not have a tissue stage [24].

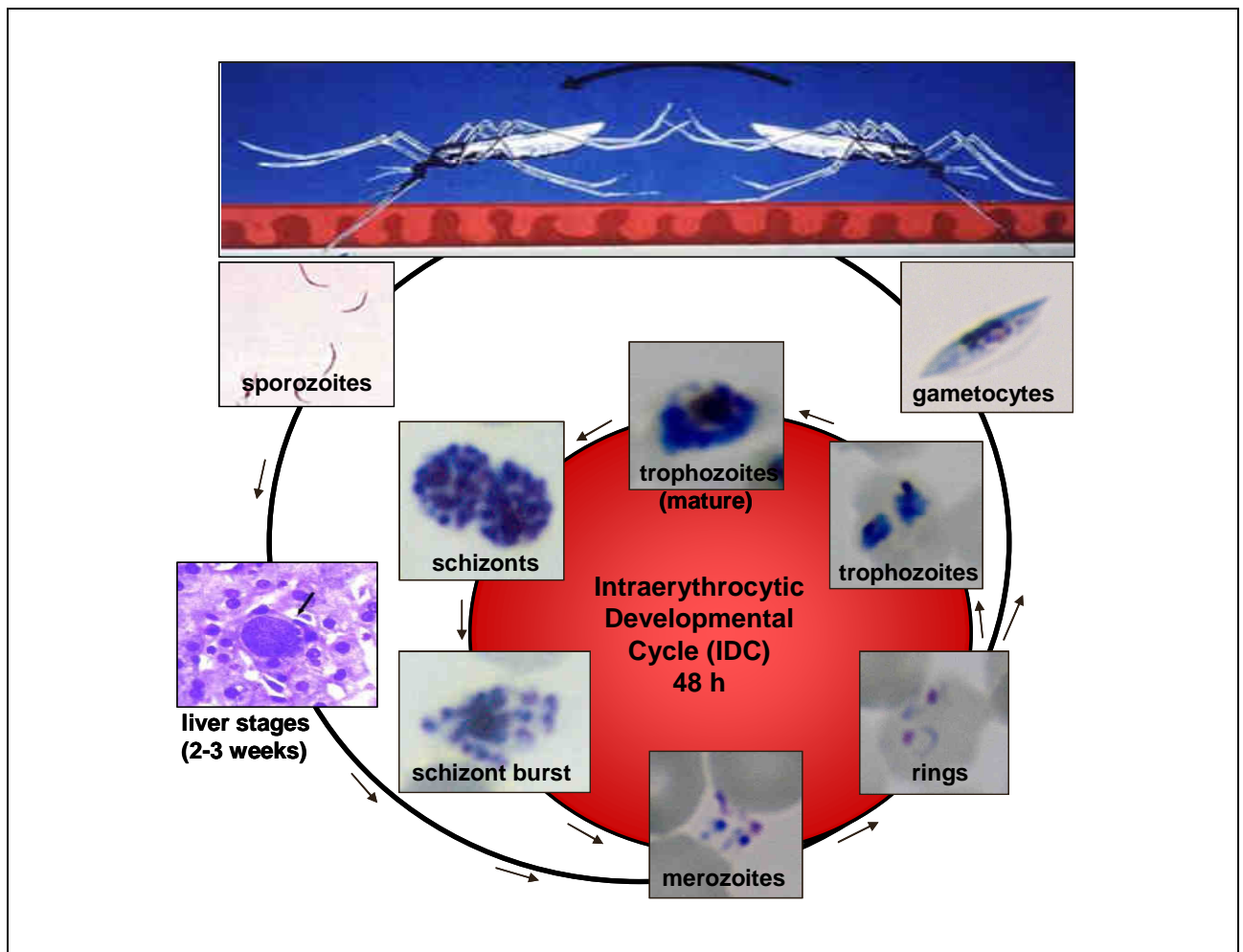


Fig. 1.2 Giemsa-stained thin smears depicting the life cycle of 3D7 *P. falciparum* (compiled from own photographs, sporozoites and liver stages from <http://images.google.com>)

During the IDC most parasites undergo asexual development from rings to trophozoites to schizonts (Fig. 1.2). The asexual parasites digest the host haemoglobin in their acidic food vacuoles to provide in their amino acid requirements [26], but this process is also necessary to provide room for parasite growth within the erythrocyte [27]. The haemoglobin degradation results in the generation of free radicals and haem, which is polymerised with the aid of lipids to form an insoluble pigment, haemozoin [28].

The IDC of *P. falciparum* lasts ~48 h. Blood schizonts release up to 32 merozoites [29]. The synchronous merozoite release causes the typical febrile attacks on days 1 and 3 in falciparum malaria, hence named "tertian malaria". More erythrocytes are invaded by the released merozoites and the next IDC commences. The cycle continues until the death of the host or death of the parasites due to drug treatment or acquired partial immunity [24]. A few erythrocytic parasites differentiate into sexual forms, named gametocytes. When infected blood containing gametocytes is ingested by a female *A. gambiae* mosquito, the male gametocyte exflagellates and male gametogenesis and fertilisation of the female gamete occurs in the mosquito gut. The zygote develops into an oocyst in the gut wall of the mosquito and infective sporozoites eventually invade the insect salivary glands to be released during the next human blood meal [24].

1.4 HUMAN MALARIA SPECIES

Humans have been regarded as the natural hosts of four species of malaria, namely *P. falciparum*, *P. malariae*, *P. vivax* and *P. ovale* [24], but there are more than 100 *Plasmodium* species that infect a variety of hosts such as reptiles, birds, rodents, primates and other mammals [9]. Each species causes a characteristic illness and has unique morphological features in blood smears under the microscope [24]. *P. vivax* is the most prevalent world-wide, and *P. falciparum* is the most dangerous and virulent species that causes malignant malaria, which is associated with severe complications such as cerebral malaria, renal failure and pulmonary affection [24, 30]. *P. falciparum* infection is potentially lethal due to its ability to invade erythrocytes of all ages (compared to *P. vivax* that invades only a subpopulation, i.e. the reticulocytes [31]), resulting in overwhelming parasitaemias and enhanced growth rate. Moreover, it has the capacity to adhere (cytoadherence) to the peripheral microvasculature (capillaries and venules) through sequestration. The parasitised erythrocytes attach to the venular endothelium via parasite-derived proteins that are expressed on the erythrocytic surface, e.g. erythrocyte membrane protein 1 (PfEMP1) [32], and remain attached until rupture and merozoite release [33]. Thus, the ring stage is the predominant form seen in the peripheral circulation [33]. By hiding in the microvasculature, the falciparum parasites avoid clearance by the immune system through the spleen [32], whereas *P. vivax*, *P. ovale* and *P. malariae* infected erythrocytes are not sequestered and are more successfully removed, therefore causing only benign human malaria without the danger of fatal complications [24]. Infected erythrocytes are also able to adhere to uninfected erythrocytes (i.e. rosetting), which can cause thrombus formation, resulting in tissue oxygen deprivation [34, 35].

The widely held view of four human malaria species was recently challenged by reports of *P. knowlesi* infection in humans [36]. The first naturally acquired case of *P. knowlesi* in a human male was documented in 1965 [37], but the vector, *A. hackeri*, was afterwards demonstrated to be predominantly zoophagic and the threat was dismissed [38]. However, recent surveillance detected a large focus (120/208 patients) of this simian malaria parasite in the human population of Malaysian Borneo, indicating the significance of zoonotic malaria transmission [36]. The natural hosts of *P. knowlesi* are the long-tailed and pig-tailed macaques and

banded leaf monkeys, but it has been shown to be able to infect a wide range of other primates, including man. These diverse primate groups diverged millions of years ago and it is unlikely that the parasite's ability to infect such a variety of hosts is a recent adaptation or that human susceptibility to *P. knowlesii* is new [38]. Human-to-human transmission in South-East Asia was probably prevented by the restriction of the vector to a jungle habitat, which overlaps with the natural environment of the macaques and due to cross-species competition with the other *Plasmodium* species, already established in human populations. The recent success of malaria-control programmes in this region, combined with human population expansion and habitat destruction of the natural hosts, could have provided the opportunity leading to the observed host-switching [38]. The significant threat of a fifth species of human malaria should be recognised and it should be included in current malaria eradication and drug discovery programmes.

1.5 THE PATHOGENESIS AND CLINICAL PRESENTATION OF MALARIA

Falciparum malaria causes an acute illness with initially non-specific symptoms including fever, headache, malaise, mild jaundice, hyperventilation, hepatosplenomegaly, myalgia etc. [25]. The fever peaks occur at the time of erythrocyte rupture with the release of merozoites and malaria toxins [e.g. glycosylphosphatidylinositol (GPI)]. These toxins induce the secretion of pro-inflammatory cytokines by the macrophages and parasite antigens stimulate T-cells to directly secrete or induce cytokine production by other cells [33, 35]. The tertian episodes of fever and erythrocyte destruction often lead to severe anaemia and other complications specific to *P. falciparum* infection, such as cerebral malaria, anaemia, hypoglycemia, renal failure and noncardiac pulmonary oedema. In the non-immune patient, these complications may occur in isolation or in combination, resulting in an often complex clinical syndrome [33]. However, the clinical presentation of severe disease in the previously exposed African child differs and renal failure and noncardiac pulmonary oedema do not occur [33].

Severe malaria is one of the potentially fatal complications of *P. falciparum* infection. It was previously regarded as either severe anaemia (due to erythrocyte destruction) or cerebral malaria (due to small blood vessel obstruction of the brain), but nowadays it is recognised to be a complex multi-system disorder with many similarities to sepsis syndromes [35]. Metabolic acidosis leading to the clinical picture of respiratory distress is currently acknowledged as the strongest predictor of death in severe malaria. Hypovolaemia, exacerbated by anaemia and microvascular obstruction due to parasite sequestration, results in decreased oxygen delivery to tissues, anaerobic metabolism and lactic acidosis, but hyperlactataemia is not always present [35]. As with sepsis, cytokine-induced failure of oxygen utilisation [39] has an important role in the pathogenesis but the major influence of immunopathogenic processes, such as proinflammatory cytokine cascades resulting in complex metabolic changes and vascular physiological changes, are now recognised [35, 40]. Pro-inflammatory mediators such as the interleukins (IL), tumour necrosis factor (TNF), interferons (IFN), prostaglandins, as well as molecules such as nitric oxide (NO) and indoleamine 2,3-deaminase, are

biomarkers of severe malaria [35]. The balance and timing of secretion of both the pro-inflammatory and anti-inflammatory cytokines may be important in disease and parasite clearance, with IL-4 and IL-10 apparently protecting against severe disease, whereas increased TNF is associated with severe pathology [35]. The role of NO is controversial, but recent evidence indicates that low rather than high NO bioavailability contributes to the genesis of cerebral malaria in animals [40] and that expression of haem oxygenase-1 prevents the development thereof [41]. Haem oxygenase-1 produces carbon monoxide (CO), which prevents blood-brain barrier disruption, brain microvasculature congestion and neuron inflammation including CD8⁺ -T-cell brain sequestration. The protective effect of CO may be NO-dependent, as NO is a potent inducer of haem oxygenase-1. CO binds to haemoglobin, preventing haemoglobin oxidation and free haem generation, which triggers the cerebral malaria pathogenesis [41].

Pregnant women are particularly vulnerable to malaria and are more likely to become infected than non-pregnant women with *P. falciparum*, resulting in severe disease. This is partially due to the transient depression of cell-mediated immunity that occurs during pregnancy. Furthermore, the enhanced function of pancreatic β -cells in pregnant women resulting in a tendency to hypoglycaemia is further aggravated by the parasite's glucose requirements and decreased liver glycogen stores from decreased oral intake due to emesis and anorexia. Pregnancy-associated malaria is characterised by placental sequestration of malaria parasites in the intervillous space of the placenta, causing histological changes including leukocyte-induced damage to the trophoblastic basement membrane. The sequestration results from parasite binding to chondroitin sulphate A (CSA) receptors in the placenta and disrupts oxygen and nutrient transport across this membrane. Anti-adhesion immunoglobulin G antibodies against CSA-binding parasites are associated with protection from maternal malaria, but it only develops over successive pregnancies. Pregnancy-associated malaria can occur without clinical symptoms and the resulting placental sequestration can cause the malaria to be missed when based purely on peripheral blood smears. The effects during pregnancy differ depending on the woman's immunity, her gravidity, the trimester of pregnancy and the presence or absence of other disease. Adverse consequences of placental malaria and maternal anaemia may include spontaneous abortion, preterm delivery, low birth weight due to intrauterine growth retardation, congenital infection and a 2-fold increased risk of stillbirth [25].

Despite persistent malarial infections, neutralising antibodies that block erythrocyte invasion (as with many virus infections) do not occur because of the high degree of antigenic diversity of the malaria surface proteins [33]. Similar to other unicellular protozoa (African trypanosomes and *Babesia* sp.), bacterial pathogens (*Borrelia* sp. and *Neisseria* sp) and pathogenic fungi (*Candida* sp.), *Plasmodium* has the ability to vary surface protein expression to alter the profile of antigens exposed to the host immune system [34]. Antigenic variation involves the ability of the parasite to tightly regulate the expression of individual genes within large, hypervariable gene families, thus exposing only a small portion of the parasites' antigenic repertoire to the host

at any given time. These hypervariable gene families are the *var* (variant, 59 genes), *rifin* (repetitive interspersed family, 149 genes), *stevor* (subtelomeric variable open reading frame, ~30-40 genes) and *Pfmc-2TM* (two transmembrane protein domains, 13 genes) genes that are predominantly found in subtelomeric chromosomal regions. It appears that the degree of sequence variability within these families is almost limitless in natural parasite populations [34, 42]. In contrast to the *var* genes, the *rifin*, *stevor* and *Pfmc-2TM* genes all have a PEXEL (*Plasmodium* export element)/VTS (vacuolar transport signal) motif that is responsible for the transport of these proteins to the erythrocyte cytoplasm. The *var* and *rifin* proteins are ultimately targeted to erythrocyte surface, but the *stevor* and *Pfmc-2TM* proteins remain in the flat vesicular membranous Maurer's clefts [34]. These are parasite-derived structures within the erythrocyte cytoplasm that are postulated to function as protein-sorting compartments between the parasite and the erythrocyte membrane [43]. The most extensively studied variant antigens are the *var* multigene family, which expresses the cytoadhesive protein, PfEMP1. PfEMP1 is displayed within the knobs on the infected erythrocyte surface and binds to several host endothelial cell surface receptors, e.g. cluster determinant 36 (CD36), intercellular adhesion molecule 1, thrombospondin, complement receptor 1 and CSA. A single PfEMP1 protein is expressed at any given time and, depending on the variant, the cytoadherence and antigenic phenotype will vary dramatically. Therefore, PfEMP1 is a major virulence factor in falciparum malaria [34].

1.6 ANTIMALARIAL VACCINES

There have been more than 40 clinical trials of antimalarial vaccines in the last 25 years [44]. These preliminary vaccines generally followed three strategies of immunisation, namely to target the pre-erythrocytic liver stage, the blood stage or the sexual stage (transmission-blocking vaccines). Pre-erythrocytic stage vaccines aim to prevent sporozoite invasion of hepatocytes and/or to eliminate those already infected. Blood stage or asexual vaccines prevent merozoite invasion of erythrocytes and prevent clinical symptoms, whereas transmission blocking vaccines are designed to break the cycle of infection [45].

Currently, the focus of vaccine discovery programmes is on species-specific vaccines for *P. falciparum* and *P. vivax* in response to results of sequential heterologous infections from the 1950 - 1960s and cross-species challenge experiments from the 1970s, which determined that multi-species protection would be difficult to achieve with a single vaccine. However, combinations of antigens could provide broad protection once the successful species-specific vaccines have been developed [44]. Since *Plasmodium* is a multistage organism, a good vaccine should furthermore contain antigens from different stages (multistage vaccine) and should include several antigens from each stage (multivalent) to circumvent antigenic variation. Finally, vaccines should be simple and elicit the correct type of immune response [44]. Yet, despite many years of effort, an effective antimalarial vaccine remains elusive. Currently, there is reason for optimism due to evidence of partial human protection provided after immunisation with irradiated sporozoites, development of naturally acquired immunity after repeated malaria infections, the efficacy of vaccines based on recombinant

circumsporozoite protein and the successful protection of mosquitoes against *P. falciparum* and *P. vivax* by preliminary transmission-blocking vaccines [44].

Most vaccines tested up to now have been pre-erythrocytic stage vaccines against sporozoites or liver stage parasites consisting of synthetic peptides or recombinant proteins based on malarial antigens. However, a commonly experienced problem is difficulty in obtaining a strong and long-lasting immune response in humans [44]. Collaboration between the US Army Walter Reed Institute of Research and GlaxoSmithKline produced the pre-erythrocytic stage vaccines RTS,S and TRAP/SSP2 and the blood-stage vaccines MSP1 (merozoite surface protein 1)-3D7 and AMA1 (apical membrane antigen 1)-3D7 [44]. The RTS,S vaccine is a chimaeric fusion protein between circumsporozoite protein and the hepatitis B surface antigen, which was tested in several clinical trials. It caused a significant reduction of infection rate in Gambian adult males, but the effect was short-lived [46]. However, a phase IIb trial in Mozambican children demonstrated 35.3% efficacy against risk of clinical malaria and 48.6% against severe malaria with a good safety profile [47]. A phase IIa trial in malaria-naïve adults at the US Army Walter Reed Institute of Research provided 42 – 47% protection [48]. Based on these promising results it is hoped that a malaria vaccine will become available within the next decade.

1.7 ANTIMALARIAL THERAPEUTICS

Due to the current lack of an approved vaccine strategy, antimalarial intervention consists of drug treatment with the primary objective of eradicating malaria parasites completely from the body, i.e. to provide a cure for the disease [49]. Quinine's history of medicinal use dates back 350 years and artemisinin (qinghaosu) has been used in China for over 2000 years [24]. Most other drugs currently used in the treatment of malaria were discovered as long ago as the 1940s, e.g. chloroquine (1943), proguanil (1945), primaquine (1946) pyrimethamine (1951), halofantrine (1960s) and mefloquine (1963). Of the 1223 new drugs developed from 1970 to 1996, only three were antimalarials [50]. Most of the antimalarials have closely related structures and modes of action (resulting in cross-resistance), which underscores the urgency to progress antimalarial drug discovery. The most important antimalarial drugs, their modes of action and limitations are presented in Table 1.1.

Table 1.1 Antimalarial therapeutics and combinations

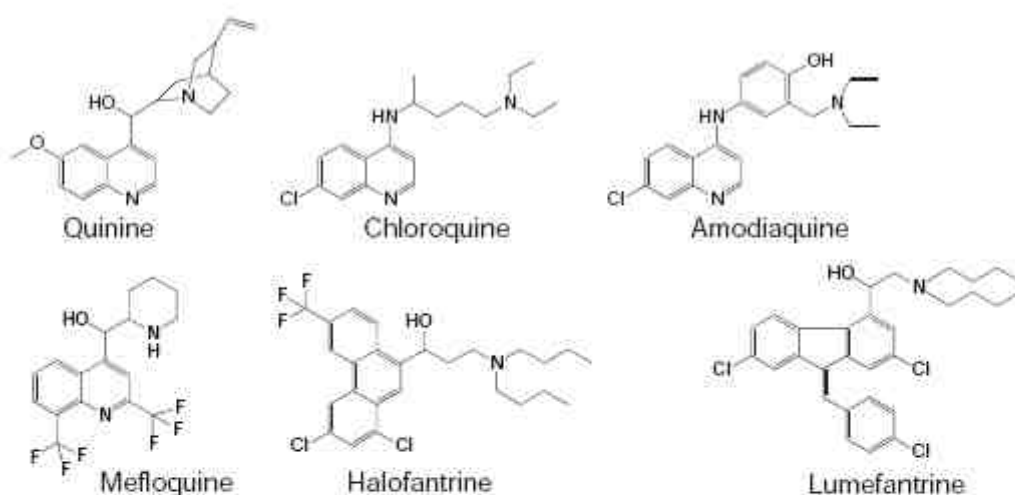
| Pharmacological class | Mode of action | Limitations |
|---|---|---|
| Quinolines and related compounds Quinine Chloroquine Amodiaquine Mefloquine Primaquine Halofantrine Lumefantrine | Inhibits haem detoxification, but exact mechanism still debated | Poor compliance, toxicity, resistance Resistance Side-effects, resistance Side-effects, resistance Resistance Side-effects, resistance, cost Cost |
| Artemisinins Arteether Artemether Artesunate | Free-radical-induced damage or inhibition of sarcoplasmic reticulum calcium-dependent ATPase 6 (SERCA), but exact mechanism still debated | Compliance, side-effects, cost |
| Antifolates Sulphadoxine Dapsone Proguanil Pyrimethamine | Inhibits dihydroopteroate synthase (DHPS) Inhibits dihydrofolate reductase (DHFR) | Resistance |
| Naphthaquinones Atovaquone | Mimics ubiquinone and interferes with mitochondrial electron transport | Resistance potential, cost |
| Antibiotics Tetracycline Doxycycline Clindamycin | Inhibits prokaryotic-like protein synthesis in the apicoplast (plastid) | Side-effects (children) |
| Antimalarial combinations Chloroquine/Proguanil Atovaquone/Proguanil Artemether/Lumefantrine Artesunate/Mefloquine Pyrimethamine/Sulphadoxine Chlorproguanil/Dapsone Pyrimethamine/Dapsone Chlorproguanil/Dapsone/Artesunate | Combination of above | Resistance Resistance, cost Resistance potential, cost Resistance potential, cost Resistance Resistance Resistance Resistance potential, cost |

Compiled from [24, 51, 52].

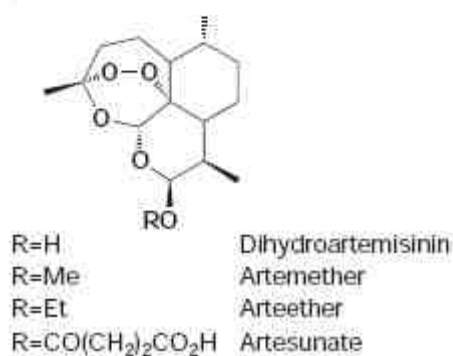
1.7.1 Quinine and related antimalarials

The quinoline antimalarials were originally derived from quinine (Fig. 1.3). Quinine is a 4-aminoquinoline and the chief alkaloid from the bark of the South American cinchona tree that was imported to Europe from Peru around 1633-1640 [51]. The quinoline drugs are blood schizontocides with high activity against the erythrocytic forms of susceptible Plasmodia as well as gametocytes of *P. vivax*, *P. ovale* and *P. malariae*, but not *P. falciparum*. They are weak bases and accumulate in the food vacuoles of susceptible parasites. As result, the pH of the acidic food vacuole increases, haem peroxidase activity is inhibited and the non-enzymatic polymerisation of haem to haemozoin is thought to be disrupted [28]. The toxic haem accumulates and kills the parasite via oxidative damage to cell membranes, proteases and other critical molecules, but the exact mode of action is not completely elucidated [53, 54].

Quinoline and related antimalarials



Artemisinin antimalarials



Other antimalarials

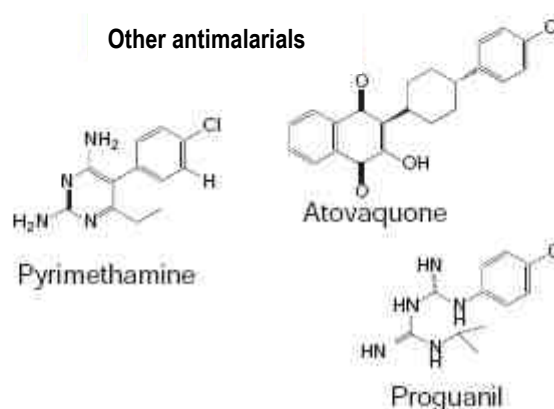


Figure 1.3 Currently used antimalarial drugs [51]

The toxicity of quinine (side-effects such as tinnitus), inconvenient dosage interval (three times daily resulting in poor compliance) and dependence on plant material for extraction motivated the development of the fully synthetic 4-aminoquinolines i.e. chloroquine and amodiaquine (Fig. 1.3) [51]. Chloroquine was already discovered in 1934 in Germany, but was not known elsewhere and was rediscovered by American scientists during World War II (1943). It has fewer side-effects than quinine and higher efficacy against malarial parasites susceptible to both drugs. Chloroquine is actually an extraordinarily safe drug for prophylaxis and cure of susceptible *P. falciparum* infections [24], but unfortunately, chloroquine resistance against *P. falciparum* is now almost global (Fig. 1.1) [51]. The use of amodiaquine has been limited since the mid-1980s due to an association with agranulocytosis, but it has retained a high degree of efficacy against the most highly chloroquine-resistant strains [51].

Mefloquine is a 4-quinoline-methanol that was first used to treat chloroquine-resistant falciparum malaria in Thailand and is currently reserved for the prevention and treatment of chloroquine-resistant and multidrug-resistant *P. falciparum* infections (Fig. 1.3). Halofantrine is a phenanthrene-methanol with blood schizontocidal properties similar to the quinoline antimalarials (Fig. 1.3). It was initially developed as an alternative to quinine

and mefloquine in the treatment of acute malarial infections of chloroquine-resistant or multidrug-resistant *P. falciparum* strains [24]. However, resistance against both mefloquine and halofantrine can develop rapidly [51] and both have contra-indications e.g. mefloquine in patients with a history of seizures or neuropsychiatric disturbances and both drugs in patients with a history of heart disease [24, 51]. The aryl-alcohol, lumefantrine, is similar to mefloquine and halofantrine, but it has a better safety profile (no neurotoxicity) and is one of the most recently approved antimalarials [51].

Drug resistance usually develops within 10 years after an antimalarial was introduced [55] and *P. falciparum* chloroquine resistance was observed for the first time about 50 years ago. Currently chloroquine resistance is the result of polymorphisms in the *pfcr1* gene located on chromosome 7 or in the *pfmdr1* gene on chromosome 5 of the *P. falciparum* genome. The *pfcr1* gene codes for the chloroquine resistance transporter (PfCRT), a vacuolar membrane transporter protein and *pfmdr1* codes for the multidrug resistance type 1 protein (MDR1), a P-glycoprotein homologue and well-characterised ABC-transporter [55]. These mutations in parasite-encoded drug transporters lead to reduced drug accumulation and therefore reduced susceptibility. The exact mechanism is controversial, but one hypothesis is that these mutations significantly change the pH of the food vacuole, resulting in reduced chloroquine accumulation. Another hypothesis is that PfCRT transports chloroquine directly out of the food vacuole. Recent evidence indicates that the chloroquine resistance conferring mutations in PfCRT enable the protein to transport chloroquine together with H⁺ ions from the food vacuole [56]. Mutations of the *pfmdr1* gene have also been implicated in *P. falciparum* resistance against quinine, mefloquine and artemisinin and resistance to atovaquone has been ascribed to point mutations in the gene encoding cytochrome bc₁ of the parasite electron transport chain [55, 57]. Gene polymorphisms that lead to non-synonymous amino acid substitutions can cause complete loss of function of the proteins involved [55].

1.7.2 Artemisinin and derivatives

Artemisinin or qinahaosu is a sesquiterpene lactone endoperoxide that is extracted from the weed *Artemisia annua* (sweet wormwood). Chinese scientists synthesised three artemisinin derivatives, two oil-soluble methyl esters named artemether and arteether and a water-soluble hemisuccinate salt of dihydroartemisinin named artesunate (Fig. 1.3) [24, 51]. The three derivatives are metabolised *in vivo* to dihydroartemisinin, the main active agent [51]. The Chinese reported rapid, safe and efficient treatment of malaria with the artemisinins in 1979 and since then more than 2 million patients have been treated successfully in China, Southeast Asia and Africa [24].

The endoperoxide moiety is essential for antimalarial activity, but substitutions of the lactone carbonyl increase potency significantly. Apparently, cleavage of the drug's endoperoxide bridge is catalysed by intraparasitic haem iron of infected erythrocytes, which is followed by intramolecular rearrangement to produce carbon-centered radicals that modify and damage specific malarial proteins by covalent interactions [24]. However,

the exact mode of action is under debate and the inhibition of the sarco/endoplasmic reticulum calcium-dependent ATPase 6 (SERCA, PfATPase6) has also been proposed [58].

Artesunate has been demonstrated to act primarily on young ring-form parasites, preventing their development to mature trophozoites [59]. Artemisinin and its derivatives are very effective in the treatment of these asexual parasites of chloroquine-sensitive, chloroquine-resistant and multidrug-resistant *P. falciparum*. The compounds also have gametocytocidal activity but do not affect liver stage parasites and can therefore not be used for chemoprophylaxis or to prevent relapses of vivax/ovale malaria. *In vitro* activity against other protozoa, e.g. *Leishmania major* and *Toxoplasma gondii*, has also been demonstrated [24].

On the negative side, the artemisinins have short half lives, necessitating treatment of 5 - 7 days, and are increasingly used in combination with drugs with longer half lives to reduce the treatment time [51] e.g. artemether/lumefantrine and artesunate/mefloquine. Furthermore, the cost of artemisinin derivatives is significantly more than that of traditional antimalarials such as chloroquine and the observation of selective brain stem neuronopathy in laboratory animals treated with a high dose of artemisinins parenterally also had a negative impact [51]. The decrease in *in vitro* susceptibility of *P. falciparum* against artemether in French Guiana [58] due to a single polymorphic mutation of the *PfATPase6* gene demanded the immediate deployment of drug combinations [58]. However, the declining efficacy of the artesunate/mefloquine combination on the Cambodia/Thailand border was recently reported, but this is most likely due to mefloquine resistance rather than artemisinin resistance, as increased copy numbers of *pfmdr1* were detected [52].

1.7.3 Antifolates

In contrast with the quinolines and artemisinins, the antifolates were not derived from plants. These drugs were mostly generated through knowledge of cell biology and synthetic medicinal chemistry [51]. Nucleotide biosynthesis and amino-acid metabolism require one-carbon transfer reactions, which are dependent on completely reduced folate co-factors. The antifolates target one of two subsequent enzymes in folate metabolism, either dihydrofolate reductase (DHFR) or dihydroopteroate synthase (DHPS) [51]. However, the effects of inhibition are only visible late in the life cycle due to failure of nuclear division during schizont formation [24].

The commonly used antimalarial combination pyrimethamine/sulphadoxine inhibits both DHFR and DHPS [51]. The success of the combination lies in the synergism of the two components. However, resistance against pyrimethamine/sulphadoxine has increased substantially and its use is nowadays restricted to suppressive treatment of chloroquine-resistant falciparum malaria in regions where antifolate resistance has not yet developed [24]. The molecular basis behind the resistance to pyrimethamine/sulphadoxine is characterised best of all antimalarial resistance. Point mutations at five codons (codon 16, 51, 59, 108, 164) of the *dhfr* gene

are implicated in conferring resistance to pyrimethamine by decreasing its binding affinity to the enzyme. In the same way specific point mutations (codon 436, 437, 540, 581 and 613) in the *dhps* gene have been identified to result in a decreased binding affinity of DHPS for sulphadoxine, other sulphonamides and the sulfone dapson [55, 60]. The selection for point mutations in *dhfr* and *dhps* are not equal, but appear to occur in *dhfr* first and mutations in *dhps* are selected only if most parasites in a population carry a double or triple mutant allele of *dhfr*. The reason for this asymmetry may be due to importance of DHFR to enable *P. falciparum* to salvage exogenous folate, thus bypassing the *de novo* biosynthesis via DHPS. However, inhibition of DHFR via pyrimethamine hampers the use of exogenous and synthesised folate by the parasite [60]. Apart from point mutations, another reason for the rapid selection for antifolate resistance is the long elimination half lives of both pyrimethamine (81 h) and sulphadoxine (116 h), resulting in the selection of resistance against these drugs when blood levels decrease below therapeutic concentrations [60].

In an effort to overcome pyrimethamine resistance and to restore the antifolates in regions of drug resistance, medicinal chemistry efforts have identified improved DHFR inhibitors, e.g. the biguanides. Chlorproguanil retains activity against most pyrimethamine-resistant parasite strains and is administered in combination with dapson and artesunate to prevent further development of resistance (Table 1.1) [51]. These three drugs all have half lives of less than a day, resulting in reduced selection pressure for resistance [60].

1.8 ANTIMALARIAL DRUG TARGETS

One of the initial steps in rational drug development is the identification and subsequent validation of drug targets in *Plasmodium* [61]. The efficacy and specificity of anti-infective drugs depend on their ability to interfere with metabolic pathways or proteins of pathogens that are essential for survival but also significantly different from those of the host to enable selective toxicity [51]. Developmental stages of the IDC are specifically targeted, since the asexual parasites are responsible for all the clinical symptoms of malaria and are therefore the focus of most antimalarial drugs and potential vaccine strategies. Moreover, distinct organelles, such as the food vacuole, the apicoplast and the acrystate mitochondrion with its limited electron transport system, are also regarded as potential drug targets [51]. Both the apicoplast (plastid) and mitochondrion are prokaryote-like organelles inside the eukaryotic parasite. The apicoplast houses enzymes involved in type II fatty acid biosynthesis, a non-mevalonate pathway for isoprenoid biosynthesis and haem biosynthetic pathways, whereas the mitochondrion contains a complete citric acid cycle [62]. A post-genome survey of *Plasmodium* identified about 50 proteins as potential antimalarial targets [54]. These potential targets belong to the following broad biological functions: energy metabolism, coenzyme and prosthetic group metabolism, protein modification, lipid metabolism, deoxyribonucleic acid (DNA) replication and transcription, haemoglobin digestion and antioxidant defence. The targets include a bifunctional, key-regulatory and biosynthetic enzyme of polyamine and methionine metabolism, S-adenosylmethionine decarboxylase/ornithine decarboxylase (PfAdoMetDC/ODC) [54], which will be discussed in more detail in the following paragraphs.

1.9 POLYAMINE METABOLISM

1.9.1 The biological importance of polyamines

The polyamines are small, aliphatic compounds containing two or more amino groups, which in eukaryotes mainly include the diamine putrescine (1,4-diaminopropane), the triamine spermidine [N-(3-aminopropyl)-1,4-diaminobutane] and the tetra-amine spermine [N,N¹-bis(3-aminopropyl)-1,4-butanediamine] (Fig. 1.4). At physiological pH these polycations interact electrostatically with numerous anionic macromolecules, thereby stabilising DNA, ribonucleic acid (RNA), nucleotide triphosphates [e.g. adenosine triphosphate (ATP)], phospholipids and proteins [63, 64]. These interactions with polyamines can alter DNA conformation, regulate replication and transcription, strengthen membranes, regulate ion channels and protect DNA and phospholipids from oxidative stress [63-67]. However, polyamines are also implicated in apoptosis [67]. Polyamine depletion generally causes cytostasis or growth arrest, which implies that these molecules are involved in cell cycle progression and regulation and it is speculated that polyamines regulate cyclin degradation [63, 68]. Therefore, polyamines are essential for cellular growth, differentiation and macromolecular synthesis and are ubiquitous components of all living cells, except two orders of Archaea [63].

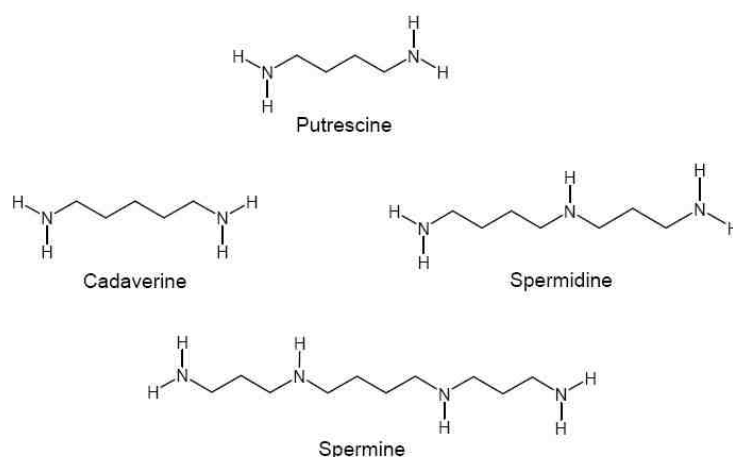


Figure 1.4 Chemical structures of the natural polyamines

A fourth polyamine, cadaverine, is actually a diamine and structural analogue of putrescine, with only an additional methylene group (Fig. 1.4) [69]. Most research on cadaverine has been performed in prokaryotes [70-73], but the importance thereof in plants has also been demonstrated [74, 75]. Cadaverine was shown to have functions similar to the other polyamines, including protection against oxidative stress [76] and involvement in root development [75]. Recently, the first cadaverine aminopropyl transferase, with functions similar to spermidine synthase, was identified in *Pyrococcus furiosus* [72]. In protozoa, cadaverine sustained growth of a *L. donovani* ornithine decarboxylase (ODC)-deletion mutant [77], but almost nothing is known about the biological role of cadaverine in Plasmodia.

Polyamine metabolism is particularly important in rapidly proliferating cells and has been exploited in the treatment of cancer [63] and parasitic diseases [78]. It is also a potential target for antimalarial therapeutic intervention [54, 79]. The various inhibitors and effects of inhibition will be discussed in Chapter 2.

1.9.2 The biosynthesis of polyamines

The natural polyamines (excluding cadaverine) are synthesised by means of six interdependent enzyme reactions in eukaryotes, starting from L-arginine (via arginase to L-ornithine) and L-methionine [via S-adenosylmethionine (AdoMet) synthetase to AdoMet]. Ornithine decarboxylation via ODC forms putrescine, which combines with decarboxylated AdoMet (dcAdoMet) from AdoMet decarboxylase (AdoMetDC), to produce spermidine through the aminopropyltransferase action of spermidine synthase. In most organisms a second aminopropyltransferase reaction involving dcAdoMet occurs via spermine synthase and leads to the formation of spermine [80]. Polyamine metabolism of mammalian cells is shown in Fig. 1.5.

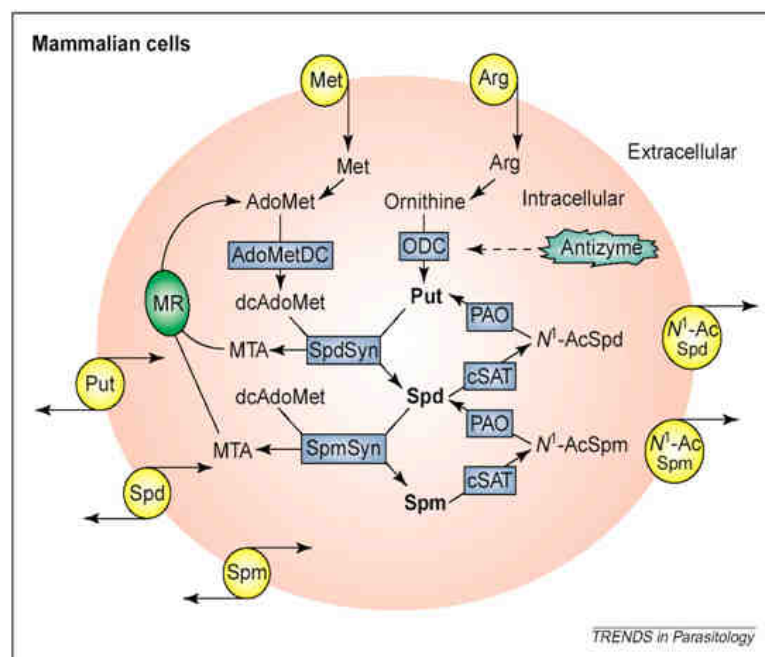


Figure 1.5 Polyamine metabolism in mammalian cells [81].

AdoMet, S-adenosylmethionine; AdoMetDC, S-adenosylmethionine decarboxylase; cSAT, cytosolic N1-acetyltransferase specific for spermidine and spermine; dcAdoMet, decarboxylated S-adenosylmethionine; MR, methionine recycling pathway; MTA, methylthioadenosine; N1-AcSpd, N1-acetyl spermidine; N1-AcSpm, N1-acetyl spermine; ODC, ornithine decarboxylase; PAO, polyamine oxidase; Put, putrescine; Spd, spermidine; SpdSyn, spermidine synthase; Spm, spermine; SpmSyn, spermine synthase.

In mammalian cells, the regulation of ODC and AdoMetDC (and thus polyamine levels) occurs at the transcriptional, translational and post-translational levels [81]. ODC is positively and negatively feedback-regulated by the polyamines, resulting in increased biosynthesis when polyamine concentrations are low and decreased synthesis when concentrations are high. The feedback regulation is a combination of post-transcriptional regulation and the induced expression of antizyme, which is a unique ODC-specific inhibitor. ODC can also be released from antizyme upon growth stimuli by another unique protein, named antizyme

inhibitor, which has higher affinity for antizyme than ODC [63]. As a result of quick degradation, ODC and AdoMetDC have short half lives, i.e. 15 min and 35 min, respectively [81]. Apart from the regulation of biosynthesis, polyamine levels are also regulated by transport, excretion and interconversion, i.e. spermine can be converted back to spermidine and spermidine to putrescine (Fig. 1.5) [81]. The interconversion pathway is mediated by cytosolic N₁-acetyltransferases (specific for spermidine and spermine) and polyamine oxidase [81]. The intricate regulation of polyamines further underscores their importance. Low polyamine concentrations or depletion generally impair growth and cellular differentiation, resulting in growth arrest (cytostasis). However, both polyamine depletion and accumulation can also stimulate programmed cell death or apoptosis. Thus, the effects of polyamines and their regulation are generally very complex [63].

In *P. falciparum*, ODC and AdoMetDC are transcribed as a single transcript and are translated into one hinge-linked bifunctional protein, PfAdoMetDC/ODC [82]. Up to date, only monofunctional ODC and AdoMetDC has been detected in other organisms [83], but the enzyme complex is bifunctional in at least three Plasmodia (*P. falciparum*, *P. berghei* and *P. yoelii*) [84]. Plasmodial polyamine biosynthesis occurs as described for mammalian cells, but spermine synthesis is now believed to be catalysed by spermidine synthase as well (Fig. 1.6) [85]. The diamine, cadaverine, is synthesised by decarboxylation of lysine via lysine decarboxylase (LDC) [69], the function of which in Plasmodia is currently unknown [79]. Plasmodia do not have an antizyme homologue and in contrast with the short half lives of the mammalian enzymes, PfAdoMetDC/ODC has a half life of ~2 h. Similar differences in the intracellular turn-over rate of ODC in Trypanosoma compared to mammals (hours versus 15 min) is partially responsible for the selective toxicity and relative safety of ODC inhibitors such as DL- α -difluoromethylornithine (DFMO) against the causative agent of African sleeping sickness, *Trypanosoma brucei gambiense* [81]. The longer half lives of the parasite enzymes result in a longer-lasting inhibitory effect of DFMO on the parasite than on the host. Recently, it was shown that trypanosomal AdoMetDC uniquely requires a protein called prozyme, which dimerises with the parasite's AdoMetDC and is an essential allosteric activator thereof [86]. *Plasmodium* does not have a polyamine interconversion pathway and there are differences in the regulation of ODC and AdoMetDC in comparison to mammals and trypanosomes. *P. falciparum* ODC activity is feedback-regulated to a greater extent by its product, putrescine, than mammalian ODC, putrescine does not stimulate the parasite's AdoMetDC, whereas it does stimulate the mammalian enzyme [81] and from recombinant AdoMetDC expression studies it was concluded that *Plasmodium* does not have a prozyme homologue [81, 87].

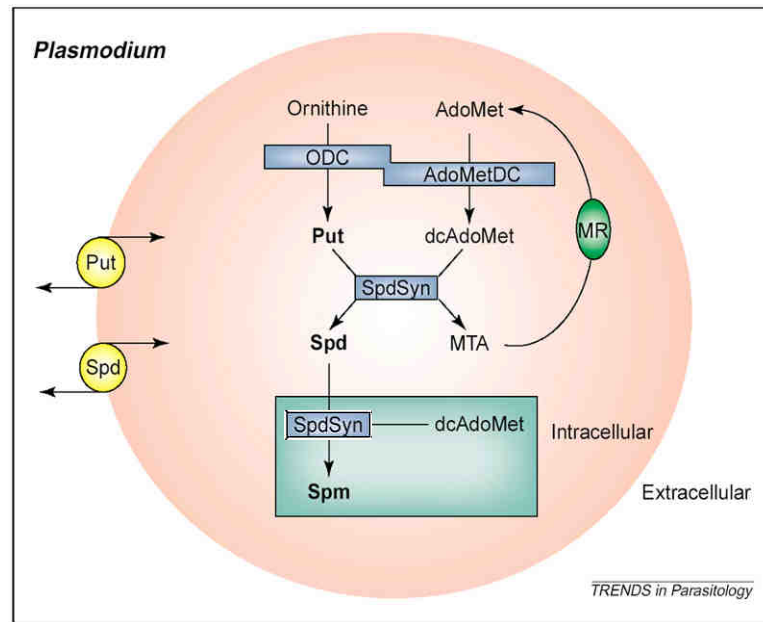


Figure 1.6 Polyamine metabolism in *Plasmodium* (slightly modified from [81]).

AdoMet, S-adenosymethionine; AdoMetDC, S-adenosylmethionine decarboxylase; dcAdoMet, decarboxylated S-adenosylmethionine; MR, methionine recycling pathway; MTA, methylthioadenosine; ODC, ornithine decarboxylase; Put, putrescine; Spd, spermidine; SpdSyn, spermidine synthase; Spm, spermine.

Human erythrocytes are anuclear and do not contain ODC or AdoMetDC. However, ODC and AdoMetDC activity and, therefore polyamine concentrations, are markedly increased in *P. falciparum*-infected erythrocytes [88]. This elevated decarboxylase activity is maximal in the early trophozoite stage [88] when the major macromolecular synthesis occurs [89] and consequently polyamine levels increase with the development from rings to schizonts (Fig. 1.7) [90].

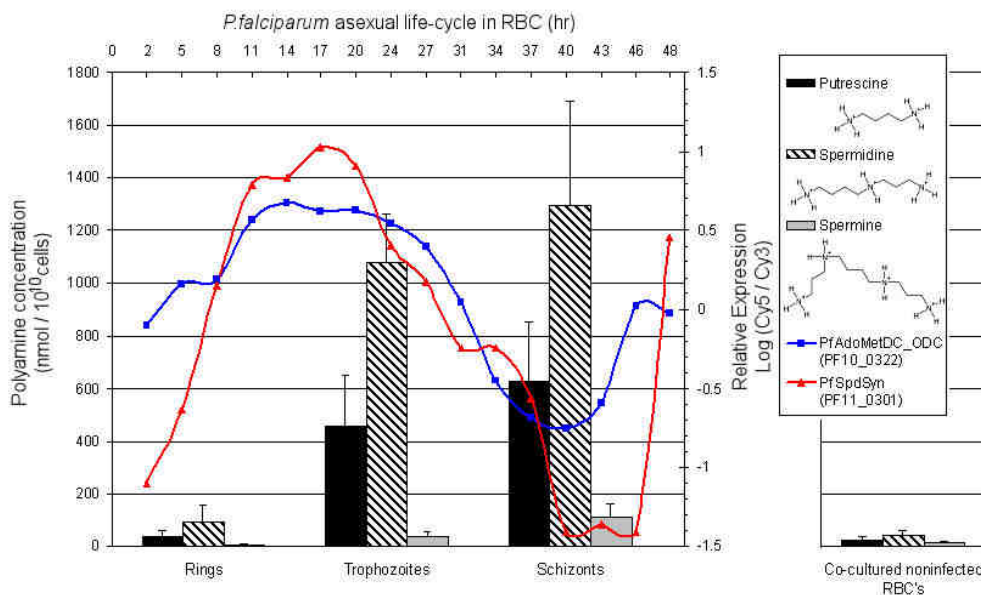


Figure 1.7 Composite diagram of polyamine levels [90] and biosynthetic enzyme transcript levels (PfAdoMetDC/ODC and spermidine synthase) [91] during the IDC of *P. falciparum* (Williams *et al.*, manuscript in preparation).

In addition to PfAdoMetDC/ODC, *P. falciparum* has other bifunctional proteins such as dihydrofolate reductase/thymidylate synthase (DHFR/TS) [92, 93] and dihydroopteroate synthase/dihydroxymethylpterin pyrophosphokinase (DHPS/PPPK) [94]. Organisation into bifunctional proteins may have biological advantages such as metabolic channelling and domain-domain interactions, which could facilitate synthesis of the respective products or regulation of the partner-domain's activity [87]. However, substrate channelling is unlikely in the case of PfAdoMetDC/ODC since another enzyme, spermidine synthase, is required to metabolise the putrescine and dcAdoMet to spermidine [82]. Furthermore, when both active sites of PfAdoMetDC/ODC were inhibited separately, it was concluded that they function independently and that domain-domain interaction is not required [87]. It is advantageous that only one bifunctional protein needs to be regulated to control polyamine synthesis in *P. falciparum* [87], but this advantage to the parasite also provides unique drug-targeting opportunities. PfAdoMetDC/ODC is furthermore unique due to the presence of parasite-specific inserted amino acids that almost double the size of the protein (330 kDa) compared to homologues in other organisms [84]. Parasite-specific inserts have also been reported for other *P. falciparum* proteins [84] and from experimental data these inserts appear to have a regulatory role [95]. These unique regions provide additional opportunities for selective inhibition of PfAdoMetDC/ODC as an antimalarial drug target [84].

1.10 MOLECULAR ASPECTS OF MALARIA

1.10.1 Sequenced *Plasmodium* genome data

The genome sequences of six *Plasmodium* species have now been published. The complete sequences of the *P. falciparum* 3D7 strain and the rodent malaria *P. y. yoelii* 17XNL clone [96, 97] appeared in 2002 and the genomic data of two more rodent malaria species, the *P. berghei* ANKA clone and *P. chabaudi* AS clone, were published in 2005 [98]. Recently, the genome sequences of the human malaria *P. vivax* Salvador 1 strain and the human/simian malaria *P. knowlesi* H strain, along with a comparative analysis with *P. falciparum*, were released [99, 100]. Thus, this genus has the highest number of sequenced species of any eukaryotic organism yet [61].

Comparative analysis of the publicly available *Plasmodium* genomes revealed that they are all haploid with a standard size of 23 – 27 Mb, which is distributed among 14 linear chromosomes between 0.5 – 3.0 Mb in size. The base composition varies among the different species, with the rodent and *P. falciparum* genomes being extremely A+T-rich (80.6% on average and close to 90% in introns and intergenic regions in *P. falciparum*) in contrast with the more G+C-rich *P. knowlesi* and *P. vivax* genomes (37.5% and 42.3%, respectively) [30, 96, 99, 101]. Each *Plasmodium* genome has in the order of 5000 - 6000 predicted genes, most of which (51%) contain at least one intron and ~60% are orthologous among the different species [30, 98]. The difference in gene number is the result of differential gene expansion in distinct lineages and the presence of large variant gene families that are involved with antigenic variation [30]. The unique genes of the different species are

often localised within the subtelomeric regions and code for immunodominant antigens [30]. The mean gene length of the three sequenced human malarias (including *P. knowlesi*) is ~2.2 to 2.3 kb, compared to the average of 1.3 to 1.6 kb in other organisms [96, 101]. The reason for these long gene lengths is not known and this is compounded by the fact that these long genes usually encode hypothetical proteins with unknown function [96]. Gene-mapping studies of conserved genes have shown that gene location, order and even exon-intron boundaries have been preserved over large regions across the three sequenced rodent *Plasmodium* species and *P. falciparum* [30].

In addition to the nuclear genome, the parasites also have a linear mitochondrial genome of ~6 kb in the case of *P. falciparum*, which is the smallest mitochondrial genome known [102], and a ~35 kb circular apicoplast genome [96]. The *P. falciparum* nuclear genome exhibits minimal redundancy in transfer RNA (tRNA) and encodes 43 tRNAs [96] compared to the ~30 of *Homo sapiens* [103]. The parasite tRNAs bind all 64 possible codons except TGT and TGC that both specify cysteine (Cys). As no other codons specify Cys, it is possible that these tRNA genes are located within the currently unsequenced regions, since Cys is incorporated into *P. falciparum* proteins [96]. The small *P. falciparum* mitochondrial genome does not encode any tRNAs [104] compared to the 22 tRNA of the circular 16.6 kb human mitochondrial genome [105]. The *P. falciparum* mitochondrion therefore imports tRNAs from the cytoplasm, whereas the apicoplast genome encodes sufficient tRNAs for protein synthesis within the organelle [106].

The *P. falciparum* genome does not contain tandemly repeated ribosomal RNA (rRNA) gene clusters as seen in many other eukaryotes, but it contains individual 18S-5.8S-28S rRNA units at loci on seven of the chromosomes [96]. The sequence of the particular rRNA genes is distinct in the different units and the expression of each unit is developmentally regulated, depending on the stage of the parasite life cycle [107]. It is anticipated that by transcribing different rRNAs at different life stages, the parasite could change its ribosomal properties and the translation rate of all or specific messenger RNA (mRNA), which could alter the cell growth rate or cell development pattern. Previously, the rRNA expressed in the mosquito was described as S (sexual)-type and that expressed in the human host as A (asexual)-type [96]. Parasite rRNA is also species-specific and can be assessed for diagnostic purposes [36].

More than 60% of the predicted 5268 open reading frames (ORFs) of *P. falciparum* have no sequence similarity to genes from other sequenced organisms [96]. The absence of sequence similarity complicates characterisation of the unknown ORFs, but might hold the answer to finding selective drug targets [29]. There is currently a dedicated initiative aimed at improving the annotation status of *P. falciparum* led by the *Plasmodium* database, PlasmoDB (www.plasmodb.org).

1.10.2 Plasmodium transcriptome data

Whole genome transcriptional profiling of the *P. falciparum* life cycle was performed in two concurrent studies in 2003 [29, 108]. Bozdech and colleagues published a high-resolution transcriptome analysis of the IDC of highly synchronised HB3 parasites over 48 h at 1 h intervals [29]. Le Roch and colleagues presented the transcriptome of nine parasite stages, including the mosquito salivary gland sporozoites, seven periodic asexual stage parasites (free merozoites and different stages spanning from early ring forms up to mature schizonts) and the sexual stage gametocytes, but excluding liver stage parasites [108]. However, recently a combined transcriptome and proteome survey of *P. yoelii* liver stage parasites [109] and the IDC transcriptome of *P. vivax* appeared [110].

By ordering the transcripts according to phase and frequency of gene expression (i.e. order according to expression peaks) as determined with fast Fourier transformation, Bozdech *et al.* demonstrated the unprecedented mode of transcriptional regulation of the malaria parasite with more than 75% of the transcripts produced only once per cycle just before they are required (Fig. 1.8) [29]. There is a clear relationship between transcriptional regulation and developmental progression of *P. falciparum* through the IDC. In contrast with the cell cycle of *Saccharomyces cerevisiae* and human HeLa cells, where only 15% of the genome is periodically regulated, the IDC resembles early development of *Drosophila melanogaster* when 80% of the genome is expressed. The continuous cascade of *P. falciparum* expression starts with genes involved with generalised cellular processes such as protein synthesis, followed by DNA replication and ending with genes encoding proteins required for invasion [29]. In contrast with the polycistronic gene expression of related organisms such as *Leishmania*, contiguous genes along the nuclear chromosomes are rarely co-regulated in *P. falciparum*, whereas expression from the apicoplast genome is polycistronic and highly co-regulated [29]. Both the mitochondrion and apicoplast are thought to have a prokaryotic origin via evolutionary endosymbiotic events [111] and the maturation and protein expression of these organelles appear to be synchronised to the second half of the IDC [29].

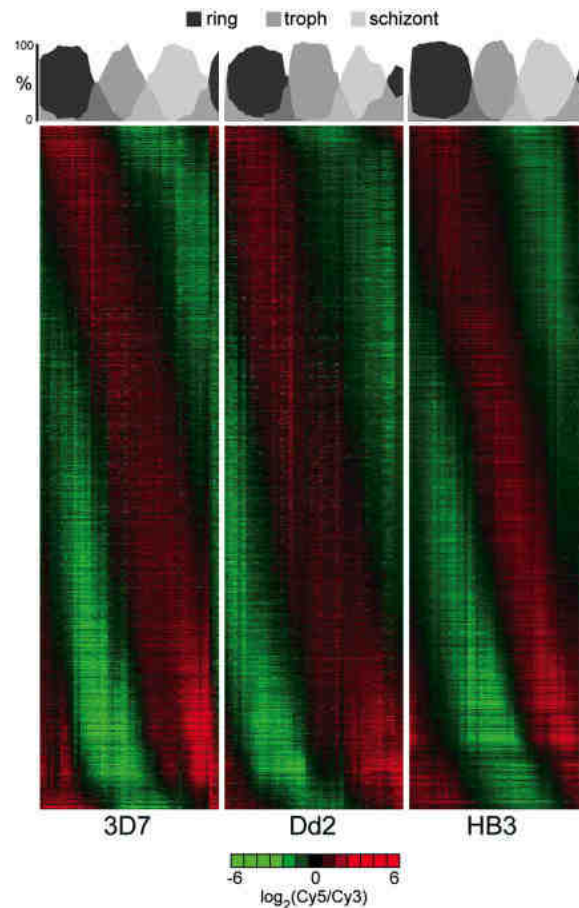


Fig. 1.8 The 48 h IDC transcriptomes of 3D7, Dd2 and HBR *P. falciparum* demonstrating the “just in time” mode of transcription across the three strains with differential expression mainly in subtelomeric regions [91].

Le Roch and colleagues demonstrated the stage-specific gene expression of different parasite stages and that the transcripts of genes with similar functions had similar expression profiles, therefore clustering together. Based on this observation they claimed to identify the potential roles of more than 1000 hypothetical proteins. They also found that genes that were involved in similar processes, such as growth and maintenance, were localised in specific chromosomal regions [108], in contrast to Bozdech and colleagues who found that contiguous genes are rarely co-regulated [29].

The IDC transcriptome of strain HB3 was subsequently followed by a comparative analysis of the IDC transcriptomes of strains HB3, Dd2 and 3D7, each of which was originally derived from different geographical regions and with distinct drug sensitivity phenotypes (Fig. 1.8) [91]. Surprisingly, there was little difference between the transcriptional profiles obtained for the three strains and the main differences were in the genes coding for surface antigens [91].

Similar to *P. falciparum*, the IDC of *P. vivax* is characterised by extensive transcriptional control and each biological function is timed to a specific period of the IDC. The IDC expression profiles of most of the *P. vivax* genes are identical to those of their *P. falciparum* syntenic orthologues, but there are partial shifts in the transcriptional profiles of 22% of genes and dramatic differences in those of 11% of genes. These changes

result in significant alteration in the timing of specific biological functions such as haemoglobin degradation, host-parasite interaction, protein export and DNA replication. Moreover, the non-syntenic *P. vivax* genes are predominantly activated at the schizont/ring transition, which indicates that the inter-species differences may have derived from events during invasion and early intraerythrocytic development [110].

Since publication, the transcriptome data of the 2003 *P. falciparum* studies have proven indispensable as reference of the expected gene expression during normal parasite development and as baseline in comparative studies of environmental perturbation and genetic alteration.

1.10.3 The *P. falciparum* proteome and interactome

A comprehensive study of the *P. falciparum* sporozoite, merozoite, trophozoite and gametocyte proteomes appeared in the same year as the *P. falciparum* genome sequence [96, 112]. Over 2415 proteins were confidently identified with multidimensional protein identification technology (MudPIT) among these stages, which is almost half of the predicted ~5300 proteins of the parasite. The majority of the proteins expressed in each stage correlated well with the stage physiology, but surprisingly several of the antigenically variant *var* and *rif* genes, known to be expressed on the erythrocyte surface, were also detected in sporozoites [112].

The sporozoite proteome is markedly different from the other stages with approximately 49% unique proteins, mainly including cell surface (e.g. host cell invasion peptides from *var* and *rifin* genes) and organellar proteins. Only 25% of the sporozoite proteins are also expressed in other parasite stages. Merozoites, trophozoites and gametocytes all have between 20% and 33% unique and between 39% and 56% common proteins. The shared proteins are mostly involved with housekeeping functions, e.g. transcription factors, histones, ribosomal proteins and cytoskeletal proteins [112]. It appears as if the specific stage proteomes include those proteins that are required to survive the circumstances to which a particular stage is exposed, e.g. the merozoite proteome includes abundant proteins for cell recognition and invasion (via active actin-myosin processes), the trophozoites express proteins to mediate cytoadherence (knob-associated HRP) and haemoglobin digestion, the gametocyte proteome includes enzymes from the mitochondrial tricarboxylic acid cycle and oxidative phosphorylation as an adaptation to life within the mosquito, whereas the asexual blood stages are mostly dependent on anaerobic respiration (glycolysis and pyruvate-lactate conversion). Survival of *P. falciparum* parasites under a variety of complex circumstances, such as vertebrate/invertebrate and intracellular/extracellular environments, thus requires specialised protein expression at specific stages [112].

In total, 46% of the predicted gene products were successfully identified in one of the four *P. falciparum* stages examined. In an attempt to infer protein function on a global scale, including many of the unidentified proteins, the *P. falciparum* interactome was modelled by integrating *in silico* and functional genomics data within a

Bayesian framework [113]. The resulting network covered 68% of the genome and protein function for more than 2000 unidentified proteins could be inferred, based on association [113].

In another investigation, comparative analysis of protein network topologies and the controlling, highly connected nodes indicated an evolutionary conservancy and homogeneity of biological networks. The *P. falciparum* interactome network was analysed by combining experimental results (*P. falciparum* interactome with genomic and proteomic data from other well-studied model organisms) and those of computational methods [114]. Functional clustering of the combined network of protein interactions revealed clusters of proteosomal, ribosomal and spliceosomal activities that were previously reported lacking in the experimental interactome dataset [115]. Moreover, the controlling nodes in the *P. falciparum* interactome were shown to feature an oligarchy of highly interacting proteins, indicating the presence of the so-called 'rich-club' phenomenon, where controlling nodes are well connected to one another [114]. These results signify a topological signature in the parasites' interactome, which covers parasite-specific biological features mainly revolving around invasion [61].

1.10.4 The *P. falciparum* metabolome

Very little is known regarding global *Plasmodium* metabolism or the metabolome, but recently two-dimensional nuclear magnetic resonance (2D-NMR) was used to identify and quantitate more than 50 metabolites using four different extractants with varying degrees of hydrophylicity/lipophylicity from isolated mature *P. falciparum* trophozoites [116]. The metabolite profiles obtained were generally similar, but perchloric acid was found to provide the most comprehensive metabolite profile. The isolated trophozoites contained significant amounts of various amino acids (from haemoglobin digestion), including millimolar levels of 4-aminobutyrate (GABA). Malate and most of the other tricarboxylic acid cycle intermediates were also detected, which indicated a role of oxidative energy metabolism in the trophozoite [116] in contrast with the postulation of ubiquinone regeneration and pyrimidine synthesis being the only function of the mitochondrion during the asexual stage [102]. Furthermore, glutathione, phospholipid precursors (phosphocholine and phosphoethanolamine) and polyamines were found to be major intracellular metabolites [116].

Despite the limited information on the *P. falciparum* metabolome, the integration of parasite genomic data (i.e. enzyme homologues) with known metabolic processes from the Kyoto Encyclopedia of Genes and Genomes (KEGG, <http://www.genome.jp/kegg/>) enabled the construction a parasite-specific website of metabolic processes, Malaria Parasite Metabolic Pathways (MPMP, <http://sites.huji.ac.il/malarial/>). KEGG maps were regarded as valid if homologues for three to four consecutive enzymes could be identified in the *P. falciparum* genome or if biochemical evidence indicated enzyme functionality. However, for most pathways the enzymes involved have not yet been tested independently. The metabolic maps also indicate the stage-dependent

transcription of the genes involved as transcriptomics clocks, which reveals whether genes that code for enzymes from the same biological process are coordinated in their expression or not [117].

1.10.5 Gene regulation in *P. falciparum*

Characteristic eukaryotic transcription requires the assembly of a multisubunit pre-initiation complex at the site of the promoter. RNA polymerase II is not able to locate and bind promoters in itself, but combines with general transcription factors (TFIIA, B, D, E, F and H) to form a pre-initiation complex that can bind to the DNA [118]. Initial searches with similarity-based clustering identified all 12 subunits of RNA polymerase II in the *P. falciparum* genome, but these initial experiments failed to find the general transcription factors except for the TATA-binding protein [119]. More recent analyses using search algorithms based on secondary structure overcame many of the computational challenges presented by the numerous AT-stretches resulting in low-amino-acid complexity regions, and identified homologues to many of the outstanding general transcription factors [120]. The extreme A+T-richness of the *P. falciparum* genome, which is more than 90% in intergenic regions, may indicate a unique set of binding interactions that underlie transcriptional control in the parasite, e.g. there is a positive correlation to the degree to which nuclear factors bind specific regions of the calmodulin promoter and the length of the poly(dA)poly(dT) stretches within that region [121].

Recently an expanded family of Apicomplexan Apetala2 (ApiAP2) transcription factors were discovered *in silico* in the genomes of four *Plasmodium* species [122], followed by experimental evidence of the DNA-binding specificities of 2 of the 26 ApiAP2 members in *P. falciparum* [123]. Subsets of these proteins are expressed throughout the IDC i.e. in the ring, trophozoite, early-schizont and late-schizont stages, and this cascade was proposed to regulate stage-specific transcription within the parasite [123].

Similar to other eukaryotic organisms, *P. falciparum* uses epigenetic mechanisms to control phenotypic states of inheritable expression, e.g. in the absence of DNA modification, the active or silenced state of *var* gene expression is inherited by daughter parasites in subsequent IDC cycles [124]. Epigenetic machinery is generally well conserved in *Plasmodium* and all four core histones required for nucleosome assembly (H2A, H2B, H3 and H4), as well as the variant histones (H3.3, CenH3, H2AZ and H2Bv), have been identified in the genome [125]. The dynamic nature of nucleosome-associated chromatin is attributed to various post-translational modifications on the N-terminal tails of the different histones. These modifications affect chromatin structure by altering interactions between histones and DNA or by affecting the recruitment of chromatin-associated proteins. Acetylation of lysines and methylation of lysines and arginines on histones H3 and H4 have been studied best and all of these modifications are found on critical residues of *Plasmodium* histones. Modified nucleosomes can mediate transcriptional control by altering the physical interactions between histones and DNA or by binding other regulatory proteins. However, the mere presence of

nucleosomes within the genome is an indication of decreased transcriptional activity and active promoters are usually located in “nucleosome-free” regions [118].

Reversible modification of DNA provides another mechanism for epigenetic control of gene expression, which typically involves methylated bases e.g. 6-methyl-2-deoxyadenine (6mA) or 5-methyl-2-deoxycytosine (5mC). Previously, partial methylation of a CpG dinucleotide was demonstrated in the DHFR/TS gene during the IDC [126] and *in silico* analysis revealed a greater than expected incidence of CpG dinucleotides in intergenic regions less than 500 bp from genes [127]. However, in contrast to these results, liquid chromatography/electron spray ionisation mass spectrometry (LC-ESI/MS) could not detect any methylation of 2-deoxycytosine bases within *P. falciparum* genomic DNA (gDNA) [124].

In recent years there have been controversial reports regarding the role of transcriptional regulation versus post-transcriptional control in *Plasmodium* [128]. The evidence supporting both sides of the debate will be discussed in detail in Chapters 3 and 4.

1.10.6 Manipulation of the *Plasmodium* genome

The –omics technologies (transcriptomics, proteomics, metabolomics etc.) form part of the functional genomics platform, which also includes gene manipulation. Genetic manipulation via transfection is a powerful method to establish gene function and enables the identification of genes responsible for specific phenotypes (forward functional genomics) [129]. Initial attempts at *P. falciparum* transfections were unsuccessful because of technical difficulties [130], but current transfection technology of *Plasmodium* has improved significantly and several papers reporting success have been published in recent years [129, 131, 132]. RNA interference (RNAi) is still a highly controversial issue, since there is currently no evidence for the homologues of the RNAi machinery within the parasite [133].

1.11 FUNCTIONAL GENOMICS FOR DRUG DISCOVERY AND TARGET VALIDATION

The availability of full genome sequencing and microarrays late in the 1990s was accompanied by enthusiasm that these technologies would aid in identifying drug targets of small molecules. This anticipation was based on early experiments in which it was demonstrated that treatment with particular drugs resulted in the altered transcription of the pathways containing these drugs' targets due to feedback inhibition [134, 135]. However, deciphering the significance of the large amount of data obtained from microarray studies is the biggest challenge of this method [136] and many of these early studies simply downplayed the fact that the transcription of many other pathways were also affected [135]. Yet, despite scepticism, the application of such whole genome approaches has been useful in elucidating the mechanism of drug action and resistance for a number of unicellular organisms [137-139]. Antibacterial drug discovery in particular has benefited greatly from the application of functional genomics techniques (especially transcriptomics), which improved knowledge of

gene function, bacterial physiology, the effects of antibiotics on bacterial metabolism, *in vitro* target identification and the mode of action of novel antibacterial compounds [140]. Therefore, functional genomics has now become an indispensable tool in the drug discovery process [141, 142] due to its capacity to monitor the effects of perturbations at a global level, as opposed to the molecular level of the more traditional methods. In the urgent search for novel antimalarials, the introduction of functional and structural genomics and bioinformatics at the very early stages of the discovery pipeline can accelerate the discovery of new and robust antimalarial drugs and novel targets and serve to validate these targets (Fig. 1.9) [61, 143, 144].

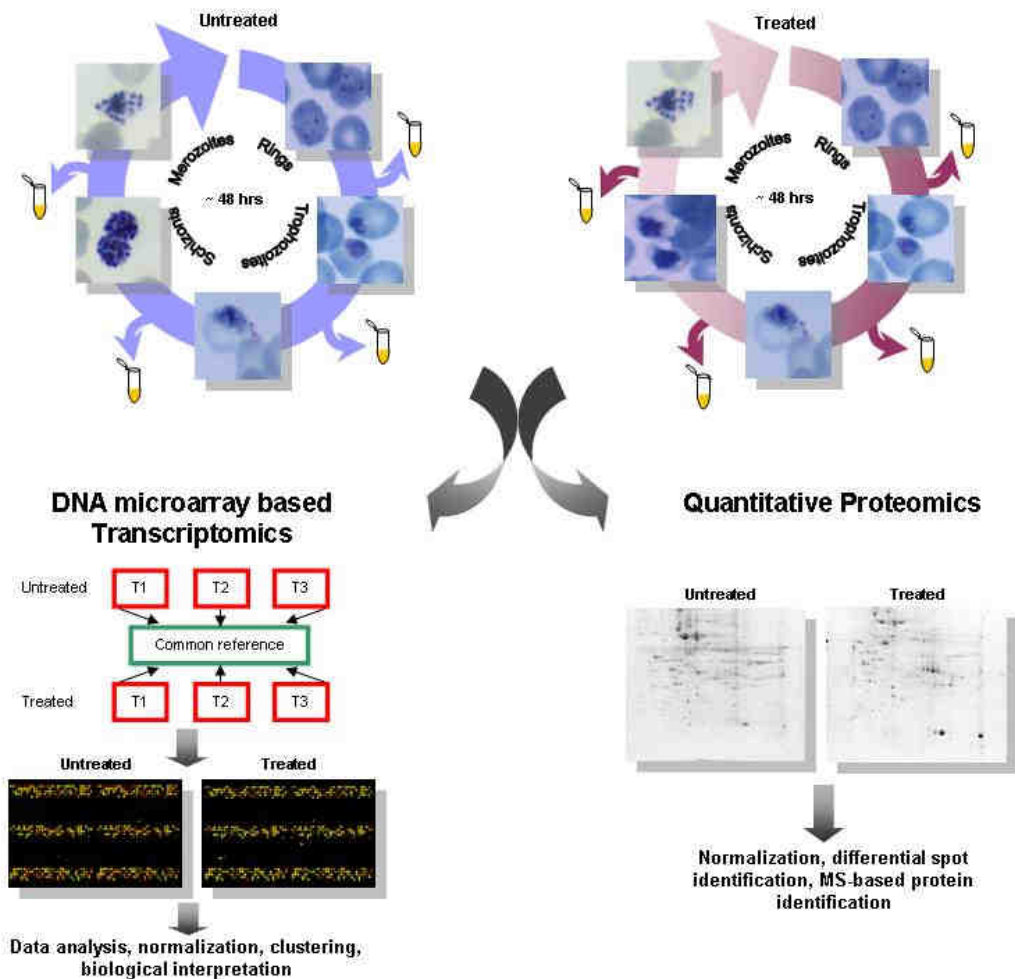


Fig. 1.9 The proposed experimental layout for the application of transcriptome and proteome analysis to drug-challenged malaria parasites. Duplicate, synchronised *P. falciparum* asexual cultures should be maintained in parallel for untreated and drug treated cultures. Simultaneous RNA and protein isolation should be performed at the highest frequency possible. Changes in transcript levels can be compared to proteome changes with e.g. quantitative 2D-gel electrophoresis [61].

1.12 RESEARCH OBJECTIVES

The study presented here was aimed at elucidating the physiological response of the malaria parasite during cyto-stasis as a result of polyamine depletion induced by the co-inhibition of both catalytic sites of the bifunctional protein PfAdoMetDC/ODC. To achieve this goal, polyamine biosynthesis inhibitors were carefully selected and characterised to ensure complete inhibition of PfAdoMetDC/ODC and a functional genomics investigation was conducted, which included the global profiling of the transcriptional, proteomic and

metabolomic response of the perturbed 3D7 *P. falciparum* parasites. The ultimate objective of the investigation was to validate PfAdoMetDC/ODC as a potential drug target for antimalarial therapeutic intervention.

Chapter 2 describes the determination of the median inhibitory concentrations (IC_{50}) of various inhibitors of PfAdoMetDC/ODC. The results obtained were used to determine the treatment dosages and most appropriate inhibitors to be used for co-inhibition during the functional genomics investigations.

Chapter 3 presents the transcriptional response of *P. falciparum* after co-inhibition of both catalytic sites of PfAdoMetDC/ODC with specific inhibitors and cytostatic drugs, as determined via oligonucleotide microarray analysis.

Chapter 4 describes the proteomic and metabolomic analyses of PfAdoMetDC/ODC co-inhibited parasites and completes the functional genomics investigation by examining specific hypotheses resulting from the study with focussed biochemical assays.

Chapter 5 presents a concluding discussion of the scientific contribution of the study, the most important research highlights and the future perspectives.

The knowledge gained from this study has led to the following contributions in scientific journals and at conference proceedings:

Papers:

Van Brummelen A.C., Birkholtz L-M and Louw, A.I. (2008) A critical evaluation of antimalarial drug sensitivity methods for testing cytostatic drugs (Manuscript in preparation).

Williams M., Niemand J., van Brummelen A.C., Clark K., Wells G., Burger P., Reeksting S., Birkholtz L-M and Louw A.I. (2008) Polyamines in *Plasmodium*: peculiarities and possibilities (Manuscript in preparation).

Van Brummelen A.C., Olszewski K.L., Wilinski D., Llinás M., Louw A.I and Birkholtz L-M. (2008) Co-inhibition of *Plasmodium falciparum* S-adenosylmethionine decarboxylase/ornithine decarboxylase reveals perturbation-specific compensatory mechanisms by transcriptome, proteome and metabolome analyses (*J. Biol. Chem*, 10.1074/jbc.M807085200, In Press).

Birkholtz L-M., van Brummelen A.C., Clark K., Niemand J., Maréchal E., Llinás M., Louw A.I. (2008) Exploring functional genomics for drug target and therapeutics discovery in *Plasmodia*. *Acta Trop.* **105**, 113-123.

Conference proceedings:

Birkholtz L-M., van Brummelen A.C., Clark K. and Louw A.I. (2008) Functional genomics investigations of polyamine depleted *Plasmodium falciparum* reveal compensatory responses and novel metabolic activities (poster). Polyamines: Forty years of mammalian ornithine decarboxylase, Kuopio, Finland.

Van Brummelen A.C., Wilinski D., Llinás M., Louw A.I. and Birkholtz L-M. (2008) Co-inhibition of S-adenosylmethionine decarboxylase/ornithine decarboxylase of *Plasmodium falciparum* reveals compensatory mechanisms in the transcriptome (poster). Molecular Approaches to Malaria, Lorne, Australia.

Van Brummelen A.C., Llinás M., Wilinski D., Louw A.I. and Birkholtz L-M. (2007) Transcriptional profiling of polyamine depletion in *Plasmodium falciparum* (paper). Molecular and Cell Biology Group Symposium (MCBG), Pretoria, South Africa. Best oral presentation award.

Van Brummelen A.C., Birkholtz, L-M and Louw, A.I. (2006) Comparative transcriptomics for target validation of plasmodial AdoMetDC/ODC (poster). The 11th International Congress of Parasitology, Glasgow, Scotland.

Van Brummelen A.C., Birkholtz, L-M and Louw, A.I. (2006) Critical evaluation of antimalarial drug sensitivity methods for cytostatic compounds (poster). 20th Meeting of the South African Society for Biochemistry and Molecular Biology (SASBMB), Pietermaritzburg, South Africa.

CHAPTER 2

A CRITICAL EVALUATION OF ANTIMALARIAL DRUG SENSITIVITY METHODS FOR TESTING CYTOSTATIC DRUGS

2.1 INTRODUCTION

Continuous drug-screening efforts for new antimalarial therapeutics, including target-based and lead-based endeavours, is of critical importance since most antimalarials last only ~10 years in the clinical setting before drug resistance develops [55]. One way of delaying the development of drug resistance is by using compounds in combination (e.g. artemether/lumefantrine and the historically used chloroquine/proguanil and pyrimethamine/suphadoxine) because the parasite then has to mutate at several sites simultaneously to become resistant to the treatment regimen, which is much less likely than the occurrence of a single mutation conferring resistance to a single drug [55]. A drug combination selectively targeting polyamine and methionine metabolism, i.e. inhibition of both polyamine biosynthesis and transport, may be a useful therapeutic alternative to delay the development of drug resistance [81, 145].

2.1.1 Polyamine biosynthesis inhibitors

DFMO (eflornitine, Fig. 2.1) is one of the most studied polyamine biosynthesis inhibitors that was initially synthesised by Metcalf and colleagues [146]. DFMO is an enzyme-activated, irreversible inhibitor of ODC, which decreases putrescine levels [90], usually resulting in cytostasis [147]. It is currently being tested as cytostatic, antineoplastic agent in several anticancer clinical trials [148, 149], but it is clinically used only to treat West African trypanosomiasis (sleeping sickness) due to *T. brucei gambiense* [150]. East African trypanosomiasis due to *T. brucei rhodesiense* is tolerant to DFMO due to higher specific ODC activity and faster enzyme turn-over in these parasites [151].

In vitro, the compound halts the plasmodial IDC in the trophozoite stage [152] in a cytostatic manner, meaning that it causes growth arrest due to polyamine depletion without cytotoxicity, although the parasite eventually dies after 67 h exposure to the drug [153]. The effects of DFMO in *Plasmodium* can be alleviated by the addition of putrescine or spermidine [90, 153] as well as high concentrations of the diamine, cadaverine (0.4 mM) [154], but there are contradictory reports on the efficacy of spermine to restore growth after DFMO inhibition [90, 153, 154]. A concentration of 5 mM DFMO was demonstrated to inhibit ODC of the chloroquine-resistant FCR-3 by more than 99%, whereas 10 mM DFMO ensured complete growth arrest *in vitro* [154].

However, *in vivo* a 2% solution of DFMO only limited *P. berghei* erythrocytic schizogony without increasing the survival time of the infected mice [155].

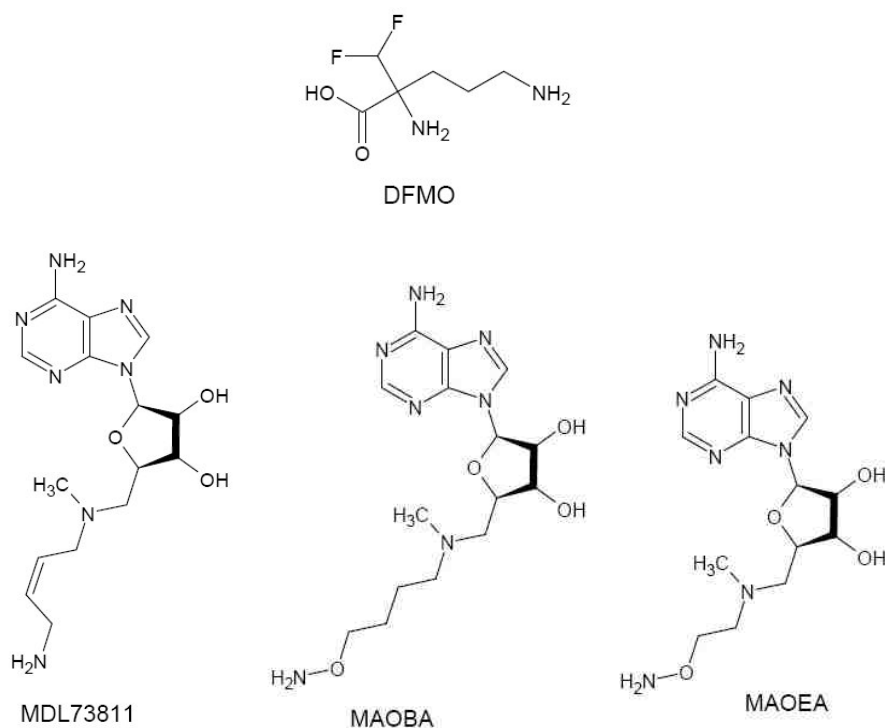


Fig. 2.1 Chemical structures of DFMO, MDL73811, MAOBA and MAOEA.

Another classic inhibitor of polyamine and methionine metabolism is the irreversible AdoMetDC inhibitor, 5'-{[(Z)-4-amino-2-butenyl]methylamino}-5'-deoxyadenosine (MDL73811 or AbeAdo, Fig. 2.1) [156]. Similar to DFMO, MDL73811 also arrests the plasmodial IDC in the trophozoite stage [153] due to a decrease of spermidine and spermine, but not putrescine. Instead, putrescine increases 3- to 4-fold [153]. MDL73811 inhibition can thus be reversed by the addition of spermidine or spermine, but not putrescine [153]. The *cis*-butenyl isomer of MDL73811 is the active form, whereas the *trans*-butenyl isomer (MDL74391) is about 15 - 20 times less efficient in inhibiting AdoMetDC [153]. After 48 h treatment of *P. falciparum* cultures *in vitro* the IC₅₀ of MDL73811 varied between 1 and 3 μ M for chloroquine-sensitive (D6 and NF54) and chloroquine-resistant (W2, FCR-3 and ITG2) strains, respectively [153]. However, similar to DFMO, MDL73811 had no effect on mice infected with *P. berghei* [153], but it was very effective against both *T. brucei brucei* and *T. brucei rhodesiense*-infected mice [157].

Other AdoMet analogues and irreversible AdoMetDC inhibitors include 5'-deoxy-5'-[N-methyl]-N-[2-(aminooxy)ethyl]amino]adenosine (MAOEA, Fig. 2.1) [158] and 5'-deoxy-5'-[N-methyl]-N-[2-(aminooxy)butyl]amino]adenosine (MAOBA, Fig. 2.1). These analogues have tertiary nitrogens instead of sulfonium atoms (as in AdoMet) and have side chains of variable length ending in reactive groups, e.g.

aminoxygroups [159]. MAOEA was initially tested in murine leukaemia L1210 cells and was found to decrease the cellular content of dcAdoMet, 5-methylthioadenosine, spermidine and spermine [160]. MAOEA was also demonstrated to be active against *T. brucei brucei* ($IC_{50} = 1.3 \mu M$), but increasing the length of the side chain (e.g. MAOBA) or swapping the methyl group (attached to the nitrogen) for an ethyl group caused reduced potency [159]. According to the literature MAOEA has not yet been tested in malaria (nor MAOBA), but because of its activity in trypanosomiasis, it was anticipated that this compound would also inhibit the growth of Plasmodia.

Bis(benzyl)polyamine analogues such as N',N'-bis{3-[(phenylmethyl)amino]propyl}-1,7-diaminoheptane (MDL27695) are spermine analogues with elongated central methylene chains and benzyl-substituted terminal amines [161]. Their antimalarial activity increases when the central methylene chain length is increased. This increase in potency is related to higher lipid solubility and uptake of the compounds into host erythrocytes, compared to the more water-soluble free-amine analogues that are more than 1000 times less potent [161]. Treatment of rat hepatoma cells with $1 \mu M$ MDL27695 repressed ODC and AdoMetDC by 50% after 8 h [162]. In *Leishmania donovani*, $10 \mu M$ MDL27695 inhibited ODC by 36% and AdoMetDC by 58% with accumulation of putrescine and spermidine [163]. *In vitro* treatment of *P. falciparum* with MDL27695 resulted in an IC_{50} of $3.0 \mu M$ for the chloroquine-sensitive strain D6 and a 15-fold higher IC_{50} for the chloroquine-resistant strain, FCR-3 [161]. However, MDL27695 at its *in vivo* IC_{90} of 15 mg/kg suppressed only 70% of the *P. berghei* parasitaemia in subsequent experiments and had a cure rate of only 21% (3/14) [161].

MDL73811 is approximately 1000 times more active than DFMO against *P. falciparum in vitro* [153], but neither of these on their own, nor the potent bis(benzyl)polyamine analogue, MDL27695, cures *P. berghei in vivo* [153, 155, 161]. The potent *in vitro* antimalarial activity and the absence of *in vivo* efficacy of these compounds can be explained by exogenous polyamine salvage from the host [145]. However, the combination of MDL27695 and DFMO, which inhibits ODC, AdoMetDC and exogenous polyamine import, cured 100% (14/14) of *P. berghei*-infected mice [161]. A polyamine transporter has not yet been identified in the *P. falciparum* genome, but a drug combination selectively inhibiting both polyamine biosynthesis and transport may provide a promising antimalarial strategy [145].

2.1.2 Antimalarial drug sensitivity methods

Drug sensitivity methods are indispensable tools for the surveillance of drug resistance and for establishing therapeutic guidelines. Antimalarial drug efficacy depends primarily on the ability of these compounds to kill malaria parasites by interfering with essential metabolic processes. This reduces their multiplication and allows the immune system to remove them from the circulation. Drug efficacy varies according to the sensitivity of each parasite clone within the natural population, which is referred to as drug sensitivity [12]. In addition to

surveillance and prevention of drug resistance, drug development programmes rely on accurate measurement of drug sensitivity to identify the most suitable candidates for further characterisation.

There are several approaches to assess the susceptibility of *P. falciparum* to antimalarial drugs. The most classical method is determining the therapeutic response or efficacy *in vivo*, which was originally defined in terms of parasite clearance as sensitive (S) or three degrees of resistance (RI, RII and RIII) [12]. *In vivo* tests nowadays include molecular analysis to distinguish true recrudescence (i.e. reappearance of disease after it has been quiescent) from re-infection and pharmacokinetic tests to identify host-related factors, such as poor absorption [12]. A different approach is to measure the drug sensitivity *in vitro* since this allows for the complete exclusion of host-related factors such as host immunity and provides a more objective perspective of the inherent drug sensitivity than the *in vivo* tests [12].

Traditional *in vitro* tests measure the effect of the antimalarial drugs on the growth and development of malaria parasites. This can be determined by several methods, e.g. the World Health Organisation (WHO) microtest, isotopic assays, parasite lactate dehydrogenase (LDH) assay, double-site enzyme-linked LDH immunodetection (DELI) assay and the histidine- and alanine-rich protein 2 (HRPII) assay [12]. In all these tests the growth of drug treated cultures is measured relative to drug-free control, but the parasite density and haematocrit (i.e. inoculum) and developmental stage of the parasites have to be controlled since these parameters can have a significant impact on the outcome of the assays [12]. The WHO microtest [164] uses schizont maturation as a measure of parasite growth [12], but in analogy, parasite growth can also be measured by determining the increase in the percentage of infected erythrocytes (parasitaemia) during a culture period of 48 to 96 h. Reading the test results via microscopy is particularly labour-intensive and prone to variability of interpretation, but methods have been developed that allow the automated reading of results, e.g. via a flow cytometer or various indirect measurements of parasitaemia. The tritium-labelled hypoxanthine incorporation assay determines the ability of antimalarial compounds to inhibit parasite growth by causing the reduced uptake of this radio-labelled nucleic acid precursor by the parasite [165]. The technique allows for a high degree of automation and is considerably faster to perform than tests based on morphological assessment. However, isotopic assays have mostly been replaced with other methods because of restrictions on the use of radioactive material [12].

LDH was one of the first plasmodial enzymes that were shown to be electrophoretically, immunologically and kinetically distinct from the host and was initially used primarily as an indicator of the presence of malaria parasites for diagnostic purposes. The levels of parasite LDH correspond to the parasite density and rapidly decrease upon initiation of treatment and the resulting lowered parasite densities [12]. Parasite LDH is distinguishable from the host LDH due to its requirement for the 3-acetyl pyridine adenine dinucleotide (APAD), which is an analogue of nicotinamide adenine dinucleotide. Makler and colleagues used this

knowledge to develop an assay that determines parasite growth inhibition profiles by measuring the enzymatic activity of the parasite homologue as an indirect indication of parasite growth [166]. However, the assay requires initial parasite densities of 1 – 2% and was found to be insensitive for field application, which led to the development of a new LDH assay. The new LDH or DELI assay measures enzyme levels via immunodetection using two monoclonal antibodies that specifically recognise parasite LDH [167], which makes the assay considerably more sensitive than the original method [12].

Another addition to the list of *in vitro* drug sensitivity methods is the HRP_{II} enzyme-linked immunosorbent assay (ELISA) [168], which measures the production of HRP_{II} by *P. falciparum* during the course of its growth and multiplication [12]. HRP_{II} levels are closely correlated to parasite density and development. The assay also uses a double-site sandwich ELISA and is ~10 times more sensitive than the isotopic assay [12].

In this chapter, several AdoMetDC inhibitors were considered for use in combination with the established ODC inhibitor, DFMO, to obtain complete inhibition of both catalytic sites of PfAdoMetDC/ODC for subsequent functional genomics investigations (Chapters 3 and 4). These compounds were evaluated by performing several biochemical assays, including calculating their IC₅₀s under the particular laboratory conditions and determining the appropriate dosages to be used in combination. In order to achieve these objectives, several established antimalarial drug sensitivity methods were critically evaluated to determine the most appropriate assay for testing cytostatic drugs, such as the polyamine biosynthesis inhibitors.

2.2 MATERIALS AND METHODS

2.2.1 *In vitro* cultivation of asexual *P. falciparum* cultures

Continuous *P. falciparum* asexual cultures of the chloroquine-sensitive 3D7 strain were maintained *in vitro* according to a modified Trager and Jensen method [169], which supports intracellular parasite development. The erythrocyte preparation, culture thawing and general maintenance are described below.

Type A+ blood was collected in ethylenediamine tetra-acetic acid (EDTA) vacuum-tubes, transferred to centrifuge tubes using aseptic technique and centrifuged at 2500 g for 5 min at room temperature (Hermle Z320 centrifuge). The serum and buffy-coat were aspirated and an equal volume of wash medium [RPMI-1640 (SIGMA, Missouri, USA) supplemented with 0.4% (w/v) D-glucose (SIGMA), 88 mg/l hypoxanthine (SIGMA), 48 mg gentamycin (SIGMA), buffered with 12 mM HEPES (SIGMA) and 21.4 mM sodium bicarbonate (Merck, Darmstadt, Germany) per litre MilliQ (distilled, de-ionized, 0.22 filter sterilised) H₂O], was added. The erythrocytes were resuspended and centrifuged at 2500 g for 5 min, after which the supernatant was aspirated. The wash procedure was repeated four to five times to reduce the presence of leukocytes. Washed erythrocytes were resuspended in an equal volume of wash medium and stored at 4°C. The wash medium was aspirated and replaced three to four times per week to preserve the erythrocytes.

A glycerol-frozen aliquot of asexual *P. falciparum* 3D7 parasites was removed from liquid nitrogen storage and quickly thawed in a water bath at 37°C. The thawed aliquot was transferred to a centrifuge tube under sterile conditions in a laminar flow cabinet. The osmotic potential of the thawed stock was gradually reduced by the drop-wise addition of 200 µl 12% (w/v) sodium chloride (NaCl) solution, followed by pipette-mixing for ~10 - 20 s and then the drop-wise addition of 1.8 ml 1.6% NaCl, again followed with mixing for ~10 - 20 s. The parasites were collected by centrifugation at 2500 g for 5 min at room temperature. The supernatant was aspirated and 10 ml culture medium [wash medium with 0.5% (m/v) Albumax II (purified lipid-rich bovine serum albumin, Invitrogen, Paisley, UK)], preheated to 37°C, was added. This was followed by 500 µl freshly collected, washed, type A⁺, packed erythrocytes to establish a ~5% haematocrit culture. The erythrocytes were suspended and transferred to 75 cm² Cellstar culture flasks (Greiner bio-one, Frickenhausen, Germany) and gassed for 30 s with a special gas mixture containing 90% nitrogen, 5% oxygen and 5% carbon dioxide (Afrox, Johannesburg, South Africa). The flasks were sealed air-tight and incubated at 37°C.

Parasite growth was monitored daily by visual microscopic inspection of thin smears, which were fixated by methanol (MeOH) and stained with a 10% (v/v) Giemsa stock solution (Merck) in phosphate buffered saline (PBS, 137 mM NaCl, 2.7 mM KCl, 10 mM phosphate, pH 7.4). Parasitaemia was calculated by counting the equivalent of 1000 erythrocytes using the Miller technique for reticulocyte counting [170] at a 1000 times enlargement with a Nikon Labophot microscope. This counting technique requires an evenly distributed erythrocyte smear across the microscope field, which is then divided into equal-sized squares, i.e. four in the case of the Nikon Labophot. The total number of erythrocytes (infected and uninfected) in one of the four squares was counted, but the infected erythrocytes across the whole field, i.e. all four squares, were counted without moving the field. The same procedure was followed in randomly adjacent fields until a total of 250 erythrocytes were counted in the single squares. By extrapolation, the equivalent of 1000 erythrocytes was inspected for parasites (250 erythrocytes x 4 blocks). The number of parasites per 1000 erythrocytes was then divided by 10 for the percentage parasitaemia, which was generally maintained at 3 to 5%. Culture medium was replaced daily and the parasites were gassed with the special gas mixture before incubation at 37°C. Once thawed, cultures were not grown for longer than 3 months to prevent genetic alteration. Ring-stage (5 – 10% parasitaemia) parasite-infected pellets were cryopreserved with an equal volume of freezing medium (28% glycerol/wash medium) on a regular basis and stocks were preserved at -180°C in liquid nitrogen.

2.2.2 Sorbitol synchronisation of growth stage

Parasites were synchronised once a week in the ring stage with the Lambros and Vanderberg method [171] with minor modifications. Cultures of 20 ml were transferred to a centrifuge tube and centrifuged at 2500 g for 5 min at room temperature. The supernatant was aspirated, 4 ml of 15% sorbitol solution (preheated to 37°C) was added, mixed well and incubated for 5 min at 37°C. The suspension was centrifuged at 2500 g for 5 min,

the supernatant removed and 8 ml of 0.1% (w/v) glucose solution (preheated to 37°C) was added and mixed well. The suspension was incubated for 5 min at 37 °C and centrifuged at 2500 g for 5 min at room temperature. The supernatant was aspirated and the infected erythrocytes were resuspended in culture medium to restore the ~5% haematocrit (including the lysed erythrocytes). The culture was divided into two culture flasks and 5 ml culture medium and 250 µl packed erythrocytes were added to each to replace the erythrocytes lysed during synchronisation. The cultures were gassed as mentioned and incubated at 37°C.

2.2.3 Parasite growth and drug sensitivity assays

Drug treatment in 96-well plate format was performed on synchronised, early ring-stage parasites and samples for direct and indirect parasitaemia quantitation assays were treated in parallel (duplicate plates) as described below.

2.2.3.1 Drug treatment and plate storage until analysis

Stock solutions of the ODC inhibitor, DFMO, and the AdoMetDC inhibitors MAOBA, MAOEA and MDL73811, as well as chloroquine (cytotoxic drug control), were prepared by dissolving the compounds in PBS followed by sterilisation with a 0.22 µM Minisart syringe filter (Sartorius Stedim Biotech, Göttingen, Germany). Aliquots were stored at -20°C and were diluted just before use in culture medium to achieve the desired concentrations. DFMO was kindly provided by P. Woster (Wayne State University, Michigan, USA), MAOEA and MAOBA were gifts from J. Secrist (Southern Research Institute, Alabama, USA), MDL73811 was obtained from Sanofi-Aventis (USA) and chloroquine diphosphate from SIGMA.

Drug dilution series consisting of eight two-fold dilutions were prepared for each drug and 50 µl of each concentration was pipetted in quadruplicate into sterile 96-well flat-bottomed culture plates with lids (Greiner bio-one Cellstar). The same volume of culture medium was aliquoted into eight wells for quadruplicate uninfected and untreated controls. Duplicate plates were prepared to enable method comparison under exactly the same culture and treatment conditions. After preparing the drug containing plates, the cultures were removed from the incubator, thin smears were prepared and the parasitaemia calculated as discussed in section 2.2.1. The haematocrit was estimated after centrifugation at 2500 g for 5 min in graduated tubes (100 µl increments). The parasitaemia was adjusted to 1% with uninfected A⁺ erythrocytes and the haematocrit to 10% with culture medium. A volume of 50 µl synchronised, early ring-stage cultures were then pipetted into all the wells (excluding the uninfected control wells) for a final haematocrit of 5%, i.e. an inoculum (parasitaemia x haematocrit) of 5. The haematocrit of uninfected A⁺ erythrocytes was also adjusted to 10% and 50 µl volumes were pipetted into the remaining wells. The plates were covered and placed inside a disinfected gas chamber, sealed, gassed with a special gas mixture for 5 min and grown at 37°C in a humid atmosphere for a complete life cycle of 48 h.

After the incubation period, the success of the treatment was evaluated by microscopical inspection of Giemsa-stained thin smears of the wells containing the untreated, highest and lowest drug concentration before continuing with the drug sensitivity assays. With successful treatments one plate was sealed and frozen at -20°C for the parasite LDH (PF13_0141) [166] and HRPII (pHRPII_830) ELISA assays [168] and the other was fixed (see below) for fluorescence activated cell sorting (FACS) [172].

Plates destined for FACS analysis were fixed with an equal volume of 4% (w/v) D-glucose/10% (v/v) Tris-saline (10 mM Tris, 150 mM NaCl, 10 mM NaN₃)/10% (v/v) formaldehyde and adjusted to a final pH of 7.3 with sodium hydroxide (NaOH) [172, 173]. A ~10% (v/v) formaldehyde solution was prepared from 3 in 10 parts 35% (v/v) formaldehyde (SIGMA). Erythrocyte lysis occurred if all the components of the fixing solution were not prepared fresh and therefore the solution was prepared just before use and tested on an uninfected erythrocyte sample of 5% haematocrit before addition to the plates, to prevent lysis compromising the experiment. Fixed plates were stored at 4°C for FACS analysis.

2.2.3.2 Indirect parasitaemia quantitation assays

2.2.3.2.1 Lactate dehydrogenase (Malstat) assay

The LDH assay measures the parasitic conversion of L-lactate to pyruvate resulting in the reduction of APAD. The reduced APAD in turn reduces nitroblue tetrazolium (NBT) and forms a blue formazan product, which is measured spectrophotometrically [12]. The LDH assay was performed according to Makler and colleagues [166], as follows: The Malstat reagent (pH 9) was prepared [0.2% (v/v) Triton-X 100 in 0.1 M Tris-HCl followed with the addition of 2.1% (w/v) lithium-lactate and 0.022% (w/v) APAD] and stored at 4°C. A volume of 100 µl Malstat reagent was pipetted into the wells of a non-sterile 96-well plate. The thawed, drug treated culture plates were resuspended and 6 µl of culture lysate was transferred to its corresponding well in the Malstat-containing plate. The drug treated plates were afterwards returned to storage at -20°C for subsequent HRPII ELISA analysis. NBT/phenazine ethosulphate (PES) was mixed 20 to 1 in PBS and 25 µl was added to the wells as chromogen. The plates were foil-covered and incubated in the dark at room temperature for 20 - 30 min until the reaction was terminated by the addition of 30 µl of 10% acetic acid. The concentration of the blue formazan product was determined with a Multiskan Ascent ELISA scanner (Thermo LabSystems, Massachusetts, USA) at an absorbance of 650 nm. The percentage response was calculated relative to that of the untreated parasite controls (Eq. 2.1) and the IC₅₀ was calculated with concentration response curves as described in section 2.2.3.4.

$$\text{Percentage response} = \frac{(\text{drug treated response} - \text{background response})}{(\text{untreated response} - \text{background response})} \times 100 \quad \dots\dots\text{Equation 2.1}$$

2.2.3.2.2 Histidine-rich protein II (HRPII) ELISA

The HRPII assay is a double-site sandwich ELISA i.e. binding of a mouse primary anti-HRPII antibody to the HRPII antigen forms a complex that is recognised by an anti-mouse horseradish peroxidase (hrp)-conjugated secondary antibody (hrp-conjugate). Excess unbound antibodies are removed and the conjugated hrp of the bound secondary antibody catalyses the oxidation of o-phenylenediamine by hydrogen peroxide, resulting in a yellow chromogenic product, 2,3-diaminophenazine, which is measured spectrophotometrically [168, 174]. The assay was performed with two commercially available monoclonal antibodies kindly provided by M. Bubb from the National Bioproducts Institute (Pinetown, South Africa) according to the protocol of H. Noedl (<http://malaria.farch.net>) [168]. 96-Well plates were coated overnight with 100 ng of anti-HRPII IgM capture antibody at 4°C and then blocked with 2% (w/v) bovine serum albumin (BSA, Roche) in PBS for 2 h at room temperature. The plates were washed three times with 0.05% Tween 20 in PBS in a Wellwash 4 ELISA washer (Labsystems, Helsinki, Finland), air dried, sealed in aluminium-plastic covers and stored with dessicant at -20°C until used.

On the day of the analysis, the drug treated culture plates (treated as discussed in section 2.2.3.1 and used for the LDH assay prior to the HRPII ELISA) were freeze-thawed twice to ensure lysis of the red blood cells and membranes. Cell lysates (initial inoculum = 5) were diluted 1/40 with PBS to prevent antigen overload (determined assay capacity < 0.15 initial inoculum) and 100 µl was transferred to each well of the pre-coated anti-HRPII IgM plates. The plates were incubated for 1 h at room temperature and subsequently washed three times with 0.05% Tween 20 in PBS. After the wash step, 100 µl of 1/3000 diluted, hrp-conjugate in 2% (w/v) BSA/1% (v/v) Tween 20/PBS (pH = 7.4) was added and incubated for a further 1 h. [This conjugate dilution was determined to provide optimal signal (linear to the inoculum size) for the particular batch of IgM with a 1/40 sample dilution, but had to be titrated with every new batch. Such titration was performed with a checkerboard design: the 96-well plate was coated with two concentrations of anti-HRPII IgM (usually 50 and 100 ng) and a sample dilution series (e.g. initial inoculum of 5 to 0.02) was distributed on the horizontal axis of the plate and different conjugate dilutions (e.g. 1/2000, 1/4000 and 1/6000) on the vertical axis]. After incubation with the anti-mouse secondary antibody, the plates were washed again three times and 100 µl of substrate (1 mg/ml o-phenylenediamine/0.8 mg/ml hydrogen peroxide in 0.1 M trisodium citrate/citric acid buffer, pH 4.5) was added as chromogen. After 10, 20 and 30 min incubation in the dark, the absorbance of the resulting yellow product was read at 450 nm with a Multiskan Ascent ELISA scanner. HRPII readings were corrected by subtracting the average HRPII value of the culture at the beginning when drug treatment was initiated [time zero (t_0)]. Triplicate readings were used to compile dose response curves.

2.2.3.3 Direct parasitaemia quantitation assays

2.2.3.3.1 FACS analysis

Drug treatment of cultures with an initial inoculum of 5 was performed for 48 h as discussed in section 2.2.3.1. The success of the treatment was first evaluated via thin smears before continuing with plate fixation as discussed in section 2.2.3.1. Fixed plates were stored at 4°C and were stable for weeks to months until FACS analysis was performed.

Samples were subsequently resuspended and 50 µl was transferred to 1 ml PBS inside 5 ml FACS tubes (Beckman Coulter, California, USA). The samples were stained with 0.525 µM of the membrane-permeable, fluorescent dye thiazole orange (SIGMA) that intercalates into DNA and RNA, thus differentiating the parasitised erythrocytes from the anuclear uninfected erythrocytes [172, 175]. To prevent quenching of the dye, samples were protected from light until the completion of the analysis. The samples were incubated for 1 h at room temperature and afterwards kept on ice until analysis with an Epics XL.MCL flow cytometer (Beckman Coulter) with laser excitation at 488 nm and fluorescence detection at 525 nm. The flow cytometer was initially calibrated with a series of fixed ring (8.6%, 4.3%, 2.15%, 1.08%, 0.54%, 0.27% parasitaemia) and trophozoite (6.4%, 3.2%, 1.6%, 0.8%, 0.4%, 0.2% parasitaemia) infected erythrocytes and the instrument was set to differentiate between uninfected, ring infected and trophozoite infected erythrocytes according to the size (forward scatter) and granularity (side scatter) of the detected fluorescence. At the start of every FACS run, uninfected erythrocytes and untreated parasite controls of known parasitaemia and parasite stage were analysed to ensure that the instrument settings were correct. In view of the cost of the analysis all samples were analysed in duplicate and not triplicate as with the other drug sensitivity assays, but a total of 50000 fluorescent events (cells) were counted to reduce the variation between replicates. Pearson correlation of the parasite counts by FACS and microscopy was calculated in Excel. The Pearson correlation is a measure of similarity i.e. the strength of the linear relationship between two variables or datasets and ranges between -1 (anti-correlated) and 1 (perfectly correlated).

2.2.3.4 Concentration-response curves

GraphPad Prism v. 4.0 software (GraphPad Software Inc., California, USA) was used to construct sigmoidal concentration-response curves according to the four-parameter logistic equation (Hill equation), including the baseline response (Bottom), the maximum response (Top), the curve slope (Hill slope) and the IC₅₀, i.e. the concentration that elicited a response halfway between the curve maximum and the baseline, as presented in Equation 2.2 [176].

$$Y = \text{Bottom} + \frac{(\text{Top} - \text{Bottom})}{1 + 10^{(\text{LogIC}_{50} - X) \cdot \text{HillSlope}}}$$

.....Equation 2.2 [176]

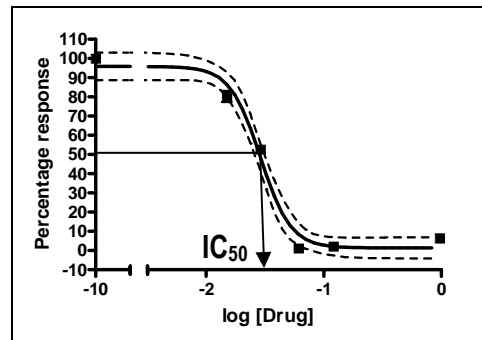


Figure 2.2 Sigmoidal concentration-response curve used by GraphPad Prism 4.0 software to calculate the median inhibitory concentration (IC_{50}). The 95% confidence zone around the best-fit curve is indicated with a dotted line [176].

The software compiles concentration-response curves by performing mean background (uninfected control) subtraction, log transformation of the X-values (concentrations in μM or mM), normalisation of the Y-values (response) against the mean untreated control as a percentage and non-linear regression to obtain a sigmoidal concentration-response curve with variable slope (Fig. 2.2).

2.2.3.5 Propidium iodide (PI) membrane integrity assay

To exclude potential cytotoxicity at the high concentrations of DFMO and MDL73811 used to prevent parasites escaping cytotaxis and causing asynchrony [154], drug treatment at 5 mM DFMO, 5 μM MDL73811 and the combination was performed and membrane integrity was assessed with propidium iodide (PI). This DNA-binding probe does not pass through intact membranes and nuclear staining indicates membrane permeabilisation [177], which is an indirect measure of chemical cytotoxicity [178]. PI fluorescence was detected with FACS using similar methodology as described in section 2.2.3.3.1. An Epics XL.MCL flow cytometer with laser excitation at 488 nm and fluorescence detection at 585 nm was set to count at least 50000 fluorescent events or 300 s. Samples were assayed immediately after drug treatment as formaldehyde fixing was found to cause membrane perforation. Samples were resuspended and 25 μl was transferred to 1 ml PBS inside 5 ml FACS tubes. These were incubated in the dark, on ice for 15 min with 0.04 μM PI (SIGMA), before FACS analysis. Positive controls of membrane damage were prepared by exposing samples to 0.05% saponin for 1 min, followed by PI addition and immediate analysis. As opposed to the general FACS procedure where it was required to differentiate between uninfected and different stages of parasitised erythrocytes, the aim here was to assess membrane damage and the FACS instrument had to be recalibrated for PI penetration and fluorescence. To test the efficacy over a wide range of parasitaemias, chicken erythrocytes, which are nucleated as opposed to human erythrocytes, were saponin-lysed to simulate 100% parasitaemia and were used for instrument calibration purposes.

2.3 RESULTS

For functional genomics investigations of polyamine-depleted *P. falciparum* (Chapters 3 and 4) DFMO was chosen as the inhibitor of choice for ODC since it is a selective and specific enzyme-activated, irreversible inhibitor of this enzyme [147] and one of the most widely studied and characterised polyamine biosynthesis inhibitors [146]. For co-inhibition of both the catalytic sites of the bifunctional PfAdoMetDC/ODC, three alternative AdoMetDC inhibitors were considered and tested to be used with DFMO, namely MDL73811 [156], MAOEA [158] and MAOBA (Fig. 2.1 B-D). To determine the IC₅₀s of these compounds, three different drug sensitivity assays were evaluated for suitability for screening such cytostatic drugs. Serial dilutions of the compounds were prepared and 3D7 *P. falciparum* parasites were treated as described (section 2.2.3.1) for 48 h. The same sample sets were analysed in parallel with the LDH assay, HRPII ELISA and FACS to enable comparison of the results obtained.

2.3.1 Validation of signal to inoculum linearity

Linearity of absorbance versus parasite inoculum (parasitaemia x haematocrit/sample dilution) was carefully optimised for the two colorimetric assays, the HRPII ELISA and the LDH assay. For the HRPII assay, the quantity of anti-HRPII IgM and hrp-conjugate, the optimal culture dilution and colour reaction time was determined with a checkerboard design (described in section 2.2.3.2.2) to prevent overloading the capacity of the assay with too much antigen. This optimisation had to be repeated for every new batch of IgM and hrp-conjugate obtained, but in general the combination of 100 ng anti-HRPII IgM, 1/2000 to 1/4000 diluted hrp-conjugate and a sample inoculum dilution ≤ 0.15 was used, resulting in a signal that was linear with the sample inoculum when incubated for 20 - 30 min. A conjugate dilution of 1/3000 was subsequently used (Fig. 2.3). The HRPII assay was by far the most sensitive of the three assays tested and could detect an inoculum of as low as 0.025 (parasitaemia of 0.005% with a 5% haematocrit).

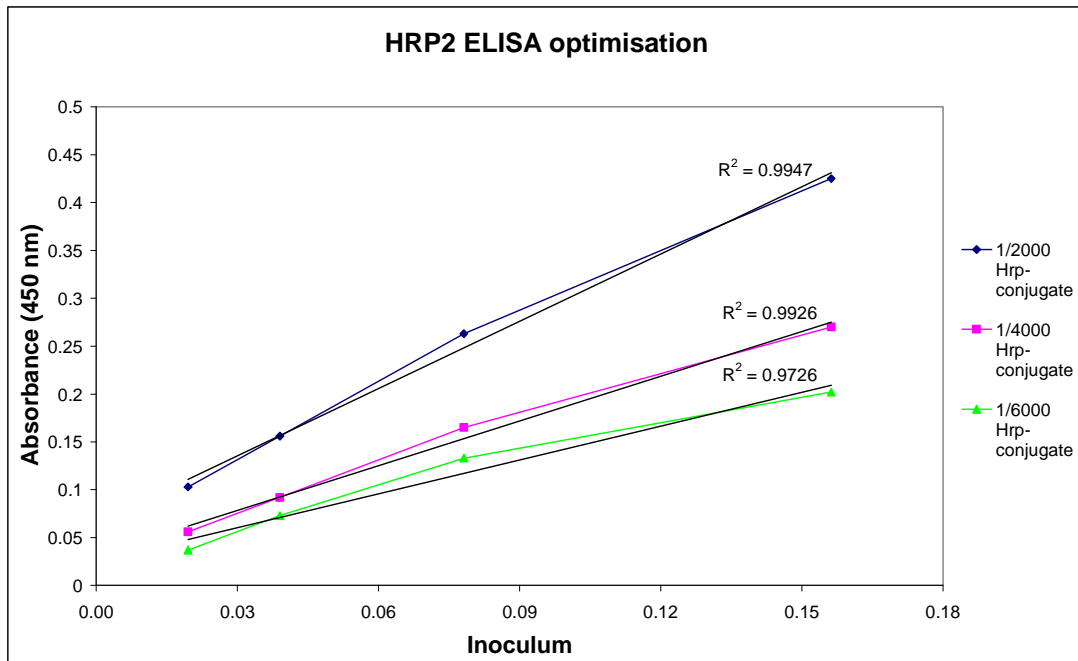


Fig. 2.3 HRPII ELISA optimisation of the hrp-conjugate dilution and sample inoculum.

Similarly, the linearity of the LDH assay was determined by measuring the LDH activity of a series of inocula (varying parasitaemia/haematocrit and sample dilution) (Fig. 2.4). This enzymatic assay (versus the antigen-antibody HRPII assay) has a higher capacity for larger inocula (higher than 2.0 for ring stage parasites, Fig. 2.9), and the upper plateau was not reached in any of the assays performed. Samples with an initial inoculum of 5 were routinely diluted to an inoculum of 0.2 to prevent haemoglobin interference with the colour reaction.

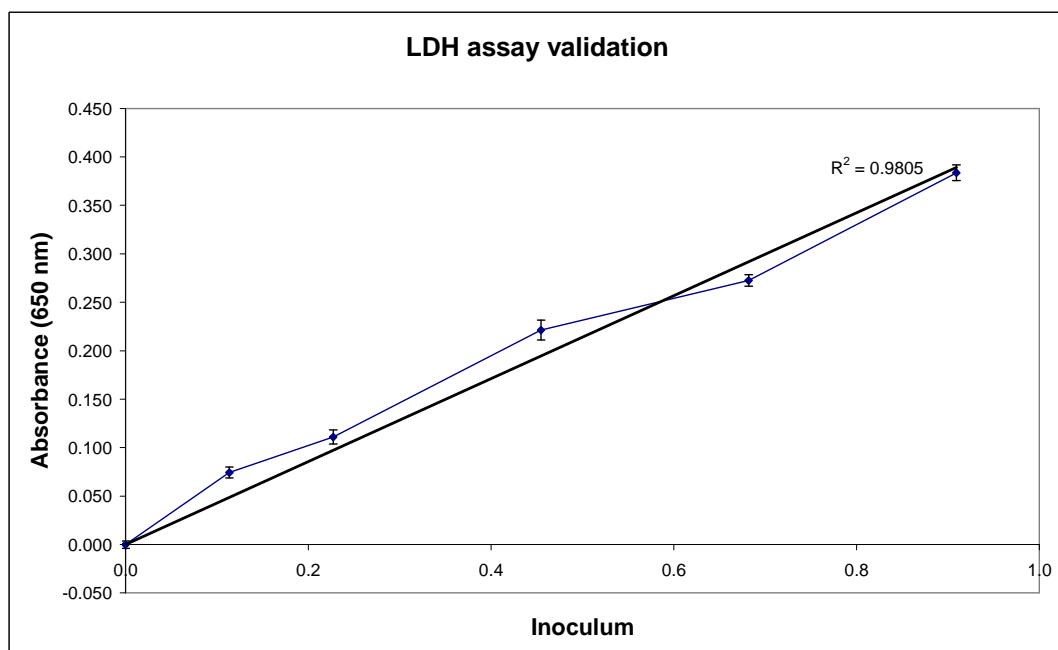


Fig. 2.4 Validation of signal to inoculum linearity of the LDH assay.

The accuracy of the FACS instrument was validated by a series of ring and trophozoite-infected erythrocytes with known parasitaemia that were prepared by microscopy (Fig. 2.5). The thiazole orange fluorescent dye used for FACS analysis, intercalates with DNA, resulting in a fluorescent signal for parasitised erythrocytes, but not with anuclear, uninfected erythrocytes [175]. Similar to previous reports [172, 175] there was excellent correspondence between the fluorescent parasite counts (FACS) and the Giemsa-stained parasite counts (microscopy, Fig. 2.5). FACS and microscopical data had a Pearson correlation > 0.99 for both rings and trophozoites. However, FACS analysis had a sensitivity of only about 0.5% parasitaemia.

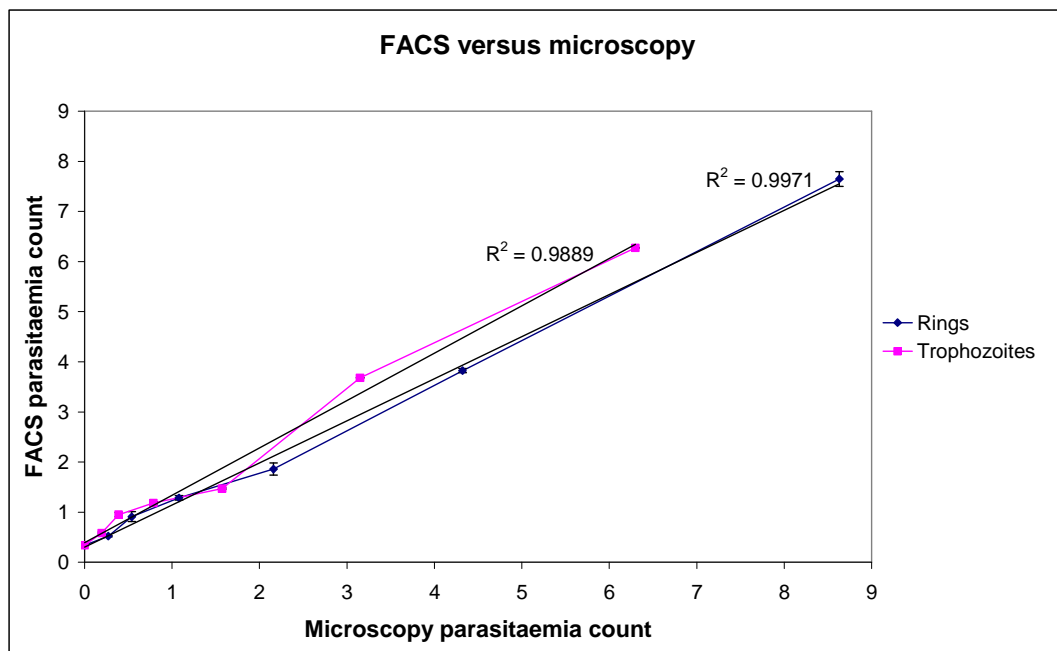


Fig. 2.5 Linearity of parasite counts by FACS analysis versus microscopy

Based on the size (forward scatter) and granularity (side scatter) of the fluorescence, uninfected and parasitised erythrocytes containing different parasite stages could be differentiated (gating) [172]. When forward (Y-axis) and side scatter (X-axis) of fluorescence was plotted, the signal of the uninfected erythrocytes (least granular) lay furthest to the left, followed by the rings (moderately granular) and the signal of the trophozoites (most granular) appeared furthest to the right on the horizontal axis (Fig. 2.6). The method was not set to differentiate schizonts from the other parasite stages, but the signal of such mature parasites would be expected at the far right on the horizontal axis because of their high granularity.

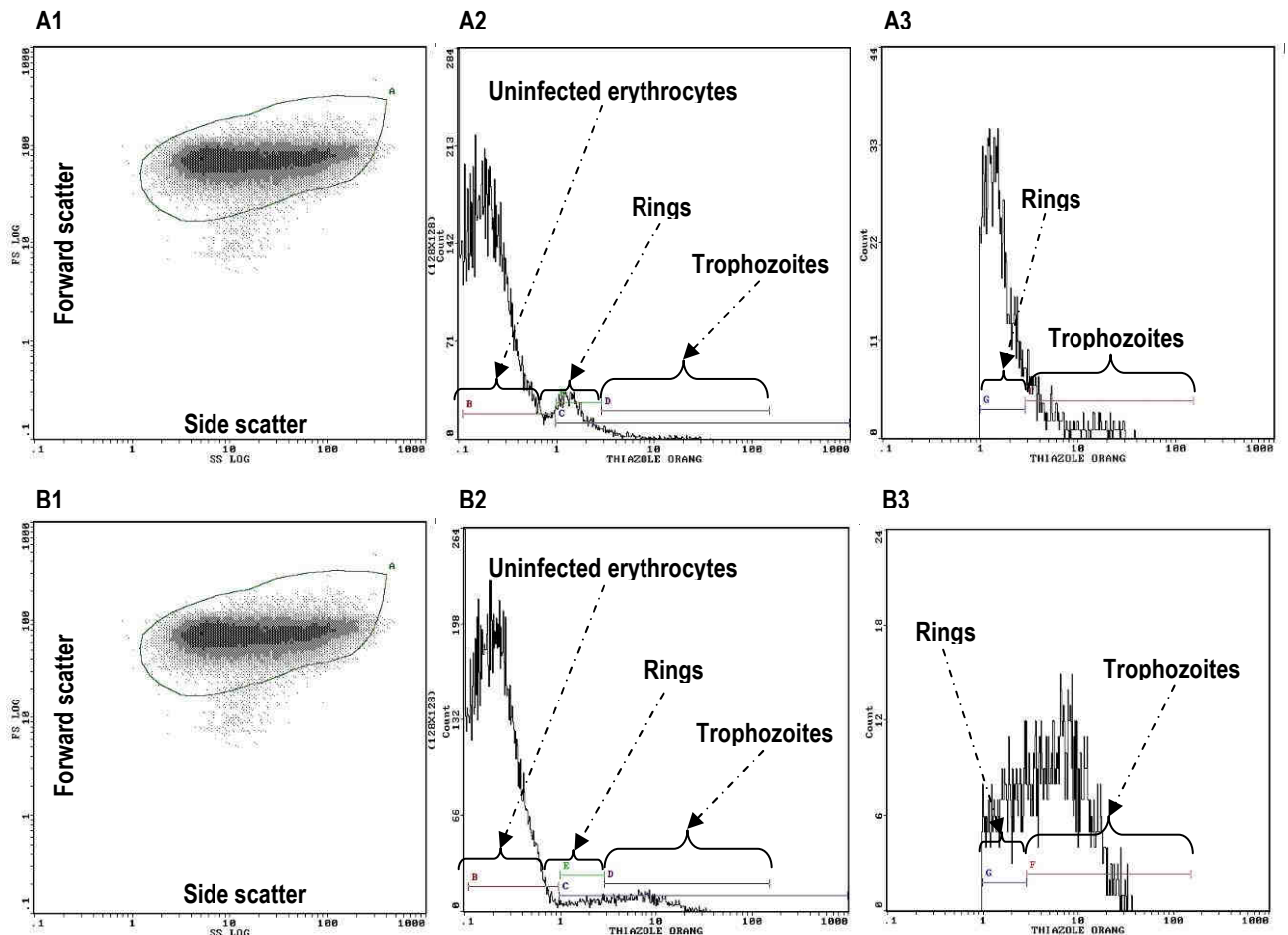


Fig. 2.6 Typical FACS images illustrating the forward (size) and side scatter (granularity) of the fluorescence, which was used to differentiate between uninfected, ring and trophozoite-infected erythrocytes (gating). Note that the sample in A contained mainly ring-stage parasites (A3), whereas the sample in B contained both rings and trophozoites (B3).

2.3.2 Concentration-response curves and IC_{50} s

The data obtained from the LDH assay, HRPII ELISA and FACS were used to compile concentration-response curves of the four cytostatic drugs in order to calculate their IC_{50} s. Chloroquine was always included as drug treatment control, albeit cytotoxic. The shape of the concentration-response curves obtained for chloroquine was always sigmoidal (S-shaped, Fig. 2.7) and the IC_{50} s across the different assays were relatively consistent (28 - 34 nM) and comparable with the published value of 50 nM for the chloroquine-sensitive 3D7 strain (Table 2.1) [179].

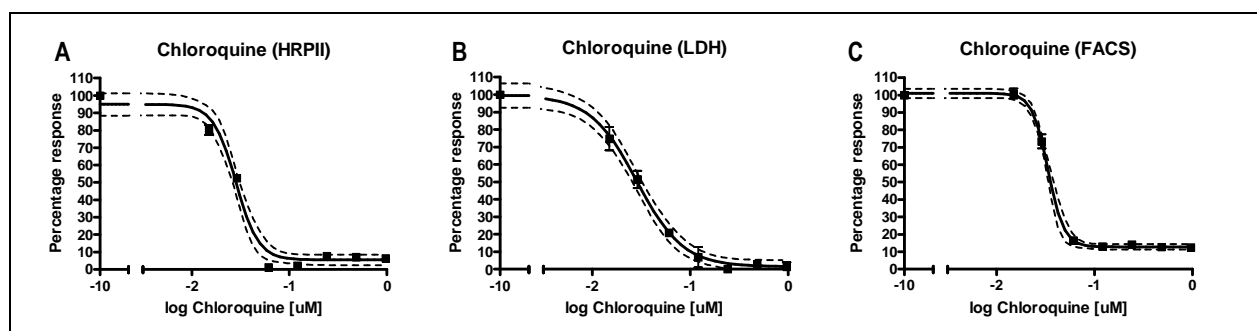


Fig. 2.7 Concentration-response curves of chloroquine from data derived of **A)** HRPII ELISA, **B)** LDH assay and **C)** FACS analysis. The 95% confidence intervals around the best-fit curves are indicated. All three curves are truly sigmoidal with little variation.

However, despite the general success of the drug treatment and dosage ranges used, as evaluated by microscopy, the curves obtained for the cytostatic drugs were often not truly sigmoidal (Fig. 2.8).

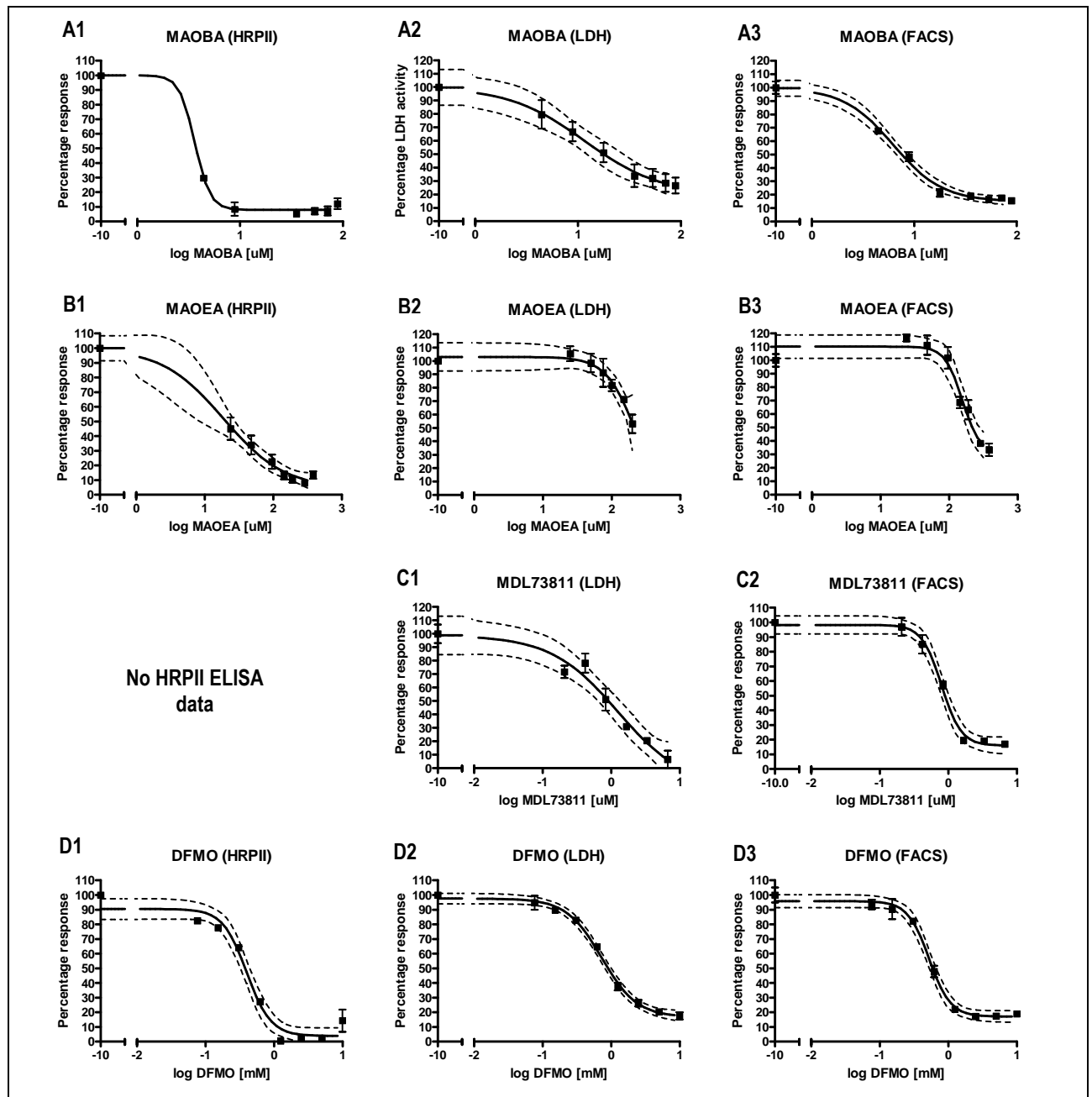


Fig. 2.8 Concentration-response curves of cytostatic compounds **A)** MAOBA, **B)** MAOEA, **C)** MDL73811 and **D)** DFMO using indirect (HRPII ELISA and LDH assay) versus direct (FACS) parasitaemia quantitation assays. The 95% confidence intervals around the best-fit curves are indicated, except for A1.

This was especially true for the concentration-response curves obtained for MAOBA and MAOEA from the two colorimetric assays and their resulting IC_{50} s (Table 2.1) varied significantly across replicates with large 95% confidence intervals, whereas the curves compiled from the FACS data were usually truly sigmoidal and the IC_{50} s had acceptable variation. The graphical 95% confidence interval of the MAOBA HRPII ELISA data could not be calculated by the software (Fig. 2.8A1). The concentration-response curve compiled from the LDH

assay data of MDL73811 was also not truly sigmoidal, but HRPII ELISA data were not generated due to the unavailability of the assay at the time when the drug was obtained.

It should be kept in mind that the software algorithm attempts to force the data into a sigmoidal shape, but that the data points should ideally be distributed uniformly on the curve to be regarded as truly sigmoidal. Since the three assays were performed on exactly the same samples, comparable results were expected. The IC₅₀s for DFMO across the different assays varied between 400 and 730 μM, which is in the same order as the published value of 1.3 mM for chloroquine-sensitive strains of *P. falciparum* [90, 153]. The values for MDL73811 varied between 0.58 and 0.80 μM, which is comparable with the published IC₅₀ of 1 μM for chloroquine-sensitive parasites. No published values are available for MAOBA and MAOEA, since these have not previously been tested in Plasmodia.

Table 2.1 IC₅₀ values obtained with three different drug sensitivity assays

| Compound | IC ₅₀ values (μM) with 95% confidence interval | | |
|-------------|---|---------------------------|---------------------------|
| | HRPII ELISA (Indirect method) | LDH (Indirect method) | FACS (Direct method) |
| Chloroquine | 0.028 (0.026 to 0.031) | 0.028 (0.024 to 0.033) | 0.034 (0.032 to 0.036) |
| MAOEA | 18.83 (12.22 to 29.02) | 433.5 (5.667 to >1000) | 156.3 (122.6 to 199.3) |
| MAOBA | 3.635 (1.899 to 6.955) | 11.6 (5.226 to 25.77) | 6.228 (5.323 to 7.286) |
| MDL73811 | - | 0.577 (0.391 to 0.852) | 0.798 (0.690 to 0.923) |
| DFMO | 400.6 (331.9 to 483.5) | 729.6 (633.7 to 840.1) | 526.4 (461.8 to 600.0) |

The inconsistencies obtained for some of the cytostatic drugs with the colorimetric assays versus FACS compared to the generally reliable data of chloroquine were subsequently proposed to be due to the difference in mechanism and stage of action of the cytotoxic chloroquine compared to the cytostatic compounds. Chloroquine kills parasites rapidly in the ring stage and when parasitaemias of drug treated parasites and untreated controls are compared 48 h later to calculate the percentage response, the parasites that survived have developed into rings again and their HRPII content or LDH activities are compared to those of the ring controls. However, the cytostatic drugs cause parasite growth arrest in the trophozoite stage [153, 154] and depending on the concentration (within the series of drug dilutions), alter the synchronisation of the parasite population due to arrest of the affected parasites compared to the normal progression of the unaffected parasites. In order to calculate the IC₅₀ after treatment for 48 h, varying degrees of asynchronous trophozoites (arrested) and subsequent ring stage parasites are compared with the untreated, synchronised ring controls (Eq. 2.1). This is not problematic when the parasites are physically counted (microscopy or FACS), but indirect quantitation of parasitaemia based on metabolism (HRPII content and LDH activity), will lead to data

inconsistencies and reproducibility problems. This is due to the fact that parasite metabolism is not equal across the IDC, but reaches a maximum in the trophozoite stage [29, 89].

To prove this hypothesis, the HRP2 content and LDH activity across different (synchronised) parasite stages were investigated. As demonstrated earlier, both the HRP2 content and LDH activity were linear with the parasite inoculum, but the slope of these straight lines was very different depending on the parasite stage (Fig. 2.9A, B). These results confirm the conundrum entered into when comparing metabolic activities across different parasite stages after growth arrest of the treated parasites versus normal progression of untreated controls.

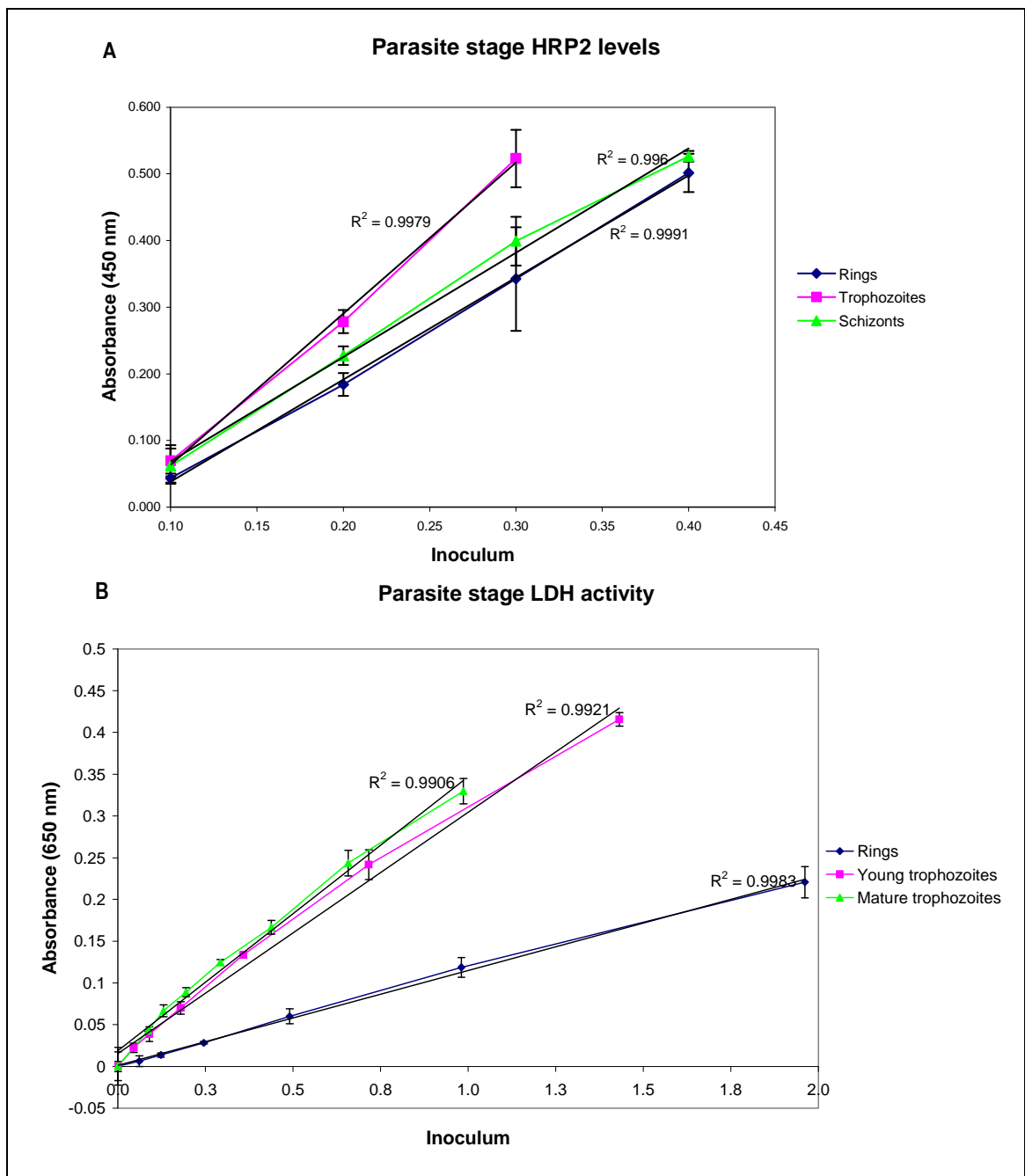


Fig. 2.9 Parasite stage-specific levels of **A)** HRP2 as detected by HRP2 ELISA assay and **B)** LDH activity according to the LDH assay.

The LDH enzyme activity increased with development from rings to young and subsequently mature trophozoites, whereas the HRP_{II} content of the trophozoites was the highest and the contents of rings and schizonts were very similar. However, LDH transcripts peak at 18 h post-invasion (hpi) according to the 3D7 IDC transcriptome (Fig. 2.10A, <http://malaria.ucsf.edu>) [91] and the proteins have delayed translation as described in section 4.3.1.2. HRP_{II} transcripts peak at 6 hpi (Fig 2.10B). The transcript half lives and translation times of the histidine-rich proteins are not known, but HRP_{II} was previously reported to be mainly secreted during the second half of the IDC with a marked rise during schizont development and rupture [180]. This is in contrast with the results presented here and peculiar considering the time of peak expression (6 hpi) and just-in-time transcriptional mechanism of *P. falciparum* [29].

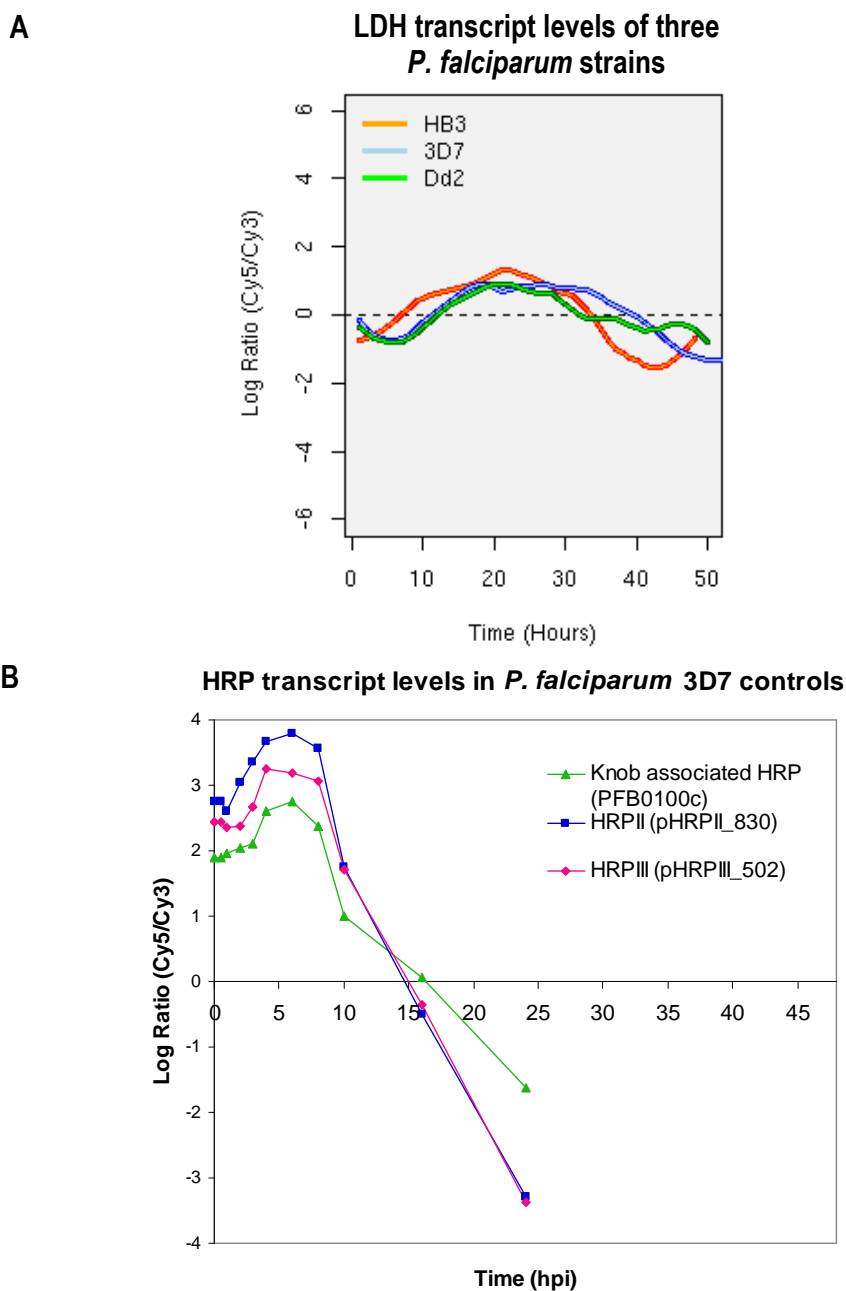


Fig. 2.10 Transcript levels of **A)** LDH of strains HB3, 3D7 and Dd2 during the complete IDC (<http://malaria.ucsf.edu>) [91] and **B)** the three histidine-rich proteins of 3D7 parasites during the first 24 h of the IDC (M. Llinás, unpublished data).

2.3.3 DFMO and MDL73811 interaction during PfAdoMetDC/ODC co-inhibition

The IC₅₀s of DFMO and MDL73811 were determined as 0.53 mM and 0.8 μM (from FACS data) for the particular laboratory conditions as described in section 2.3.2. However, the effect of the drug combination during PfAdoMetDC/ODC co-inhibition could be additive (1+1=2), synergistic (1+1>2) or antagonistic (1+1<2). Synergistic or antagonistic interactions would have necessitated dose alterations for treatment with the combination. To investigate this, the fixed-ratio method of investigating drug interaction [181] was applied whereby a dilution series of DFMO and MDL73811 was prepared in a fixed-ratio combination of their IC₅₀s (0.53 mM versus 0.8 μM). The highest concentration of the combination series contained eight times the IC₅₀ of both the drugs, which was then two-fold diluted until 0.0625 times the IC₅₀s. A 2-fold dilution series starting from 16 times the IC₅₀s of the individual compounds was also prepared and assayed in parallel. The concentration-response curves obtained for DFMO, MDL73811 and the combination are presented in Fig. 2.11.

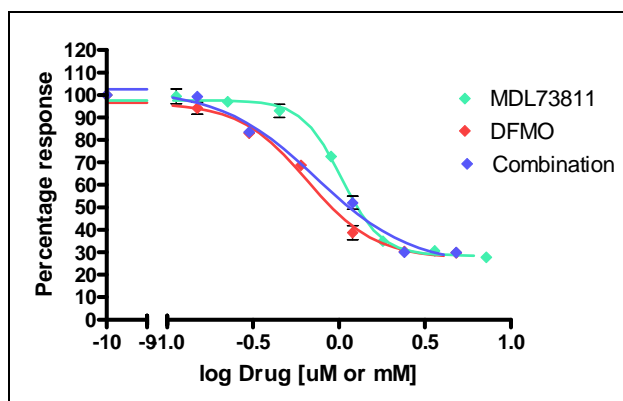


Fig. 2.11 Concentration-response curves of MDL73811 (concentration in μM), DFMO (concentration in mM) and the combination compiled with GraphPad Prism v.4 from FACS data.

The curves compiled for the individual drug treatments correlates well with those of the combination of DFMO and MDL73811, which means that the total effect of the combination is the sum of that of the individual treatments i.e. additivity (Fig. 2.11). This corresponds with previous reports [153, 154]. Antagonism would have caused the position of the combination curve to shift towards the right of the MDL73811 and DFMO curves and with synergism it would have shifted towards the left.

2.3.4 PI membrane integrity assay of PfAdoMetDC/ODC co-inhibition

Both DFMO and MDL73811 cause growth arrest of *P. falciparum* in the trophozoite stage due to polyamine depletion, but the effects are cytostatic [154]. However, to ensure that dosages as high as five times the IC₅₀ of both drugs in combination remained cytostatic for use in the subsequent functional genomics investigations (Chapters 3 and 4), parasites were incubated with PI following drug treatment [178]. This DNA-binding probe does not pass through intact membranes and nuclear staining thus indicates membrane permeabilisation [177], which is an indirect measure of chemical cytotoxicity [178]. In contrast with the FACS procedure for drug

susceptibility testing (section 2.2.3.3.1), which differentiated between the uninfected and different stages of parasitised erythrocytes (Fig. 2.6), the PI assay was aimed to assess membrane damage and the FACS instrument had to be recalibrated to detect PI penetration and fluorescence. To test the procedure over a wide range of parasitaemias, chicken erythrocytes, which are nucleated as opposed to human erythrocytes, were saponin-lysed and used as positive control to simulate membrane-damaged, parasitised erythrocytes (Fig. 2.12).

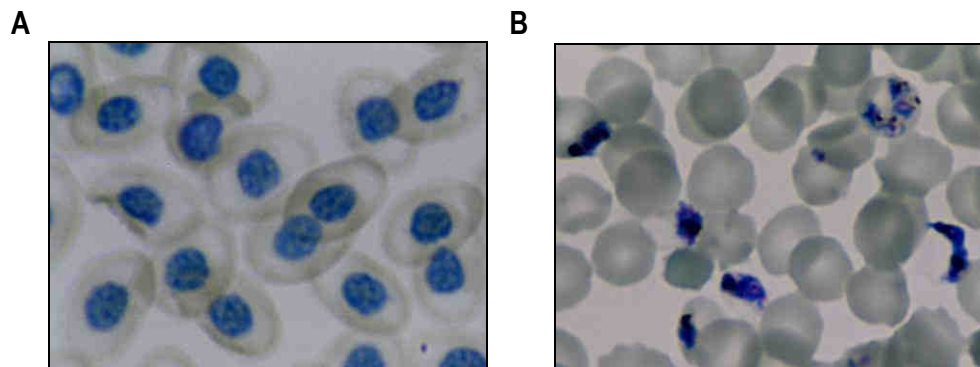


Fig. 2.12 Giemsa-stained thin smears of **A)** chicken erythrocytes, which contain nuclei and **B)** 3D7 *P. falciparum*-infected human erythrocytes.

In the absence of saponin, the chicken erythrocytes were not detected, but saponin treatment allowed PI penetration and nuclear fluorescence, resulting in a 96.2% “parasitaemia” (Table 2.2.). However, anuclear human erythrocytes were not detected despite saponin treatment. Similarly, parasitised erythrocyte controls were not detected without saponin treatment. The procedure was subsequently applied to assess erythrocyte membrane integrity after treatment with the combination of 5 mM DFMO and 5 μ M MDL73811, but parasites could not be detected above the background, indicating that PI did not penetrate and that the membranes of parasitised erythrocytes remained intact despite the high dosages used for treatment (Table 2.2).

Table 2.2 PI assay and FACS analysis of PfAdoMetDC/ODC co-inhibited *P. falciparum*

| Sample | % Parasitaemia |
|--|----------------|
| Chicken erythrocytes + PI | 0.03 |
| Chicken erythrocytes + saponin + PI | 96.2 |
| Human erythrocytes + saponin + PI | 0 |
| 4-5% <i>P. falciparum</i> trophozoite controls + PI | 0.25 |
| 4- 5% <i>P. falciparum</i> trophozoite controls + saponin + PI | 4.74 |
| 5 mM DFMO-treated <i>P. falciparum</i> + PI | 0.09% |
| 5 μ M MDL73811-treated <i>P. falciparum</i> + PI | 0.10% |
| DFMO/MDL73811 combination + PI | 0.08% |

2.4 DISCUSSION

In this chapter, three AdoMetDC inhibitors were considered for use in combination with DFMO in functional genomics investigations of PfAdoMetDC/ODC co-inhibited *P. falciparum*. The IC₅₀s of these cytostatic drugs had to be determined and in the process three high-throughput drug sensitivity methods (HRPII ELISA, LDH

assay and FACS) were evaluated to determine the most appropriate method for testing cytostatic compounds. HRPII levels and LDH activity are closely associated with parasite density and development [12], whereas FACS analysis physically counts the number of infected erythrocytes based on their DNA contents and fluorescence [175]. Of the three methods tested, the HRPII ELISA assay was the most sensitive and could detect inocula as low as 0.025 (e.g. 0.005% parasitaemia, 5% haematocrit), but the assay capacity was easily overloaded with antigen and sample dilution was required.

The accuracy of drug sensitivity assays such as these three are critical in resistance-surveillance and drug discovery programmes. These assays measure the proliferation or growth of drug treated parasites relative to a drug-free control. Since variables such as parasite inoculum (haematocrit and parasitaemia) and the stage-dependent action of the drugs tested can influence the outcome of the assays, it is important to control these factors (including parasite stage) when the assays are performed [12]. However, cytostatic drugs, such as the polyamine biosynthesis inhibitors, cause growth arrest in the trophozoite stage [153, 154], whereas the untreated controls progress as usual according to the IDC. Thus, despite starting with a synchronised culture, the cytostatic action of these compounds will cause arrest of a proportion of the parasites and normal progression of the balance, resulting in varying degrees of synchronisation depending on the drug concentration within the dilution series. When stage-independent, direct counting methods such as microscopy or FACS analysis are used to measure parasitaemia, these cytostatic effects on synchronisation have no influence. However, when indirect measures of parasitaemia based on metabolic activity (HRPII content or LDH activity) are applied, inconsistent and variable results may be obtained due to the stage-dependence of these metabolism-based assays. This was especially true for MAOEA and MAOBA. It is well established that parasite metabolism is not equal across the IDC, but reaches a maximum in the trophozoite stage [89]. Therefore, drug discovery efforts employing only methods based on indirect assessment of parasitaemia may obtain inaccurate results and potentially miss novel compounds with cytostatic modes of action, which is far from ideal at a time when every potential antimalarial should be considered. Cytostatic drugs are known to have therapeutic potential in parasitic diseases and DFMO is currently the safer, clinically used alternative in the treatment of West African trypanosomiasis [78]. It is, therefore, suggested that more than one method (direct and indirect measures of parasitaemia) be used in parallel for drug screening to avoid missing potential hits.

Previously, IC_{50} s for DFMO, MDL73811 and various 3-aminoxyl-1-aminopropane derivatives [90, 153, 154] were determined with the tritium-labelled hypoxanthine incorporation assay, which monitors DNA synthesis as an indication of parasite growth [165]. Drug treatment is usually performed in the early ring-stage for 24 h, after which 3H -hypoxanthine is added for 18 h [165]. The assay therefore also measures parasitaemia indirectly based on DNA synthesis, but the assay is terminated at ~42 hpi, i.e. before schizogony. For these cytostatic drug treatments, DNA synthesis of untreated schizont controls would be compared to varying degrees of

arrested trophozoites and schizonts, which may have similar DNA metabolic activities considering that DNA metabolism peaks during the late trophozoite/early schizont stages [29]. Therefore, this assay did not give reason to doubt the methodology used for any of the cytostatic compounds [90, 153, 154], but if performed over 48 h and schizogony occurred, similar problems could have been experienced as with the colorimetric assays used in this investigation.

Different levels of synchronisation and parasite stage are well-known problems in susceptibility surveillance for *P. vivax*, which is predominantly asynchronous compared to *P. falciparum* isolates that are mostly synchronous. Recent *P. vivax* surveillance studies of various drugs in Papua Indonesia with the schizont maturation test demonstrated that *in vitro* susceptibility was correlated to the initial parasite stage and isolates that were predominantly in the trophozoite stage had a 2-fold higher IC₅₀ than those predominantly in the ring stage [182]. Furthermore, the surveillance studies also indicated a correlation between the *in vitro* susceptibility and the duration of the assays [182]. Since the HRPII ELISA, LDH assay and FACS were performed in parallel on the same samples in this study, the standard 48 h incubation period used for most drug sensitivity assays was used. However, longer incubation times are often recommended to test slow-acting drugs, e.g. pyrimethamine/sulphadoxine [12], that primarily exert their effects in the schizont stage [183]. Longer incubation times, such as 72 h, may theoretically also solve the conundrum faced in the case of the polyamine biosynthesis inhibitors, since the arrested trophozoites would then be compared with controls that progressed to the subsequent trophozoite stage and not the ring stage as with 48 h incubation, resulting in comparable metabolic measurements (incl. HRPII and LDH levels). It is currently not clear why the results obtained with the colorimetric analyses of MAOEA and MAOBA were so highly variable, whereas the IC₅₀s of DFMO and MDL73811, determined with the same assays, were relatively acceptable.

Due to the inconsistent results obtained for MAOEA and MAOBA, and better characterisation of ML73811 in the literature [153, 157, 184, 185], the latter drug was selected as the AdoMetDC-inhibitor of choice to be used in the functional genomics investigations. The combination of 5 mM DFMO and 5 µM MDL73811 was shown to be additive and to remain cytostatic at these high dosages. However, the inclusion of MAOEA and MAOBA in the analysis revealed opposite activities in *P. falciparum* compared to what was previously reported for *T. brucei brucei* [159]. MAOEA had an IC₅₀ of 1.3 µM in *T. brucei brucei* and analogues with longer side chains had reduced potency [159]. However, the results in *P. falciparum* showed that MAOBA with its 4-carbon-aminoxy side chain (Fig. 2.1) was 25 times more active (FACS IC₅₀ = 6.2 µM) than MAOEA with its 2-carbon-aminoxy chain (FACS IC₅₀ = 156.3 µM, Fig. 2.1). Apart from potential pharmacokinetic differences of these compounds in *Plasmodium*, the contradictory results between the two species could indicate structural differences in the active site of the *P. falciparum* versus the *T. brucei brucei* AdoMetDC. To investigate this possibility, docking studies of MAOEA and MAOBA in the active site of AdoMetDC were performed with a three-dimensional model of the AdoMetDC domain of PfAdoMetDC/ODC [186] (results not shown). These

studies revealed 15 potential conformations for MAOBA on the plasmodial active site compared to only one for MAOEA, which indicated a significantly higher probability of the first being in the correct conformation to inhibit the enzyme than with MAOEA.

In conclusion, the cytostatic mechanism of polyamine biosynthesis inhibitors resulting in growth arrest of the treated cells and normal progression of the untreated controls requires special consideration for basic comparisons of response in terms of assay methodology used and data analysis. This is particularly important when studying a multistage organism such as *P. falciparum*, which constantly develops during the IDC (Fig. 1.2) such that growth arrest compared to normal progression will result in significant differences merely due to stage. This should be kept in mind with any comparative analysis of such an organism treated with these compounds, including drug sensitivity assays. In addition, the same principle also applies to the relative quantitation of RNA, proteins and/or metabolites as is required in functional genomics investigations, hence the relative t_0 strategy applied in the following chapters.

CHAPTER 3

TRANSCRIPTIONAL PROFILING OF CO-INHIBITED PfADOMETDC/ODC

3.1 INTRODUCTION

3.1.1 Transcriptional profiling of perturbed *P. falciparum* compared to other organisms

Transcriptional profiling can be used to assess the response of cells or organisms to environmental stress, which can identify feedback mechanisms, alternative pathways and metabolic buffering systems activated to cope with a perturbation [136, 187]. The data can demonstrate how specific compounds affect regulatory networks of cellular metabolism and their effects on particular metabolic pathways [188]. The approach was applied with great success in the case of *Mycobacterium tuberculosis* [138] and *S. cerevisiae* [139]. Studies on *M. tuberculosis* revealed transcriptional signatures specific to the mode of action for several antimycobacterial drugs [138] and for *S. cerevisiae* it was shown that the transcriptional changes associated with target deletion or under-expression should theoretically mimic the effect of chemically inhibiting that target [188]. The latter makes microarray studies of drug perturbed *P. falciparum* an attractive alternative compared to gene deletion, in particular since genetic manipulation of this organism faces unique technical problems and a low success rate due to its A+T-richness and intracellular location [130]. In contrast to *M. tuberculosis* [138] and *S. cerevisiae*, the correlation of perturbation-specific events in the *P. falciparum* transcriptome was initially limited to only a few studies in malaria research [179, 189-191]. This could have been related to the multistage nature of the parasite, which challenged the experimental design of microarray and other functional genomics investigations. The limited evidence of compensatory mechanisms, the paucity of transcription factors identified in the *P. falciparum* genome [119], the small amplitude of transcriptional responses observed in *Plasmodium* upon perturbation compared to other organisms, e.g. *M. tuberculosis* [137, 138], and evidence of post-transcriptional control [128, 192, 193] (as discussed in section 4.1), caused doubt regarding the role of transcriptional regulation in the parasite. It was perceived that the parasite's transcriptional control was "hard-wired" and that transcriptional profiling during environmental perturbations was futile [128, 194, 195]. This perspective was corroborated by several perturbation-investigations of the parasite that failed to detect programmed transcriptional responses [194, 196, 197].

However, evidence supporting the role of transcriptional control in the parasite is now mounting. One of the first studies of plasmodial transcriptional profiling employed serial analysis of gene expression (SAGE) and monitored the transcriptional response of asexual parasites to 6 h chloroquine treatment [179]. More than 100 transcripts were identified as differentially affected and included the increased abundance of the transcript for

the multidrug resistance gene, *pfmdr1*, which underscored its importance in chloroquine resistance. This investigation indicated the existence of a compensatory feedback mechanism, signalling a transcriptional response to chloroquine [179]. A subsequent follow-up report identified 600 drug-responsive genes after treatment with chloroquine [196]. Since then, there have been a number of microarray studies which reported transcriptional compensation in response to environmental stress in *P. falciparum*. These include the increase of the transcript for a *rcd1+* homologue (regarded as glucose-specific) upon glucose deprivation [189] and the increased transcript abundance of two heat shock protein orthologues after exposure to elevated temperature [190]. Other microarray studies detected perturbation-specific, albeit not compensatory, effects including the specific impairment of transcription of apicoplast genes after parasites were treated with doxycycline [62] and enrichment of the differentially affected transcripts for histone H3K9 acetylation after treatment with the histone acetyltransferase inhibitor, anarcadic acid [191]. Recently, treatment with artesunate was reported to cause a transcriptional death response, but it is not clear whether the response observed was specific or generalised cytotoxicity [198]. Finally, transcriptional profiling of sphingomyelin biosynthesis inhibition, which similar to polyamine depletion results in developmental arrest in the trophozoite stage, indicated the involvement of an previously unknown tubovesicular network export-protein that was subsequently shown to be important for lipid import and parasite growth [199]. These studies demonstrated that the malaria parasite is able to respond to environmental perturbation in the transcriptome and that perturbation-specific transcriptional responses can be distinguished from the basal “just-in-time” level of transcriptional control.

3.1.2 Transcriptomics methodologies, experimental design and data analysis

Genome sequencing of humans and various organisms has provided large amounts of data and various techniques were developed to exploit this growing body of knowledge to the maximum. These include SAGE, representational difference analysis (RDA), complementary DNA (cDNA) microarrays and oligonucleotide microarrays, all of which enable the simultaneous analysis of the transcript abundance from thousands of genes [200]. SAGE is based on the isolation of unique sequence tags from individual transcripts and serial concatenation of these tags into long DNA molecules. Sequencing of the concatemer clones reveals the individual tags, which enables the rapid identification and quantitation of the cellular transcripts [201]. In RDA, the difference between two complex genomes is determined by subtractive and kinetic enrichment of restriction endonuclease fragments that are present in the one DNA population but not in the other [202]. cDNA microarray experiments involve the competitive hybridisation of two mRNA samples that have been converted into cDNA and each labelled with its own fluorescent dye (e.g. Cy3 and Cy5). The hybridisation occurs on a glass slide or chip spotted with cDNA probes. The resulting data provide information on the relative transcript abundance of the sample genes [203]. In oligonucleotide microarray, oligonucleotides are spotted or synthesised onto glass slides instead of cDNA probes. With two-colour/channel oligonucleotide arrays the relative expression between two differentially labelled samples is determined as with cDNA

microarrays, but for single-colour/channel arrays the absolute gene expression values of a single sample are determined [203].

Operon Biotechnologies (Cologne, Germany) provides commercial 70-mer spotted arrays or array-ready oligonucleotide sets for in-house spotting. In addition to spotted arrays, various other competing technologies for commercial oligonucleotide microarrays have emerged. These include the use of either full-length cDNAs, or presynthesised/*in situ* synthesised oligonucleotide probes [204]. The pioneering work in this field was performed by Affymetrix (Santa Clara, California, USA) and consequently their GeneChips are regarded as the optimal method for transcriptional profiling. The GeneChip technology uses a combination of light-directed (photolithography) and solid-phase DNA synthesis of 25-mer oligonucleotides *in situ* on the slide. Agilent (Palo Alto, California, USA) technology synthesises 60-mer oligonucleotides *in situ* at or near the surface of the slide by inkjet printing using phosphoramidite chemistry, whereas NimbleGen (Madison, Wisconsin, USA) technology uses a digital micromirror device instead of the photolithographic masks for *in situ* synthesis of 24 to 70-mer oligonucleotides. A major advantage of oligonucleotide arrays is that they are designed *in silico* without the need for clone libraries and tedious sequencing for identification purposes [204]. The longer 60 to 70-mer oligonucleotide lengths provide higher sensitivity compared to the shorter 24 or 25-mers [204].

In microarray experimental design a key issue is whether to use direct or indirect comparisons i.e. to make the comparison within or between slides. In direct comparison the differential transcript abundance between two samples is directly measured on the same slide, but in indirect comparison the differential abundance of the two samples is determined on separate slides compared to a common reference. The common reference can be an external RNA or cDNA reference pool or a composite pool containing all the samples. In time course microarray experiments RNA is extracted from samples harvested at several time points after a form of treatment or stimulation. These samples can also be compared to a common reference or directly using a sequential or loop design (Fig. 1.9, Fig. 3.1). The experimental design usually depends on the number of hybridisations to be performed, i.e. the number of time points and the number of replicates. When the main focus is on the relative changes between the time points, the reference design is the better choice. In contrast to the sequential and loop designs, the reference design has the further advantage that the normalised data (i.e. \log_2 -ratios) can be directly compared (through the reference), which simplifies data analysis and interpretation [203].

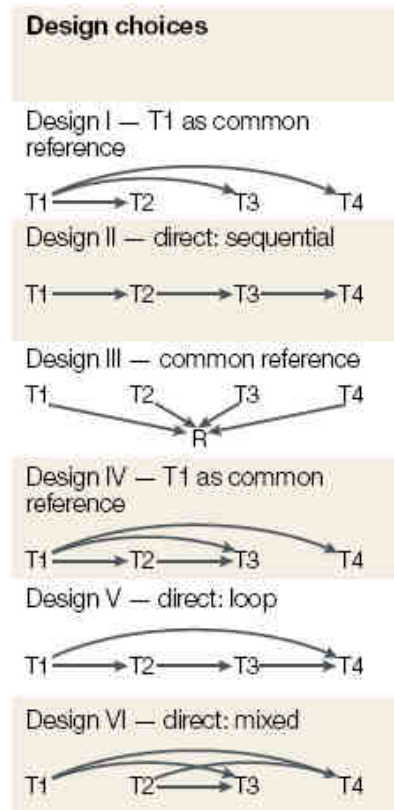


Fig. 3.1 Six designs of microarray time course experiments (image obtained from [203]). Designs I and II require only three slides, whereas the other four designs require four [203].

After hybridisation, the data are collected by scanning the two independent fluorescent images (e.g. Cy3 and Cy5) of the co-hybridised species (e.g. one for the sample and one for the reference) from each slide at high resolution. The spot relative fluorescence intensities (e.g. Cy5/Cy3) are normalised during scanning by adjusting the photon multiplier tube (PMT) settings to compensate for differences in labelling and detection efficiencies (i.e. dye bias) such that $Cy5/Cy3 \approx 1$. The quality of every spot is inspected and bad quality spots are flagged and subsequently removed from the dataset. Subsequently, the data for each gene is typically reported as a \log_2 expression-ratio (Eq. 3.1). The data can then be explored via different analyses, such as clustering, to identify genes that are co-regulated, i.e. with similar expression profiles [200].

$$\text{GeneX } \log_2\text{-ratio} = \log_2 \left\{ \frac{\text{normalised value of treated sample}}{\text{normalised value of reference}} \right\} \quad \dots\dots\text{Equation 3.1}$$

For differential transcript abundance analysis, various software packages are available for normalisation and statistical analysis, such as the R statistical environment (<http://www.r-project.org/>). Data normalisation for two-colour arrays will be discussed. Within R, data are normalised, first within the same slide to remove local background artefacts or edge effects. Various diagnostic plots can be compiled to visualise the data before and after normalisation to determine the most appropriate normalisation method to apply. For closely related samples with similar expression, a scatterplot of Cy5 versus Cy3 (or their logarithms) would result in data

distribution in a straight line approximately (slope ≈ 1) if labelling and detection for both samples were equal. However, this is not necessarily true and normalisation involves calculating the best-fit slope using regression techniques such as locally weighted scatterplot smoothing (LOWESS) [200]. Global LOWESS normalisation is usually performed if the background is homogenous, but if there are significant differences in the distribution of \log_2 -ratios among the print-tips (visualised as print-tip boxplots, Fig. 3.14), print-tip LOWESS is recommended [205]. Robust spline normalisation is a compromise between print-tip and global LOWESS [206], which uses regression splines instead of LOWESS curves to shrink the individual print-tip curves towards a common value according to Bayesian rules. This technique introduces little variation into good quality arrays with limited spatial variation (localised artefacts), but also improves the data from arrays with significant spatial variation [206]. After within-slide normalisation, between-slide normalisation is performed, such as quantile normalisation or scaling, to standardise the distribution of \log_2 -ratios across the different slides [205]. Quantile normalisation was initially proposed for Affymetrix-style single-colour arrays and ensures that the fluorescence intensities (i.e. Cy3 or Cy5) have the same empirical distribution across both fluorescent channels for all the arrays (Fig. 3.16). Rquantile or Gquantile normalisation is particularly useful when using a reference design to normalise the common reference values across all the slides. Rquantile is used when the reference is labelled with Cy5 (red) or Gquantile when labelled with Cy3 (green). With every data analysis step diagnostic plots are compiled and evaluated to determine the suitability of the data transformation. When satisfactory distributions of \log_2 -ratios are obtained, the replicate data are consolidated and differential transcript abundance (also referred to as differential expression, but actually the function of mRNA expression and decay) between samples can be calculated. With a reference design, the differential transcript abundance of any sample combination can be determined (e.g. treated compared to untreated or to a time zero).

Microarray data should be reported in sufficient detail, including information on the applied methodology and analysis. This ensures the simple interpretation and independent verification of the data as stipulated by the minimum information about a microarray experiment (MIAME) convention [207]. Public microarray database repositories such as ArrayExpress (<http://www.ebi.ac.uk/microarray-as/ae>) and the NCBI's Gene Expression Omnibus (GEO, <http://www.ncbi.nlm.nih.gov/geo>) require detailed MIAME information during data deposition, which enables meta-analyses across different microarray platforms and comparison between different datasets.

Presented here is transcriptional profiling of *P. falciparum* during cyto-stasis using a spotted, 70-mer oligonucleotide microarray platform and employing a reference experimental design. Cyto-stasis was induced by polyamine depletion via co-inhibition of both catalytic sites of PfAdoMetDC/ODC with DFMO and MDL73811. These drugs are specific inhibitors of PfAdoMetDC/ODC [147] and therefore the transcriptional profiles obtained should be characteristic of the effects of polyamine-depletion on the parasite [138]. A reference point for quantitative analysis of differential expression was defined and several transcripts with

altered profiles could be detected, including some from polyamine and methionine metabolism. Transcriptome analysis revealed polyamine-specific compensatory responses to alleviate the perturbation, which supports the role of transcriptional regulation in polyamine and methionine metabolism of *Plasmodium*.

3.2 MATERIALS AND METHODS

3.2.1 Ensuring the correct treatment dosage for the transcriptomics investigation

3.2.1.1 Growth morphology studies

3D7 *P. falciparum* cultures were maintained *in vitro* as discussed in section 2.2.1. A small-scale morphology study was performed to ascertain that complete arrest occurred at the treatment concentrations and to determine the exact sampling times for the transcriptomics investigation. Parasites were synchronised by consecutive sorbitol treatments as discussed in section 2.2.2 and treated in the late schizont stage with 5 mM DFMO and 5 μ M MDL73811 and the combination thereof. The parasite morphology was monitored microscopically at 6 h intervals for a complete 48 h life cycle using Giemsa-stained thin smears.

3.2.1.2 Radio-labelled substrate assays

To ensure complete enzyme inhibition of DFMO/MDL73811-treated (T) and untreated (UT) 3D7 cultures (sampled at ~10% parasitaemia, 3% haematocrit) at 5 mM DFMO and 5 μ M MDL73811, the decarboxylase activities of AdoMetDC and ODC were determined after PfAdoMetDC/ODC co-inhibition according to the original method of Assaraf and colleagues [88]. In principle, the 14 C-labelled substrates S-adenosyl-L-[14 C]methionine (56.2 mCi/mmol, Amersham Biosciences, Buckinghamshire, England) and L-[1- 14 C]ornithine (47.7 mCi/mmol, Amersham Biosciences) were incubated with the culture lysates and the release of 14 CO₂ was measured. Cultures were sampled in the early (19 hpi) and mature trophozoite (34 hpi) stages. Samples of 10 - 15 ml were centrifuged at 2500 g for 5 min and the pellet washed three times with an equal volume of PBS, after which 500 μ l was transferred to a cryotube and stored at -70°C. Uninfected erythrocytes were sampled and processed in the same way to serve as a negative control. A volume of 1 ml buffer A (40 mM Tris-HCl, 1 mM dithiothreitol (DTT), 1 mM EDTA, 0.1 mM phenylmethanesulphonylfluoride, pH = 7.4) [88] was added, the samples freeze-thawed three times (alternating between -70°C and 37°C) and then centrifuged at 8000 g for 20 min at 4°C. The cell lysate supernatants were aspirated, mixed and kept on ice. Reactions were performed in 50 ml glass tubes in duplicate. Whatman 2 filter paper (Merck) was folded lengthwise and inserted into 2 ml open-ended microfuge tubes onto which 40 μ l hydroxide of hyamine (PE Applied Biosystems, California, USA) was absorbed to trap released 14 CO₂. Two hundred microlitres of cell lysate supernatant was pipetted to the bottom of the glass tubes on ice. This was followed by 50 μ l of reaction mixture containing 7.2 μ M 14 C L-ornithine (100 nCi) and 40 μ M pyridoxal-5-phosphate (PLP) in buffer A, or 7.2 μ M 14 C AdoMet (50 nCi) only, in buffer A. Filter paper-containing tubes (standing upright inside the glass tubes) were inserted at the bottom of the glass tubes, followed by a rubber stopper to prevent CO₂ escape.

The assays were allowed to take place at 37°C for 30 min (ODC) or 60 min (AdoMetDC) in a ZHWY-110X shaking water bath (Shanghai ZHICHENG Analytical Instruments Manufacturing Co., Shanghai, China). The reactions were terminated with the injection of 500 µl 30% trichloro-acetic acid and free ¹⁴CO₂ was diluted with regular CO₂, by the addition of 500 µl 0.1 M NaHCO₃. The tubes were once again incubated for 30 min (ODC) or 60 min (AdoMetDC) at 37°C. The filter papers were transferred into 4 ml Pony-Vial H/I tubes (PE Applied Biosystems) and 4 ml of Ultima Gold XR scintillation fluid (PE Applied Biosystems) was added. The radioactivity was determined with a Tri-Carb series 2800 TR liquid scintillation counter (PE Applied Biosystems) until at least 10000 events were recorded for each sample. The average disintegrations per minute (DPM) was calculated from the average counts per minute (CPM) corrected for quenching as determined by ¹⁴C-standards. The results were analysed with QuantaSmart (PerkinElmer, Connecticut, USA) software and total activity was calculated (Eq. 3.2)

$$\text{Total activity} = \text{DPM} \times \text{nmol substrate} / \text{ml cell lysate} \times \text{min incubation time} \quad \dots\dots \text{Equation 3.2}$$

3.2.2 Drug treatment for the transcriptomics investigation

Parasites were synchronised by consecutive sorbitol treatments, as described in section 2.2.2, for three generations [171]. Drug treatment with the combination of 5 mM DFMO and 5 µM MDL73811 occurred in the late schizont stage (42 hpi) at ~2% parasitaemia and 3% haematocrit. After schizogony these parasites proliferated up to a parasitaemia of about 10% in both the treated and untreated cultures. Treatment was performed in duplicate (i.e. two biological replicates, assigned A and B) alongside untreated controls. Culture medium (with and without drug) was replaced halfway through the time course (i.e. about 18 hpi), but before the first sampling, to prevent metabolic stress of the parasites. Drug treated and untreated samples of 15 ml (10% parasitaemia and 3% haematocrit) were harvested at three time points within the trophozoite stage ($t_1 = 19$ hpi, $t_2 = 27$ hpi and $t_3 = 34$ hpi), based on the morphology of untreated parasites after microscopic inspection of Giemsa-stained thin smears. These were centrifuged at 2500 g for 5 min, the supernatant aspirated and replaced with 15 ml PBS. The pellet was resuspended by pipette-mixing, centrifuged at 2500 g for 5 min and the supernatant aspirated once more. The PBS-washed infected erythrocyte pellet was stored at -70°C until RNA isolation could be performed.

3.2.3 RNA isolation

RNA was isolated under RNase-free conditions according to the Chomczynski and Sacchi [208] method with a few additional lysis steps. The monophasic, phenol/guanidine thiocyanate solution in TRI-Reagent inhibits RNase activity and lyses the sample material. The homogenate is then separated into aqueous and organic phases by the addition of chloroform followed by centrifugation. RNA partitions in the aqueous phase, DNA in

the interphase and proteins in the organic phase. The RNA was then precipitated from the aqueous phase with ethanol (EtOH).

Total RNA was extracted from frozen infected erythrocyte pellets collected from 15 ml culture samples with the RNeasy (Qiagen, Germany) kit. The erythrocytes were lysed by freeze-thaw, but to ensure optimal parasite lysis three additional steps were performed. A volume of 1.2 ml lysis buffer was added to each pellet, which was then centrifuged for 2 min at 15700 g through a QIA-Shredder column (Qiagen) for physical rupture. The flow-through was split in two aliquots and 600 μ l TRI-Reagent was mixed with each in a 2 ml microfuge tube. After 5 min incubation at room temperature, 400 μ l chloroform was added, vortexed and incubated at room temperature for 10 min. The samples were centrifuged at 15700 g for 15 min and the upper aqueous phase of each was transferred to a clean tube without disturbing the interphase. The RNA was precipitated with 700 μ l 70% EtOH; the aliquots were combined and loaded onto RNeasy columns. The RNA was washed several times according to the kit instructions with two different buffers and a 15 min on-column treatment with 27 units (U) DNaseI (Qiagen) was performed to degrade any residual gDNA contamination of the RNA. The RNA was finally eluted with RNase-free H₂O and the concentration was determined by measuring the absorbance at 260 nm by ultraviolet (UV) spectrophotometry with a NanoDrop-1000. The absorbance is multiplied by one absorbancy unit, which equals 40 ng/ μ l for RNA [209]. Purity from protein contamination was estimated from the 260 nm/280 nm ratio, which should be 1.8 – 2, as proteins have maximum absorbance at 280 nm [209]. RNA was stored at -70°C to retain stability until cDNA synthesis.

RNA integrity was assessed with denaturing formaldehyde/agarose gel electrophoresis. All buffers were prepared using diethyl pyrocarbonate (DEPC)-treated H₂O (3 h treatment at 37°C with 0.1% DEPC in MilliQ H₂O and autoclaved twice to eliminate residual DEPC), glassware was rinsed with 0.5 M NaOH and disposable plastic was autoclaved twice. Gels consisting of 1.2% (w/v) agarose in FA buffer [20 mM 3-(N-morpholino)propanesulfonic acid (MOPS, SIGMA), 5 mM sodium acetate, 1 mM EDTA] with 0.67% (v/v) formaldehyde and 0.1 μ g/ml ethidium bromide were prepared. Samples of 2 μ g RNA were mixed with 5 x RNA loading buffer [0.16% (w/v) bromophenol blue in 20% (v/v) glycerol containing 4 mM EDTA (pH 8), 2.66% (v/v) formaldehyde and 30.84% (v/v) deionised formamide], incubated at 65°C for 5 min and then cooled on ice before loading onto the gel. The formaldehyde and the formamide in the buffers function to denature RNA secondary structures. Electrophoresis was performed using a 10 x 14 cm electrophoresis system with FA buffer. A voltage of 5 V/cm gel was applied for 2 h (~50 V) and the gel was visualised on a UV transilluminator (Spectroline TC-312 A) at 312 nm.

3.2.4 cDNA synthesis

Due to the limited amount of RNA (15 to 20 µg) obtained from the early time points, an RNA pool consisting of equal ratios of all twelve samples to be used as common reference (reference design microarray experiment) could not be compiled. The 12 µg RNA required for cDNA synthesis per sample was therefore aliquoted and the remaining RNA from both sets of biological replicates (A, B) was pooled to obtain a representative RNA reference pool (144 µg RNA in total). First-strand cDNA synthesis was initiated from 12 µg of total RNA with 775 pmol random primer 9 (New England Biolabs, Massachusetts, USA) and 250 pmol oligo-dT₂₅ (Integrated DNA Technologies, Iowa, USA) by incubation at 70°C for 10 min followed by cooling on ice for 10 min. Reverse transcription and amino-allyl incorporation were performed simultaneously as described [210], but the reaction time was extended overnight at 42°C using 480 U of SuperScript III RNase H⁻ reverse transcriptase (Invitrogen), 10 mM DTT and a mixture of deoxynucleotide triphosphates (dNTPs) in a 2A:1C:1G:2U/T ratio [1 mM deoxyadenosine triphosphate (dATP), 500 µM deoxycytidine triphosphate (dCTP), 500 µM deoxyguanosine triphosphate (dGTP), 500 µM deoxythymidine triphosphate (dTTP) and 500 µM aminoallyl-deoxyuridine triphosphate (dUTP) from Fermentas Life Sciences, Ontario, Canada]. The high A+T mixture of dNTPs was used to provide sufficient nucleotides for A+T-rich cDNA synthesis of *P. falciparum*. Contaminating RNA was removed by hydrolysis with 0.5 M EDTA and 1 M NaOH at 65°C for 15 min and the reactions were purified with the Wizard SV Gel and PCR Clean-Up System (Promega, Wisconsin, USA) according to the manufacturer's recommendations. The kit works on the principle that DNA binds to a silica matrix in the presence of chaotropic salts [211]. These salts are then removed with an alcohol-based wash buffer and the DNA is eluted in a low-ionic-strength solution or water. In the order of 6 – 8 µg cDNA was obtained from 12 µg RNA starting material. The cDNA was divided into aliquots of 2 µg each, which were dried under vacuum and stored at -20°C to retain stability.

3.2.5 Oligonucleotide array spotting and slide post-processing

Long 70-mer oligonucleotides, previously designed based on uniqueness within the genome and proximity to the 3' end of the gene open reading frames [210], were spotted in-house at the Lewis-Sigler Institute Microarray Facility (Princeton University) onto poly-lysine coated glass slides. The oligonucleotide identifiers and sequences are provided (Supplementary CD). The oligonucleotides were cross-linked onto the slides by exposure to 60 mJ UV in a Stratalinker. Post-processing was performed as described [210] by soaking the slides in a mixture of 3x saline sodium citrate (SSC) and 0.2% sodium-dodecylsulphate (SDS) at 65°C for 5 min followed by MilliQ H₂O for 30 s. They were rinsed in EtOH and then dried by centrifugation at 200 g for 5 min. The oligonucleotide spots were rehydrated by soaking the slides for 1 min in 0.5xSSC and the slides were then quick-dried on a heat block at 99°C for 1 - 2 s. Blocking solution was prepared by dissolving succinic acid anhydride in 1-methyl-2-pyrrolidinone to obtain a 1.6% (w/v) solution and adding 15 ml 1 M sodium borate (pH 8) immediately afterwards as buffer. The slides (on slide-rack) were plunged vigorously up and down in the

buffering solution for 30 s while keeping them beneath the level of the solution. These were incubated for another 5 min on a horizontal shaking platform at low speed and subsequently removed from the solution and the excess blocking solution drained by lifting and tilting the rack for 5 s. The slides were submerged into MilliQ H₂O and gently pushed back and forth for 5 s and then incubated for 60 s. The blocking step was repeated with the same buffered blocking solution and plunging for 30 s, followed by incubation with gentle shaking for 5 min. The slides were again rinsed in MilliQ H₂O with plunging for 10 s, followed by a brief rinse with 95% EtOH and subsequently dried by centrifugation for 5 min at 200 g.

3.2.6 Cy dye cDNA labelling

The aminoallyl-dUTPs that were incorporated during cDNA synthesis were coupled to either Cy3 (reference pool) or Cy5 (samples) fluorescent dyes (Amersham Biosciences) in 0.1 M NaHCO₃/Na₂CO₃ (pH = 9.0) for a minimum of 1 h in the dark at room temperature. Free dye was removed with DNA Clean and Concentrator-5 columns (Zymo Research, California, USA). The kit works on the same principle as the Wizard SV Gel and PCR Clean-Up System Wizard SV Gel and PCR Clean-Up System (described in section 3.2.4). The samples were eluted through the columns and loaded onto the membrane a second time before washing with 200 µl wash buffer. The wash step was repeated and the samples eluted with 20 µl elution buffer. The fluorescently labelled cDNA was kept in the dark for a brief period (1-2 hours) until the hybridisations were set up. Labelling efficiency was calculated (Eq. 3.3) and should ideally be at least 10 labelled nucleotides in 1000 for hybridisation purposes.

$$\text{Labelling efficiency (number of labelled nucleotides per 1000)} = \frac{\text{pmol dye} \times 324.5 \text{ pg/pmol}^a}{\text{ng DNA}} \quad \dots\dots\text{Equation 3.3}$$

a. The average mass of a dNTP

3.2.7 Oligonucleotide array hybridisation, washing and scanning

The methodology of Bozdech and colleagues was followed as briefly described [210]. Post-processed slides were positioned (array-side upwards) inside a hybridisation chamber and the arrays were covered by clean dust-free lifter slips (Erie Scientific Company, New Hampshire, USA). The probe mixture was prepared by combining 25 pmol of Cy5-labelled sample and 25 pmol Cy3-labelled reference with 0.5xSSC, 0.8 mg/ml polyadenylic acid (SIGMA), 26 mM HEPES (pH 7) and 0.24% (w/v) SDS. These were denatured in a heat block at 99°C for 2 min and then cooled for 5 min at room temperature. The ~50 µl labelled cDNA probe mixture was slowly injected underneath the lifter slip covering the array, taking care not to inject bubbles. Immediately after injecting all the probes, the chamber was covered and sealed by tightening the screws. The chamber was kept horizontal and submerged in a water bath at 65°C for overnight incubation (20 h). The chambers were subsequently quickly removed from the water bath and unscrewed while being kept horizontal. The slides had been submerged one by one in washing solution 1 [0.6xSSC, 0.03% (w/v) SDS] in such a way

that the lifter slip gently lifted and settled to the bottom of the dish without scratching the arrays. After all the slides were submerged and positioned inside the slide rack, it was plunged up and down for 30 s and then incubated for about 1 min. The slides were individually transferred into another rack into washing solution 2 (350 ml MilliQ H₂O with 0.06xSSC) and as before the slide rack was plunged up and down for 30 s followed by incubation for 1 min. The slides were then dried individually in a high-speed ArrayIt microarray centrifuge (TeleChem International, Inc., California, USA). The arrays were scanned with an Axon GenePix 4000A scanner (Molecular Devices, California, USA) and the images were analysed with Axon GenePix Pro 6.0 software (Molecular Devices).

3.2.8 Data analysis

3.2.8.1 Exploratory data analysis

The GenePix default flagging parameters were applied in combination with visual inspection to assess and define spot quality. Array data were stored in the Princeton University Microarray database (PUMAdb, <http://puma.princeton.edu>). The normalised Cy5/Cy3 log₂-ratios of the data were retrieved from PUMAdb. The technical replicates were averaged (arithmetic mean) in EXCEL and data were filtered in CLUSTER 2.1.1 [212] for transcripts with 100% data present in all the time points. Hierarchical data clustering was performed using uncentered correlation and average linkage to calculate the distance between clusters in CLUSTER 2.1.1 with display in TREEVIEW 1.0.12 [212]. Hierarchical clustering is an unsupervised, agglomerative method that joins the transcript data of single genes/oligonucleotides to form groups, which are further joined and eventually results in a single hierarchical tree that can be easily visualised and interpreted [200]. The distance or similarity measure used were based on the Pearson correlation, as defined in section 2.2.3.3.1, but instead of the standard calculation (centered), uncentered correlation was performed, which assumes that the mean is zero even if not. This compensates for vectors (transcript profiles) with the same shape that are offset relative to each other by a fixed value and thus results in a standard Pearson correlation for these [212]. Average linkage indicates that the distance between the clusters were calculated using average values as opposed to minimum (single linkage or nearest neighbour) or maximum (complete linkage or furthest neighbour) values [200]. All treated and untreated data were clustered together but the treated data were also clustered with UT_{t1} (relative t₀) only. A phaseogram was compiled from mean centered, log₂-ratios that were ordered in PERL according to the phase of gene expression in the 3D7 IDC transcriptome (<http://malaria.ucsf.edu>) [91] and displayed in TREEVIEW 1.0.12. The phase and frequency of expression of the IDC transcriptome was determined with fast Fourier transform [29, 91], a complex mathematical procedure that is used to isolate individual components of signals (e.g. waves) to determine the amplitude and phase of a particular frequency component. Pearson correlation coefficients (r) are commonly used in global expression profiling [29, 62, 91] to determine the similarity between sample profiles, between replicates etc. and were calculated in EXCEL.

3.2.8.2 Differential transcript abundance analysis

3.2.8.2.1 Linear models for microarray data (LIMMA) analysis

For differential transcript abundance analysis, data quality and normalisation methods were evaluated using data diagnostic tools from the MARRAY software package in R [213] on GenePix data and flagged values received a zero weight. Background subtraction (offset = 50) and robust spline normalisation were applied within each array, followed by Gquantile normalisation between arrays due to the common reference design of the microarray experiment. Differential abundance analysis was performed with the linear models for microarray data (LIMMA) software package within R (<http://www.r-project.org/>, [206, 214]). With a common reference design, LIMMA is similar to ordinary analysis of variance or multiple regression except that a linear model is fitted to the data for every oligonucleotide. Significance is calculated with moderated t-statistics using a simple Bayesian model in order to make the analyses robust even for a small number of arrays [206]. Differential abundance was calculated compared to UT_{t1} , defined as relative t_0 . Genes in at least one treated time point with transcript abundance greater than 1.7-fold (\log_2 -ratio ≥ 0.75 or ≤ -0.75) in either direction compared to relative t_0 , and p-values (adjusted for multiple hypothesis false discovery rate) of less than 0.05, were regarded as differentially affected. Data within these limits of transcripts represented by multiple oligonucleotides were averaged.

3.2.8.2.2 EDGE time course analysis

Differential abundance analysis was in addition performed with EDGE 1.1.208 software [215] on \log_2 -ratios normalised in PUMAdb. EDGE was specifically designed for microarray time course experiments. It models the expression over time and calculates the statistical significance by considering sources of dependence over time [215]. EDGE was applied with a Q-value cut-off of 0.1% ($p < 0.02$) for significance and no fold change cut-off. Since the software was designed to determine differential expression over time e.g. treated over three time points versus untreated over three time points, it had to be forced to compare all the treated time points to UT_{t1} (relative t_0) by defining the covariates such that instead of providing the replicate data of UT_{t2} and UT_{t3} , the data of UT_{t1} were repeatedly used for all three untreated time points.

3.2.8.3 Additional data analysis

The differentially affected transcripts (LIMMA dataset) were classified into functional groups using gene ontology (GO) terms obtained from the database for annotation, visualisation and integrated discovery (DAVID, <http://david.abcc.ncifcrf.gov/>, [216]) and PlasmoDB 5.3 (<http://www.plasmodb.org>, [217]). The GO identifiers were sorted in EXCEL.

The LIMMA dataset was also compared with the PlasmoDB 5.3 general feature format file (.gff file) to search for clusters of adjacently located genes with differentially affected transcripts, where a cluster was regarded as four or more genes within a window of six adjacent genes. The analysis was performed in EXCEL.

To investigate the possible enrichment of the LIMMA dataset for transcripts of proteins functionally connected to polyamine and methionine metabolism, the dataset was manually compared with the *in silico* predicted *P. falciparum* interactome [113] of PfAdoMetDC/ODC with DHPS/PPPK (PF08_0095) as control.

3.2.9 Real-time PCR validation of differential transcript abundance data

The differential abundance analysis was validated by performing the polymerase chain reaction (PCR) in real-time using a LightCycler 1.5 and FastStart DNA MasterPLUS SYBR Green I kit (Roche Diagnostics, Mannheim, Germany). Primers with a melting temperature (T_m) around 55°C and a product length of 150 - 170 bp were designed using Oligo v.6.71 software (Table 3.1). The relative abundance of three transcripts with increased (PFL1885c, PFD0285c, PFF0435w) and three with decreased (PF08_0131, PFD0830w, PFI1090w) abundance levels were confirmed. Real-time PCR was performed in triplicate on the cDNA sample with maximum fold change compared to relative t_0 . Comparable starting levels of cDNA across the different samples were obtained by adjusting template concentrations according to the relative amount of a putative cyclophilin (PFE0505w). The thermocycling programme was as follows: A 10 min pre-incubation period at 95°C was followed by 35 cycles of 10 s at 95°C, 5 s at 55°C and 7 s at 72°C, according to the manufacturer's instructions. After amplification, melting curve analysis was performed to exclude primer-dimer interference. Fold change was calculated compared to relative t_0 .

Table 3.1 Real-time PCR primer information

| PlasmoDB | Annotation | 5' - 3' Primer sequence | T_m^a | Size (bp) |
|-----------|--------------------------------|------------------------------------|---------|-----------|
| PFE0505w | Cyclophilin Fwd | AAT TCT TTG ACC ATC TTA ATC ATT C | 54.8 | 167 |
| | Cyclophilin Rev | CAA AAC AAT TTT ACT TCC TTG GGT TA | 56.9 | |
| PFD0285c | Lysine decarboxylase Fwd | AGA GGG ATA TGG ATT GGT AGA | 55.9 | 161 |
| | Lysine decarboxylase Rev | TTC TCT TCA TGT ATG ATA CAG TA | 53.5 | |
| PFF0435w | Ornithine aminotransferase Fwd | CAA CTT TGG TCC ATT CGT ACC | 57.9 | 165 |
| | Ornithine aminotransferase Rev | GCT ACA CCT GGG AAA TAA CTA TC | 58.9 | |
| PFL1885c | Ca/calmodulin prot kinase2 Fwd | CGC ATT GGA AGC ATT ACA TTC TA | 57.1 | 154 |
| | Ca/calmodulin prot kinase2 Rev | ACA TCT CAT ATT CAT TGA TGG ACT G | 58.1 | |
| PFI1090w | AdoMet synthetase Fwd | TTT AGA TTA CAA AAC GGC AGA GAT AA | 56.9 | 160 |
| | AdoMet synthetase Rev | AGG CAT ATA ATT CTC AGT TTC ATC AG | 58.5 | |
| PF08_0131 | 1-Cys-peroxiredoxin Fwd | TAC TCC CGT TTG TAC CAC TGA | 57.9 | 162 |
| | 1-Cys-peroxiredoxin Rev | ATA TCC CAC TTA TCT AGG TTT C | 54.7 | |
| PFD0830w | DHFR/TS Fwd | AAC CTT TAA GCA ATA GGA TAA ATG | 54.2 | 164 |
| | DHFR/TS Rev | TTG ATA AAC AAC GGA ACC TC | 53.2 | |

a. Melting temperature was calculated with the formula: $T_m = 69.3 + (0.41 \times \%GC) - (650/\text{primer length})$ [218].

Fwd = forward and Rev = reverse primers.

3.3 RESULTS

3.3.1 Ensuring the correct treatment dosage for the functional genomics investigations

The IC_{50} s of DFMO ($IC_{50} = 0.53$ mM) and MDL73811 ($IC_{50} = 0.8$ μ M) for 3D7 *P. falciparum* under the particular laboratory conditions were determined in section 2.3.2. In a previous suppressive-subtractive

hybridisation/microarray study of DFMO-treated *P. falciparum*, a treatment-dose of 10 mM was used [219]. In the combination with MDL73811 it was decided to use only 5 mM DFMO (i.e. 9x IC₅₀), which was previously demonstrated to inhibit ODC of the chloroquine-resistant FCR-3 strain by more than 99% [154], and 5 μM MDL73811 (i.e. 6x IC₅₀), since MDL73811 is approximately 1000 times more active than DFMO against *P. falciparum in vitro* [153]. Treatment at these high concentrations was to ensure complete parasite arrest in order to prevent parasites escaping cytostasis and causing asynchrony [154]. For the same reason, the drugs were added in the schizont stage as opposed to the ring stage. On occasion, cytostatic arrest was achieved only for a subset of the parasite population treated in the early ring stage due to the synchronisation window being between 8 and 12 h, which resulted in escape and normal progression of the more mature ring forms. However, treatment in the schizont stage ensured arrest of the whole population and the addition of DFMO in the schizont stage was previously shown to affect neither merozoite invasiveness nor ring development [88, 220].

To ensure that both drugs contributed equally to the growth arrest at the dosages applied, a parasite growth morphology study with 5 mM DFMO and 5 μM MDL73811 separately and in combination was performed. This was additionally important since the IC₅₀s could be determined at an inoculum of maximum 5 (1% parasitaemia and 5% heamatocrit) as described in section 2.3.2, but to obtain enough RNA for microarray analysis, a parasite population of at least an inoculum of ~30 (10% parasitaemia, 3% haematocrit) was required [29, 108]. Parasite morphology was carefully monitored at 6 h intervals to determine the exact sampling times (just before and during growth arrest) for the functional genomics investigations. Both drugs on their own caused growth arrest from the trophozoite stage with no visible effect during the ring stage, as reported [153, 154]. The growth arrest was clear from about 27 hpi when compared to the untreated controls, but not in the samples taken 6 h prior. However, parasites treated with the drug combination appeared smaller and slightly more delayed compared to the separate treatments (Fig. 3.2), which can be attributed to the additive effect of the two drugs.

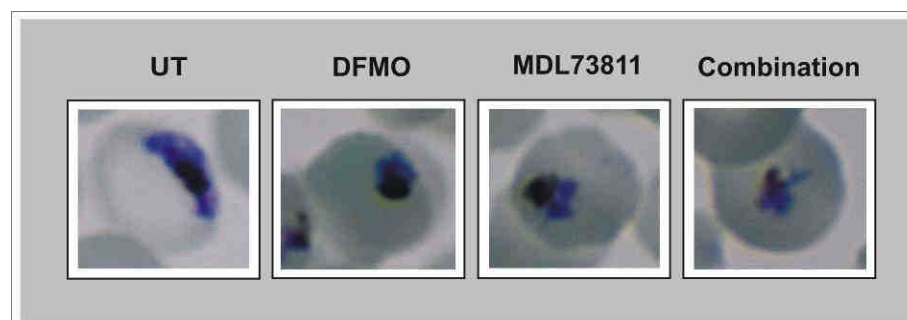


Fig. 3.2 Giemsa-stained thin smears of untreated *P. falciparum* and cultures treated with either 5 mM DFMO or 5 μM MDL73811 or the combination of 5 mM DFMO/5 μM MDL73811 result in growth arrest at ~27 hpi.

Parasite sampling times for the functional genomics investigations (after treatment with the combination of 5 mM DFMO and 5 μ M MDL73811) were subsequently selected to be in the early ($t_1 = 19$ hpi), mid ($t_2 = 27$ hpi) and mature ($t_3 = 34$ hpi) trophozoite stages (before and during cyto-stasis) such that the expression period of PfAdoMetDC/ODC (12 to 40 hpi) would be spanned. The complete inhibition of AdoMetDC and ODC activities of the 3D7 parasite strain was confirmed under these treatment conditions with radio-labelled substrate (S-adenosyl-L-[14 C]methionine and L-[14 C]ornithine) assays of the decarboxylase activities after PfAdoMetDC/ODC co-inhibition. No decarboxylase activity above background was observed in the treated samples (T_{t_1} , T_{t_3}) compared to normal increasing enzyme activities of ODC and AdoMetDC in the untreated controls (UT_{t_1} , UT_{t_3} , Fig. 3.3), as expected from previous reports [88]. Enzyme inhibition by both DFMO and MDL73811 are specific and irreversible [147].

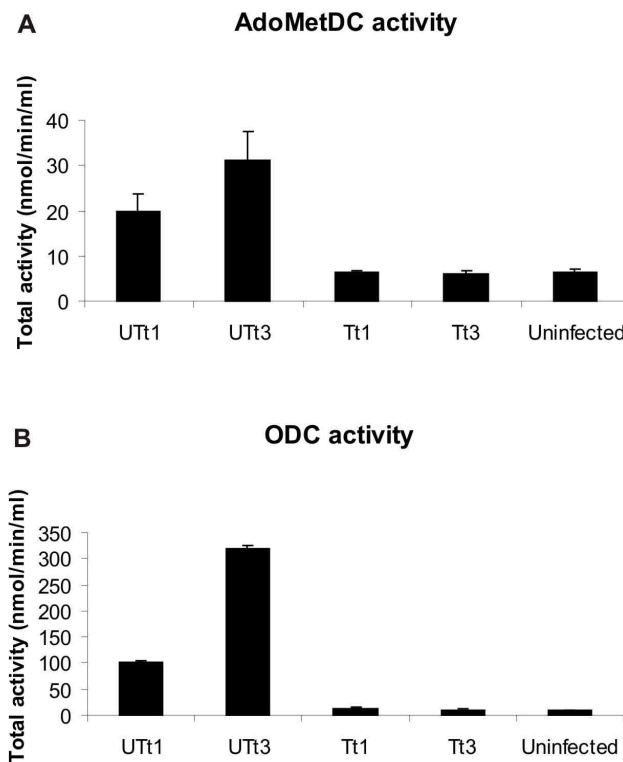


Fig. 3.3 Total activity (nmol/min/ml lysate) of **A**) AdoMetDC and **B**) ODC, based on the release of $^{14}\text{CO}_2$ from lysates of untreated and DFMO/MDL73811-treated parasites after incubation with S-adenosyl-L-[14 C] methionine or L-[14 C]ornithine, respectively ($n=2$). Cultures were sampled at $t_1 = 19$ hpi and $t_3 = 34$ hpi.

3.3.2 Transcriptomics sampling, RNA isolation and cDNA synthesis

Based on the parasite growth morphology study, DFMO/MDL73811-treatment was performed in the schizont stage at about 42 hpi (real t_0) and parasites were sampled at $t_1 = 19$ hpi, $t_2 = 27$ hpi and $t_3 = 34$ hpi of the next life cycle, for the isolation of RNA to be used as starting material in the subsequent microarray analysis (Fig. 3.4).

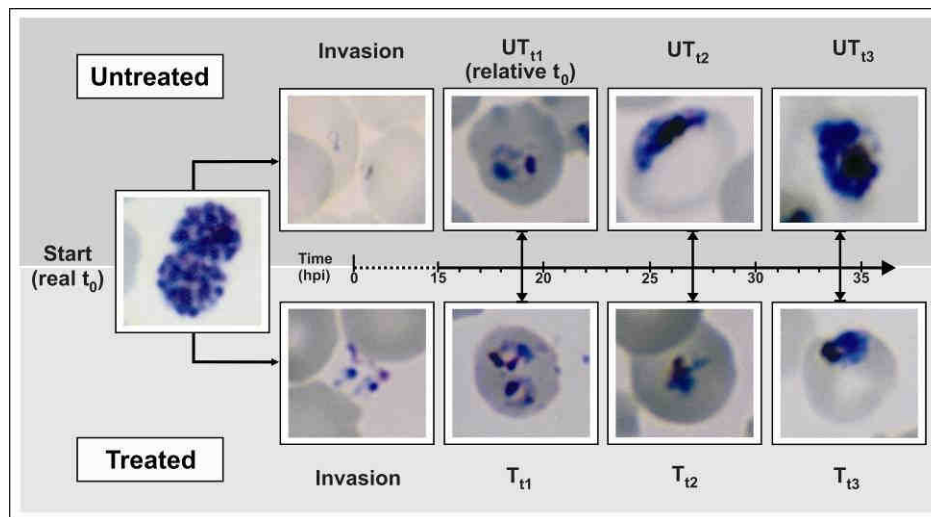


Fig. 3.4 Transcriptomics sampling times. Giemsa-stained thin smears of untreated *P. falciparum* and cultures treated with the combination of DFMO/MDL73811. Samples were taken at $t_1 = 19$ hpi, $t_2 = 27$ hpi and $t_3 = 34$ hpi. Growth arrest was morphologically visible from T_{t_2} .

The purity and quality of the RNA were assessed with denaturing agarose/formaldehyde gel electrophoresis (Fig 3.5). The sharp definition of the 28S and 18S rRNA species, higher intensity of the 28S band and minimal smearing confirmed the integrity of the samples. Furthermore, 260/280 nm ratios between 1.9 and 2.0 were obtained, which indicated purity from protein contamination [209].

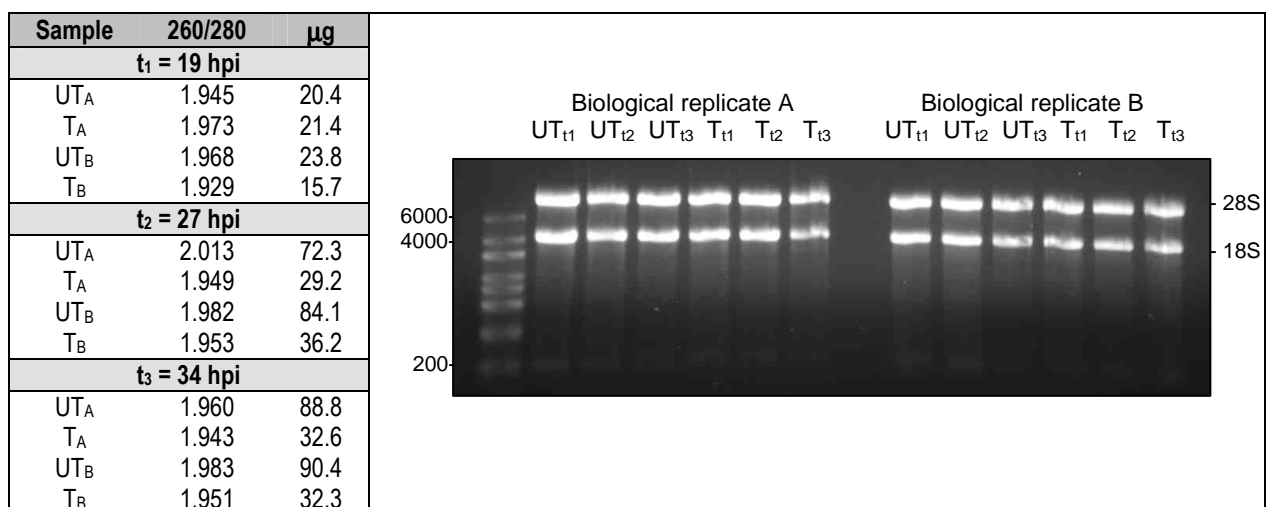


Fig. 3.5 The total RNA yield obtained from 15 ml cultures (10% parasitaemia, 3% haematocrit) over the time course is tabled and the 260/280 nm ratios are shown. RNA integrity was further assessed with denaturing agarose/formaldehyde electrophoresis where 2 μg samples were loaded onto a 1.2% agarose/formaldehyde denaturing gel with high range RNA ladder (Fermentas Life Sciences). 28S and 18S rRNA are visible, but the 5S rRNA was removed during isolation.

Note that for mRNA enrichment purposes all RNA species smaller than 200 nucleotides (e.g. 5S rRNA and tRNA) are selectively excluded by the RNeasy protocol (RNeasy manual). Cytostatic growth arrest was observed in the RNA yields obtained since the level was approximately maintained in the treated samples from t_1 to t_3 (20 - 30 μg), whereas it increased in the untreated samples (70 - 90 μg), as expected during normal development (Fig. 3.5) [221]. The cDNA synthesis protocol [210] was optimised by increasing the amount of reverse transcriptase from 150 U to 480 U and the reaction time from 120 min to overnight. In this manner the

cDNA yield from 12 μg of total RNA was increased about 3-fold ($\sim 2 \mu\text{g}$ cDNA to $\sim 6 \mu\text{g}$ cDNA). Only 2 μg cDNA is required for sufficient labelling and hybridisation and therefore several technical replicate hybridisations could be performed from the same RNA sample.

3.3.3 Oligonucleotide microarray analysis

Transcriptional profiling of untreated versus PfAdoMetDC/ODC co-inhibited parasites was performed on non-commercial arrays spotted with 8088 70-mer oligonucleotides, which represented 5332 unique genes [210] (Supplementary CD). Note that the microarray analysis quantitates steady-state mRNA, which for any gene is a function of both the rate of transcription and the rate of mRNA decay [128], and is therefore referred to as transcript abundance here. A reference design microarray experiment was performed, i.e. the cDNA of the various samples were co-hybridised with a composite reference pool from all the samples included in the experiment. Treated and untreated samples (two biological replicates) were taken at three time points (12 samples) and two technical replicate hybridisations were performed for each. Thus a total of 24 hybridisations were performed and 20 were of acceptable quality (e.g. total number of detectable spots, limited background etc.) to be used for data analysis. Cytostasis caused arrays of treated samples to have an overall yellow appearance (similar to self-self hybridisations) compared to untreated samples at t_2 and t_3 , which had a more colourful (red, yellow, green) display typical of differential expression (Fig. 3.6). The yellow appearance was due to enrichment of the reference pool with early transcripts resulting from the parasite arrest.

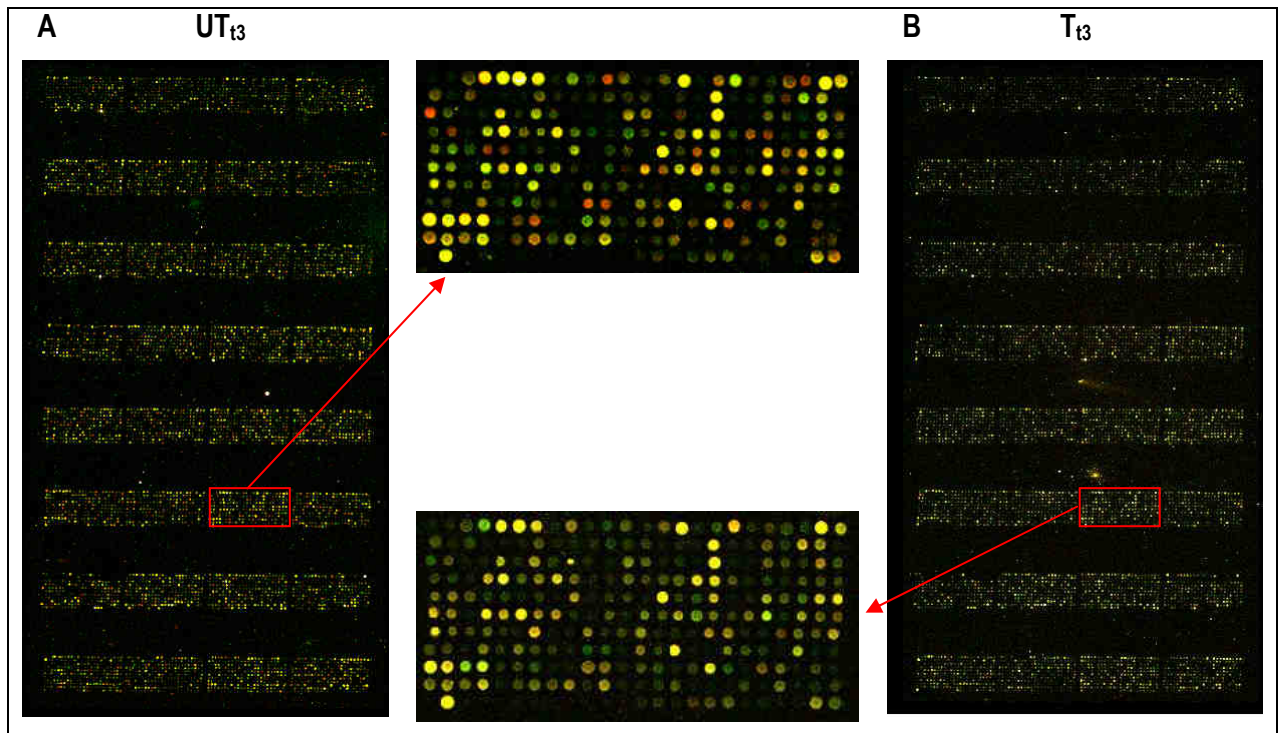


Fig. 3.6 Typical 70-mer oligonucleotide spotted arrays of **A)** UT_{t_3} and **B)** T_{t_3} with one block enlarged. The slide from T_{t_3} had an overall yellowish appearance (similar to self-self hybridisation) due to enrichment of the reference pool with early transcripts from arrested parasites, whereas the slide from UT_{t_3} was colourful as is typical of differential expression on microarray.

3.3.4 Exploratory data analysis

3.3.4.1 Hierarchical clustering of data with those of other perturbations

Exploratory data analysis was mainly performed in CLUSTER 2.1.1 with hierarchical clustering of normalised \log_2 -ratios, which was then displayed in TREEVIEW 1.0.12. The PfAdoMetDC/ODC co-inhibition data were clustered with microarray data of *P. falciparum* exposed to a series of perturbations, including several antimalarial drugs and environmental stressors (Fig. 3.7, data used by courtesy of M. Llinás, unpublished data) sampled 1, 2, 4, 6, 8, 12, 16 and 24 h post-treatment (treatment occurred at invasion). The PfAdoMetDC/ODC co-inhibition data are at the far right with the two biological replicate sets (A, B) displayed separately. The perturbation controls for the Llinás perturbation data are at the far left. Because of the different periods of sampling of the PfAdoMetDC/ODC co-inhibition data ($t_1 = 19$ hpi, $t_2 = 27$ hpi and $t_3 = 34$ hpi) and the Llinás perturbation data (1 – 24 hpi), clustering between genes (Fig. 3.7) was not informative, but when clustering between arrays (Fig. 3.8) was performed, UT_{t1} and T_{t1} as well as T_{t2} and T_{t3} respectively, clustered together and were relatively close on the hierarchical tree. UT_{t2} and UT_{t3} also clustered together but completely separately from the rest of the data along with the latest control (24 h) of the Llinás perturbation data. Biological replicates always clustered together. These results indicated the reproducibility of the PfAdoMetDC/ODC co-inhibition data in terms of replicates, but more importantly it confirmed that the data obtained were comparable with other *P. falciparum* datasets (based on the clustering together of the untreated controls) e.g. the 3D7 IDC transcriptome [91]. Furthermore, the relative closeness of the UT_{t1} with T_{t1}, T_{t2} and T_{t3} again illustrated the effect of cyto-stasis, whereas UT_{t2} and UT_{t3} clustered on their own branch at the bottom of the tree due to normal parasite progression. The data shown in Fig. 3.8 are those for the transcripts of PfAdoMetDC/ODC in all the different perturbations.

Hierarchical clustering was performed with both the complete set of PfAdoMetDC/ODC data (treated and untreated) and the treated parasite data with UT_{t1} only (Supplementary CD and website at http://genomics-pubs.princeton.edu/PfAdoMetDC_ODC). The latter comparison revealed two large arrest clusters that were maintained at either high (red) or low (green) transcript abundance with a correlation coefficient of 0.94 for both clusters. Clusters of transcripts with differential abundance over the time course were also revealed, including one that contained several polyamine pathway-related transcripts (Fig. 3.9).

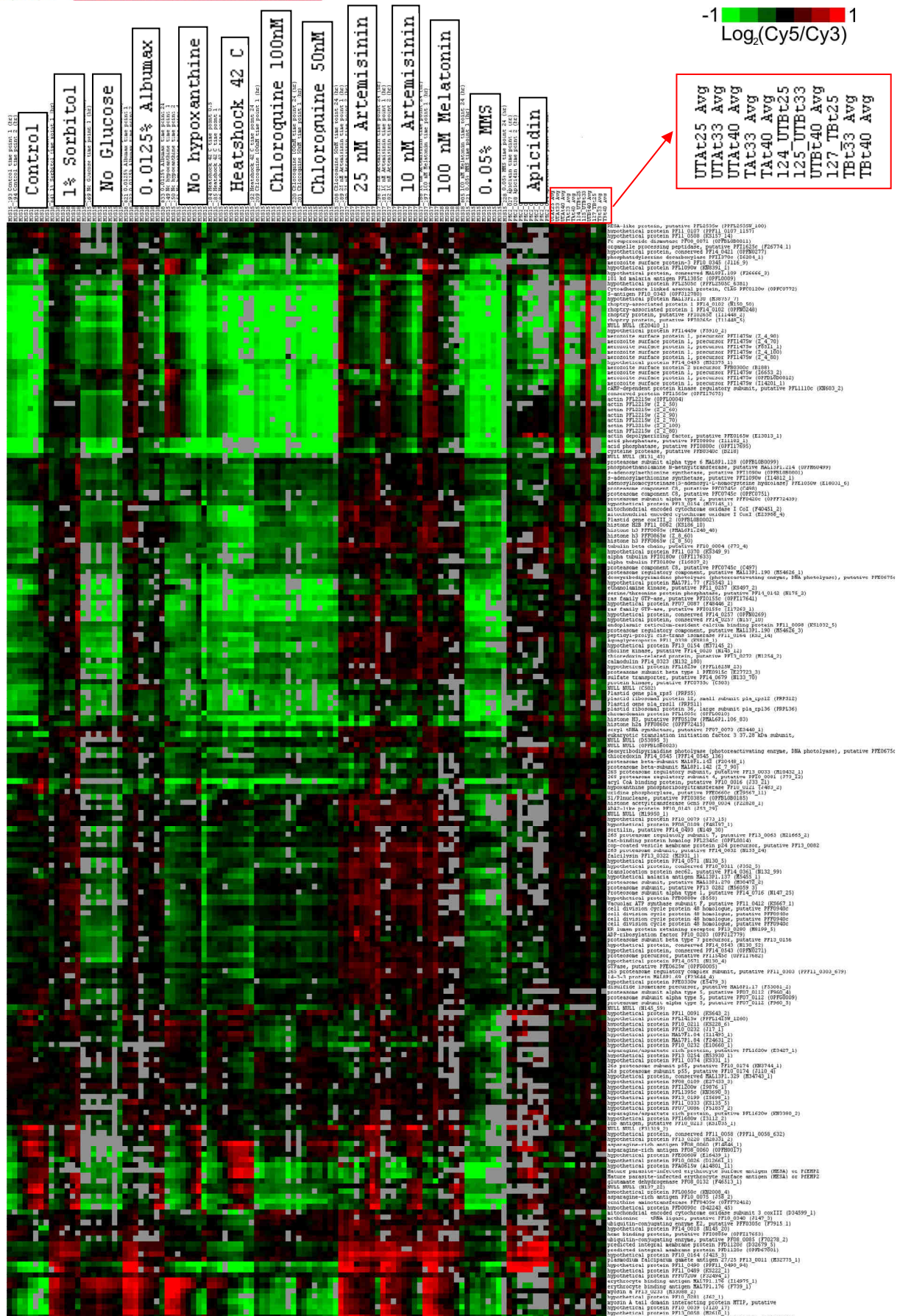


Fig. 3.7 Hierarchical data clustering between genes of the PfAdoMetDC/ODC co-inhibition data ($t_1 = 19$ hpi, $t_2 = 27$ hpi and $t_3 = 34$ hpi) and the Linás perturbation data (1 to 24 hpi) was not informative due to the different sampling periods of the two sets (M. Linás, unpublished data). MMS = methyl methane sulfonate.



Fig. 3.8 Hierarchical data clustering between arrays of the PfAdoMetDC/ODC co-inhibition data and the Llinás perturbation data indicate the effect of cytosstasis with the clusters of UT₁₁ and T₁₁ as well as T₁₂ and T₁₃ being relatively close, whereas UT₁₂ and UT₁₃ clustered completely separately, albeit with the latest control of the Llinás perturbation data (M. Llinás, unpublished data). The data shown are those for the transcript of PfAdoMetDC/ODC. The sampling times indicated are post-treatment.



Fig. 3.9 A tight cluster (correlation coefficient = 0.89) containing several polyamine pathway transcripts (framed), including PfAdoMetDC/ODC, produced by hierarchical data clustering of UT₁₁ with T₁₁, T₁₂ and T₁₃.

3.3.4.2 Hierarchical clustering of data related to polyamine and methionine metabolism

Exploratory hierarchical clustering of the transcripts from polyamine and methionine metabolism on their own resulted in two relatively tight clusters (correlation values of 0.78 and 0.94, respectively, Fig. 3.10) indicating that gene expression of this pathway does not occur at the same time for all transcripts, i.e. it is not all in phase. The time points chosen combined with the transcriptional arrest appear to reveal a biphasic nature of polyamine and methionine metabolism gene expression, but a more sophisticated bioinformatics approach and inclusion of all the genes involved (e.g. all methyltransferases etc.) may indicate more phases. Gene expression for RNA and DNA synthesis is normally in phase in *P. falciparum* [222], but transcription of the genes of the glutathione and thioredoxin systems [222], and the pentose phosphate pathway [223], were also demonstrated not to be all in phase with at least two expression peaks in the IDC.

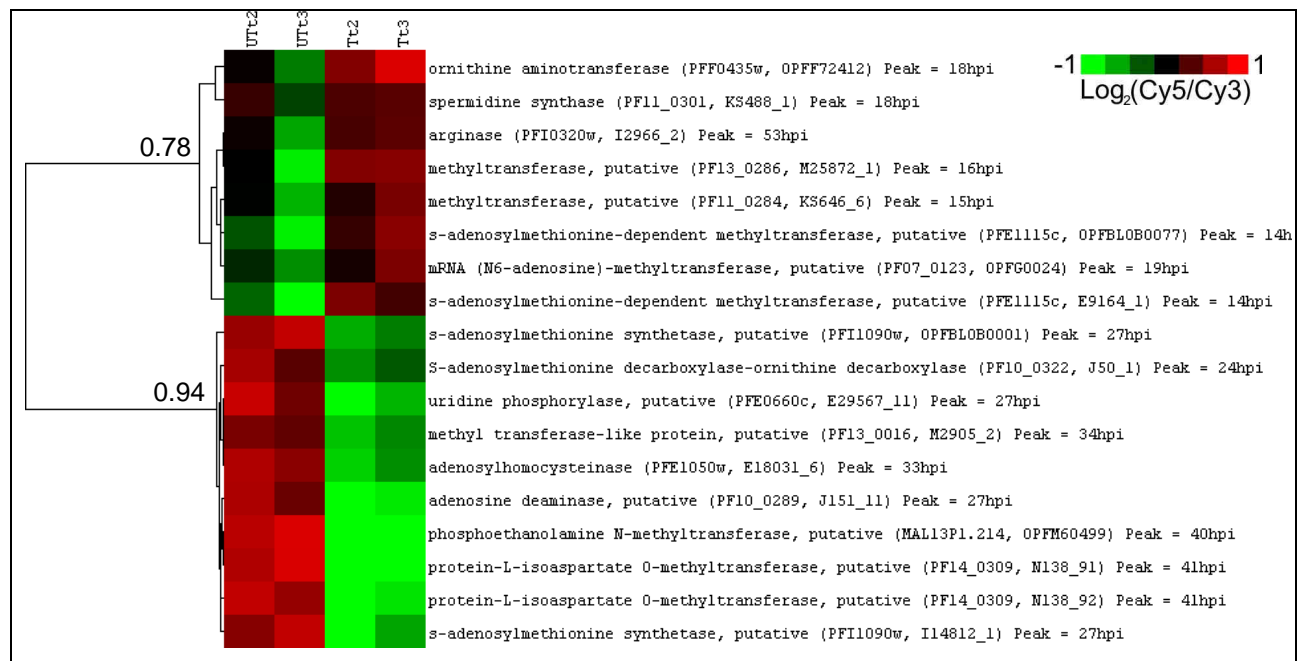


Fig 3.10 “Biphasic” segregation of the expression/peak abundance of polyamine and methionine metabolism transcripts visible as two relatively tight clusters due to the transcriptional arrest of treated samples (T_{t2}, T_{t3}) and normal progression of untreated controls (UT_{t2}, UT_{t3}). This division was particularly clear at t₂ and t₃, as demonstrated.

3.3.4.3 Phase-ordering and correlation calculations

Fast Fourier analysis was applied to calculate the apparent phase and frequency of gene expression in the IDC transcriptome [29, 91]. By ordering the PfAdoMetDC/ODC co-inhibition data according to the phase of expression, as determined for the 3D7 strain (Fig. 1.8) [91], cytosclerosis was revealed as a generalised transcriptional arrest across T_{t1} to T_{t3} with normal IDC progression visible in UT_{t1} to UT_{t3} (Fig. 3.11A). In general, expression of genes that were already transcribed before the effect of the treatment (IDC peak expression before or around t₁) were unchanged, whereas genes that were not yet transcribed (IDC peak expression in second half of 48 h cycle e.g. t₂ and t₃) showed no or low transcript abundance. Not surprisingly,

growth arrest occurred after the transcriptional arrest and was morphologically visible only from T_{12} with parasites appearing small and distressed compared to their untreated counterparts (Fig. 3.4)

In order to use the IDC transcriptome as a reference time line (i.e. of transcript expression times), Pearson correlation was used to align the PfAdoMetDC/ODC co-inhibition data with each of the one hourly time points of the 3D7 IDC transcriptome [91]. UT_{t1} (19 hpi) had the highest correlation at 14 - 15 hpi with T_{t1} to T_{t3} following closely thereafter at 15 - 16 hpi (Fig. 3.11B) as opposed to UT_{t2} and UT_{t3} , which correlates at 33 hpi and 44 hpi of the 53-hour 3D7 IDC cycle [91], respectively. This analysis corroborated the transcriptional arrest and estimated the approximate time thereof as 15 - 16 hpi (according to the 3D7 IDC transcriptome), which correlates with the start of PfAdoMetDC/ODC expression (transcript produced from 12 – 40 hpi).

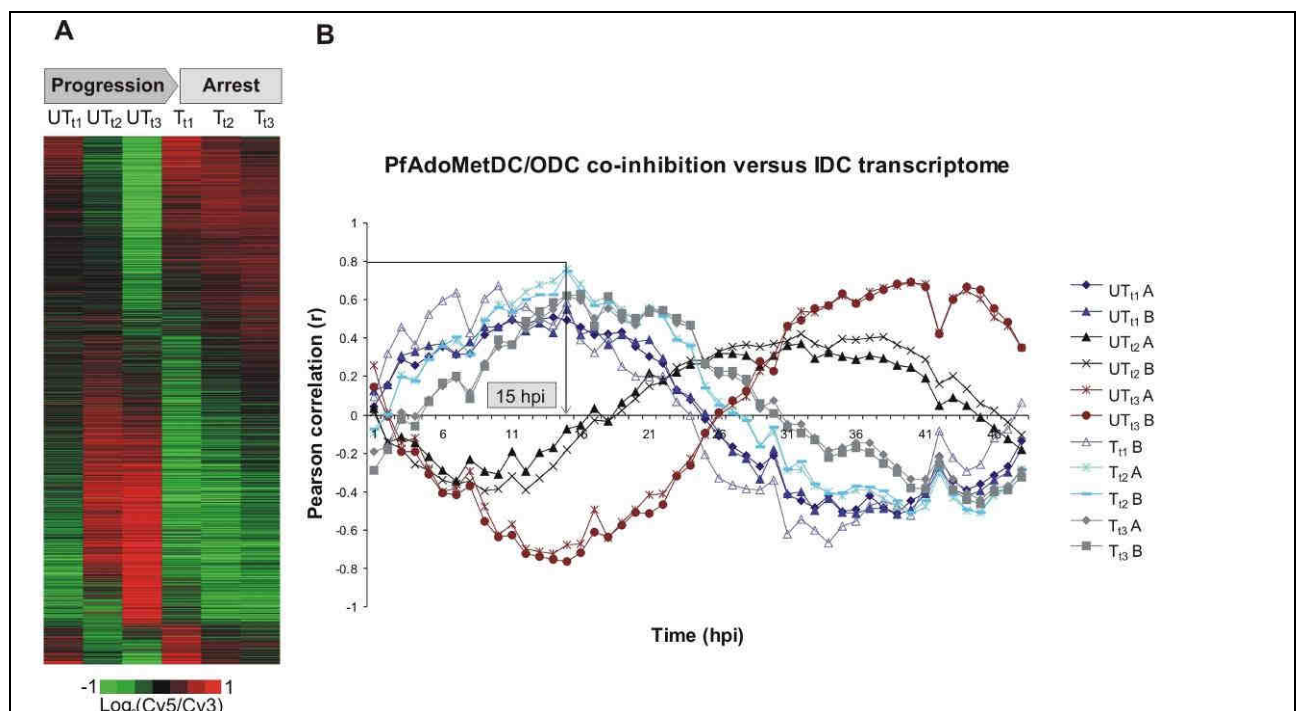


Fig. 3.11 A) A phaseogram depicting the transcriptional profiles of untreated versus PfAdoMetDC/ODC co-inhibition data over three time points (t_1 to t_3) by ordering 3206 oligonucleotides according to the phase of expression. Transcriptional arrest is visible in T_{t1} to T_{t3} . **B)** Pearson correlation between the PfAdoMetDC/ODC co-inhibition data and the one hourly time points of the 3D7 IDC transcriptome. The treated samples have a correlation profile similar to UT_{t1} (relative t_0) with the highest correlation at ~15-16 hpi, illustrating the approximate time of transcriptional arrest. Data of the respective biological replicates (A, B) are shown separately (T_{t1} had only one biological replicate due to technical difficulty).

Pearson correlation within the PfAdoMetDC/ODC co-inhibition data also indicated transcriptional arrest, since relatively close correlations were observed between the treated parasite data (T_{t1} versus T_{t2} : $r = 0.77$, T_{t2} versus T_{t3} : $r = 0.89$, T_{t1} versus T_{t3} : $r = 0.61$) and each of these compared to UT_{t1} (r ranging from 0.57 to 0.72). In contrast, data at t_2 and t_3 were uncorrelated ($r = 0.07$) and anti-correlated ($r = -0.61$) respectively compared to the matched untreated parasite data (Table 3.2). This is due to the transcriptional arrest of treated and normal progression of untreated parasites. In comparison, in the absence of transcriptional arrest, the array data of doxycycline-treated versus untreated *P. falciparum* were still highly correlated ($r = 0.8$) after 55 h [62].

Table 3.2 Pearson correlation within the PfAdoMetDC/ODC co-inhibition transcript data

| Comparison | Pearson correlation (r) |
|-----------------------------------|-------------------------|
| T _{t1} :UT _{t1} | 0.72 |
| T _{t2} :UT _{t2} | 0.07 |
| T _{t3} :UT _{t3} | -0.61 |
| T _{t2} :UT _{t1} | 0.72 |
| T _{t3} :UT _{t1} | 0.57 |
| T _{t1} :UT _{t2} | 0.77 |
| T _{t2} :UT _{t3} | 0.89 |
| T _{t1} :UT _{t3} | 0.61 |

Thus, three different analyses (phase ordering, Pearson correlation with the 3D7 IDC transcriptome [91] and within the PfAdoMetDC/ODC co-inhibition data) confirmed the transcriptional arrest observed as a result of the perturbation. Data reproducibility was calculated and technical replicates had a correlation of 0.93 and biological replicates a correlation of 0.88 on average. Reproducibility of the biological replicate can be visualised in the comparison with the 3D7 IDC transcriptome where the replicate sinusoidal curves obtained can almost be superimposed (Fig. 3.11B).

3.3.5 Differential transcript abundance analysis

Comparison of the clustered PfAdoMetDC/ODC co-inhibition data with the IDC transcriptome indicated a few genes with the same expression time but with an opposite response to the perturbation, e.g. the increased abundance of the transcript for ornithine aminotransferase (OAT, PFF0435w) and the decreased abundance of that for enolase (PF10_0155), though both have normal peak expression at 18 hpi. Hence the transcriptional arrest was not merely due to the normal mRNA abundance level of IDC co-expressed genes being maintained, but transcripts of specific genes with the same expression time were differentially affected. To identify the transcripts most affected by the perturbation, a quantitative approach was followed with LIMMA as well as EDGE analysis. However, the global transcriptional arrest caused by PfAdoMetDC/ODC co-inhibition negated the direct comparison of treated and untreated data at t_2 and t_3 , as this standard approach would have detected mainly growth/stage differences. Therefore, in differential transcript abundance analysis all treated time points were compared to UT_{t1} defined as a relative t_0 . Comparison to the real t_0 would also primarily have identified stage differences, since drug treatment was performed in the late schizont stage of the life cycle, but cytostasis and sampling occurred in the early trophozoite stage of the next cycle.

3.3.5.1 Data normalisation

Microarray data quality and normalisation methods were evaluated using data diagnostic tools from the MARRAY software package in R [213] on GenePix data (R-script on Supplementary CD). The red (Cy5) and green (Cy3) background of every array was inspected for global or localised effects and presence in one or both channels (Fig. 3.12). Local artefacts and edge effects (visible at the top in the red background image, Fig 3.12) indicated background subtraction and that a spatial normalisation approach such as print-tip LOWESS should be used as opposed to global normalisation. Background subtraction with an offset of 50 was used to

avoid negative or zero-corrected intensities [206]. However, when print-tip LOWESS was applied the red/green density plots (shown in Fig. 3.16) indicated a serious error, appearing as data degeneracy of one or more arrays. This was subsequently solved when the prerequisite of print-tip LOWESS was considered, namely that it requires data from at least 150 spots [206]. The spotter used has 32 print-tips, which each spotted 264 spots (11 rows of 24 spots each), but in a few blocks only ~120 spots had a signal because of low intensity transcripts. Thus, print-tip LOWESS was not justified, in which case global LOWESS or robust spline normalisation is recommended [206]. To avoid the global approach as explained above, robust spline normalisation, which is a compromise between print-tip and global LOWESS [206], was applied within arrays to remove systematic error such as dye bias.

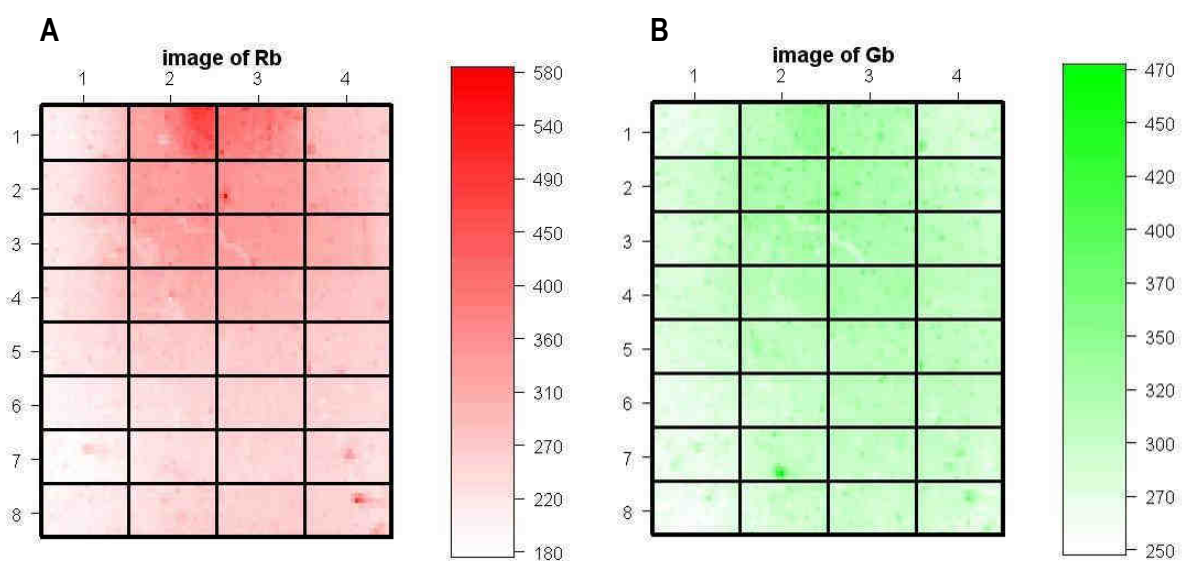


Fig 3.12 A) Red and B) green background images of a typical array (111_TAt33) presented in MARRAY. Note the localised artefacts in both images and edge effect towards the top of the array in the red background image.

Quantile normalisation was applied between arrays to ensure the same distribution of spot intensities in the green (Cy3) channel across all the arrays (adjusting the red or Cy5 channel accordingly) without changing the \log_2 -ratios (M-values). Gquantile between-slide normalisation is specifically applicable to common reference microarray experiments where the reference is labelled with Cy3, whereas Rquantile is applied in experiments where the samples are labelled with Cy3 and the reference with Cy5.

\log_2 -ratios (M) versus average intensities (A) plots were used to confirm that the applied normalisation had the desired effect. On these plots, the centre of distribution of \log_2 -ratios should ideally be zero, the ratios should be independent of spot intensity and the fitted line should be parallel to the intensity axis [205]. After performing normalisation, the data spread of the example complied better with the ideal (Fig. 3.13).

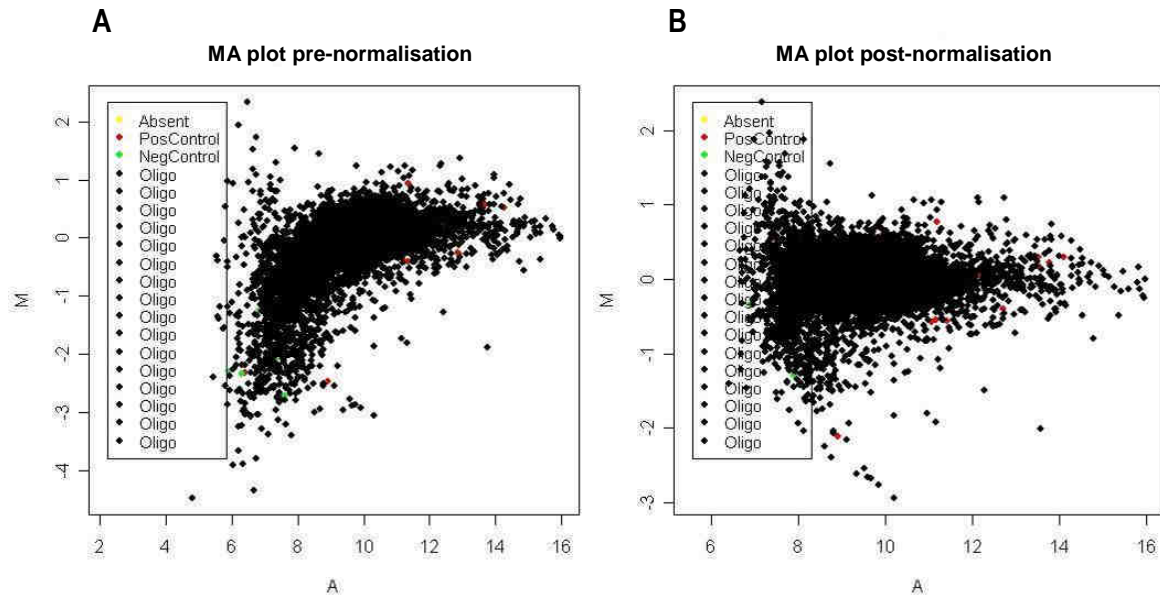


Fig 3.13 MA-plots from a typical array (125_UTBt33) **A)** before and **B)** after data transformation (background subtraction, robust spline and Gquantile normalisation). Note that the post-normalisation data comply better with the ideal, i.e. the centre of distribution of the M-values is around zero and should a line be fitted through the data, it will be parallel to the A-axis.

Robust spline normalisation in addition had a smoothing effect on the distribution of the log-ratios among the print-tip groups (Fig. 3.14), which reduced technical bias as a result of, for example, the unequal deposition of oligonucleotides or different size spots resulting from the different print-tips.

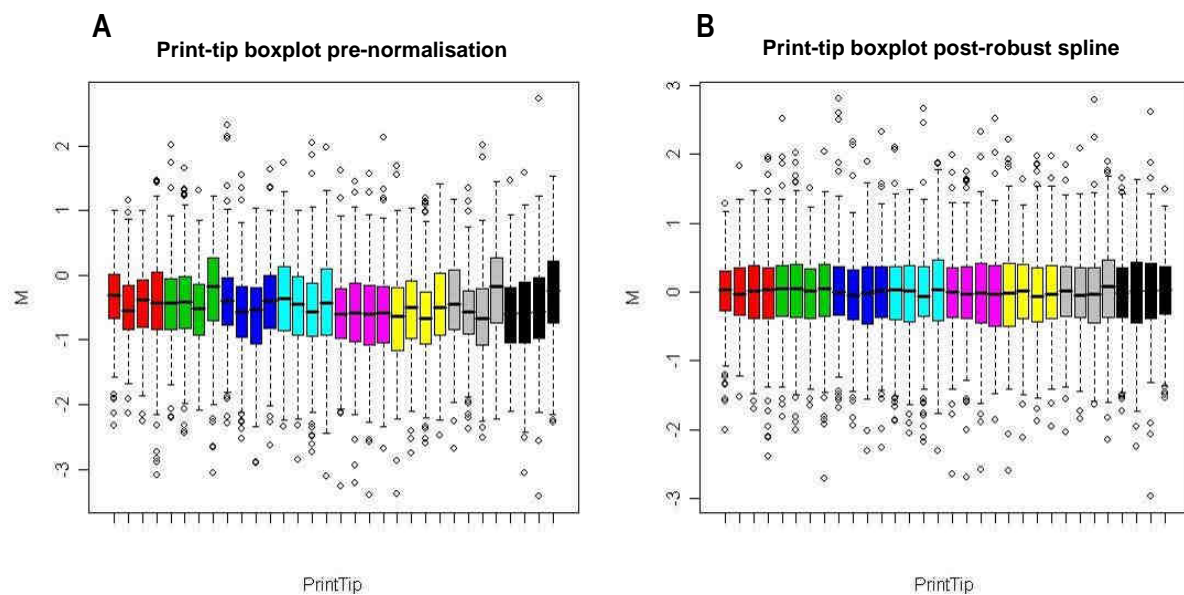


Fig 3.14 Print-tip boxplots of the log₂-ratio distributions of the 32 blocks (equivalent to the 32 print-tips) from a typical array (116_TBt25), **A)** before and **B)** after data transformation (background subtraction, robust spline normalisation).

Log₂-ratio boxplots and intensity boxplots across all arrays (Fig. 3.15) illustrated that the log₂-ratios remained unchanged although intensities across the different arrays were equalised after normalisation.

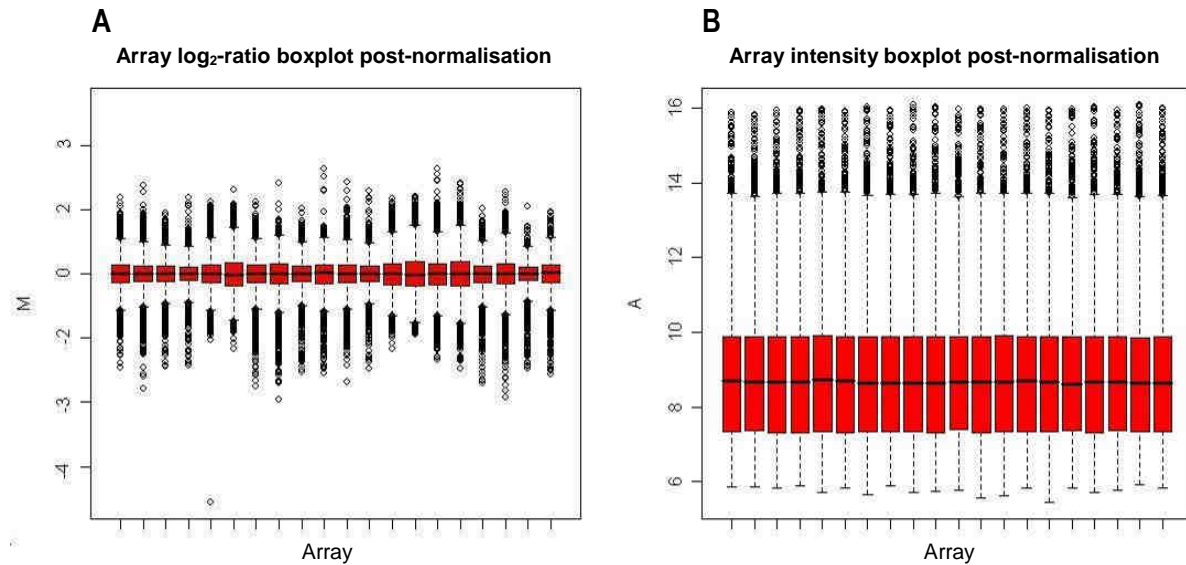


Fig 3.15 **A**) Boxplots of log₂-ratios (M) and **B**) intensities (A) across all arrays post-normalisation (background subtraction, robust spline and Gquantile normalisation). Although the intensities across the different arrays were equalised, the log₂-ratios are independent and did not change.

Red/green (Cy5/Cy3) density plots indicated a dye bias towards the green channel for several arrays prior to normalisation but this was improved revealing only one density curve for the green channel subsequent to Gquantile normalisation (Fig. 3.16). Thus, all the arrays were normalised according to the green (Cy3, reference pool) channel, enabling subsequent comparison of the log₂-ratios (Cy5/Cy3).

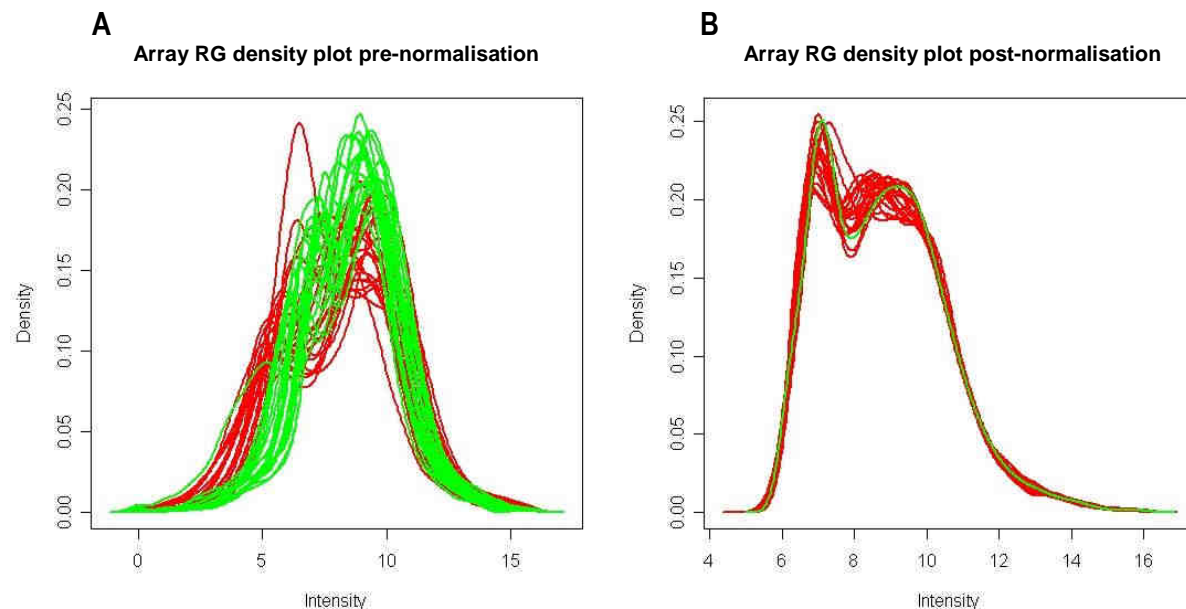


Fig 3.16 Red/Green density plots of all the arrays **A**) before and **B**) after data transformation (background subtraction, robust spline, Gquantile normalisation). Note that after Gquantile normalisation only one curve is visible for the green channel in all the arrays.

3.3.5.2 LIMMA data analysis

After obtaining a satisfactory intensity distribution within and across the arrays according to the diagnostic plots, differential transcript abundance between the samples was calculated for all the oligonucleotides in

LIMMA. Over the time course, the abundance of 538 transcripts from 5332 unique genes represented on the array, was significantly differentially affected (1.7-fold change in either direction; \log_2 -ratio ≥ 0.75 or ≤ -0.75 ; $p < 0.05$) compared to the relative t_0 (Appendix A). Of these, 171 transcripts were increased (up to 3.2-fold) and 377 were decreased (down to 5-fold), with the transcripts of 10 apparently unrelated genes falling in both categories by displaying an increase in t_1 as well as a decrease in t_2 and/or t_3 . A selected subset of the differentially affected transcripts is presented in Table 3.3, including eight transcripts from polyamine and methionine metabolism and three methyltransferases. Note that several of the transcripts (marked with *) with decreased abundance in the table also clustered together during the exploratory analysis (Fig. 3.9) e.g. PF10_0322, PFI1090w, PFE10_0289, PFE0660c, PF14_0598, PF08_0131, P13_0141, PFF1300w, PF14_0018, PFE0675c, PF14_0187, PF14_0378. The complete LIMMA dataset of 538 transcripts is presented in Appendix A.

Table 3.3 Biological functions of a subset of the transcripts differentially affected according to LIMMA as a result of PfAdoMetDC/ODC co-inhibition

| PlasmoDB ID | Annotation | Fold change ^a | IDC time of peak expression (hpi) ^b |
|---|--|--------------------------|--|
| Polyamine and methionine metabolism | | | |
| PF10_0322* | PfAdoMetDC/ODC | -1.9 | 24 |
| PFD0285c | Lysine decarboxylase, putative | 2.8 | 25 |
| PFF0435w | Ornithine aminotransferase | 1.9 | 18 |
| PFI1090w* | AdoMet synthetase | -2.4 | 27 |
| PFE1050w | Adenosylhomocysteinase | -1.9 | 33 |
| PF10_0289* | Adenosine deaminase, putative | -2.6 | 27 |
| PFE0660c* | Uridine phosphorylase, putative | -3.2 | 27 |
| PF10_0340 | Methionine-tRNA ligase | -1.7 | 33 |
| <i>Methyltransferases</i> | | | |
| MAL13P1.214 | Phosphoethanolamine N-methyltransferase, putative | -2.8 | 40 |
| PF14_0309 | Protein-L-isoaspartate O-methyl transferase, putative | -1.9 | 41 |
| PF14_0526 | Generic methyltransferase | -2.9 | 37 |
| Potential polyamine associated effects | | | |
| PF14_0316 | DNA topoisomerase II | -1.7 | 50 |
| PFL1885c | Calcium/calmodulin-dependent protein kinase 2, putative | 2.4 | 50 |
| PF07_0065 | Zinc transporter, putative | -2.4 | 40 |
| Oxidative stress defence | | | |
| PF08_0131* | 1-Cys-peroxiredoxin | -3.2 | 34 |
| PF14_0192 | Glutathione reductase | -1.7 | 34 |
| PF14_0187* | Glutathione S-transferase | -1.8 | - |
| Energy metabolism | | | |
| <i>Oxidative phosphorylation</i> | | | |
| Col | Cytochrome oxidase I, putative | -2.0 | - |
| CoxI | Cytochrome oxidase I, putative | -1.7 | 53 |
| CoxIII_2 | Mitochondrial encoded cytochrome oxidase subunit 3 | -2.0 | - |
| PF11_0412 | Vacuolar ATP synthase subunit F, putative | -1.8 | 34 |
| MAL7P1.75 | Mitochondrial ATP synthase F1, epsilon subunit, putative | -1.8 | - |
| PFE0970w | Cytochrome c oxidase assembly, putative | -1.7 | 24 |
| PF13_0121 | Dihydrolipoamide succinyltransferase | -1.7 | 27 |
| <i>Glycolysis</i> | | | |
| PF10_0155 | Enolase | -2.0 | 18 |
| PF13_0141* | L-lactate dehydrogenase | -1.8 | 18 |
| PF14_0378* | Triose-phosphate isomerase | -1.8 | 18 |
| PF14_0598* | Glyceraldehyde-3-phosphate dehydrogenase | -2.1 | 27 |
| PFF1300w* | Pyruvate kinase | -1.9 | 28 |
| DNA replication | | | |

| | | | |
|------------------------------|---|------|----|
| PF11_0117 | Replication factor C subunit 5, putative | -2.1 | 34 |
| PF11_0087 | Rad51 homologue, putative | -2.0 | 35 |
| PF13_0095 | DNA replication licensing factor mcm4-related | -2.2 | 42 |
| PF13_0291 | Replication licensing factor, putative | -1.8 | 34 |
| PF14_0081* | DNA repair helicase, putative | -1.7 | - |
| PF14_0112 | POM1, putative | -2.0 | 37 |
| PF14_0254 | DNA mismatch repair protein Msh2p, putative | -1.8 | 32 |
| PF14_0314 | Chromatin assembly factor 1 p55 subunit, putative | 2.4 | - |
| PF14_0601 | Replication factor C3 | -2.0 | 34 |
| PFB0180w | 5'-3' Exonuclease, putative | -1.9 | 26 |
| PFB0895c | Replication factor C subunit 1, putative | -2.0 | 33 |
| PFD0470c | Replication factor A protein, putative | -2.5 | 34 |
| PFD0685c | Chromosome associated protein, putative | -2.0 | 40 |
| PFD0830w | Dihydrofolate reductase-thymidylate synthase | -2.0 | 33 |
| PFD0950w | Ran binding protein 1 | 2.0 | - |
| PFE0675c* | DNA photolyase | -2.2 | 36 |
| PFF1470c | DNA polymerase epsilon, catalytic subunit A, putative | -1.7 | 36 |
| PFI0235w | Replication factor A-related protein, putative | -1.8 | 33 |
| PFI0530c | DNA primase, large subunit, putative | -1.8 | 35 |
| Transcription factors | | | |
| PF11_0241 | Hypothetical protein with Myb-like domains | 1.8 | - |
| PFL0465c | C2H2-type zinc-finger transcription factor, krox1 | 2.0 | - |
| PFE1245w | CCCH-type zinc-finger protein | 1.7 | 26 |
| PFD0560w | Hypothetical protein with a TATA-box -like domain | 1.7 | 32 |
| PFE0415w | Transcription factor IIB, putative | -1.8 | - |
| Translation | | | |
| MAL13P1.327 | Ribosomal protein S17 homologue, putative | 1.7 | 22 |
| PF07_0080 | 40S ribosomal protein S10, putative | 1.9 | 16 |
| PF10_0038 | Ribosomal protein S20e, putative | 2.3 | 15 |
| PF11_0454 | Ribosomal protein, 40S subunit, putative | 2.0 | - |
| PF13_0014 | 40S ribosomal protein S7 homologue, putative | 1.8 | 15 |
| PF13_0171 | 60S ribosomal protein L23, putative | 2.0 | 13 |
| PF13_0228 | 40S ribosomal subunit protein S6 | 1.8 | 13 |
| PF14_0205 | Ribosomal protein S25 | 2.4 | 23 |
| PF14_0231 | Ribosomal protein L7a, putative | 1.8 | 21 |
| PF14_0579 | Ribosomal protein L27, putative | 2.1 | 21 |
| PF14_0709 | Ribosomal protein L20, putative | -2.6 | 32 |
| PFB0455w | Ribosomal L37ae protein, putative | 1.7 | 16 |
| PFC0535w | 60S ribosomal protein L26, putative | 2.0 | - |
| PFC1020c | 40S ribosomal protein S3A, putative | 1.7 | 15 |
| PFE0185c | 60S ribosomal subunit protein L31, putative | 1.8 | 14 |
| PFI1585c | 30S ribosomal protein S6-like protein, putative | 1.8 | - |
| Cell cycle mediators | | | |
| PF13_0328 | Proliferating cell nuclear antigen | -3.3 | 40 |
| PF14_0604 | Hypothetical protein with cyclin homology | -1.7 | 2 |
| PFL1330c | Hypothetical protein with cyclin homology | 1.8 | 37 |

a. Average fold change calculated at the time point of maximum change

b. Transcript peak expression time according to the 3D7 IDC transcriptome [91]

* Transcripts that clustered together after hierarchical clustering (Fig. 3.9)

(-) No data available

The majority (70%) of the differentially affected transcripts were decreased, equally so for polyamine and methionine metabolism with the abundance of only two transcripts, OAT and LDC (PFD0285c), being increased ~2-fold and 2.8-fold, respectively (Fig 3.17). The transcript level for PfAdoMetDC/ODC, the protein of which was targeted by DFMO and MDL73811, was decreased by ~2-fold (Fig. 3.17). Thus, despite the transcripts for LDC and PfAdoMetDC/ODC being expressed at approximately the same time in the IDC (25 hpi and 24 hpi respectively), the transcript for LDC was increased and that of PfAdoMetDC/ODC was decreased,

which illustrates the differential effect of the co-inhibition on the abundance of specific transcripts, despite the generalised transcriptional arrest. Other affected transcripts from polyamine and methionine metabolism include AdoMet synthetase (PF11090w), adenosylhomocysteinase (PFE1050w), a putative adenosine deaminase (PF10_0289), uridine phosphorylase (PFE0660c) and methionine-tRNA ligase (PF10_0340). The transcripts for putative methionyl-tRNA formyltransferase (MAL13P1.67) and proline carboxylate reductase (MAL13P1.284) could not be detected.

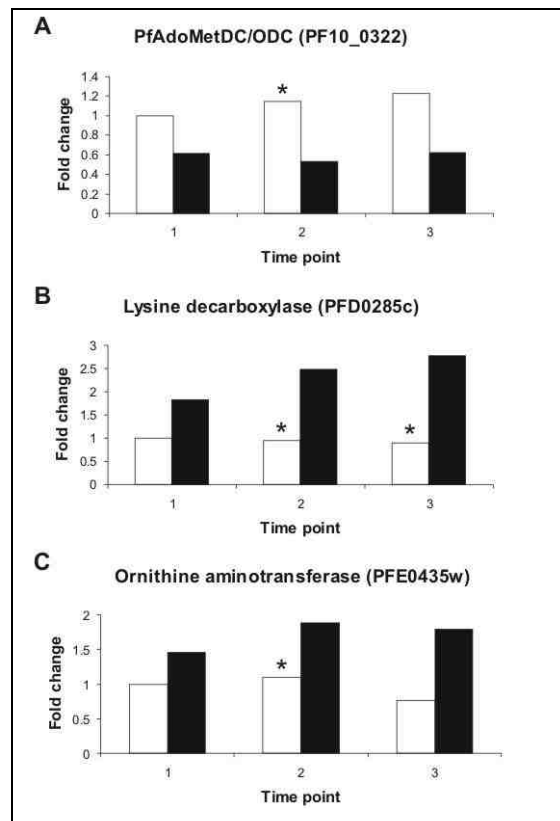


Fig. 3.17 Transcript profiles of **A)** PfAdoMetDC/ODC, **B)** lysine decarboxylase and **C)** ornithine aminotransferase compiled from the PfAdoMetDC/ODC co-inhibited (black bar) and untreated (white bar) *P. falciparum* cultures sampled at $t_1 = 19$ hpi, $t_2 = 27$ hpi and $t_3 = 34$ hpi according to untreated parasite morphology. Fold change was calculated compared to relative t_0 ($p < 0.05$ except where indicated with *)

Several of the transcripts with decreased abundance translate to proteins that are known to require polyamines for optimal functioning, protection or gene expression in other organisms (Table 3.3). These, for example, include the transcript for DNA topoisomerase II (PF14_0316) [224], three oxidative stress defence transcripts [225] and transcripts involved with zinc transport and energy metabolism [226], which were all decreased. In addition, the transcript for a putative calcium/calmodulin-dependent protein kinase 2 (PFL1885c) was increased 2.4-fold and it is known that polyamines inhibit this protein [227]. Furthermore, the transcript abundance of several transcription factors was increased (PF11_0241, PFL0465c, PFE1245w, PFD0560w) and polyamines have been shown to act as transcriptional repressors. This may be indirectly via the regulation of specific transcription factors [226] e.g. c-Myc was shown to increase upon polyamine depletion [228].

3.3.5.3 EDGE time course analysis

Differential transcript abundance analysis was performed in addition with EDGE 1.1.208 software [215]. EDGE was specifically designed to calculate the significance of differential abundance in microarray time course experiments [215]. EDGE identified 718 significantly differentially affected unique transcripts (Fig. 3.18, Appendix B) compared to relative t_0 versus the 538 identified by LIMMA. The EDGE results include the transcripts for LDC, OAT and spermidine synthase (PF11_0301), but it do not indicate fold change or even direction of change. There was only about 35.6% overlap between the EDGE and LIMMA differential abundance data sets, but EDGE uses a default Q-value cut-off of 0.1% ($p < 0.02$) for significance and no fold change cut-off compared to the $p < 0.05$ significance and 1.7-fold change cut-offs specified in LIMMA. However, since EDGE was written for proper time course analysis with parallel time point comparison, the software had to be forced to compare all three treated time points with the relative t_0 , which potentially interfered with the statistical calculations. For this reason and because of the advantage of definite fold change cut-offs with LIMMA, the LIMMA dataset of 538 was regarded as the dataset of choice to be used for further analysis.

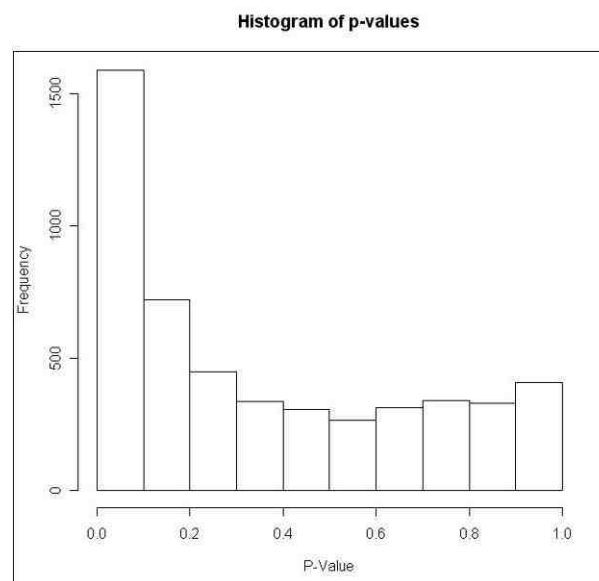


Fig 3.18 EDGE output in the form of a histogram of p-values of the oligonucleotides with changed expression. Note that the abundance of more than 1500 of the 5056 oligonucleotides analysed (including repeats and NULL-controls) changed during the time course with $p < 0.1$. However, when the Q-value significance cut-off of 0.1% ($p < 0.02$) was used, 718 unique transcripts (823 oligonucleotides) showed significant differential abundance.

3.3.6 GO assignment of differentially affected transcripts

The 538 transcripts identified by LIMMA were classified into 14 functional groups (Fig. 3.19) using GO terms obtained from DAVID and PlasmDB. Most transcripts with increased abundance were related to RNA metabolism (9%), translation (10%) and host/parasite interaction (11%), whereas those with decreased abundance mostly represented DNA (7%) and primary metabolism (8%, including carbohydrate, lipid and energy metabolism). The increased abundance of transcripts associated with host/parasite interaction (including surface antigens) is regarded as a general stress response [189, 196]. Transcripts related to the

clusters were found among the decreased abundance transcripts and none among the increased abundance transcripts. The seven clusters were distributed over chromosomes 7, 10 and 11, respectively (Table 3.4).

Table 3.4 Adjacent gene clusters with decreased abundance transcripts

| Chromosome | Cluster 1 ^a | Cluster 2 ^a | Cluster 3 ^a |
|--------------|---|---|---|
| MAL7 | MAL7P1.6 MAL7P1.7 PF07_0005 PF07_0006 | MAL7P1.170 MAL7P1.173 MAL7P1.176 PF07_0129 MAL7P1.177 | - |
| MAL10 | PF10_0014 PF10_0015 PF10_0016 PF10_0017 PF10_0019 PF10_0020 PF10_0021 PF10_0022 PF10_0023 PF10_0024 PF10_0025 | PF10_0152 PF10_0153 PF10_0154 PF10_0155 | - |
| MAL11 | PF11_0037 PF11_0039 PF11_0040 PF11_0041 | PF11_0364 PF11_0365 PF11_0367 PF11_0368 | PF11_0503 PF11_0504 PF11_0505 PF11_0508 PF11_0509 |

a. A cluster was defined as four or more genes within a window of six adjacent genes of which the transcripts were present within the dataset. Seven such gene clusters were detected, namely two on MAL 7, two on MAL10 and three on MAL11.

Particularly significant was a cluster of eleven genes on chromosome 10 (PF10_0014 to PF10_0025) that lie back-to-back on the same strand, with only one gene (PF10_0018) in the entire stretch of ~41,000 bases not present in the LIMMA dataset (Fig. 3.20). PF10_0018 produces a low abundance transcript, which was most likely affected in the same way, but was not detected.

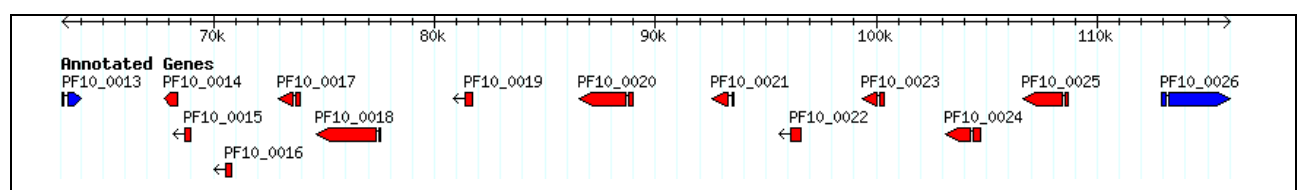


Fig. 3.20 Eleven gene cluster from chromosome 10 (PF10_0014 to PF10_0025) where the transcripts of eleven adjacently located genes (red arrows) were all decreased except for the low abundance transcript of PF10_0018, which could not be detected due to low signal intensity. Figure constructed within PlasmODB 5.3.

Decreased transcription of co-localised genes may be due to a common transcription factor that became non-functional in the absence of polyamines. These twelve genes (including PF10_0018) were therefore analysed for motifs identified in other organisms with Transfaq and RSA tools, via the MADIBA database (<http://www.bi.up.ac.za/MADIBA/MADIBA.html>), as well as MEME (<http://meme.sdsc.edu/>) and Weeder (<http://159.149.109.16/Tool/Ind.php>), but a meaningful motif could not be identified. Finding known motifs in

the *P. falciparum* genome is a well-known problem, which is ascribed to divergence from other organisms and the high A+T-rich content of the genome [128, 229]. TATA-box-like motifs are characteristic of regulatory regions in other organisms but occur at random in the *P. falciparum* genome [128]. However, the genes within the identified clusters are not all co-expressed under normal conditions according to the 3D7 IDC transcriptome [91] (Table 3.5) and nuclear expression of contiguous genes is rarely co-regulated in *P. falciparum* [29]. A more likely explanation for the co-regulation may therefore be partial DNA unwinding due to polyamine depletion [230], thereby causing genes previously buried within the nucleosome particle to become more exposed to e.g. oxidative damage.

Table 3.5 IDC mRNA expression profiles of the eleven gene cluster from chromosome 10

| PlasmoDB ID | Oligo ID | IDC time of peak expression (hpi) | IDC expression profile |
|-------------|-----------|-----------------------------------|------------------------|
| PF10_0015 | opfj12802 | 53 | |
| PF10_0016 | j3_21 | 28 | |
| PF10_0017 | 33_20 | 37 | |
| PF10_0018 | j33_18 | 0 | |
| PF10_0019 | j33_16 | 10 | |
| PF10_0020 | j33_15 | 42 | |
| PF10_0021 | j33_12 | 9 | |
| PF10_0022 | j33_11 | 6 | |
| PF10_0023 | j33_10 | 53 | |
| PF10_0024 | j33_6 | 5 | |
| PF10_0024 | kn1473_2 | 4 | |
| PF10_0025 | f67629_1 | 6 | |
| PF10_0025 | j33_5 | 6 | |

The data above were obtained from the 3D7 IDC transcriptome (<http://malaria.ucsf.edu>) [91].

3.3.8 PfAdoMetDC/ODC-interactome data comparisons

In contrast to most other environmental perturbations of *P. falciparum* that have been evaluated on the transcriptome level, e.g. glucose deprivation [189], heat-shock [190] and even chloroquine treatment [179, 196], the exact protein and pathway targeted by DFMO/MDL73811 in this study were known, which enabled specific transcripts to be evaluated. The presence of eight transcripts from polyamine and methionine metabolism in the LIMMA dataset indicated the potential enrichment for transcripts from proteins functionally connected to this pathway or to PfAdoMetDC/ODC. To investigate this observation further, the LIMMA dataset was compared with the *in silico* predicted interactome data of PfAdoMetDC/ODC [113]. These networks were constructed using among others the IDC transcriptome [29, 113]. The transcripts of 23% of all the predicted binding partners of PfAdoMetDC/ODC were present in the LIMMA dataset, including 60% (12/20) of the top 20 scored (highest prediction) proteins (Table 3.6). To assess the possibility of random overlap, the LIMMA dataset was also compared with the interactome data of another bifunctional protein from outside the polyamine pathway and unaffected by the treatment, namely DHPS/PPPK (PF08_0095). The transcripts of

only about 10% of the predicted binding partners of this protein and only 10% (2/20) of the top 20 scored proteins were present in the dataset of 538 (Table 3.6). The interactome is a theoretical interaction prediction that still requires experimental verification, but this analysis may indicate enrichment of the LIMMA dataset for transcripts of proteins functionally connected to PfAdoMetDC/ODC or polyamine and methionine metabolism. The complete interactomes of these proteins and data comparison are provided in Appendix C.

Table 3.6 Interactome data comparisons

| Score ^a | Protein ID | Description | Present in LIMMA dataset |
|---|------------|---|--------------------------|
| PfAdoMetDC/ODC top 20 binding partners | | | |
| 9.53 | PF11_0317 | Structural maintenance of chromosome protein, putative | |
| 8.31 | PFE0195w | P-type ATPase, putative | |
| 7.98 | PFA0390w | DNA repair exonuclease, putative | |
| 6.62 | MAL8P1.99 | Hypothetical protein | Yes |
| 6.62 | PF11_0427 | Dolichyl-phosphate b-D-mannosyltransferase, putative | |
| 6.62 | PF07_0129 | ATP-dependent acyl-coa synthetase | Yes |
| 6.62 | PFA0590w | ABC transporter, putative | Yes |
| 5.9 | PF10_0260 | Hypothetical protein | |
| 5.9 | PF13_0348 | Hypothetical protein | |
| 5.7 | PF14_0053 | Ribonucleotide reductase small subunit | Yes |
| 4.71 | PFD0685c | Chromosome associated protein, putative | Yes |
| 4.71 | PFC0125w | ABC transporter, putative | Yes |
| 4.71 | PF14_0709 | Ribosomal protein L20, putative | Yes |
| 4.71 | PF08_0131 | 1-Cys peroxiredoxin | Yes |
| 4.71 | PF11_0117 | Replication factor C subunit 5, putative | Yes |
| 4.71 | PF11_0181 | Tyrosine tRNA ligase, putative | Yes |
| 4.71 | PFB0180w | 5'-3' Exonuclease, N-terminal resolvase-like domain, putative | Yes |
| 4.71 | PFL2180w | 50S Ribosomal protein L3, putative | |
| 4.71 | PF14_0097 | Cytidine diphosphate-diacylglycerol synthase | |
| 4.71 | PF14_0081 | DNA repair helicase, putative | Yes |
| DHPS/PPPK top 20 binding partners | | | |
| 10.32 | PF13_0140 | Dihydrofolate synthase/folylpolyglutamate synthase | |
| 8.31 | PFL0740c | 10 kd chaperonin, putative | |
| 8.31 | PF11_0258 | Co-chaperone GrpE, putative | |
| 8.31 | PF13_0180 | Chaperonin, putative | |
| 7.98 | PF08_0006 | Prohibitin, putative | |
| 7.98 | PFL1475w | Sun-family protein, putative | |
| 5.96 | PF13_0234 | Phosphoenolpyruvate carboxykinase | |
| 5.96 | PF11_0188 | Heat shock protein 90, putative | |
| 5.96 | PF14_0656 | U2 snRNP auxiliary factor, putative | |
| 5.96 | PF14_0242 | Arginine n-methyltransferase, putative | |
| 5.9 | PFB0953w | Hypothetical protein | Yes |
| 5.9 | MAL7P1.209 | AAA family ATPase, putative | |
| 5.9 | PFF0945c | Long-chain fatty-acid Co-A ligase and oxalyl Co-A decarboxylase | |
| 5.9 | PFE0060w | Hypothetical protein | |
| 5.9 | PF11_0076 | Hypothetical protein | |
| 5.9 | PFF0775w | Pyridoxal kinase-like protein | |
| 5.9 | PF10_0013 | Hypothetical protein | |
| 5.9 | MAL8P1.124 | Hypothetical protein | |
| 5.9 | PF14_0705 | Hypothetical protein | |
| 5.9 | PFE1245w | Zinc finger protein, putative | Yes |

a. Probability score for functional linkage

3.3.9 Real-time PCR validation of differential transcript abundance data

The accuracy of the microarray data was validated with real-time PCR of three increased and three decreased transcripts including LDC, OAT and AdoMet synthetase. At the time, two complete hybridisation sets (unamplified and amplified) had been performed (amplified results not shown) and very limited quantities of cDNA were available. Several plasmodial “housekeeping” genes from other studies were considered to be used as loading control to obtain comparable starting levels e.g. ribosomal protein L37A, chromatin binding protein, Ser/Thr protein kinase [231] and LDH [179]. However, transcript levels of these either fluctuate during the IDC or were affected by PfAdoMetDC/ODC co-inhibition (Appendix A). However, the log₂-ratios of a putative cyclophilin (PFE0505w) remained relatively unchanged across the different samples in the PfAdoMetDC/ODC co-inhibition data (Fig. 3.21A) and in the IDC transcriptome (Fig. 3.21B), and was used as “housekeeping” or cDNA loading control.

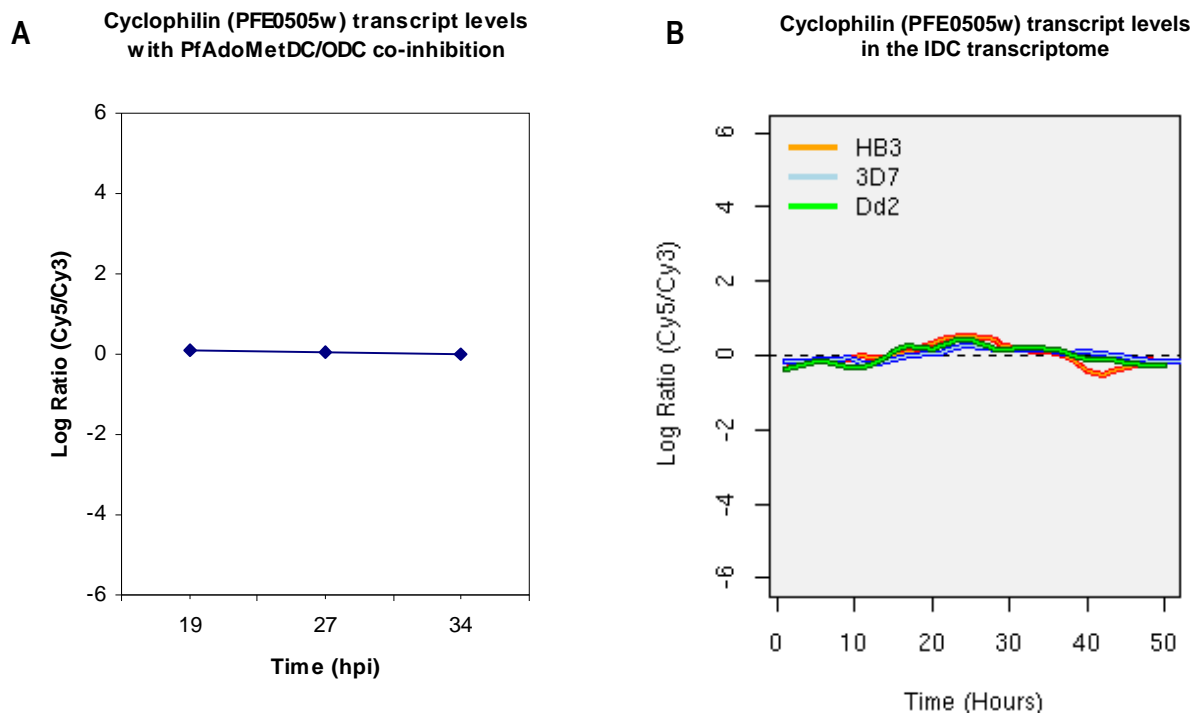


Fig. 3.21 The relatively constant transcription profile of the putative cyclophilin (PFE0505w) in **A**) the PfAdoMetDC/ODC co-inhibition data and **B**) the IDC transcriptome of three parasite strains (image in B obtained from <http://malaria.ucsf.edu>, [91]) enabled its use as “housekeeping” or cDNA loading control.

A five-part cDNA dilution series (1, 1/10, 1/20, 1/50 and 1/100) of the putative cyclophilin was prepared. The amplification process was visualised in real-time by plotting fluorescence against the cycle number on a logarithmic scale (Fig. 3.22). The cycle at which the sample fluorescence of a specific amplification product crosses the threshold for detection (above background) is the cycle threshold (C_t) and is indicative of the abundance of that specific cDNA species within the sample.

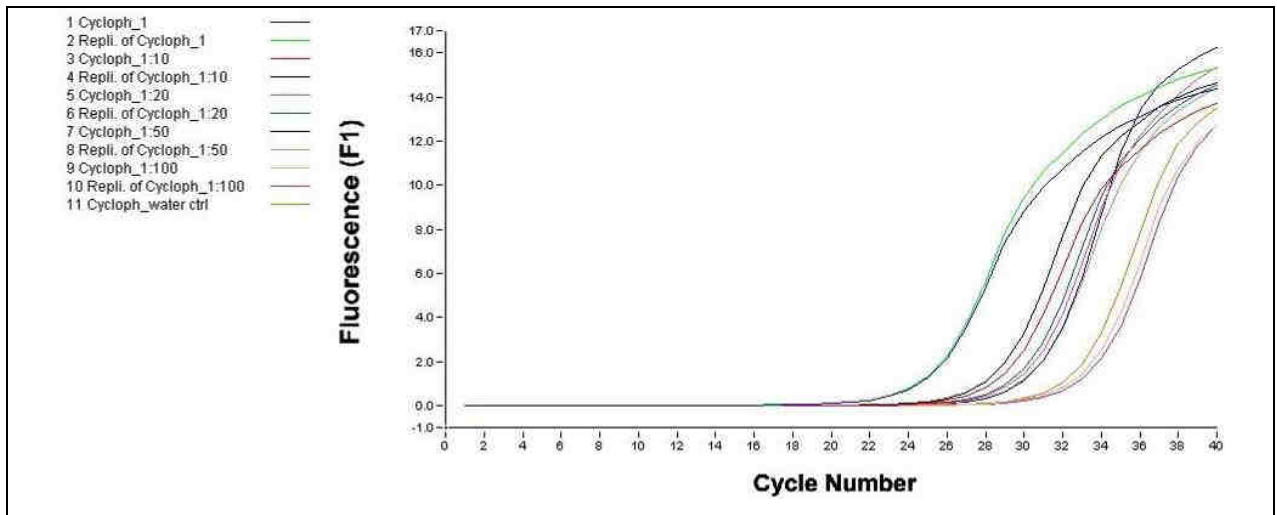


Fig. 3.22 A real-time PCR plot obtained for a five-part cDNA dilution series (1, 1/10, 1/20, 1/50 and 1/100) of the putative cyclophilin. The 1/100 dilution curve was detected in the same cycle as the negative water control, which indicated primer-dimer formation.

Melting curve analysis was performed to distinguish the correct amplification products from primer-dimers, since the SYBR Green dye intercalates non-specifically into all double-stranded DNA (Fig.3.23).

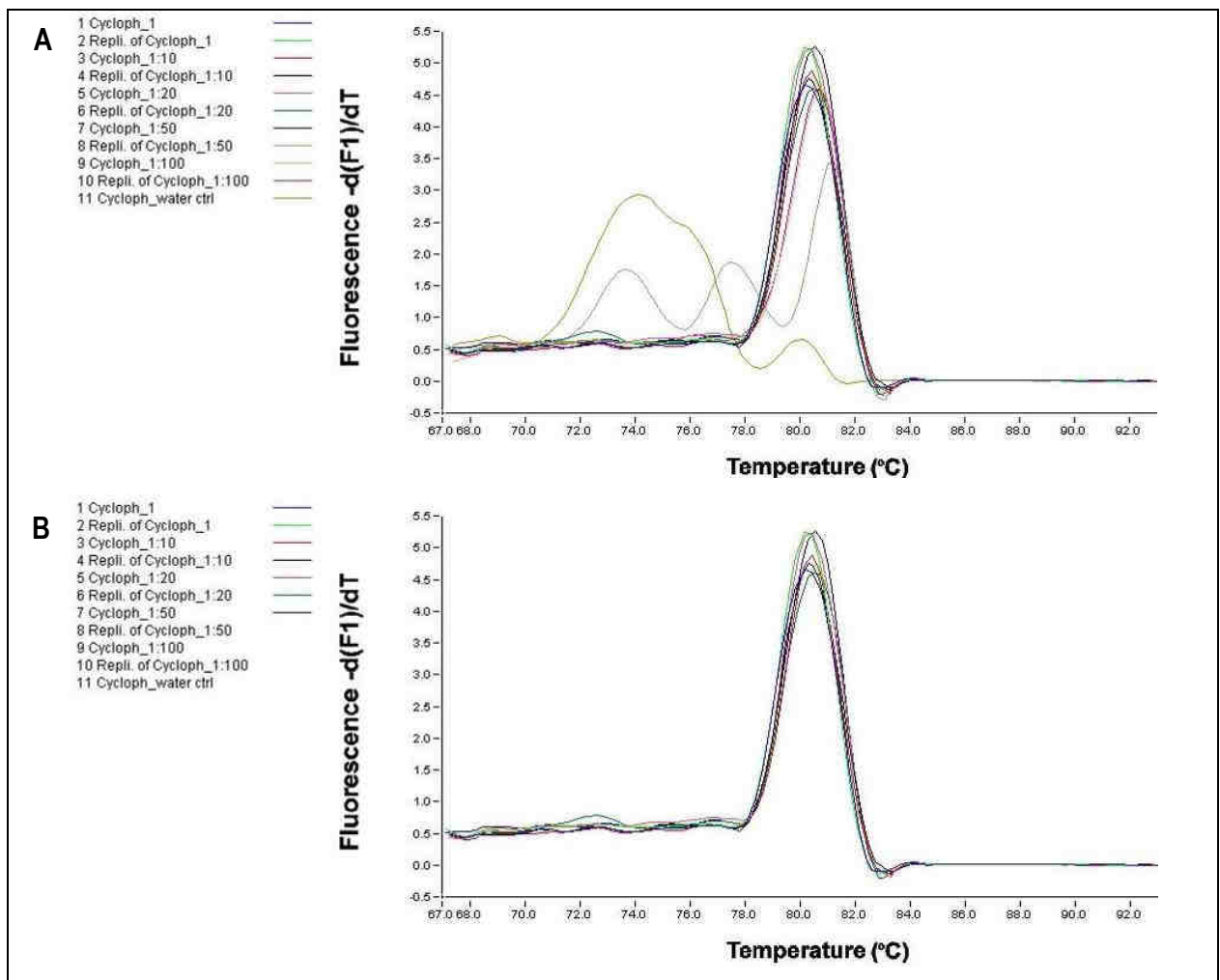


Fig. 3.23 Melting curve analysis of the amplification product of cyclophilin. **A)** The five-part cDNA dilution series confirmed primer-dimer formation at the higher sample dilutions (1/100 and 1/50 replicate). **B)** These values were subsequently excluded from the analysis and a 1/5 sample dilution were routinely used.

The short primer-dimers dissociate at a lower temperature than the 160-170 bp gene-specific products, which usually had a $T_m \approx 80^\circ\text{C}$ (Fig. 3.23). Primer-dimers were detected in the very dilute samples (i.e. 1/50 to 1/100) and these data were excluded from the analysis. Sample dilutions of 1/5 were routinely used.

A standard curve was compiled from the C_t -values of the putative cyclophilin dilution series (Fig. 3.24) and was used to estimate the amount of cDNA of the six transcripts of interest (Table 3.7). The amount of cDNA obtained for the specific transcripts was divided by the amount of the putative cyclophilin in that same sample to normalise for the variation in sample concentration and resulted in a relative cDNA ratio or fold change.

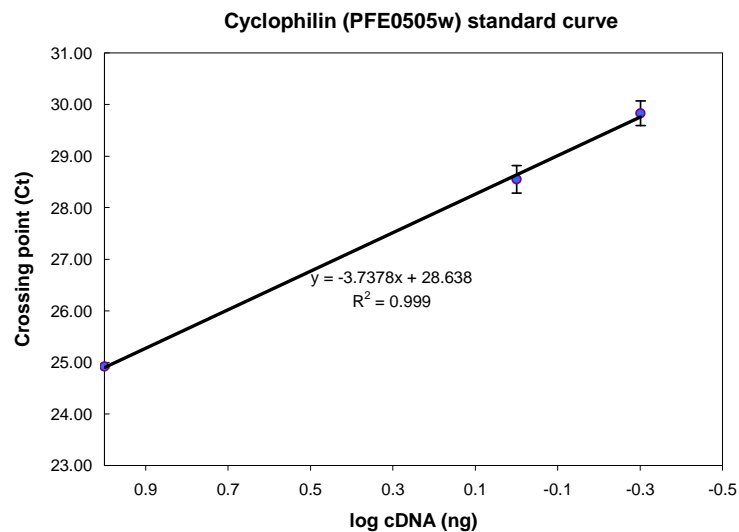


Fig. 3.24 A standard curve of the putative cyclophilin (PFE0505w).

Fold change values obtained with the two different mRNA quantitation techniques i.e. microarray and real-time PCR, were relatively consistent for the six transcripts tested (Table 3.7), which confirmed the reliability of the microarray analysis. Relatively low abundance transcripts within the dataset were validated by the inclusion of LDC and DHFR/TS. However, LDC cDNA levels were so low that they could not be assessed in the 1/5 dilution without primer-dimer formation and were therefore measured in the undiluted cDNA stock to obtain reliable data. Similarly, for DHFR/TS, of which the transcript abundance decreased with PfAdoMetDC/ODC co-inhibition (Table 3.3), cDNA levels could not be measured in the sample of maximum fold change (T_{11}), but were subsequently detected in T_{13} .

Table 3.7 Microarray data validation with real-time PCR

| PlasmoDB ID | Annotation | Time point ^a | Fold change to relative t ₀ | |
|-----------------------|---|-------------------------|--|---------------------------|
| | | | Oligo array (±SD) ^b | Rt PCR (±SD) ^c |
| PFL1885c | Calcium/calmodulin-dependent protein kinase 2 | t ₃ | 2.43 (±0.18) | 1.74 (±0.40) |
| PFD0285c ^d | LDC | t ₃ | 2.78 | 1.71 (±0.19) |
| PFF0435w | OAT | t ₃ | 1.88 | 2.14 (±0.30) |
| PF08_0131 | 1-Cys-peroxiredoxin | t ₃ | 0.35 | 0.42(±0.14) |
| PFD0830w ^d | DHFR/TS | t ₁ | 0.50 (±0.05) | Not detected ^e |
| | | t ₃ | 0.62 (±0.03) | 0.35 (±0.04) |
| PFI1090w | AdoMet synthetase | t ₁ | 0.42 | 0.53 (±0.07) |

a. Treated sample of maximum increase/decrease in transcript abundance

b. Data of transcripts with multiple oligonucleotides ($p < 0.05$) were averaged, the standard deviation of the mean in parentheses.

c. Real-time PCR was performed in triplicate with the standard deviation of the mean indicated in parentheses.

d. Relatively low abundance transcripts

e. Not detected in sample of maximum decrease in abundance (t₁) and repeated for t₃

3.4 DISCUSSION

The ability to measure the expression of thousands of genes in a single experiment simultaneously assured the rapid adaptation of DNA microarray into most biomedical research fields [232]. However, one of the biggest challenges to microarray studies is deciphering the significance of the wealth of information obtained from high-quality raw data [136]. In this study, cautious experimental design was used to ensure that the data obtained would be maximally informative regarding the effects of the perturbation [61]. A reference design microarray experiment was performed to enable easy comparison between samples and to simplify data analysis. Secondly, synchronous parasites were treated (with DFMO and MDL73811) to limit the background noise of various parasite stages to enable the detection of transcriptional responses above the basal transcriptional level in the IDC. Thirdly, two biological and two technical replicates were included to enable statistical analysis to determine the significance of the observations. Fourthly, a time course study was performed to assess the effects of the perturbation at the highest possible resolution i.e. samples were harvested over three time points. Initial assessment of the quality of the data included visual inspection of the arrays and data flagging, followed by a series of diagnostic analyses to ensure appropriate data correction and normalisation. These analyses indicated that local background subtraction and robust spline normalisation had to be performed within each array to correct for spatial effects, whereas Gquantile between array normalisation enabled consolidation of replicates and cross-sample comparison for differential abundance analysis with LIMMA. The statistical significance of differential transcript abundance was calculated with moderated t-statistics [206] and only transcripts with at least a 1.7-fold change ($\log_2\text{-ratio} \geq 0.75$ or ≤ -0.75) and $p < 0.05$ were regarded as differentially affected. These thorough analyses confirmed data quality, which indirectly determined the reproducibility and reliability of the derived gene lists (e.g. the LIMMA dataset) and the validity of the resulting biological conclusions [232]. The raw microarray data and detailed information on the

experimental methodology and analysis (MIAME) were subsequently submitted to GEO, as required for publication purposes and to enable independent verification and meta-analyses.

Transcriptional profiling of cells treated with cytostatic drugs has previously been performed in cancer [233, 234] but global transcriptome studies with cytostatic drugs in multistage organisms such as *P. falciparum* have not yet been reported. The cytostatic effect of DFMO or MDL73811 inhibition on PfAdoMetDC/ODC in *P. falciparum* is well established [153, 154], but the exact mechanism by which polyamine depletion (induced by these drugs) results in growth inhibition, was not yet elucidated [235]. To aid in a better understanding of this process, the physiological response of *P. falciparum* during polyamine depletion induced cytostasis was evaluated on a transcriptional level. Transcriptional arrest was observed with three different analyses (phase ordering, Pearson correlation with the 3D7 IDC transcriptome [91] and within the PfAdoMetDC/ODC co-inhibition data). The transcriptional arrest preceding and resulting in cytostatic growth arrest due to polyamine depletion was demonstrated here for the first time to our knowledge in any organism. *P. falciparum* is a multistage organism and the transcriptional arrest of treated and normal transcriptional progression of untreated parasites was clearly visible when the data were ordered according to peak expression times within the IDC (Fig. 3.11A). Pearson correlation calculations indicated that the approximate time of transcriptional arrest occurred in the late ring/early trophozoite stage, which correlates to the time of PfAdoMetDC/ODC transcription and the subsequent availability of the protein for drug inhibition (Fig. 3.11B). Complete enzyme inhibition occurred soon after protein expression (Fig. 3.3) and underscored the enzyme-specific inhibitory effects of DFMO and MDL73811 [153, 154]. The exact mechanism by which polyamine depletion results in transcriptional arrest is not clear, but the importance of polyamines in macromolecular synthesis (including RNA and proteins, e.g. transcription factors) [88], optimal ribosome function [236] and the association of the main fraction of polyamines with RNA [64] has been demonstrated. In this study, the increased transcript abundance of several putative transcription factors and ribosomal components were detected (Table 3.3), which could indicate an attempt to induce transcription and translation (as opposed to DNA replication) in order to overcome the transcriptional arrest caused by the perturbation.

Despite the generalised transcriptional arrest, 538 transcripts with fold changes ranging between maximum 3.2-fold up and 5-fold down (Appendix A) were shown to be differentially affected with LIMMA analysis. The range of fold change detected is in agreement with other transcriptome reports of perturbed Plasmodia where relatively small amplitude transcriptional responses were detected [62], especially in the increased abundance datasets [189, 196]. These changes were quantitated compared to a relative t_0 , which was used as reference point for quantitative analysis throughout the whole functional genomics investigation. Due to the transcriptional arrest of the treated and normal progression of untreated parasites, the standard parallel time point comparison approach of treated versus untreated would have indicated stage and life cycle differences and not the perturbation-specific effects of polyamine depletion. A similar relative t_0 strategy and fold change

cut-off were used in the analysis of the artesunate-perturbation of *P. falciparum* [198]. Furthermore, Temez and colleagues also compared trophozoites that were arrested by the inhibition of sphingomyelin biosynthesis with trophozoite controls rather than ring controls, to limit the detection of stage-specific transcriptional differences as opposed to perturbation-specific differences [199]. Both these studies used synchronised parasites [198, 199], as well as a relative t_0 strategy, and both detected perturbation-specific transcriptional responses similar to the study reported here. In comparison, the reported perturbations of Plasmodia that failed to detect programmed transcriptional responses generally employed asynchronous cultures [194, 196]. The transcriptional arrest demonstrated after PfAdoMetDC/ODC co-inhibition would have been masked if asynchronous cultures had been used and defining a reference point for quantitative analysis, i.e. relative t_0 , would have been difficult. The use of synchronised cultures also enabled comparison with the IDC transcriptome and transcripts with treated profiles that deviated from their IDC profiles further corroborated the findings of the differential abundance analysis. It appears as if the parasite attempts to respond to environmental stress on the transcriptional level with a specific though small amplitude response, removed from the normal transcriptional control and these non-random changes may potentially be missed if asynchronous cultures are used [128].

The 538 transcripts include eight transcripts from polyamine and methionine metabolism that were differentially affected (Fig. 3.25). The presence of these eight transcripts in the LIMMA dataset suggested the potential enrichment of the data for transcripts from proteins functionally connected to this pathway or to PfAdoMetDC/ODC. Therefore, the LIMMA dataset was compared with the *in silico* predicted interactome data of PfAdoMetDC/ODC [113], which revealed 12/20 of the top 20 (highest probability) scored binding partners of PfAdoMetDC/ODC within the dataset compared to only 2/20 of the top 20 binding partners of an unrelated bifunctional protein, DHPS/PPPK, and corroborated the enrichment for transcripts from polyamine and methionine metabolism (Table 3.6).

The LIMMA dataset was furthermore classified into 14 functional groups (Fig. 3.19) using GO terms obtained from DAVID and PlasmoDB. In many cases, the co-inhibition caused both an increase and a decrease in abundance of transcripts representing the same biological process, e.g. proteolysis. These paradoxical effects of polyamines or depletion thereof are not uncommon, e.g. in mammalian cells polyamine depletion increased the half life of long-lived proteins, but decreased the half life of short-lived proteins [237]. In the current investigation, the highest percentages of increased transcripts were related to RNA metabolism, translation and host/parasite interaction, whereas most of the decreased transcripts represented DNA and primary metabolism (including carbohydrate, lipid and energy metabolism). The increase in abundance of transcripts associated with host/parasite interaction (including surface antigens) is regarded as a general stress response [189, 196]. More than half of the dataset (51%) represents hypothetical proteins with unknown biological function at the current time, which limits data interpretation. Recently, a database for GO annotation prediction

of *P. falciparum* was released, named PlasmoDraft [238]. Instead of sequence homology, PlasmoDraft uses post-genomic (transcriptomic, proteomic and interactomic) data for “guilt by association”, based on the similarity of gene expression profiles. This database could suggest identities and the biological significance for many of these hypothetical proteins. The dataset of 538 was validated with real-time PCR of three increased and three decreased transcripts and their differential abundance was confirmed (Table 3.7). Relatively low abundance transcripts within the dataset were validated by the inclusion of LDC and DHFR/TS in the real-time PCR strategy.

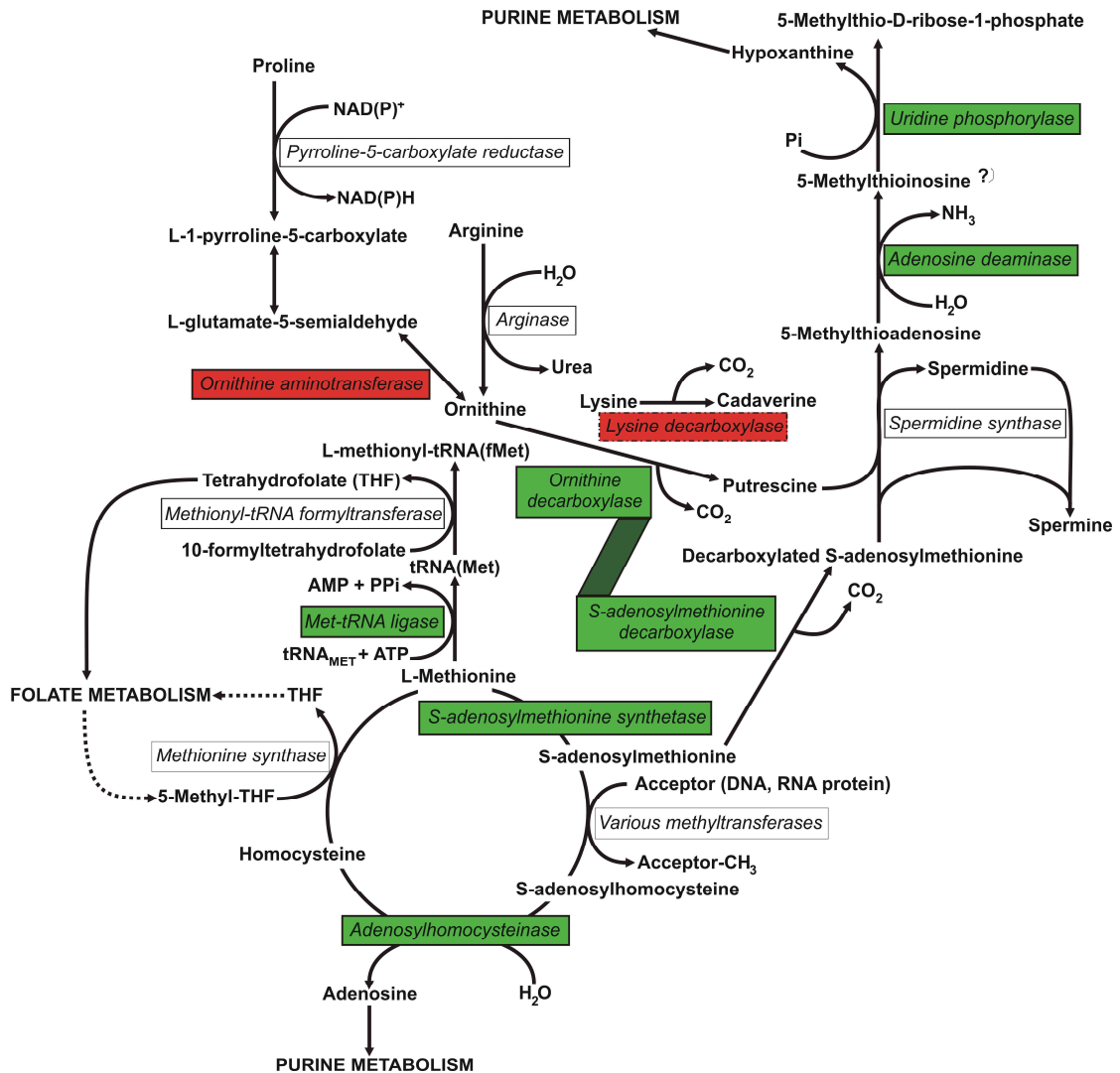


Fig. 3.25 Polyamine and methionine metabolism (adapted from MPMP at <http://sites.huji.ac.il/malarial/>). Plasmodial spermine synthesis is currently believed to be catalysed by spermidine synthase as indicated [85]. Enzymes of which the transcript abundance was significantly increased due to PfAdoMetDC/ODC co-inhibition are indicated in red and those significantly decreased are indicated in green.

The abundance of the majority (~70%) of the 538 transcripts was decreased with PfAdoMetDC/ODC co-inhibition. However, in two investigations of DFMO-induced polyamine depletion (Loikkanen, 2005, PhD thesis, University Oulu)[219] the majority of transcripts were increased. The latter study used twice the DFMO dose and similar exposure times compared to the co-inhibition study reported here. However, MDL73811-treatment

of *T. brucei brucei* resulted in a 20-fold increase of AdoMet [157], which is the principal biological methyl donor in trans-methylation of e.g. DNA, RNA, proteins and phospholipids [239]. The accumulation of AdoMet, rather than polyamine depletion, was proposed to be the antitrypanosomal mechanism of MDL73811 [157]. Therefore, the general transcriptional suppression observed in the current investigation could be due to transcriptional silencing as a result of AdoMet accumulation causing hypermethylation of e.g. histones [125] or 2-deoxycytosine bases within gDNA. However, there is contradicting evidence as to the latter as an epigenetic mechanism in *Plasmodia* [124, 126, 127]. In addition to polyamine depletion, co-inhibition of PfAdoMetDC/ODC may potentially alter the methylation status of *P. falciparum* due to increased levels of AdoMet. The decrease of the transcript for AdoMet synthetase (PF11090w, Table 3.3) may act as a compensatory strategy induced to maintain AdoMet levels. The exact mechanism behind this regulation needs to be elucidated, but AdoMet concentration in MDL73811-treated mammalian cells was effectively regulated through substrate feedback inhibition of AdoMet synthetase activity [240]. This is not the case in *P. falciparum* as it was demonstrated that AdoMet does not allosterically regulate AdoMet synthetase [79], but regulation of AdoMet synthetase by AdoMet at the transcriptional level needs to be investigated. In contrast, the trypanosomal AdoMet synthetase is apparently poorly regulated, resulting in the substantial accumulation of AdoMet with AdoMetDC inhibition [157]. S-adenosylhomocysteine (AdoHcy) is the major by-product of AdoMet-dependent trans-methylation and a competitive inhibitor of trans-methylation reactions [239, 241]. The AdoMet/AdoHcy ratio is an indicator of cellular methylation status and a decrease in this ratio is associated with reduced methylation potential [241]. Therefore, the decrease in abundance of the transcript for adenosylhomocysteinase (PFE1050w), which catalyses the hydrolysis of AdoHcy [241], may be an attempt to restore the AdoMet:AdoHcy ratio and cellular methylation status. Transcriptome analysis of individually inhibited *P. falciparum* AdoMetDC and ODC is currently under way to distinguish between the effects of polyamine depletion with and without the proposed AdoMet accumulation. AdoMet levels and the role of gDNA methylation in the mode of action of MDL73811 in *Plasmodium* are discussed further in Chapter 4.

The transcript for PfAdoMetDC/ODC was decreased ~2-fold with DFMO/MDL73811-treatment (Fig. 3.25, Table 3.3). In accordance, the transcripts for the proteins DHFR/TS and DHPS/PPPCK, targeted by pyrimethamine and sulphadoxine in the study of antifolate-treated *P. falciparum*, were also decreased [197]. DHFR/TS expression is regulated by the binding of the protein to its own mRNA, thus acting as a negative feedback to control its own translation [242]. A similar mechanism could apply to PfAdoMetDC/ODC, but this needs to be elucidated. The decrease in the transcripts for a putative adenosine deaminase (PF10_0289) and uridine phosphorylase (PFE0660c) was postulated to be due to decreased spermidine synthesis (resulting from reduced levels of putrescine and dcAdoMet) and thus less production of 5-methylthioadenosine and subsequently 5-methylthioinosine. An extensive metabolomics investigation was subsequently performed to resolve these hypotheses, as is discussed in Chapter 4.

Polyamines interact with DNA, RNA and proteins [63, 64] and it is, therefore, difficult to discriminate where their main regulatory effects are. In the present investigation, many of the differentially affected transcripts translate proteins that are known to require polyamines for optimal functioning in other organisms (Table 3.3). These include the transcript for DNA topoisomerase II (PF14_0316), which was decreased with PfAdoMetDC/ODC co-inhibition and it was shown in mammalian cells that the enzyme activity also decreased upon polyamine depletion [224]. Moreover, polyamines inhibit calcium/calmodulin-dependent protein kinase 2 [227] and stimulate casein kinases [243]. In accordance, the transcript for a putative calcium/calmodulin-dependent protein kinase 2 (PFL1885c) was increased and that of casein kinase I (PF11_0377) was slightly decreased by DFMO/MDL73811-treatment in *P. falciparum*. Polyamines protect macromolecules from peroxidation reactions [65, 66] and increase the expression of oxidative stress defence genes (including glutathione reductase) in *Escherichia coli* [225]. In the absence of polyamines in the current investigation, the transcripts for the antioxidant protein 1-cys-peroxiredoxin (PF08_0131), as well as glutathione reductase (PF14_0192) and a putative glutathione S-transferase (PF14_0187), were all decreased. Polyamines were also shown to increase the expression of genes related to energy metabolism and iron/zinc transport in *E. coli* [226]. In the current investigation, seven transcripts associated with oxidative phosphorylation (Col, CoxI, CoxIII_2, PF11_0412, MAL7P1.75, PFE0970w, PF13_0121); five concerned with glycolysis (PF10_0155, PF13_0141, PF14_0378, PF14_0598, PFF1300w) and the transcript for a putative zinc transporter (PF07_0065) were significantly decreased. Although there are differences between polyamine metabolism of different organisms [82], these analogies may indicate that polyamines have a regulatory or stabilising effect on the transcripts of these proteins in *P. falciparum*.

Polyamines can also act as transcriptional repressors, which may be indirectly via the regulation of specific transcription factors [226]. Expression of the transcription factor c-Myc was shown to increase upon polyamine depletion [228]. PfAdoMetDC/ODC co-inhibition caused increased transcript abundance of several transcription factors (Table 3.3), including that of a hypothetical protein (PF11_0241) with Myb-like domains (SANT, Homeodomain-like and Myb domains, <http://www.plasmodb.org>). The Myb proteins, e.g. PfMyb1, are sequence-specific transcription factors that regulate the expression of genes implicated in growth and cell cycle regulation [244]. Furthermore, there was an increase in abundance of the transcript for a C2H2-type zinc-finger transcription factor, krox1 (PFL0465c) and two other putative transcription factors, namely a putative CCCH-type zinc-finger protein (PFE1245w) and a hypothetical protein (PFD0560w) with a TATA-box binding protein-like domain (<http://www.plasmodb.org>). Interestingly, a TATA-binding protein-associated factor was shown to be important in the regulation of mammalian polyamine transport for maintenance of basal polyamine levels [88] [245]. In addition, the transcript abundance of a putative transcription factor iib (PFE0415w) was decreased.

Polyamines are required for the degradation of cyclin B1 mRNA in the G1-phase of the classic eukaryotic cell cycle to commit cells to enter the S-phase for completion of the cycle [68]. On the other hand, polyamines stabilise cyclin D1, which upon their depletion result in the decrease of this cyclin and cell cycle arrest [63, 68]. Growth arrest in the trophozoite stage of *P. falciparum* due to ODC and/or AdoMetDC inhibition resembles the late-G1 of the eukaryotic cell cycle [88]. The homologues of these specific cyclins are not yet known within the *P. falciparum* genome but three cyclin-associated transcripts were differentially affected as a result of the perturbation (Table 3.3). The transcripts for proliferating cell nuclear antigen (PF13_0328) and a hypothetical protein (PF14_0604) with cyclin homology (<http://david.abcc.ncifcrf.gov/>) were both decreased. In addition, the transcript for a hypothetical protein (PFL1330c), implicated in cell cycle regulation within the liver stage [246], was increased. The transcript levels of none of the protein kinases associated with cyclins in *P. falciparum* were differentially affected.

Several clusters of adjacently located genes with a co-ordinated decrease in transcription were identified (Table 3.4), including an eleven gene cluster from chromosome 10 (PF10_0014 to PF10_0025, Fig. 3.20). However, the genes within these clusters are not normally all co-expressed according to the 3D7 IDC transcriptome [91], making the decrease/dysfunction of a common transcription factor unlikely. Moreover, nuclear expression of contiguous genes are rarely co-regulated in *P. falciparum* [29]. A more logical explanation may therefore be partial DNA unwinding due to polyamine depletion [230], thereby causing genes previously buried within the nucleosome particle to become more exposed to e.g. oxidative damage. The observed differential co-regulation of these transcripts after polyamine depletion reiterates a perturbation-specific effect on the transcriptome as a result of polyamine depletion.

The most dramatic perturbation-specific transcriptional response observed was the 2.8-fold increase in abundance of the transcript for LDC and ~2-fold increase of that for OAT (Table 3.3, Fig. 3.17). Both of these proteins are intricately involved with polyamine metabolism and their differential abundance indicates a transcriptional mechanism or potential compensatory feedback to overcome the perturbation (Fig. 3.25). The increase in the transcript for OAT may be a compensatory mechanism or buffering effect to prevent toxic ornithine accumulation [247] as a result of ODC inhibition by DFMO. OAT regulates ornithine metabolism and catalyses both synthesis of ornithine from glutamate-5-semialdehyde when levels are low and its degradation to proline and glutamate when present in excess [248]. Lysine decarboxylation produces cadaverine, a diamine and structural analogue of putrescine with one additional methylene group (Fig. 1.4) [69]. LDC activity and cadaverine accumulation have been reported to alleviate ethylene inhibition of arginine decarboxylase and AdoMetDC in pea seedlings [74] and 0.4 mM cadaverine reversed DFMO-induced growth arrest to some extent in *P. falciparum* [154]. Otherwise there is little known about the biological role of LDC or cadaverine in *P. falciparum*, but the Plasmodial recombinant enzyme was successfully expressed and lysine decarboxylation could be demonstrated [79]. The transcripts for LDC and PfAdoMetDC/ODC are expressed at approximately

the same time in *P. falciparum* (25 hpi and 24 hpi respectively), which is expected, should LDC serve as a compensatory mechanism for polyamine/diamine biosynthesis. The transcript for LDC was increased and that of PfAdoMetDC/ODC was decreased, again illustrating the differential effect of the co-inhibition on the abundance of specific transcripts despite the generalised transcriptional arrest. The increase in the transcript for LDC may indicate a potential resistance mechanism, should PfAdoMetDC/ODC be clinically targeted in future. Interestingly, a lysine decarboxylase-like protein was also among the LIMMA dataset, but it was 2.5-fold decreased. This protein is much smaller than LDC (39 kDa versus 280 kDa) and it also contains a putative LDC domain (PlasmoDB 5.4), but activity has not yet been demonstrated. An arginine decarboxylase (associated with putrescine biosynthesis in microorganisms and higher plants, [81, 249]), has not yet been identified within the *P. falciparum* genome (C Wrenger, personal communication).

The programmed compensatory mechanisms (as opposed to a random transcriptional response), which resulted in the highly specific increased abundance of the OAT and LDC transcripts upon polyamine depletion, are also supported by other transcriptome studies of polyamine-depleted *P. falciparum*. Increased transcript levels of OAT were reported after treatment with DFMO alone [219], but were not affected when the downstream enzyme, spermidine synthase (which should not result in ornithine accumulation), was inhibited (J. Becker, unpublished data). However, an increase in LDC transcript abundance was recently also detected with both ODC (K. Clark, unpublished data) and spermidine synthase inhibition (J. Becker, unpublished data), to compensate for the resulting polyamine depletion. In contrast, the transcripts for neither OAT nor LDC were increased after exposure of *P. falciparum* to a variety of perturbations, including a series of antimalarial drugs and environmental stressors (M. Llinás, unpublished data) [189, 196, 198]. It therefore appears as if the increased abundance of LDC and OAT are transcriptional responses specific to the perturbation of polyamine metabolism in *P. falciparum*.

In this chapter the differential abundance of specific transcripts involved in polyamine and methionine metabolism as compensatory responses, as well as the co-regulation of clusters of genes as result of the perturbation, provides evidence of a drug-specific response. Taken together, these results, as well as evidence from other perturbations [179, 189, 190, 198, 199], provide support for the ability of the parasite to react to environmental pressure at the transcriptional level.

In the following chapter, the functional genomics investigation will proceed with proteomics and metabolomics analyses of PfAdoMetDC/ODC co-inhibited *P. falciparum* to confirm the conclusions of the transcriptomics investigation. In addition, specific hypotheses will be investigated with biochemical analyses.

3.5 RAW DATA AND SUPPLEMENTARY WEBSITE

The microarray raw data can be downloaded from PUMAdb (http://puma.princeton.edu/cgi-bin/publication/viewPublication.pl?pub_no=523) and additional data can be obtained from the supplementary website (http://genomics-pubs.princeton.edu/PfAdoMetDC_ODC) supporting the publication that resulted from this work (*van Brummelen et al. J. Biol. Chem, 10.1074/jbc.M807085200*). The microarray data can also be accessed at the NCBI's GEO [250], accession GSE13578, according to MIAME recommendations.

CHAPTER 4

TRANSCRIPTOMICS VALIDATION STRATEGIES

4.1 INTRODUCTION

4.1.1 Evidence of post-transcriptional regulation in *P. falciparum*

Gene regulation of *P. falciparum* is currently a controversial issue with evidence supporting the dominant role of post-transcriptional control [119, 128, 192, 193] on the one hand and evidence demonstrating transcriptional control [123, 179, 189, 190, 198, 199] on the other. As a result, conclusions drawn on transcriptomics data alone require validation. In addition, post-transcriptional responses to perturbations can potentially be missed if only assessed by microarray. The evidence corroborating post-transcriptional control as dominant mode of gene regulation in *P. falciparum* includes the apparent paucity of recognisable promoter elements in the genome [119], the small amplitude transcriptional responses detected upon perturbation of the parasite, conflicting results obtained when the parasite is exposed to small molecules and the recent evidence of variable mRNA decay rate and translational repression [192-194, 196, 197]. These will be discussed in more detail in the following paragraphs.

Nirmalan and colleagues studied the transcriptional [197] and the translational response [242] of antifolate-inhibited parasites, but in contrast with the decreased transcript level of the drug target DHFR/TS, a marked increase was seen on the protein level. This was specific to the inhibitor used and indicated that the parasite is able to significantly relieve constraints resulting from environmental perturbation post-transcriptionally as opposed to responding at the transcriptional level [197]. Another integrated investigation of the transcriptome and proteome of *P. falciparum* after treatment with a choline analogue also indicated more pronounced changes at the protein level without specific transcriptional responses to the drug [128]. Drug-specific effects were furthermore detected on the protein level in a two-dimensional electrophoresis (2D-GE) study of the parasite response to treatment with artemether/lumefantrine [251]. In addition, most studies of environmentally perturbed *Plasmodium* that did report compensatory transcriptional responses and supported the presence of transcriptional control mechanisms in the parasite were not confirmed on the proteome/metabolome level [179, 189, 190, 198] and several others simply failed to detect such programmed transcriptional responses [194, 196, 197].

However, probably the most important evidence of post-transcriptional control of gene expression in *Plasmodium* was the demonstration of the variation in mRNA decay rate during the IDC [193] and the presence of mechanisms resulting in translational repression [192]. The mRNA decay rate increases with parasite development during the IDC and ring-stage parasites have an average mRNA half life of about 9.5

min, which is extended to an average of 65 min during the late-schizont stage [193]. These results implied that the stage-specific mode of transcription during the IDC [29] may in fact be the result of stage-specific mRNA decay [128]. Translational repression mediated via the highly conserved DEAD-box RNA helicase, DOZI, was demonstrated in *P. falciparum* [192]. Translational repression has an important role in sexual differentiation and gametogenesis in higher eukaryotes and involves the movement of specific mRNA molecules into cytoplasmic messenger ribonucleoprotein complexes (mRNPs), which prevents their translation until release from these complexes. DOZI-mutant parasites failed to store certain transcripts (p25, p28), which were therefore targeted for degradation, whereas the transcripts in the translationally repressed mRNPs from wild-type parasites were stored for translation after fertilisation [192].

The most recent addition to the debate on the role of transcriptional control in the parasite was evidence of a cascade of AP2 transcription factors that were proposed to control transcription during the IDC [123], as discussed in section 1.10.5.

4.1.2 Integrative biology from *Plasmodium* functional genomics data

There are currently no reports nearing systems biological investigations of Plasmodia, but biological questions regarding the parasitic lifestyle are starting to be addressed. The proteome data, when combined with evidence of chromosomal clusters encoding co-expressed genes, suggest a highly coordinated expression of *Plasmodium* genes involved in common biological processes [246]. Furthermore, there appears to be a positive correlation between the abundance of transcripts and their encoded proteins during the *P. falciparum* lifecycle [246, 252]. The majority of discrepancies are attributable to a delay between transcript production and protein accumulation (translational gap), which is observed as a time-shift between detection of the transcript and its protein [246].

The most comprehensive and integrated analyses of the genome, transcriptome and proteome have been reported for *P. berghei* and *P. chabaudi chabaudi* and represent state-of-the-art of functional genomics as applied to Plasmodia [30, 253]. Hall and colleagues proposed that the parasite uses four strategies/mechanisms for gene expression during its lifecycle, which includes housekeeping genes, stage-specific genes, host-specific genes (mosquito or mammalian host) and strategy-specific genes (related to invasion, asexual replication and sexual development). Their results indicated that over half of the proteins were detected solely in one stage of the lifecycle, implying a considerable degree of specialisation at the molecular level to support the demanding developmental programme. This large dataset allowed the authors to observe post-transcriptional gene silencing of some gametocyte transcripts with the implicated involvement of a 47-nucleotide sequence motif in two-thirds of the 3'-untranslated regions of these transcripts [61].

New analysis methods are being developed to integrate transcriptomics, proteomics and metabolomics datasets, such as the Partial Least Squares (PLS) method, which was used to integrate yeast transcriptome

and metabolome data [254]. Assuming that the metabolome is a function of the transcriptome, changes due to environmental perturbations were used to model the metabolic variables with PLS. This allowed the discrimination of the effects of perturbations on the transcriptome and metabolome, the modelling of the metabolome as a function of the transcriptome and the extent of similarity between these and finally the identification of transcripts that mediate changes in the metabolome [61]. However, reports of perturbations of *Plasmodium* that integrate transcriptomics, proteomics and metabolomics data are currently not available.

4.1.3 Proteomics methodologies

Two-dimensional polyacrylamide gel electrophoresis (2D-PAGE or 2D-GE) is a powerful and high-resolution protein separation method. In the first dimension proteins are separated based on their iso-electric point (pI) and in the second based on their molecular weight (Mr). Protein mixtures are resolved in this manner over the entire gel for an average of 1000 to 1250 spots (~300 to 1000 proteins) with a weight range of 10 – 250 kDa [255, 256]. This number can be improved to 10000 spots and 3000 proteins under some conditions [255]. The technique has developed considerably in recent years and the use of immobilised pH gradient (IPG) strips for iso-electric focusing (IEF) during the first dimension has tremendously improved the reproducibility. Furthermore, advances in staining technology with fluorescent stains (e.g. SyproRuby, DeepPurple and Flamingo) allow reliable quantitation of separated proteins with high sensitivity and dynamic range compared to the limitations of the traditional silver and Coomassie brilliant blue stains [255]. The fluorescent stains have linear ranges of about three orders of magnitude compared to the covalently bound fluorescent dyes (Cy2, Cy3 and Cy5) with linear ranges of greater than four orders of magnitude [257]. Most modern gel scanners are linear up to five orders of magnitude. However, proteins differ in their staining characteristics and therefore the relationship between intensity and concentrations across different proteins are not the same. Of all the protein stains, the traditional Coomassie stain is the least sensitive with a lower limit of detection of about 10 ng protein compared, to silver and fluorescent stains that have similar sensitivity of ~1 ng protein (20 fmol for a 50 kDa protein). The fluorescent dyes are currently superior and the Cy dyes have a limit of detection as low as 125 pg protein [257]. These covalently bound Cy dyes were introduced to overcome the technical variability of 2D-GE with difference gel electrophoresis (2D-DIGE). Samples are differentially labelled with these dyes (e.g. Cy2, Cy3, Cy5) were introduced to enable differentiation between samples within the same protein mixture on a single 2D gel. The fluorophores can be resolved spectrally and matched for mass and charge to allow better spot matching and normalisation across gels, which minimises gel-to-gel variation [258]. The reproducibility of 2D-GE for quantitative proteomics can also be improved by differential tagging of samples via metabolic isotope labelling by growing cultures on medium containing either heavy- or light-isotope containing components. This was successfully applied with *P. falciparum* grown on medium containing either ¹³C,¹⁵N-isoleucine or regular isoleucine, followed with sample separation on the same gel and mass spectrometry (MS) analysis for identification and differentiation between the samples [259].

However, a significant drawback of 2D-GE is protein solubility problems, which limit the separation and detection of low-abundance and hydrophobic proteins. Multidimensional liquid chromatography (LC)-techniques have emerged to interface separated proteins/peptides directly into mass spectrometers (MS). MudPIT is an LC-based method, whereby proteins are separated depending on charge in the first dimension and hydrophobicity in the second, prior to MS analysis [260]. LC approaches also allow for differential labelling of samples via chemical tagging of proteins/peptides with stable isotopes (e.g. on the cysteine residues) known as isotope-coded affinity tags (ICAT), which enables relative quantitation during comparative studies. A more recently developed quantitative method, isobaric tags for relative and absolute quantitation (iTRAQ), employs a 4-plex set of amine reactive isobaric tags to derivatise peptides at the N-terminus and on the lysine side chains, thus labelling all the proteins in the mixture. The labelled peptides cannot be distinguished with MS (isobaric), but distinguishable signature ions are produced upon fragmentation with tandem MS (MS/MS) [261]. LC methods generally have poorer resolution than 2D-GE and can resolve only hundreds to thousands of proteins, but it can separate low molecular weights of 1 – 20 kDa and offer the additional advantage of easy automated coupling to MS for protein identification [256]. DIGE and ICAT are currently the most commonly practised techniques for gel-based and LC-based quantitative proteomics, respectively [261].

For protein identification, MS and MS/MS methodologies are most commonly used [256]. Mass spectrometers measure the mass/charge ratio (m/z) and make use of the growing knowledge of genome and protein databases where these lists of peak intensities and m/z ratios can be manipulated and compared with lists of theoretical protein digestions or fragmentations [262]. Major advances for analysing protein structure was the introduction of soft ionisation techniques such as electrospray ionisation (ESI) and matrix assisted laser desorption/ionisation (MALDI), which enable the volatilisation of biomolecules. In ESI, the sample is passed through a high-voltage needle at atmospheric pressure to produce charged droplets that desolvate prior to entrance to the high vacuum of the mass spectrometer. In MALDI, the samples are co-crystallised onto a sample plate with an organic matrix that has a conjugated ring structure to absorb at the wavelength of the laser. ESI typically induces a range of charged states, whereas only singly charged ions are usually observed with MALDI [262]. Limitations of these techniques include the limited number of peptide ions produced by trypsin digestion for MALDI analysis that are expected to co-crystallise efficiently with the matrix; the influence of the size and composition (e.g. arginine versus lysine) of the peptides on the signal detected, ESI voltage favouring certain charged states (e.g. higher voltages favour lower charged forms, but the lower charged state may not be within the mass range of the instrument) and competition between analytes for charge as they are extruded from the ESI spray droplets [262].

The ESI and MALDI platforms are combined with various mass analysers, e.g. quadrupole, time-of-flight (TOF), quadrupole ion traps and Fourier transform ion cyclotron resonance (FTICR). Quadrupoles apply radio frequency and voltages, which allows a narrow m/z ratio range to reach the detector. The technique is usually

limited in mass range and has low resolution (separate m/z from 0 to 4000). TOF analysers accelerate ions via a short voltage gradient and measure the time ions take to traverse a field free flight tube (the flight time is proportional to the square root of m/z). TOF instruments can achieve a resolution of 10000 (separate m/z of 1000.0 from 1000.1). Quadrupole ion traps focus ions into a small space with an oscillating electric field and ions are activated and ejected by electronic manipulation of the field. Ion traps are very sensitive since ions can be trapped for varying lengths of time. FTICR uses high magnetic fields to trap and cyclotron resonance to detect and excite ions with a resolution >1000000 (separate m/z of 1000.000 from 1000.001) [262].

For the proteomics investigation of PfAdoMetDC/ODC co-inhibition, as discussed in this chapter, samples were separated with 2D-GE and stained with a fluorescent stain (Flamingo) to enable the sensitive and accurate quantitation of proteins. DIGE is currently the method of choice for differential protein abundance analysis, but the required fluorescent scanner was not available. Selected proteins were subsequently identified with MS/MS (MALDI-Q-TOF), which enabled protein identification and confirmation/validation, as discussed in section 4.3.1.1.

4.1.4 Metabolomics methodologies

Enzyme-based assays for the one-by-one measurement of metabolites have been available for decades, but methods for the simultaneous quantitation of large numbers of metabolites have only become available in recent years [263]. Efforts to quantitate multiple metabolites simultaneously have included thin-layer chromatography [264], high-performance liquid chromatography (HPLC) with UV-detection [265], nuclear magnetic resonance (NMR)-spectroscopy [116] and LC-MS [263, 266, 267]. In general, the methods without MS-detection suffer from low sensitivity and specificity [263]. Global metabolomics analysis of *Plasmodium* is still in its infancy, but recently the 2D-NMR was used to identify and quantitate more than 50 metabolites from isolated mature *P. falciparum* trophozoites [116].

The LC-MS technologies, as discussed for proteomics in section 4.1.3, can also be applied for global metabolomics analysis. NMR is an alternative method that requires minimal sample preparation and is considered to have a high throughput (hundreds of samples per day). In $^1\text{H-NMR}$ an external magnetic field aligns the nuclear spin of responding proton nuclei at specific frequencies where they occur in resonance. The radiation emission or absorbance frequency during nuclei relaxation is detected, which varies depending on the number of electrons orbiting the nucleus. $^1\text{H-NMR}$ theoretically provides unique signals for chemically distinct hydrogen nuclei, which allows analyte structure determination. However, NMR has only half the sensitivity of the discussed MS-based approaches [268].

The advantage of metabolomics compared to transcriptomics and proteomics is that a particular metabolite has the same basic chemical structure irrespective of the organism from which it was extracted. Therefore, once the technology is established and quantitation challenges are overcome, a universal approach that spans

the species barriers can be adopted [269]. However, in contrast with the transcriptome and proteome, metabolite concentrations within the cell are determined by the activities of various enzymes and as a result the components of the metabolome are generally far more complex than is the case with transcripts or proteins [270]. For example, less than 30% of metabolites are involved in only two reactions, ~12% of metabolites participate in more than 10 reactions and ~4% are involved in more than 20 reactions, resulting in a high degree of connectivity in the metabolic network. Because of these complex networks of tightly connected reactions, small perturbations in the proteome can result in significant changes in the concentration of various metabolites. Therefore, metabolomics analyses provide integrative information. However, this strength is also a drawback since data interpretation in the physiological context is generally difficult [270].

Metabolomics data analyses essentially consist of raw data processing, data mining, presentation and storage. Because of instrument inaccuracies such as chromatogram shift and mass drift, raw data processing involves the deconvolution of overlapping chromatogram peaks and chromatogram alignment to overcome the drift and to enable the comparison of different datasets. Baseline correction and noise reduction can also be advantageous, but such data smoothing may lose useful information [268]. Once quantitative datasets have been obtained the fundamental approach is to compare the level of a metabolite between experimental and control samples and to use standard statistics to assess the significance of the detected differences [271]. However, high-throughput multivariate analysis or mining of all the components within a dataset requires unsupervised [e.g. principal component analysis (PCA) and hierarchical clustering] or supervised (PLS) statistical approaches that reduce the dimensionality of the data [268] and even more advanced and detailed approaches will be required to extract the full wealth of information embedded in metabolomics datasets [272].

For the metabolomics investigation of PfAdoMetDC/ODC co-inhibition, samples were analysed with LC-ESI/MS for maximum sensitivity and specificity [263], which enabled the simultaneous determination of 172 water-soluble metabolites. In combination with the transcriptomics, the proteomics and metabolomics analyses of PfAdoMetDC/ODC co-inhibition, as discussed in this chapter, complete one of the first comprehensive functional genomics investigations of perturbed *Plasmodium*. In addition, biochemical assays were performed to investigate specific hypotheses such as the induction of LDC as compensatory response to polyamine depletion and the role of DNA hypermethylation in the mechanism of MDL73811 and in the transcriptional arrest observed during cyto-stasis. By following this integrative approach, two of three perturbation-specific compensatory mechanisms as detected in the transcriptome were confirmed on both the protein and metabolite level, which corroborated their biological relevance in the malaria parasite.

4.2 MATERIALS AND METHODS

4.2.1 Proteomics

3D7 *P. falciparum* culturing and DFMO/MDL73811 treatment were performed as discussed in section 2.2.1 and 3.2.2, but in order to obtain enough protein, an 180 ml culture of 8% parasitaemia and 3% haematocrit

was treated in duplicate (two biological replicates) alongside duplicate untreated controls. Sample volumes of 60 ml were harvested from these at approximately the same three time points as for the transcriptomics investigation (section 3.2.2). The parasites were released with the addition of 60 μ l 10% (w/v) saponin (Merck) in PBS (0.01% final concentration) followed by incubation on ice for 5 min before centrifugation at 2500 g for 15 min. The erythrocyte lysates were aspirated and the parasite-containing pellets were washed four times with an equal volume of PBS before storage at -70°C.

4.2.1.1 Protein extraction and quantitation

A volume of 500 μ l strip rehydration buffer [8 M urea, 2 M thiourea, 2% (w/v) 3-[(3-cholamidopropyl)dimethylammonio]-1-propanesulfonate (CHAPS), 32.4 mM DTT with 0.7% (v/v) carrier ampholytes (IPG buffer, pH 3-10, GE Healthcare)] was added to each parasite pellet for complete solubilisation, denaturation and reduction of proteins and the two biological replicates were combined. The samples were pulse-sonicated with a Virsonic microtip sonifier for 10 cycles (a cycle consisted of 10 pulses of 1 s each at output level 2) with 1 min ice-incubation between cycles. Samples were subsequently centrifuged at 16000 g for 60 min at 4°C. The supernatant was transferred to a new microfuge tube (on ice) and the protein concentration was determined using the 2-D Quant kit (Amersham Biosciences), which uses a combination of a unique precipitant and co-precipitant (proprietary knowledge) to precipitate the sample protein quantitatively while interfering contaminants (carrier ampholytes, thiourea, detergents and reductants) remain in solution. The protein is pelleted by centrifugation and resuspended in an alkaline solution of cupric ions, which bind to the polypeptide backbone of the proteins present. A colorimetric agent reacts with the unbound cupric ions and the resulting colour density is inversely related to the protein concentration. This method is compatible with samples containing urea, thiourea and/or CHAPS as opposed to the regular Bradford protein assay [273]. A BSA dilution series was used to compile a standard curve of absorbance of the coloured reaction product at 492 nm against protein concentration, which was used to estimate the sample protein concentrations.

4.2.1.2 Iso-electric focussing (IEF)

For the first dimension separation of proteins, 400 μ g of the total protein obtained (diluted to a volume of 340 μ l with rehydration buffer) was applied to four 18 cm Immobiline DryStrip (Amersham Biosciences) IPG strips with a linear pH gradient (pH 3-10) inside ceramic strip holders (Amersham Biosciences). The use of IPG strips limits technical variation and is currently the reference method during IEF [255]. The strips were covered with 500 μ l of strip covering oil (GE Healthcare) and active rehydration at 30 V was performed for 10 h using an Ettan IPGphor II iso-electric focussing system (Amersham Biosciences) at 20°C. The voltage was gradually increased in a step-and-hold manner to 8000 V within the next 1.5 h and kept at 8000 V (step 9) for 24000 volt hours (Vh, Eq. 4.1, 4.2).

$$\text{Volt hours (Vh)} = \text{hours (h)} \times \text{Volts (V)} \quad \dots\dots \text{Equation 4.1}$$

$$\text{But during the gradient, Vh} = h \times \frac{(V_{\text{previous step}} + V_{\text{new step}})}{2} \quad \dots\dots \text{Equation 4.2}$$

The run was terminated after a total of ~35000 Vh was reached (Table 4.1).

Table 4.1 Iso-electric focussing step-and-hold programme

| | | | | |
|-----------|----------|-----------|----------------|---------|
| S1 | Step | 30 V | 10 h | 300 Vh |
| S2 | Gradient | 200 V | 0.10 h | 19 Vh |
| S3 | Step | 200 V | 0.20 h | 66 Vh |
| S4 | Gradient | 500 V | 0.20 h | 116 Vh |
| S5 | Step | 500 V | 0.20 h | 166 Vh |
| S6 | Gradient | 2000 V | 0.20 h | 416 Vh |
| S7 | Step | 2000 V | 0.45 h | 1500 Vh |
| S8 | Gradient | 8000 V | 1.40 h | 8333 Vh |
| S9 | Step | 8000 V | Up to 24000 Vh | |
| TOTAL | | ~35000 Vh | | |

4.2.1.3 Two-dimensional polyacrylamide gel electrophoresis (2D-GE)

After completion of the IEF, the strips were briefly rinsed with MilliQ H₂O. The cysteine residues were reduced with 2% (w/v) DTT (Pharmacia Biotech) for 10 min with gentle shaking at 20°C followed by carbamidomethylation with 2.7% (w/v) iodoacetamide (FLUKA, SIGMA) for another 10 min. Both the DTT and iodoacetamide were dissolved in SDS equilibration buffer [50 mM Tris-HCl, pH 6.8, 6 M urea, 30% (v/v) glycerol, 2% (w/v) SDS, 0.002% (w/v) bromophenol blue] and were prepared fresh prior to use. The strips were finally equilibrated for electrophoresis by 10 min incubation in the SDS equilibration buffer only and each strip was subsequently positioned on top of a 10% (w/v) vertical SDS-polyacrylamide gel and sealed with 0.5% (w/v) agarose for the second dimension separation. The gels were run in SDS electrophoresis buffer (25 mM Tris-HCl, pH 8.3, 192 mM glycine, 0.1% SDS) at 80 mA (limits set at 500 V, 40 W), 20°C until the bromophenol blue front reached the bottom of the gels after 4 - 5 h using a Hoefer SE 600 vertical system with a water cooling unit. The gels were removed and fixed overnight in 40% (v/v) EtOH/10% (v/v) acetic acid, with gentle shaking at 20°C. The fix solution was decanted and each gel was stained overnight with gentle shaking at 20°C with 100 ml Flamingo fluorescent gel stain (Bio-Rad, California, USA) for visualisation of proteins. Fluorescent stains are light-sensitive and gels were covered with aluminium foil from this point forward.

4.2.1.4 Gel scanning and data analysis

The gels were scanned with a Pharos FX Plus molecular imager (Bio-Rad) at high and medium intensity (PMT voltage) to enable quantitation of low abundance as well as saturated spots. Twenty-one gels were scanned and the best three of four gels were selected (triplicate technical replicates) for spot analysis using PDQuest 8.0 Advanced (Bio-Rad) software. The gels were orientated by rotation, cropped to the same size, speckle filtered (median filter) and warped for optimal alignment. Roller-ball background subtraction, LOWESS normalisation and automated spot detection and matching were performed. The automated spot matching was carefully checked by visual inspection and comparison in order to achieve maximum consensus within each

replicate group. A master image was generated including all replicate groups to be compared (i.e. one master image of UT_{t1} compared to T_{t1}, T_{t2}, T_{t3} and another master image for UT_{t1} compared to UT_{t2}, UT_{t3}) since the software could only analyse 15 gels at a time. As with the microarray data analysis (section 3.2.8), differential protein abundance was calculated in comparison to UT_{t1} (relative t₀) with PDQuest 8.0 software. Proteins in at least one treated time point with an abundance greater than 2-fold in either direction compared to relative t₀, and p-values of less than 0.05 (Student's t-test), were regarded as differentially affected. The similarity between the replicate groups and relative t₀ was determined by plotting the data on the same graph and calculating the correlation coefficient of the regression line within PDQuest.

4.2.1.5 Spot excision, destaining and trypsin digestion for protein identification

Gels containing spots of interest were visualised on a UV transilluminator at 365 nm to enable the manual excision of the proteins, which was transferred to low adhesion microfuge tubes. Spots from technical replicate gels were combined where possible, dried under vacuum and stored at -20°C. The dessicated gel pieces were rehydrated twice with 200 µl MilliQ H₂O for 10 min. The gel pieces were then washed for 10 min with 200 µl of 50% (v/v) acetonitrile (AcN) followed by 50 mM ammoniumbicarbonate, 100% AcN, 50 mM ammoniumbicarbonate, 50% (v/v) AcN and finally 100% AcN and then centrifuged under vacuum for 5 – 10 min to remove all the traces of AcN. Depending on the size and intensity of the excised spot, the gel pieces were digested with 50 – 100 ng of sequencing grade trypsin (Promega) in its provided buffer and incubated overnight at 37°C. Trypsin cleaves proteins at the carboxyl side of the amino acids lysine and arginine, except when either is followed by proline. The supernatant was collected and a further 20 µl of 70% (v/v) AcN was added to the gel pieces for 30 min. The supernatants were pooled, dried under vacuum and resuspended in 10 – 20 µl of 10% (v/v) AcN/0.1% (v/v) formic acid, depending on the size of the gel pieces. The digested peptides were mixed 1:1 with the MALDI matrix, consisting of a saturated solution of α-cyano-4-hydroxycinnamic acid (HCCA, Bruker Daltonics) in 50% (v/v) AcN/0.1% (v/v) formic acid, and 1.5 µl volumes were spotted in duplicate onto a MALDI plate. MALDI-Q-TOF was performed using a QStar Elite instrument (Applied Biosystems) equipped with a MALDI source with the assistance of S. Stoychev at the CSIR Biosciences Division. The instrument was calibrated with a commercially available peptide calibration standard containing angiotensin II, angiotensin I, substance P, bombesin, ACTH clip 1-17, ACTH clip 18-39 and somatostatin 28 encompassing a mass-range of ~1000 - 3200 Da (Bruker Daltonics, Massachusetts, USA), which was spotted onto the plates. Peptide mass fingerprints (PMF) were obtained with the first MS and the resultant mass lists were compared to a non-redundant protein database (Swiss-Prot/TrEMBL, <http://ca.expasy.org/sprot>) using MASCOT (www.matrixscience.com). Oxidation (methionine) and carbamidomethylation were set as variable and fixed protein modifications respectively, only one missed trypsin cleavage was allowed and the mass tolerance was 50 parts per million [ppm = (experimental mass in daltons – theoretical mass)/(theoretical mass expressed in parts per million), equivalent to 0.1 D for a 2 kD peptide][274]. The probability based MOWSE score (-10*LogP, with P the probability of the match being a random event) was used to estimate the

significance of the identification and was set at a confidence threshold of 5% ($p < 0.05$). The second mass analyser (Q-TOF) accelerated the peptides, resulting in collision with nitrogen gas particles and fragmentation, providing a higher resolution fingerprint, which was searched in a similar manner using MASCOT to confirm the initial identification.

4.2.2 Metabolomics

This experiment was performed in collaboration with K.L. Olszewski and D. Willinski, at Princeton University (Princeton, New Jersey, USA). DFMO/MDL73811-treatment of 60 ml 3D7 *P. falciparum* cultures of 9% parasitaemia and 2% haematocrit was performed in duplicate (two biological replicates) alongside duplicate 60 ml untreated controls as discussed in section 3.2.2. Samples of 20 ml were harvested at approximately the same three time points as for the transcriptomics and proteomics investigations. The metabolite extraction and LC-MS/MS methodology were previously developed and optimised for the simultaneous relative quantitation of water-soluble metabolites [263, 266].

4.2.2.1 Metabolite extraction and polyamine derivatisation

Of 20 ml cultured *P. falciparum* samples (two biological replicates), 10 ml was used for general metabolite analysis and 10 ml was derivatised for polyamine analysis. The cultures were pelleted by centrifugation at 2000 g for 5 min at room temperature and metabolites were serially extracted immediately thereafter. Four pellet volumes of -75°C 100% MeOH (e.g. 2 ml to a 500 μl pellet) were added at the start to flash-freeze all metabolic activity, followed with incubation on dry ice for 15 min with vigorous vortexing every 5 min. The sample was centrifuged for 5 min at 11000 g at 4°C and the supernatant removed and stored on ice. A volume of 80% (v/v) ice-cold MeOH was added to the pellet, followed with vortexing and sonification on ice in a water bath sonicator for 15 min. The sample was again centrifuged for 5 min at 11000 g at 4°C and the supernatant removed and added to the previous aliquot on ice. The last extraction step with 80% (v/v) MeOH was repeated and the supernatants from each extraction were pooled and centrifuged free of cell debris and protein. Culture medium was sampled as background control and these samples were treated in the same way as the culture samples by the addition of four volumes of -75°C 100% MeOH, then two volumes of 80% (v/v) MeOH to obtain the same dilution factor as the pellet extracts and subsequently centrifuged free of protein. All samples were analysed within 24 h of their generation and were analysed for 167 metabolites as described [263, 266, 267], as well as putrescine, spermidine, spermine, cadaverine and dcAdoMet. The synthetic dcAdoMet standard used for calibration was a kind gift from K. Samejima (Josai University, Japan); the other standards were obtained commercially.

For polyamine analysis, succinic anhydride derivatisation was performed to induce a negative charge on these polycationic molecules to retain them on the aminopropyl column during LC. A volume of 10 μl of triethylamine was added to 100 μl of cell extract and mixed, followed with a few crystals of solid succinic anhydride and vigorous vortex mixing. The derivatisation reaction was performed for 1 h at room temperature, with vortexing

every 10 min. After this incubation the samples were centrifuged to pellet any remaining solid succinic anhydride and the liquid portion of the sample was subjected to LC-MS/MS analysis using parameters previously determined with pure stock solutions of putrescine, cadaverine, spermidine and spermine.

4.2.2.2 LC-MS/MS metabolite analysis

LC-MS/MS was performed using an LC-10A HPLC system (Shimadzu Corporation, Kyoto, Japan) and a Luna aminopropyl column (250 mm x 2 mm with a 5 µm particle size (Phenomenex, California, USA) coupled to the mass spectrometer. Quantitation and run-to-run variability were controlled by the 1:10 addition of an internal standard mixture containing ¹³C/¹⁵N isotopes (alanine, aspartate, glutamate, glutamine, isoleucine/leucine, methionine, phenylalanine, serine, threonine, tyrosine and valine) encompassing a mass-range distributed over the entire chromatographic run. The LC parameters were as follows: autosampler temperature, 4 °C; injection volume, 20 µl; column temperature, 15 °C and flow rate, 150 µl/min. The LC solvents were Solvent A [20 mM ammonium acetate and 20 mM ammonium hydroxide in 5% (v/v) AcN (pH 9.45)] and Solvent B (100% AcN). The gradients were as follows: positive mode, t = 0, 85% B; t = 15 min, 0% B; t = 28 min, 0% B; t = 30 min, 85% B; t = 40 min, 85% B; and negative mode, t = 0, 85% B; t = 15 min, 0% B; t = 38 min, 0% B; t = 40 min, 85% B; t = 50 min, 85% B.

MS analyses were performed on a Finnigan TSQ Quantum Ultra triple-quadrupole MS (Thermo Electron Corporation, Massachusetts, USA), equipped with an ESI source. The ESI spray voltage was 3200 V in positive mode and 3000 V in negative mode. Nitrogen was used as sheath gas at 30 psi and as the auxiliary gas at 10 psi, and argon as the collision gas at 1.5 mTorr, with the capillary temperature 325°C. Scan time for each single reaction monitoring (SRM) event transition was 0.1 s with a scan width of 1 m/z. SRM involves selecting for ions of a specified parent molecular weight (m/z), fragmenting the parent ion at optimal collision energy to produce a particular daughter ion and then quantitating the production of ions of the daughter mass. The scanning of multiple SRM events enables the simultaneous measurement of numerous compounds in a single LC run. The LC runs were divided into time segments, with the SRM scans within each time segment limited to those compounds eluting during that time interval. For compounds eluting at the boundaries between time segments, the SRM scan corresponding to a specific compound was conducted in both time segments. The instrument control, data acquisition and data analysis were performed by Xcalibur software (Thermo Electron Corporation, version 1.4 SR1), which also controlled the chromatography system.

4.2.2.3 Metabolomics data analysis

Raw data peak quantitation was performed by Xcalibur software using 10³ as bottom quantitation limit. Biological replicate data were averaged (arithmetic mean), background subtracted and compared to the relative t₀ in EXCEL, to calculate fold change as a result of the perturbation. Treated parasite data was also compared to their parallel time point untreated controls, to determine the validity of the relative t₀ strategy for

metabolite analysis. Metabolites with a fold change of 2 were regarded as significantly changed. Pearson correlations of the complete metabolic profiles and excluding several metabolites present in excess in the medium (arginine, asparagine, aspartic acid, cystine, glutamic acid, glutamine, histidine, isoleucine, leucine, lysine, phenylalanine, proline, serine, threonine, tryptophan, tyrosine, valine, choline, niacinamide, pantothenic acid, riboflavine, thiamine, D-glucose) were calculated in EXCEL. This measure of similarity is commonly used in global expression profiling analyses [29, 62, 91].

4.2.3 Decarboxylase activity assays

LDC activity of DFMO/MDL73811-treated and untreated culture lysates was assessed by measuring $^{14}\text{CO}_2$ -release according to the methodology of Assaraf and colleagues [88], as discussed for AdoMetDC and ODC in section 3.2.1.2. L-[1- ^{14}C]lysine (56 mCi/mmol, American Radiolabelled Chemicals) were incubated with the lysates from treated and untreated 3D7 cultures (10% parasitaemia, 3% haematocrit) sampled in the early (19 hpi) and mature (34 hpi) trophozoite stages. Samples of 10 - 15 ml were centrifuged at 2500 g for 5 min, the pellet washed three times with an equal volume of PBS and then 500 μl was transferred to a cryotube and stored at -70°C . Uninfected erythrocytes were sampled and processed in the same way to serve as a negative control. A volume of 1 ml of buffer A [88] or LDC buffer [0.5M sodium acetate, 1 mM DTT, 1 mM EDTA, 0.1 mM PLP, pH = 6] [275] was added, the samples were freeze-thawed three times (alternating between -70°C and 37°C) and then centrifuged at 8000 g for 20 min at 4°C . The rest of the assay was performed as described in section 3.2.1.2, but the 50 μl reaction mixture that was added to 200 μl cell lysate consisted of 40 μM ^{14}C L-lysine (100 nCi) and 40 μM PLP in either buffer A or LDC buffer. Assays were allowed to take place at 37°C for 60 min in a ZHWY-110X shaking water bath (Shanghai ZHICHENG Analytical Instruments Manufacturing Co.).

4.2.3.1 LDC induction in *E. coli* as assay positive control

BL21(DE3) *E. coli* cells were grown overnight at 37°C to saturation in Luria-Bertani (LB)-broth [1% (w/v) tryptone, 0.5% (w/v) yeast extract and 1% (w/v) NaCl, pH 7.5] and then diluted 1:4 with either LB-broth or modified Falkow (F-MES) medium [0.5% (w/v) peptone, 0.3% (w/v) yeast extract, 0.1% (w/v) D-glucose, 0.5% (w/v) D,L-lysine and 100 mM 2-(N-morpholino) ethanesulfonic acid, pH 5.2] [275, 276]. The cells in LB-broth were grown for 6 h with aeration (agitation at 175 rpm at 37°C) and those in F-MES for 2 h with aeration followed by 4 h without (stationary at 37°C). The cultures were centrifuged at 2000 g for 20 min, the pellets were washed once with five volumes of PBS and stored at -70°C . A cell pellet of 500 μl was resuspended in either buffer A or LDC buffer and incubated with 0.1 mg lysozyme (Roche Diagnostics) for 30 min. The samples were pulse-sonicated with a Virsonic microtip sonifier for seven cycles as described in section 4.2.1.1, to ensure complete lysis, followed by centrifugation at 20000 g for 30 min at 4°C . The cell lysate supernatants were aspirated and only 10 μl bacterial lysate was included per 250 μl reaction.

4.2.4 Methylation status determination

4.2.4.1 CpG island analysis of the differential transcript abundance list

CpG island detection and analysis of the increased and decreased transcript abundance lists were performed in EMBOSS (http://emboss.sourceforge.net/apps/release/5.0/emboss/apps/nucleic_cpg_islands_group.html) using a batch file. The EMBOSS nucleic CpG island applications CpGplot, CpGreport and geecee-count were performed. In CpGplot, the observed number of CpGs is the count of the number of cytosines directly followed by a guanine, whereas the expected number in a window is the number of CpG dinucleotides expected based on the frequency of cytosines and guanines in that window (<http://www.sacs.ucsf.edu/Documentation/emboss/cpgplot.html>). CpGplot identifies CpG islands over an average of 10 windows, where the percentage composition of cytosines and guanines is over 50% and the calculated observed/expected ratio is over 0.6 for a minimum of 200 nucleotides. CpGreport scans nucleotide sequences for regions with higher than the expected frequency of the CpG dinucleotide (<http://www.sacs.ucsf.edu/Documentation/emboss/cpgreport.html>) and geecee-count calculates the fraction of guanine and cytosine nucleotides within a nucleotide sequence (<http://www.sacs.ucsf.edu/Documentation/emboss/ceegee.html>).

4.2.4.2 Global methylation assays

4.2.4.2.1 gDNA isolation

The methodology applied was similar to the strategy reported for investigating the methylation status of another protozoan, *Entamoeba histolytica* [277]. Volumes of 5 ml treated and untreated *P. falciparum* culture (10% parasitaemia, 3% haematocrit) were sampled for gDNA isolation in the early (19 hpi) and mature (34 hpi) trophozoite stages, as described in section 4.2.3. The samples were pelleted by centrifugation at 2500 g for 5 min, the pellet washed with an equal volume of PBS and then stored at -70°C. gDNA was isolated with the QIAamp Blood Mini kit (QIAGEN). This kit works on the same principle as discussed in section 3.2.4 for cDNA purification. The erythrocytes were lysed by chaotropic salts and detergents and the cellular debris was removed by filtration. The DNA was purified from the soluble part of the lysate by binding to a silica matrix [211], which was then washed with alcohol-based buffers to remove the salts. The membrane-bound DNA was treated with RNase A (Fermentas Life Sciences) for 10 min to remove contaminating RNA before the final elution of the gDNA with 200 µl water. The concentration was determined by measuring the absorbance at 260 nm by UV spectrophotometry with a NanoDrop-1000. For double-stranded DNA, one absorbancy unit equals 50 ng/µl [209]. As discussed in section 3.2.3, DNA purity was estimated from the 260 nm/280 nm ratio, which should preferably be between 1.7 – 1.9 [209].

4.2.4.2.2 Methylation negative and positive controls

Synthetic DNA was prepared by amplification of the OAT (PFF0435w) gene from a pET-15b (Novagen, Merck, Darmstadt, Germany) construct provided by K. Clark, to serve as methylation-free negative control. Plasmid DNA (20 ng) was amplified with 5 U Taq DNA polymerase (New England Biolabs), 200 µM dNTPs, 20 pmoles

of primers (forward: 5'-CTCGAGGATTTTCGTTAAAGAATTA AAAAG-3' and reverse: 5'-GCTCAGCCTCAGTTATAAGTTGTCATC-3') in standard buffer (New England Biolabs) in a total reaction volume of 100 μ l. After denaturation at 94°C, the DNA was amplified for 30 cycles (94°C for 30 s, 56 °C for 30 s, 72°C for 2 min) with a final 5 min extension step at 72°C. Gel electrophoresis analysis of the amplified product was performed with a 1.2% (w/v) agarose in TAE (40 mM Tris, 20 mM glacial acetic acid, 1 mM EDTA), pH 8) gel containing 0.5 μ g/ml ethidium bromide. A voltage of 5 - 7 V/cm was applied (~80 V) for 45 min and the gel was visualised on a UV transilluminator (Spectroline TC-312 A) at 312 nm. The amplification product was subsequently purified with the QIAquick PCR purification kit (QIAGEN) as described in section 3.6.2. OAT DNA (2.5 μ g) was methylated with 12 U M.SssI CpG methyltransferase (New England Biolabs) and 20 nmoles AdoMet in 62.5 μ l at 37°C for 2 h to be used as a methylation positive control. The methylated OAT DNA was again purified from excess AdoMet with the QIAquick PCR purification kit (QIAGEN).

4.2.4.2.3 Restriction-enzyme digestion to assess gDNA methylation

The isolated gDNA from treated and untreated *P. falciparum* cultures was digested with methylation-sensitive restriction enzymes to reveal gDNA methylation patterns. Samples of 250 ng gDNA as well as 250 ng methylated and unmethylated OAT DNA were digested with 10 U *Hpa*II (Fermentas Life Sciences) and 20 U *Dpn*I (Fermentas Life Sciences) overnight at 37°C. Cytosine methylation within the recognition site protects against *Hpa*II digestion (C \downarrow CGG), whereas *Dpn*I digestion only occurs when the adenine in its recognition site is methylated (GA \downarrow TC). The digestion products were separated on a 0.8% (w/v) agarose gel in TAE buffer containing 0.5 μ g/ml ethidium bromide as described in section 3.6.2 and 4.2.4.2.2.

4.2.4.2.4 South-Western immunoblotting

gDNA samples (UT_{t1}, UT_{t3}, T_{t1} and T_{t3}) were denatured by boiling for 5 min, followed by cooling on ice for 5 min. To ensure that signal intensity increased with increasing gDNA concentration, 500 ng and 1000 ng quantities were spotted onto a positively charged nylon membrane (Roche Diagnostics) along with 250 ng methylated and unmethylated OAT (prepared in section 4.2.4.2.2) and 1 μ l of 0.01 M 5-methylcytidine (SIGMA) as controls. The DNA was UV cross-linked for 3 min on a UV transilluminator (Spectroline TC-312 A) at 312 nm and then blocked overnight at 4°C with 2% (w/v) BSA (Roche Diagnostics) in PBS inside a small plastic resealable bag. The blocking solution was discarded and the membrane was incubated overnight at room temperature with gentle shaking in a 0.1 μ g/ml dilution of mouse anti-5-methylcytidine monoclonal IgG (AbD Serotec, Oxford, UK) in washing buffer [2% (w/v) BSA, 0.1% Tween-20 in PBS] according to the manufacturer's instructions. The membrane was washed extensively with three 10 min incubation steps in washing buffer at room temperature with gentle shaking. The membrane was subsequently incubated for 1 h with the anti-mouse hrp-conjugate followed by four 5 min washes in washing buffer, three 5 min washes with 0.1% Tween-20 in PBS and finally two 5 min washes in PBS only. All the wash steps were performed at room temperature with gentle shaking. The SuperSignal West Pico Chemiluminescence kit (Pierce, Illinois, USA)

was used as substrate for the oxidation reaction catalysed by the hrp-conjugate, as described in section 2.2.3.2.2. Usually, 4 ml of hydrogen peroxide and 4 ml of luminol provided in the kit was mixed just before use and incubated with the membrane for 5 min at room temperature with gentle shaking. Excess SuperSignal solution was removed to minimise background luminescence. The membrane was exposed to Hyperfilm ECL X-ray film for high performance chemiluminescence (Amersham Biosciences) for 5 – 6 h in the dark. The X-ray film was developed in Universal Paper Developer (Ilford) for 1.5 – 3 min until the spots became visible, briefly rinsed in MilliQ H₂O and then fixed with Rapid Paper Fixer (Ilford) for 1 min. The film was subsequently rinsed with MilliQ H₂O and left to dry at room temperature. X-ray films were scanned with a VersaDoc scanner (Bio-Rad) and densitometry analysis was performed with Quantity One (Bio-Rad) software.

4.3 RESULTS

4.3.1 Proteomics analysis of PfAdoMetDC/ODC co-inhibited *P. falciparum*

To validate the findings of the transcriptome investigation (Chapter 3), PfAdoMetDC/ODC co-inhibition was repeated and the effects of polyamine depletion and cytostasis on the parasite proteome were determined with 2D-GE. The two biological replicates of the experiment were pooled to have enough protein for three to four technical replicates, which minimised technical variability and enabled differential protein abundance analysis. A master image was generated, which represented all the spots across all the replicate groups to be compared. However, the software could analyse a maximum of 15 gels at a time and therefore one master image was prepared for UT_{t1} compared to T_{t1}, T_{t2}, T_{t3} (Fig. 4.1) and another for UT_{t1} compared to UT_{t2}, UT_{t3} (results not shown).

As was observed in the transcriptome, cytostasis resulted in a high correlation between the gels of the relative t₀ (UT_{t1}) and the three treated time points (UT_{t1} versus T_{t1}: R = 0.93; UT_{t1} versus T_{t2}: R = 0.88; UT_{t1} versus T_{t3}: R = 0.88) and a lower correlation with UT_{t2} and UT_{t3} (UT_{t1} versus UT_{t2}: R = 0.78; UT_{t1} versus UT_{t3}: R = 0.70; Table 4.2). These correlation values indicate that the cytostatic effects were more subtle in the proteome than in the transcriptome (section 3.3.4.3), but the perturbation caused an overall decrease in the number of proteins detected over the time course (UT_{t1} = 483 spots; T_{t1} = 461; T_{t2} = 409; T_{t3} = 416). A similar result was detected in the transcriptomics investigation where the majority of differentially affected transcripts were decreased, as described in section 3.3.5.2.

Table 4.2 Correlation of the 2D-GE data across replicates groups

| Comparison | Correlation of regression line (R) ^a |
|------------------------------------|---|
| UT _{t1} :T _{t1} | 0.93 |
| UT _{t1} :T _{t2} | 0.88 |
| UT _{t1} :T _{t3} | 0.88 |
| UT _{t1} :UT _{t2} | 0.78 |
| UT _{t1} :UT _{t3} | 0.70 |

a. The correlation coefficient of the regression line when the respective replicate groups were plotted on the same graph in PDQuest.

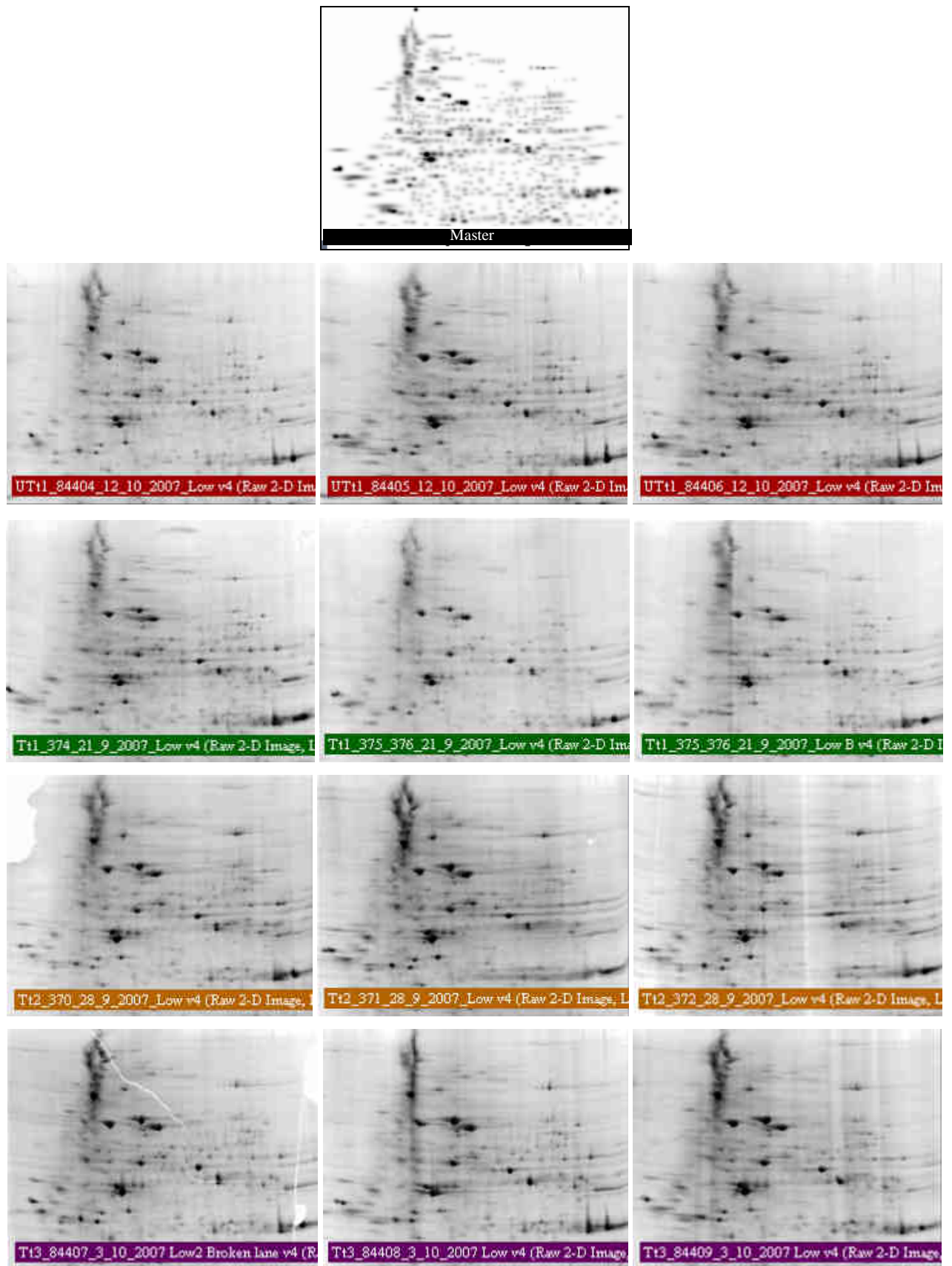


Fig. 4.1 The master image and actual images of the three best 2D-GE technical replicates used for analysis of UT₁₁ versus T₁₁, T₁₂ and T₁₃.

4.3.1.1 Differential protein abundance analysis and protein identification

As in the transcriptomics investigation, the differential abundance of proteins was calculated compared to UT_{t1}, which was previously defined as the relative t₀, a reference point just prior to the transcriptional arrest (section 3.3.5). Due to the translational gap or time delay between the appearance of the transcriptional peaks and their corresponding protein peaks [246], the relative t₀ of the proteins could arguably be later than for the transcripts. However, a high resolution reference proteome dataset, similar to the IDC transcriptome [29, 91] is still lacking [187] and a similar calculation of the approximate time of the proteomics relative t₀ could not be performed. Hence, for comparison purposes, the sampling times of the transcriptomics and proteomics investigations were kept the same and fold changes were again calculated compared to UT_{t1} with the differential abundance criteria 2-fold change and p<0.05. By following this approach, 53 spots (26 spots with an increasing and 27 spots with a decreasing profile) were regarded as differentially affected, but only 41 spots were visible to the eye for manual excision (Fig. 4.2, Appendix D).

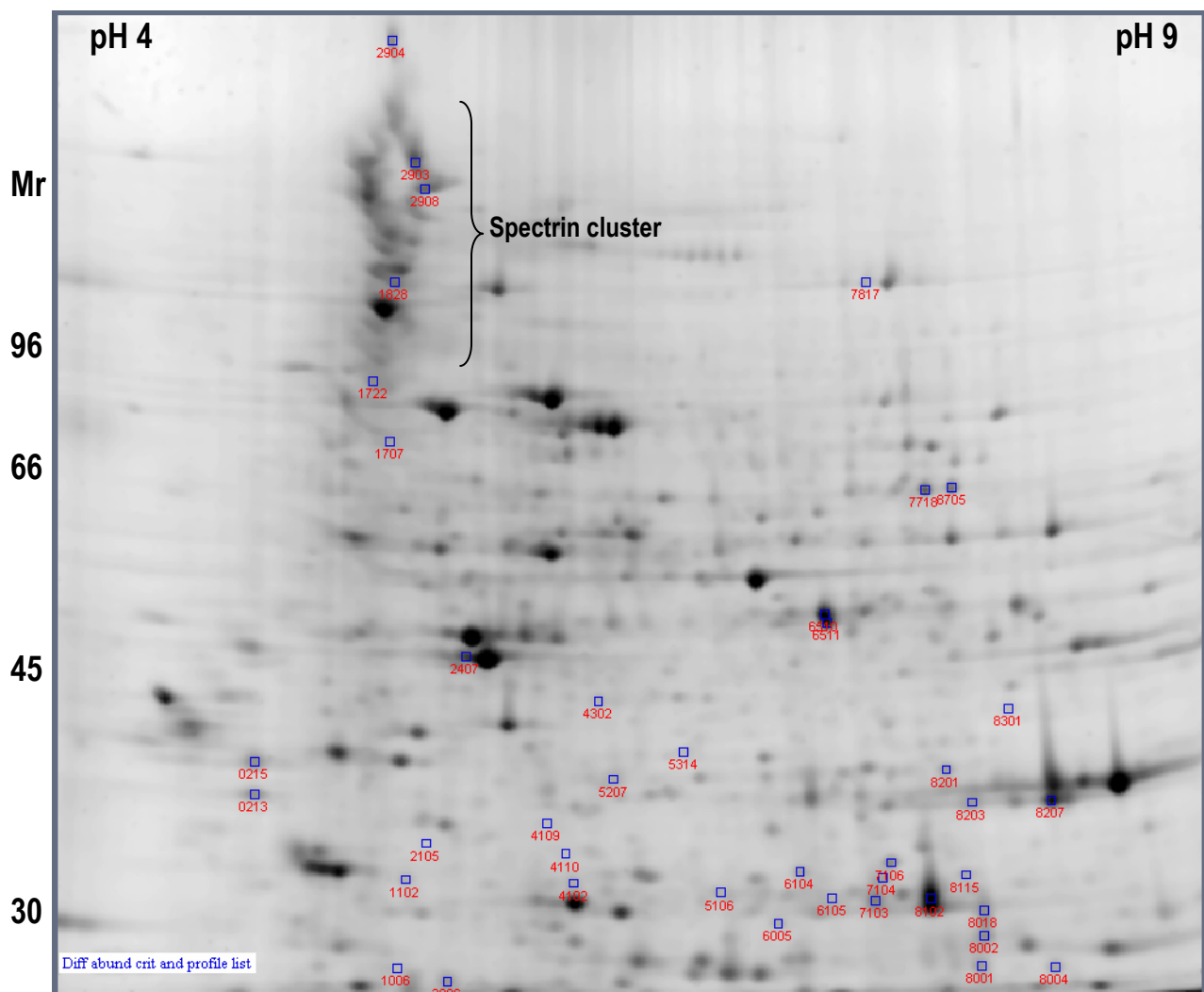


Fig. 4.2. A typical gel (UT_{t1}_84404) indicating the 41 spots with differential abundance that were visible to the eye and could be excised and processed for identification. The molecular weight (Mr) in kDa and pH variation across the gel is displayed. Note that most spots of interest were of low molecular weight and low intensity, which hampered successful identification. The standard spot numbers (SSP) as designated by PDQuest are displayed.

The excised protein spots were cleaved into smaller peptides with trypsin and the absolute masses of these were then determined by MALDI-Q-TOF, which separates singly charged peptides based on m/z , resulting in a sequence-specific PMF (Fig 4.3A) [278]. The experimentally obtained PMF were compared *in silico* with the theoretical/calculated peptide masses of proteins stored in Swiss-Prot/TrEMBL by means of the search engine MASCOT using a threshold of 5% (MOWSE score ≥ 78 i.e. $p < 0.05$). The results were statistically analysed and possible matches were indicated. However, spots excised from 2D-GE are not necessarily pure proteins, but may contain protein mixtures with the same M_r and pI characteristics, which can complicate PMF analysis. Furthermore, different peptides can sometimes have the same absolute masses, resulting in similar PMF spectra. Therefore, MS/MS validation of PMF identities was performed by fragmenting the 50 most prominent PMF peptide ions into daughter ions via acceleration and collision with nitrogen gas in the second mass analyser (Q-TOF) and again separating them according to m/z (Fig. 4.3B). These fragmented daughter ions were used to deduce the amino acid sequences of the parent peptides (Fig. 4.3B). Note that peptide fragments are indicated by a, b or c when the charge is retained on the N-terminus and x, y or z when the charge is on the C-terminus and the subscript indicates the number of amino acids in that particular fragment.

However, since the majority of the spots had low molecular weight (<30 kDa) and low intensity, only 11 proteins (27%) were successfully identified with MALDI-Q-TOF (Table 4.3). This number is in agreement with the spot identification reported in another 2D-GE plasmodial study where only 25% (50/200) of the excised proteins could be identified [251]. Although the number of spots with increasing (26 spots) and decreasing (27 spots) profiles were almost equal, 9 of the 11 proteins that could be identified showed an increase in abundance over the time course, which enhanced their identification (Appendix D).

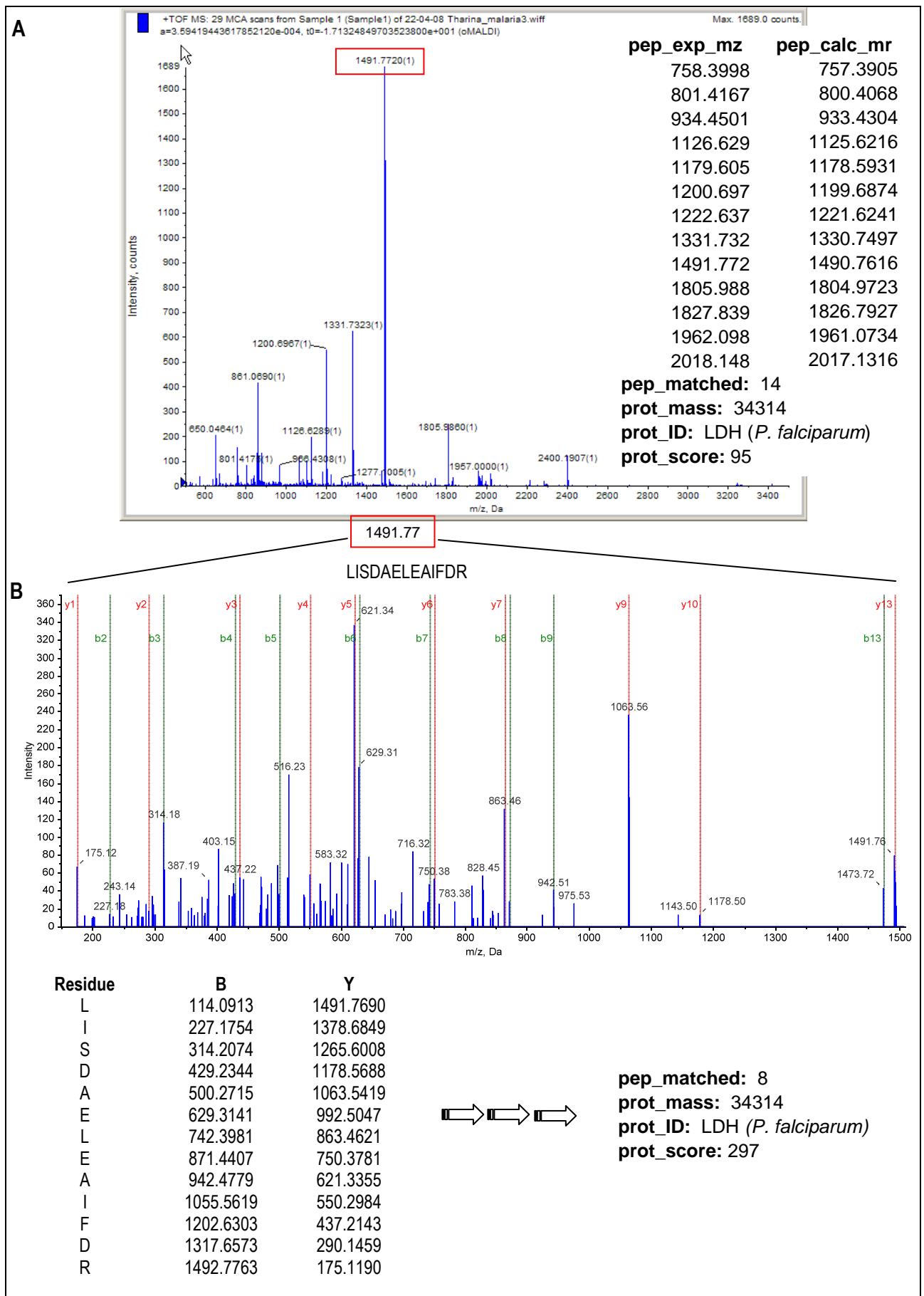


Fig. 4.3 MALDI-Q-TOF MS/MS protein identification of LDH as an example. **A)** PMF spectrum indicating the experimental and calculated molecular mass of the most prominent peptides after the tryptic digest, which was identified by MASCOT as LDH (prot_score or MOWSE score = 95). **B)** MS/MS scan indicating the amino acid sequence LISDAELEAIFDR of the parent peptide with mass 1491.77. The amino acid sequences of eight peptides were deduced in this manner, which confirmed the protein identity as LDH (MOWSE score = 297).

Table 4.3 Identification and characterisation of a subset of proteins with differential abundance

| SSP ^a | Annotation | Fold-change ^b | M _r (kDa) | pI | PlasmoDB | Peptide mass fingerprinting (PMF) | | | | MS/MS confirmation | | | |
|------------------|------------------------------------|--------------------------|----------------------|------|-----------|-----------------------------------|-----------------------|--------------|--------------------------|-------------------------|-----------------------|--------------|--------------------------|
| | | | | | | Protein ID ^c | Pep. ^d no. | %Seq. cover. | MOWSE ^e score | Protein ID ^c | Pep. ^d no. | %Seq. cover. | MOWSE ^e score |
| 1102 | Falcpain-2 | 2.9 | 27.6 | 4.96 | PF11_0165 | Q3HTL5-PLAFA | 11 | 44 | 71 | Q3HTL5-PLAFA | 4 | 13 | 134 |
| 1828 | Human erythroid α -spectrin | 4.7 | 282.0 | 4.98 | - | - | - | - | - | SJHUA | 10 | 5 | 358 |
| 2407 | Human beta-actin (fragment) | 2.7 | 41.3 | 5.56 | - | Q96HG5_HUMAN | 21 | 69 | 106 | ACTB_CAMDR | 8 | 32 | 266 |
| 2903 | Human erythroid α -spectrin | 3.3 | 280.9 | 4.98 | - | Q5VYL2_HUMAN | 52 | 30 | 110 | Q5VYL1_HUMAN | 14 | 8 | 631 |
| 2904 | Human erythroid α -spectrin | 5.9 | 280.9 | 4.98 | - | SPTA1_HUMAN | 56 | 24 | 80 | SJHUA | 9 | 5 | 201 |
| 2908 | Human erythroid α -spectrin | 2.7 | 280.7 | 4.98 | - | Q5VYL2_HUMAN | 46 | 26 | 100 | Q5VYL1_HUMAN | 17 | 11 | 652 |
| 6510 | AdoMet synthetase | -2.1 | 45.3 | 6.28 | PF11090w | Q9GN14_PLAFA | 15 | 43 | 119 | Q9GN14_PLAFA | 12 | 40 | 455 |
| 6511 | OAT | 2.2 | 46.9 | 6.47 | PFF0435w | AAG44560 | 20 | 53 | 215 | CR382399_NID | 11 | 23 | 332 |
| 7817 | Elongation factor 2 | 2.8 | 94.5 | 6.36 | PF14_0486 | Q8IKW5_PLAF7 | 34 | 32 | 81 | Q9NDT2_PLAFA | 7 | 13 | 271 |
| 8201 | Pdx1 homologue | 2.5 | 33.4 | 6.76 | PFF1025c | Q3V7I1_PLAF7 | 17 | 48 | 79 | Q3V7I1_PLAF7 | 6 | 31 | 170 |
| 8207 | LDH ^f | 2.8 | 34.3 | 7.12 | PF13_0141 | Q71T02_PLAFA | 14 | 49 | 95 | Q71T02_PLAFA | 8 | 33 | 297 |

- a. SSP is the standard spot number designated by PDQuest
- b. Fold change calculated at the time point of maximum change
- c. MASCOT search protein identifier
- d. Number of peptides identified in the mass spectrum.
- e. A MOWSE score of 78 indicates a threshold of 5% ($p < 0.05$)
- f. Note that LDH decreased from 2.8 to unchanged during the time course compared to the relative t_0

4.3.1.2 Perturbation-specific compensatory mechanisms confirmed in the proteome

Despite the limited number of spots with positive identities, meaningful results were obtained, including proteins involved in polyamine and methionine metabolism (Table 4.3). These include AdoMet synthetase, OAT and PLP synthase (pdx1, PFF1025c). The differential protein abundance of OAT and AdoMet synthetase (Fig. 4.4, Table 4.3) correlated with their transcript abundance after PfAdoMetDC/ODC co-inhibition (Table 3.3) and confirmed these compensatory mechanisms in the proteome. The ~2-fold increase in the OAT transcript corresponded with a 2.2-fold increase in the protein and the 2.4-fold decrease in the transcript for AdoMet synthetase corresponded with a 2.1-fold decrease in this protein (Fig. 4.4). The third compensatory mechanism proposed in the transcriptomics investigation, namely the induction of LDC, could not be assessed with 2D-GE due to the protein size (280 kDa), which prohibited gel penetration. However, pdx1 was increased 2.5-fold and synthesises PLP, which is an important co-factor for both PfAdoMetDC/ODC and LDC [279]. The change seen on the transcript level was delayed on the protein level in the case of LDH (Appendix D). The LDH transcript was decreased 1.7-fold and the protein was increased 2.8-fold in T_{t1} , but during the time course the protein gradually decreased (2.8-fold) to the same level as the relative t_0 (i.e. unchanged) in T_{t3} . LDH was also identified in another plasmodial study to show a delay between mRNA and protein accumulation due to the translational gap or time required for translation to occur [246].

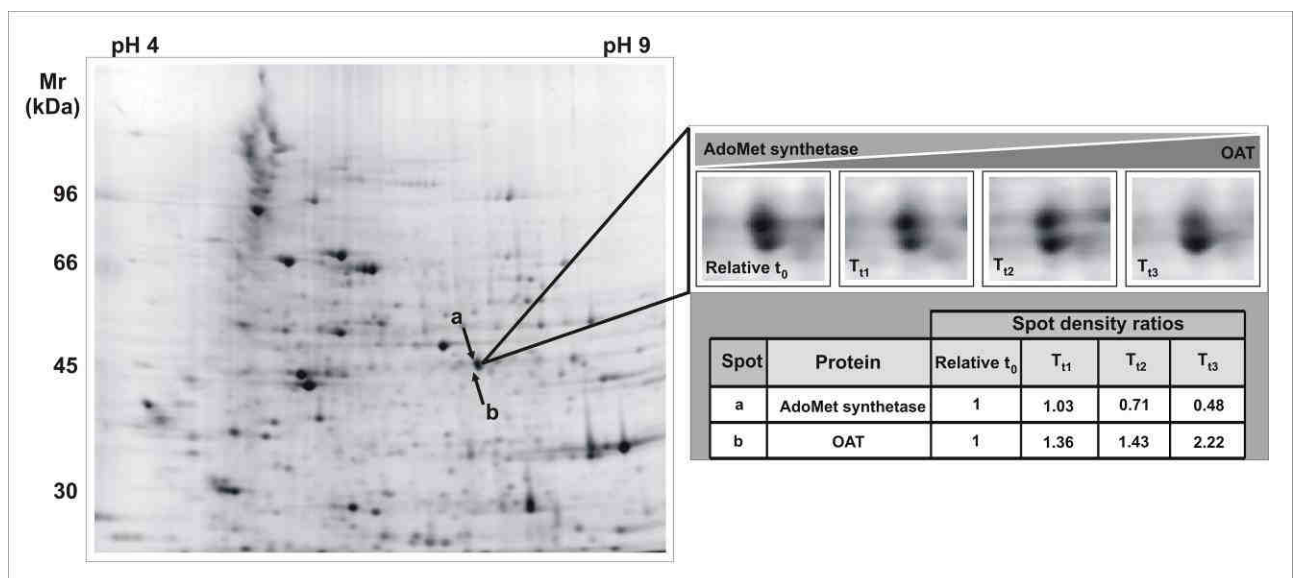


Fig. 4.4. A typical gel (UTt1_84404) with an enlarged view of (a) AdoMet synthetase and (b) OAT over the time course, including the respective spot densities. Spot density ratios were calculated compared to UT_{t1} (relative t_0) with $p < 0.05$.

Other proteins that were differentially affected as a result of the perturbation include falcipain-2 (PF11_0165) and elongation factor 2 (PF14_0486). Both these proteins are involved with protein synthesis (falcipain-2 is the principal hemoglobinase in trophozoites and supplies amino acids for translation [280]) and both were significantly increased. Moreover, GO analysis in the transcriptomics investigation (section 3.3.6) determined that 10% of the transcripts with increased abundance were implicated in translation. Falcipain-2 also cleaves human ankyrin and protein 4.1 near their carboxyl termini to enable merozoite release, resulting in reduced

association of spectrin and actin with the erythrocyte membrane. Interestingly, contaminating human spectrin and actin were both found to increase over the time course, which could be related to the increased levels of falcipain-2 (Table 4.3). Human erythroid spectrin (280 kDa) contains two subunits (α and β chains) that are each composed of 21 and 16 repetitive units respectively [281]. Truncation forms were detected as a diamond-shaped pattern from 95-150 kDa (Fig. 4.2) and were also reported in another plasmodial 2D-GE study [261].

4.3.2 Metabolomics analysis of PfAdoMetDC/ODC co-inhibited *P. falciparum*

To probe and/or validate the findings of the transcriptome investigation further, another independent PfAdoMetDC/ODC co-inhibition experiment was conducted and the effects of the perturbation were assessed on the parasite metabolome. The perturbation conditions (parasite inoculum, treatment and sampling times) of the three independently performed functional genomics experiments were replicated as far as possible. The metabolite extraction and LC-MS/MS methodology were previously developed and optimised for the simultaneous measurement of water-soluble metabolites [263, 266]. DFMO/MDL73811-treated and untreated control samples were analysed for 172 metabolites (including putrescine, spermidine, spermine, cadaverine and dcAdoMet) with LC-MS/MS [263, 266]. Reliable data were obtained for 92 metabolites (Appendix E) with the balance excluded due to levels below the detection or set quantitation limit. The latter included several relevant metabolites, such as cadaverine, spermine, dcAdoMet and PLP, that could not be detected.

As opposed to the transcriptome and the proteome, Pearson correlations revealed that the effects of cyto-stasis were less pronounced in the metabolome and the metabolic profiles of treated and untreated parasites were often similar. Pearson correlation between the metabolic profiles of the treated parasites and the relative t_0 (T_{t1} versus UT_{t1} : $r = 0.99$; T_{t2} versus UT_{t1} : $r = 0.97$; T_{t3} versus UT_{t1} : $r = 0.96$) as well as the untreated parasites at t_2 and t_3 (UT_{t1} versus UT_{t2} : $r = 0.97$; UT_{t1} versus UT_{t3} : $r = 0.96$, Table 4.4) were close to perfect correlation. However, to exclude the interference of excess amino acids, vitamins and glucose supplemented in the culture medium on the abovementioned correlations, these were recalculated without 16 amino acids, 5 co-factors, glucose-1-phosphate and glucose-6-phosphate (UT_{t1} versus T_{t1} : $r = 0.99$; UT_{t1} versus T_{t2} : $r = 0.96$; UT_{t1} versus T_{t3} : $r = 0.94$; UT_{t1} versus UT_{t2} : $r = 0.96$; UT_{t1} versus UT_{t3} : $r = 0.93$, Table 4.4). The close correlations between all samples, treated and untreated, indicate the maintenance of metabolic homeostasis during cyto-stasis.

Table 4.4 Pearson correlation of the metabolite data

| Comparison | Pearson correlation (r) | Pearson correlation (r) excl. excess medium components |
|-------------------|-------------------------|--|
| $UT_{t1}:T_{t1}$ | 0.99 | 0.99 |
| $UT_{t1}:T_{t2}$ | 0.97 | 0.96 |
| $UT_{t1}:T_{t3}$ | 0.96 | 0.94 |
| $UT_{t1}:UT_{t2}$ | 0.97 | 0.96 |
| $UT_{t1}:UT_{t3}$ | 0.96 | 0.93 |

4.3.2.1 Perturbation-specific compensatory mechanisms confirmed in the metabolome

Differential metabolite abundance during the time course was again quantitated compared to the relative t_0 and 24 metabolites were changed at least 2-fold after PfAdoMetDC/ODC co-inhibition (Table 4.5). Similar to the transcriptomics investigation (section 3.3.5.2), most of these (67%) were decreased.

Table 4.5 Metabolites with differential abundance (i.e. fold changes of more than 2 in either direction) in treated and untreated samples (relative t_0 comparison)

| Metabolite | Fold change compared to relative t_0 | | | | |
|--------------------------------|--|------------------|-----------------|-----------------|-----------------|
| | UT _{t2} | UT _{t3} | T _{t1} | T _{t2} | T _{t3} |
| 2-Methylglutaric acid | 4.9 | 7.0 | 1.7 | 3.2 | 4.2 |
| γ -Aminobutyrate (GABA) | 29.0 | 59.6 | 7.7 | 10.4 | 11.0 |
| α -Ketoglutarate | 4.5 | 5.8 | 1.2 | 2.9 | 3.9 |
| D-Sedoheptulose-7-phosphate | 2.7 | 3.5 | 1.5 | 2.1 | 1.9 |
| Glutathione disulfide | 2.0 | 2.0 | 1.2 | 2.1 | 2.1 |
| Orotate | 2.9 | 4.9 | 1.9 | 2.1 | 2.8 |
| Pipecolic acid | 4.0 | 8.9 | -1.2 | 1.2 | 2.6 |
| Pyruvate | 10.3 | 23.6 | 2.1 | 6.4 | 10.9 |
| 1,3-Diphosphateglycerate | 1.1 | -10.4 | -2.3 | -1.2 | -2.7 |
| 5-Methylthioinosine | 5.8 | 7.4 | -4.6 | -8.7 | -3.9 |
| Adenosine | -4.7 | -3.3 | 1.1 | -1.9 | -4.5 |
| D-Glyceraldehyde-3-phosphate | -8.5 | -9.6 | -1.9 | -7.2 | -7.3 |
| Dihydroxy-acetone phosphate | -9.0 | -10.3 | -1.9 | -6.2 | -7.7 |
| Fructose-1,6-bisphosphate | -1.3 | -3.5 | -1.7 | -1.3 | -2.1 |
| Glutathione | -2.0 | -2.2 | -1.1 | -2.5 | -2.4 |
| Indole | -1.7 | 1.1 | -1.6 | -2.6 | -1.9 |
| Methionine | -1.3 | -1.7 | -2.1 | -2.1 | -2.2 |
| NADH | -28.5 | -43.6 | -2.0 | -33.2 | -209.1 |
| Putrescine | 1.1 | 1.8 | ND | ND | -4.6 |
| Pyridoxine | -1.6 | -2.2 | -1.3 | -1.7 | -2.0 |
| AdoHcy | -8.4 | 4.6 | -3.8 | -1.8 | -1.1 |
| Spermidine | 1.9 | 1.4 | -5.6 | -3.0 | -2.6 |
| Tryptophan | -1.3 | -1.3 | -1.7 | -2.2 | -2.0 |
| UTP | 1.5 | 1.5 | -2.4 | 1.2 | 1.6 |

Metabolites changed >2-fold in either direction are color-indicated (red = more than 2-fold increased, green = more than 2-fold decreased). ND = not detected

Compared to the relative t_0 , the majority of the differentially affected metabolites in the treated parasites were similarly affected in the untreated controls (Table 4.5). Therefore, these changes were most likely cell cycle related peaks and not the result of the perturbation. Compellingly, the perturbation-specific effects of PfAdoMetDC/ODC co-inhibition were observed in the parasite metabolome with significantly lower levels of the polyamines (putrescine and spermidine) in the treated parasites compared to increased levels in the untreated controls (Fig 4.5A, Table 4.5), as previously described (Fig. 1.7) [88, 90]. Moreover, downstream metabolites, including 5-methylthioinosine (Fig. 4.5A, Table 4.5), were also decreased in the treated parasites only, corroborating the complete metabolic halt of polyamine metabolism after the co-inhibition. The decreased NADH levels (Table 4.5) after PfAdoMetDC/ODC co-inhibition could be the result of decreased energy metabolism as detected in the transcriptome (Table 3.3, section 3.3.6), but NADH was also decreased in the untreated controls (although ~5 times less in T_{t3}). UTP also showed a decrease at T_{t1}, but subsequently

increased. The levels of other energy intermediates (e.g. ATP and the glycolysis metabolites) were generally maintained or similarly affected in the untreated controls (Appendix E).

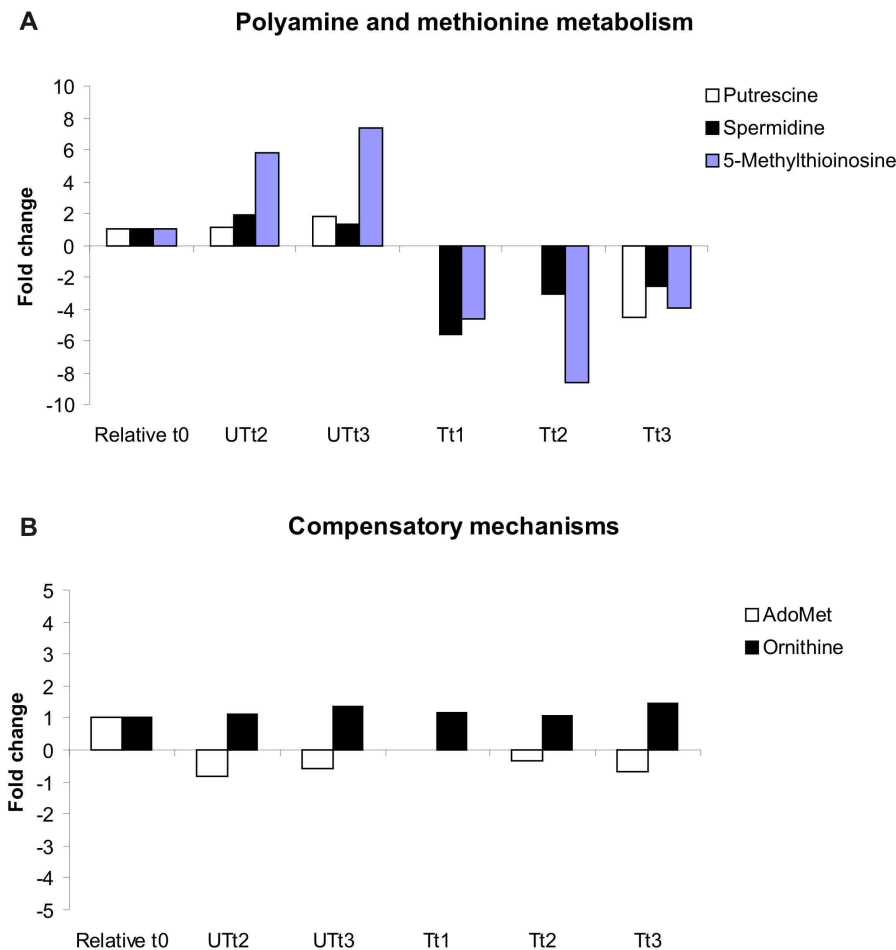


Fig. 4.5 Metabolite profiles compared to relative t_0 of **A**) putrescine, spermidine and 5-methylthioinosine downstream of PfAdoMetDC/ODC, which showed perturbation-specific decrease in the treated parasites, and **B**) ornithine and AdoMet levels directly upstream of PfAdoMetDC/ODC, which were maintained despite the complete co-inhibition. Cadaverine and spermine could not be detected. Fold changes are indicated compared to relative t_0 . Thus, the fold change of relative $t_0 = 1$ (unchanged).

The proposed compensatory responses of LDC, OAT and AdoMet synthetase were also investigated in the metabolome. The increased abundance of LDC transcripts (Table 3.3) could indicate the functional production of cadaverine from lysine in *P. falciparum*, but cadaverine could not be detected. AdoMet and ornithine levels were altered less than 2-fold compared to the relative t_0 in all of the samples and were therefore not considered as differentially affected (therefore not present in Table 4.5). In other organisms, inhibition of AdoMetDC caused an increase of the substrate AdoMet [157]. However in *Plasmodium*, AdoMet homeostasis was apparently maintained (non-differential fold change ≈ -1 , Fig. 4.5B, Appendix E). Moreover, ornithine levels also remained mostly unchanged (non-differential fold change ≈ 1 , Fig. 4.5B, Appendix E) despite the complete inhibition of PfAdoMetDC/ODC, which indicates the efficiency of the compensatory AdoMet synthetase decrease and OAT increase as observed in the transcriptome (Table 3.3) and the proteome (section 4.3.1.2).

The general maintenance of metabolic homeostasis observed, caused reservations as to whether the relative t_0 strategy, as applied here and in other metabolomics investigations [267], was appropriate for differential metabolite abundance analysis, since the metabolome is more dynamic than the transcriptome and proteome. Moreover, if homeostasis exists, then an argument could be made for standard parallel time point comparison. Therefore, comparison of metabolite levels between treated and untreated parasites was in addition performed between parallel time points, which revealed 15 metabolites with differential abundance over the time course (Table 4.6).

Table 4.6 Metabolites with differential abundance (i.e. fold changes of more than 2 in either direction) after PfAdoMetDC/ODC co-inhibition (parallel time point comparison)

| Metabolite | Fold change compared to parallel untreated control | | |
|----------------------------|--|-----------------------------------|-----------------------------------|
| | T _{t1} /UT _{t1} | T _{t2} /UT _{t2} | T _{t3} /UT _{t3} |
| 1,3-Diphosphateglycerate | -2.3 | -1.3 | 3.9 |
| γ-Aminobutyrate (GABA) | 7.7 | -2.8 | -5.4 |
| 5-Methylthioinosine | -4.6 | -50.2 | -29.0 |
| Adenosine | 1.1 | 2.5 | -1.4 |
| Lysine | 1.4 | 1.1 | 2.1 |
| Methionine | -2.1 | -1.6 | -1.3 |
| NADH | -2.0 | -1.2 | -4.8 |
| Pipecolic acid | -1.2 | -3.5 | -3.4 |
| Putrescine | ND | ND | -8.2 |
| Pyruvate | 2.1 | -1.6 | -2.2 |
| AdoHcy | -3.8 | 4.7 | -5.0 |
| Spermidine | -5.6 | -5.7 | -3.5 |
| S-ribosyl-L-homocysteine | 1.9 | -1.2 | 2.5 |
| Succinate | 1.9 | -1.7 | -2.2 |
| UTP | -2.4 | -1.3 | 1.1 |

Metabolites changed >2-fold in either direction are colour-indicated (red = more than 2-fold increased, green = more than 2-fold decreased). ND = not detected

When the results from the relative t_0 approach is compared to those of the parallel time point approach, 12/15 metabolites from Table 4.6 also appear in Table 4.5, but three metabolites uniquely appear only with parallel comparison (lysine, S-ribosyl-L-homocysteine and succinate, Table 4.6). Both analyses indicated that NADH was decreased ~5 times more after PfAdoMetDC/ODC co-inhibition in T_{t3} than in the controls (Table 4.5 and Table 4.6). However, compared to the relative t_0 , most of the metabolites followed a distinct increasing or decreasing profile in the treated or untreated samples (Table 4.5), as opposed to a variable profile with the parallel strategy (Table 4.6). In addition, using the latter approach, only three metabolites (1,3-diphosphateglycerate, methionine and UTP) demonstrated a consistent increase over the time course (compared to eight with the relative t_0 approach), but levels above 2-fold were detected among a few variable profiles (e.g. adenosine, lysine, AdoHcy and S-ribosyl-L-homocysteine, Table 4.6). Moreover, using the relative t_0 approach, specific metabolites, e.g. GABA, pipecolic acid and pyruvate, were similarly increased in the treated and untreated samples, but they had a decreasing profile after PfAdoMetDC/ODC co-inhibition according to the parallel approach. Despite the observed homeostasis, this may again be due to arrest of the treated versus normal progression of the untreated parasites, since exactly the same extraction protocol were

followed for all the samples, which would result in a higher metabolite abundance of the untreated controls simply due to parasite maturity and larger size (Fig. 3.4).

Convincingly, the parallel time point comparison between treated and untreated samples also indicated the perturbation-specific effects of PfAdoMetDC/ODC co-inhibition downstream of the bifunctional complex with a maximum 8.2-fold decrease of putrescine, 5.7-fold decrease of spermidine and 50.2-fold decrease of 5-methylthioinosine (Fig. 4.6A, Table 4.6). As before, ornithine and AdoMet levels were not identified in the differential abundance set (fold change less than 2, not present in Table 4.6) and were therefore considered as unchanged, since the levels of these metabolites were maintained in both the untreated and treated parasites (Fig. 4.6B, Appendix E). This corroborates the proposed metabolic homeostasis upstream of PfAdoMetDC/ODC and the compensatory effects of OAT and AdoMet synthetase, as well as the perturbation-specific metabolic halt downstream of PfAdoMetDC/ODC.

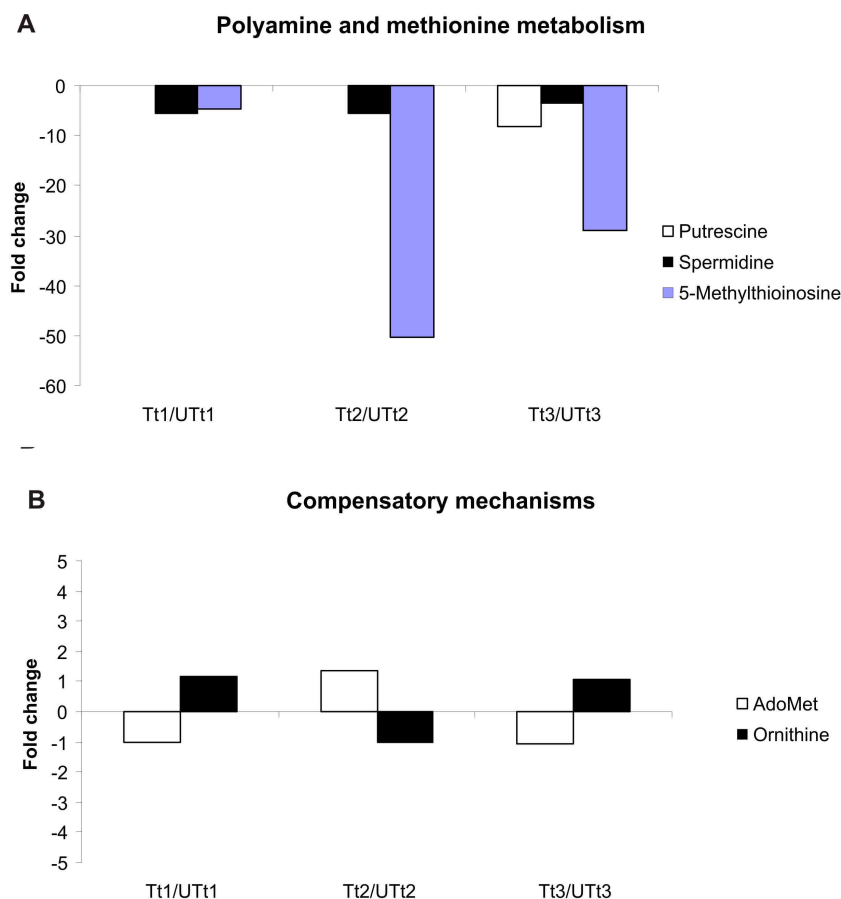


Fig. 4.6 Metabolite profiles of treated parasites directly compared to the parallel untreated controls for **A)** putrescine, spermidine and 5-methylthioinosine corroborating the perturbation-specific decrease after PfAdoMetDC/ODC co-inhibition, whereas **B)** ornithine and AdoMet levels were maintained.

4.3.3 Compensatory LDC induction during polyamine depletion investigated further

LDC activity and cadaverine accumulation reduces ethylene inhibition of arginine decarboxylase and AdoMetDC in pea seedlings [74] and cadaverine reverses DFMO-induced growth arrest of *P. falciparum* [282]. Compensatory induction of the LDC transcript was also detected after PfAdoMetDC/ODC co-inhibition of *P. falciparum* (section 3.4), but this response could not be confirmed on the protein level with 2D-GE nor could cadaverine be detected with LC-MS/MS. Therefore, to investigate the hypothesis of LDC induction as compensatory mechanism to alleviate polyamine depletion further, LDC activity of PfAdoMetDC/ODC co-inhibited parasites was biochemically determined via radio-labelled substrate (^{14}C -lysine) decarboxylase assays as described for ODC and AdoMetDC in section 3.3.1. However, no LDC activity above background could be detected in either treated or untreated *P. falciparum* cultures (Fig. 4.7). *E. coli* positive controls proved that the LDC activity assay was functional and uninfected erythrocytes were included as negative controls. Moreover, *E. coli* LDC activity was about 5-fold higher when assayed in sodium-acetate buffer (LDC buffer) [275] as opposed to the Tris-HCl (buffer A) [88], used for the AdoMetDC and ODC activity assays (section 3.3.1). This is probably due to inhibition of LDC by chloride ions as demonstrated for LDC from soybean [283]. However, no activity could be detected in the *P. falciparum* samples despite changing to the sodium-acetate buffer (without chloride ions), increasing the substrate concentration up to 100-fold (700 μM) that used for AdoMetDC and ODC activity assays or adding BSA to the reaction, as suggested for *E. coli* [71] (results not shown).

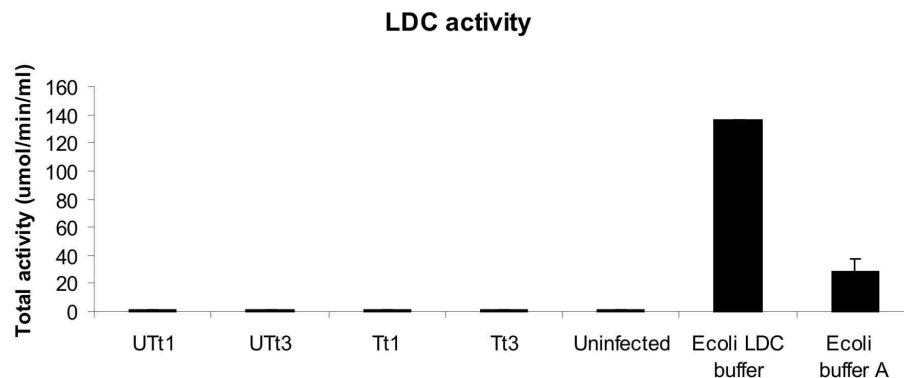


Fig. 4.7 Lack of measurable LDC activity of untreated and DFMO/MDL73811-treated parasite lysates (sampled at $t_1 = 19$ hpi and $t_3 = 34$ hpi) after incubation with L-[^{14}C]-lysine ($n=2$). Uninfected erythrocytes were used as negative control and *E. coli* lysates as positive control. Note the reduced *E. coli* LDC activity due to inhibition by chloride ions [283] in buffer A compared to the recommended LDC buffer.

In a final attempt to detect plasmodial LDC activity, a mixture of co-factors at physiological concentrations (~80 μM magnesium, manganese, thiamine, ATP and NAD respectively, with 40 μM substrate), as required by other decarboxylases [284-286], was added to the reaction in addition to PLP, but enzyme activity could not be detected in *P. falciparum*.

4.3.5 gDNA Methylation status investigation

DFMO/MDL73811-treatment of trypanosomes caused a 40-fold accumulation of AdoMet [185], which resulted in speculation of hypermethylation of nucleic acids and/or proteins as the main antitrypanosomal mechanism of MDL73811 [157]. Methylation of histones [125] or 2-deoxycytosine bases within gDNA [287] can result in transcriptional repression and might explain the decreased abundance of the majority of transcripts (70%) after PfAdoMetDC/ODC co-inhibition (section 3.3.5.2). Yet, with DFMO/MDL73811-treatment of *P. falciparum*, AdoMet levels were maintained (section 4.3.2.1) by a decrease in its synthesis among others (section 4.3.1.3). However, the conversion of AdoMet to AdoHcy (resulting in methylation) could in addition have controlled AdoMet levels [241]. To investigate the potential role of DNA methylation in the mechanism of MDL73811 in *P. falciparum*, the presence of CpG islands in the genes encoding the transcripts that were differentially affected after PfAdoMetDC/ODC co-inhibition was investigated.

4.3.5.1 CpG island analysis of the differential transcript abundance list

CpG island analysis (CpGplot, CpGreport) of the genes encoding the 538 transcripts from the LIMMA dataset (377 decreased, 171 increased), including their 1000 bp upstream/downstream regions, did not detect any CpG islands. In fact, geecee-count analysis calculated the average GC content of these genes and their surrounding regions, which was found to closely represent the average composition of the *P. falciparum* genome i.e. 18.8 – 18.4% GC versus the reported 19.4% [96] (Table 4.7).

Table 4.7 Geecee-count analysis of the genes encoding the 538 differentially affected transcripts

| Gene list | %GC content of the 538 genes | | | |
|---|------------------------------|------------------|--------------------|----------|
| | CDS | 1000 bp upstream | 1000 bp downstream | Total GC |
| Genes of increased abundance transcripts | 15.67 | 3.13 | 3.67 | 18.8 |
| Genes of decreased abundance transcripts | 14.66 | 3.73 | 4.25 | 18.39 |

Therefore, as opposed to a gene-specific methylation approach such as bisulfite sequencing [288], a genome-wide analysis strategy was applied to determine the role of DNA methylation in the observed transcriptional suppression.

4.3.4.2 Global methylation assays

The classical method of global DNA methylation analysis using methylation-sensitive restriction endonucleases (MSRE) is based on the properties of specific endonucleases to be sensitive to the methylation status of their recognition sequence. MSRE demonstrated the high abundance of 5mC in murine DNA since different digestion profiles were obtained when using enzymes with different methylation sensitivities [289], but failed to demonstrate the genetic methylation pattern in *D. melanogaster* [290]. Instead a powerful immunological approach revealed the presence of 5mC in *D. melanogaster* DNA [290]. Both these strategies

were attempted here to determine the methylation status of *P. falciparum* gDNA isolated from samples of two time points ($t_1 = 19$ hpi and $t_3 = 34$ hpi) after PfAdoMetDC/ODC co-inhibition.

4.3.4.2.1 Methylation-sensitive restriction endonucleases

Due to the contradictory evidence of cytosine methylation [124, 126, 127] in *P. falciparum* gDNA (section 1.10.5) and the known role of adenine methylation in other low eukaryotes [291], both methylation types were investigated by including two enzymes with different methylation sensitivities: *HpaII*, which recognises C↓CGG but does not cleave when the cytosines are methylated (5mC), and *DpnI*, which recognises the sequence GA↓TC but only cleaves when the adenine is methylated (N⁶-methyladenine). No difference in the digestion profiles of gDNA from PfAdoMetDC/ODC co-inhibited or untreated parasites could be detected after either *HpaII* or *DpnI* overnight digestion (Fig. 4.8).

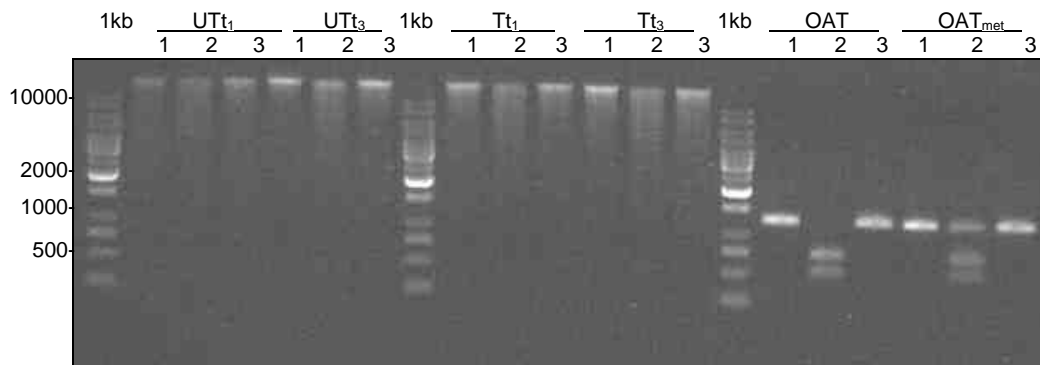


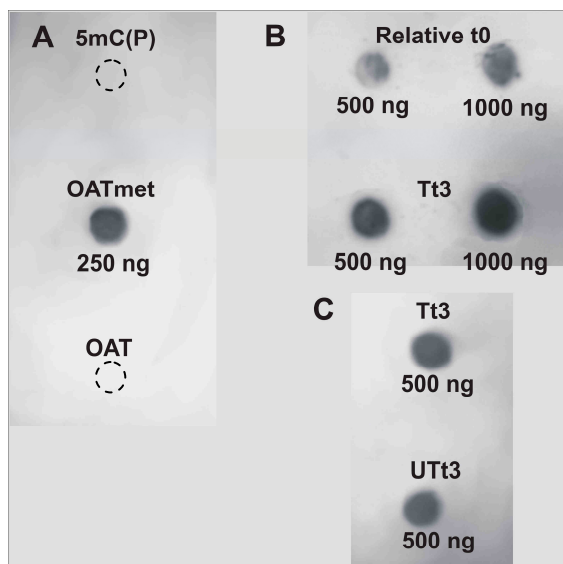
Fig. 4.8 Gel electrophoresis of 250 ng digested and undigested gDNA on 0.8% agarose, to assess methylation after PfAdoMetDC/ODC co-inhibition. Lane 1: undigested gDNA, lane 2: *HpaII* digested and lane 3: *DpnI* digested gDNA of treated (T) and untreated (UT) parasites at $t_1 = 19$ hpi and $t_3 = 34$ hpi, respectively. A synthetic unmethylated (OAT = 250 ng) and methylated control (OAT_{met} = 250 ng) DNA are included. Molecular size is indicated with a 1 kb ladder.

However, the partial protection of cytosine-methylation against *HpaII* digestion was visible in the M.SssI (CpG methyltransferase)-treated synthetic DNA control (Fig. 4.8 OAT_{met} lane 2). Three detectable bands including the original 1245 bp OAT amplicon, as well as the 725 bp and 520 bp fragments (flanking the CCGG restriction site), are visible, compared to the unmethylated OAT *HpaII* digest where the amplification product was completely digested with only two bands visible (Fig. 4.8 OAT lane 2). Although two *DpnI* sites occur in OAT DNA, the amplicon was not cleaved, indicating that N⁶-methyladenine was not present. These controls confirmed that MSRE can theoretically distinguish different 5mC methylation patterns, but the methodology was not sensitive enough to reveal specific methylation profiles in *P. falciparum* and gDNA methylation differences as a result of PfAdoMetDC/ODC co-inhibition could not be demonstrated.

4.3.4.2.2 South-Western immunoblotting

The low sensitivity of MSRE analysis demanded a more sensitive approach, such as immunoblotting, to establish the methylation status after PfAdoMetDC/ODC co-inhibition and to clarify the paradox concerning

5mC within the *P. falciparum* genome [124, 126, 127]. By including both 5-methylcytidine [5mC(P)] and synthetically prepared (and thus unmethylated) OAT as negative controls and OAT_{met} as positive control, the specificity of the antibodies for 5mC within gDNA was determined (Fig. 4.9A). Methylated RNA species can cause false positive results [277] and therefore contaminating RNA was removed during DNA isolation with RNase A treatment. The initial experiment (Fig. 4.9B) indicated a higher abundance of 5mC in T₁₃ compared to the relative t₀ as determined by densitometry. Moreover, the 5mC signal versus the gDNA mass (i.e. 5mC quantity) was approximately linear (Fig. 4.9 Table). However, since the putative DNA(cytosine-5)-methyltransferase (MAL7P1.151) transcript peaks between 14 and 23 hpi according to the 3D7 IDC transcriptome [91] (i.e. around t₁) and the transcript was not affected by PfAdoMetDC/ODC co-inhibition (Chapter 3), it was decided to determine the gDNA methylation of UT₁₃ (Fig. 4.9C) as well. Interestingly, the m5C content and thus gDNA cytosine-methylation of T₁₃ and UT₁₃ (based on spot density) was the same. It therefore appears as if the increased methylation detected was time-dependent (t₃) and not the result of PfAdoMetDC/ODC co-inhibition.



| Experiment | Sample | gDNA mass (ng) | Total spot density ^a |
|------------|-------------------------|----------------|---------------------------------|
| B | Relative t ₀ | 500 | 14068 |
| | | 1000 | 27855 |
| | T ₁₃ | 500 | 31255 |
| | | 1000 | 50194 |
| C | T ₁₃ | 500 | 31832 |
| | UT ₁₃ | 500 | 32193 |

a. Total spot density = area (mm²) x density (CNT/mm²)

Fig. 4.9 South-Western blot of 5mC in *P. falciparum* gDNA. **A**) 1 nmole of 5-methylcytidine [5mC(P)], 250 ng artificially methylated OAT (OAT_{met}), 250 ng unmethylated OAT; **B**) 500 ng and 1000 ng relative t₀(UT₁₃), 500 ng and 1000 ng T₁₃; **C**) 500 ng T₁₃ and 500 ng UT₁₃. The total spot densities of the two separate experiments (**B** and **C**) are tabled.

4.4 DISCUSSION

In this chapter, conclusions drawn from the transcriptomics investigation of PfAdoMetDC/ODC co-inhibited *P. falciparum*, resulting in polyamine depletion, were validated in the proteome and metabolome. Moreover, biochemical assays were performed to investigate specific hypotheses such as the induction of LDC as compensatory response to polyamine depletion and the role of DNA hypermethylation in the mechanism of MDL73811. As with the transcriptomics investigation, the effects of cytotaxis could be detected in the proteome with the number of detectable spots decreasing in the treated samples over the time course (483 to 409). However, correlation calculations indicated that the effects of cytotaxis were subtle in proteome (T₁₃

versus UT_{t1} : $R = 0.88$) and even more so in the metabolome (T_{t3} versus UT_{t1} : $r = 0.96$) compared to the transcriptome (T_{t3} versus UT_{t1} : $r = 0.57$). Yet, differential abundance analysis of the treated time points compared to UT_{t1} (regarded as a relative t_0 and reference point for quantitative analysis through the whole functional genomics investigation) detected 53/500 protein spots and 24/92 metabolites compared to the 538/5332 transcripts with differential abundance as a result of the perturbation.

Technical limitations of some of the techniques applied were evident, such as the poor proteome coverage of 2D-GE [260]. Despite the excellent resolution, relatively easy, inexpensive performance and theoretical capability of detecting more than 5000 protein spots [292], only about 500 trophozoite stage proteins (including protein variants and contaminating host proteins) i.e. ~10% of the *P. falciparum* proteome, were accessible. In comparison, a recently “improved” 2D-GE method for *P. falciparum* detected only 239 spots [293] and ~300 spots were obtained from *T. cruzi* epimastigotes [294]. Yet, MudPIT confidently identified 1036 trophozoite stage proteins covering 42% of the predicted *P. falciparum* proteome [112]. The poor proteome coverage is explained among others by protein solubility constraints (e.g. membrane proteins) and exclusion due to extreme pI and/or protein size [255]. The latter caused two important polyamine metabolism proteins, PfAdoMetDC/ODC (330 kDa) and LDC (280 kDa), not to be assessable with 2D-GE since they were too large for gel penetration. In addition, the limited identification of low molecular weight and low abundance proteins resulted in the successful identification of only ~30% of the already restricted dataset. In future studies, the 2D-GE proteome coverage may be increased by fractionation [251] or by using larger gels (24 cm) with better resolution, but techniques such as MudPIT, ICAT or iTRAQ [295] should definitely be considered to improve the identification of low abundance proteins and the coverage of the *Plasmodium* proteins interrogated.

The time course approach has proven indispensable, particularly in the 2D-GE investigation. The visible increase of OAT and decrease of AdoMet synthetase, located adjacently on the 2D-image, confirmed that these changes were indeed in response to the perturbation and not due to technical artifacts. Furthermore, transcriptional responses that were delayed on the protein level (LDH) due to the translational gap [246], could have been regarded as contradictory to the transcriptomics results if only one time point had been assessed.

Pearson correlation calculations of the metabolomics data revealed the general maintenance of metabolic homeostasis and many of the metabolites that showed a 2-fold change compared to the relative t_0 in the treated parasites were similarly affected in the untreated controls. Therefore, differential metabolite abundance was also determined compared to the parallel untreated controls (standard approach). Both strategies indicated perturbation-specific effects downstream to PfAdoMetDC/ODC with the decrease of putrescine, spermidine and 5-methylthioinosine in the treated parasites. Otherwise, homeostasis was generally maintained and ornithine and AdoMet levels were not significantly altered despite the complete inhibition of PfAdoMetDC/ODC. However, the results obtained with the parallel time point comparative approach were

generally more variable over the time course and in some cases metabolite levels could have appeared to decrease after treatment simply because lesser amounts were extracted due to the smaller size of the arrested parasites compared to the more mature, untreated controls. For this reason the relative t_0 strategy is also regarded as the better approach to follow for analysis of metabolomics data during cytostasis, but if the metabolite samples could be quantitatively loaded onto the LC-MS/MS instrument, this problem could be resolved to some extent. Standardisation of the metabolite extraction efficiency/yield against an internal biomarker (internal standard) would be ideal. Another limitation of the metabolomics methodology applied here is that the sample replication encompassed only two biological replicates and no technical replicates. The variation detected with the parallel time point approach could thus have included technical variation, although the variation between biological replicates should exceed technical variation and the latter should be equal regardless of the analysis approach applied. The limited replication furthermore constrained statistical analysis, since most statistical methodologies (e.g. Student's t-test) require at least three replicate values and the statistical significance of the obtained results could therefore not be calculated. Reports on metabolomics investigations of *Plasmodium* are currently extremely scarce [116] and the data analysis performed here was limited to differential abundance analysis and Pearson correlation calculations. In other organisms intricate computational approaches and data visualisation methods (e.g. PCA, hierarchical clustering and PLS), similar to microarray data analysis [254, 296], are now being performed. In the investigation presented here the overall aim of the proteomics and metabolomics analyses was to confirm certain hypotheses resulting from the transcriptomics investigation, which was achieved with the fundamental analysis described, but a more in-depth analysis approach could certainly reveal metabolic effects of the perturbation not determined here.

Two of the three perturbation-specific compensatory transcriptional responses, namely the increased abundance of OAT, as well as the decreased abundance of AdoMet synthetase, showed coordinated responses in the proteome and metabolome. An integrated view of the results regarding polyamine and methionine metabolism from the complete functional genomics investigation is presented in Fig. 4.10. The increase in the transcript and protein levels of OAT and the maintenance of ornithine concentrations in the metabolome provides evidence for the compensatory effects of OAT during PfAdoMetDC/ODC co-inhibition and confirms its role in the regulation of ornithine in the parasite. The significant increase of the protein pdx1 could be an additional compensatory attempt to activate PfAdoMetDC/ODC (and potentially LDC) since both ODC and LDC are PLP-dependent decarboxylases [279].

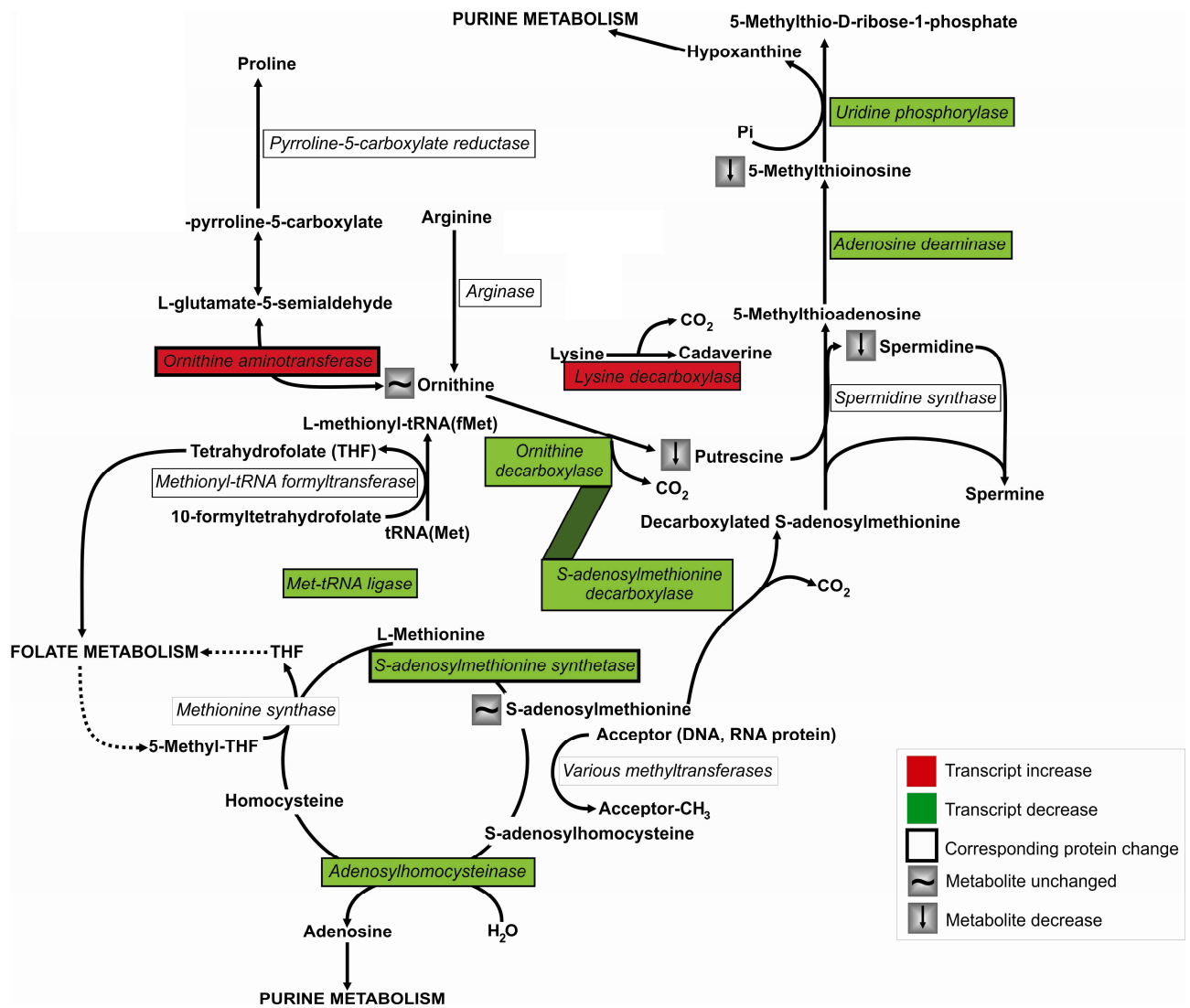


Fig. 4.10 Polyamine and methionine metabolism (adapted from MPMP at <http://sites.huji.ac.il/malarial/>). The minimal synthesis of spermine in *Plasmodium* is currently believed to be catalysed by spermidine synthase, as indicated [85]. Enzymes of which the transcript abundance was significantly increased are indicated in red and those significantly decreased are indicated in green, whereas proteins with confirmed corresponding abundance are framed with a thick border. Metabolites that were decreased at least 2-fold are indicated.

DFMO/MDL73811-treatment of trypanosomes caused a 40-fold accumulation of AdoMet [185], resulting in speculation on hypermethylation of nucleic acids and/or proteins being the main antitrypanosomal mechanism of MDL73811 [157]. However, in the present study of DFMO/MDL73811-treated *P. falciparum*, AdoMet levels were maintained. Several mechanisms could maintain metabolic homeostasis during a perturbation such as regulation of enzyme activity or protein production. This study revealed a decrease in both the transcript and protein of AdoMet synthetase that may act as a compensatory strategy to maintain AdoMet levels. The exact mechanism behind this regulation needs to be elucidated, but in MDL73811-treated mammalian cells the AdoMet concentration was effectively regulated through substrate feedback inhibition of AdoMet synthetase activity [157, 240]. The Plasmodial enzyme activity was recently reported not to be allosterically regulated by AdoMet [79], but based on the data presented here, AdoMet could regulate the transcript and protein levels of AdoMet synthetase. In contrast, the trypanosomal enzyme is poorly regulated, resulting in the substantial accumulation of AdoMet after AdoMetDC inhibition [157]. Moreover, the proposed difference in regulation of

AdoMet synthetase between *Trypanosoma* and *Plasmodia*, resulting in hypermethylation with polyamine depletion in the first case and possibly only polyamine depletion in the second, may be the reason for the success of MDL73811 in *T. brucei rhodesiense*-infected mice [184], and failure of MDL73811 in *P. berghei*-infected mice [153].

Hypermethylation as partial mechanism of MDL73811 in *Plasmodium* was further investigated since the methylation of histones [125] or 2-deoxycytosine bases within gDNA [287] can result in transcriptional repression, which could explain the decreased abundance of the majority of transcripts (70%) after PfAdoMetDC/ODC co-inhibition (section 3.3.5.2). Although AdoMet levels were maintained, the conversion of AdoMet to AdoHcy (resulting in methylation) could also have controlled the AdoMet concentration [241], in addition to decreased AdoMet synthesis. AdoHcy is the major by-product of AdoMet-dependent transmethylation and a competitive inhibitor of trans-methylation reactions [239, 241]. A decrease in the AdoMet/AdoHcy ratio would result in reduced methylation [241]. AdoHcy increased from -3.8 to unchanged in T_{11} to T_{13} and from -8.4 to 4.6 in UT_{11} to UT_{13} in the data compared to the relative t_0 (Table 4.5, Appendix E). This could indicate the increased conversion of AdoMet to AdoHcy through methyltransferase or the decreased hydrolysis of AdoHcy via adenosylhomocysteinase (the transcript decreased 2.6-fold, Table 3.3). There has been contradictory evidence on cytosine-methylation as an epigenetic mechanism in *Plasmodium* [124, 126, 127], but DNA(cytosine-5)-methyltransferase homologues have been predicted in three of the human malaria parasites [*P. falciparum* (MAL7P1.151), *P. knowlesi* (PKH_021170) and *P. vivax* (Pv081670)] according to PlasmoDB 5.4. Therefore, the DNA methylation potential of the genes encoding the 538 differentially affected transcripts was determined by CpG-island bioinformatics analysis and the extent of gDNA methylation of DFMO/MDL73811-treated and untreated parasites was determined with MSRE and 5mC-antibodies. Bioinformatics analyses could not predict any CpG-islands in the differentially affected transcript data and MSRE had insufficient sensitivity to indicate differences in the digestion profiles of treated and untreated parasite gDNA. However, in contrast to other reports [124, 126, 127], the highly sensitive South-Western immunoblotting detected the presence of 5mC in *P. falciparum* gDNA of treated and untreated parasites, despite the low GC content of the genome (19.4% GC-rich) [96]. 5mC-Methylation apparently increases during development (tested from 19 hpi to 34 hpi) and was not influenced by the perturbation, i.e. the gDNA of treated and untreated parasites at t_3 was similarly methylated. This may be explained by the expression of the putative DNA(cytosine-5)-methyltransferase (MAL7P1.151) early in the trophozoite stage (transcript peaks between 14 and 23 hpi according to the 3D7 IDC transcriptome) i.e. at around t_1 . The proposed stage-dependent gDNA methylation (as opposed to perturbation-dependent methylation) was further substantiated by the fact that AdoMet levels in both treated and untreated parasites were maintained during the time course. From the results obtained, it was concluded that MDL73811 does not result in hypermethylation of *P. falciparum* gDNA.

The compensatory induction of LDC to alleviate polyamine depletion remains to be confirmed in *Plasmodium*, since the protein could not be detected by 2D-GE nor cadaverine with LC-MS/MS. LDC activity assays with ¹⁴C-labelled lysine were subsequently conducted to elucidate this hypothesis, but plasmodial LDC activity could not be demonstrated, whereas convincing activity of the *E. coli* positive control confirmed the integrity of the assay. It may be that LDC is not a constitutive enzyme in *P. falciparum* and that it is only induced upon polyamine depletion, which would explain the lack of activity in the untreated controls. This is supported by the fact that putrescine and spermidine were shown to inhibit LDC in a regulatory manner in *E. coli* [297], which may occur at the transcript level, resulting in increased LDC transcription only upon polyamine depletion. Experts in the field of malaria polyamine research from the Bernard Nocht Institute for Tropical Medicine, Hamburg, Germany [79], could also not demonstrate any LDC activity in *P. falciparum* cultures (I Muller, personal communication), but the recombinant enzyme was successfully expressed and lysine decarboxylation could be demonstrated [79]. However, if the plasmodial LDC is inhibited by the other polyamines, activity should have been detected in the treated/polyamine depleted parasites due to the induction of LDC protein expression. However, DFMO-inhibition of LDC activity has been described in *Selenomonas ruminantium* [73] and cannot be excluded in the case of the plasmodial LDC. Another possibility is that the plasmodial LDC is not stable under the conditions used for storage, sample preparation or assay or that it requires a co-factor which was not provided. Western blot analysis would indisputably confirm an increase in the LDC protein, but successful protein expression of this 280 kDa protein will be required to enable antibody generation for this strategy.

Similar to other studies of *Plasmodium* [246, 252], changes in transcript and protein levels as a result of PfAdoMetDC/ODC co-inhibition were generally correlated, e.g. AdoMet synthetase, OAT and LDH, though the latter was delayed. In some cases small incremental changes on the transcriptional level (e.g. falcipain-2 and pdx1) resulted in significant changes on the protein level, which could be attributed to post-transcriptional regulation of these particular enzymes. Alternatively, it may indeed be that small amplitude transcriptional responses can result in momentous alterations of the corresponding protein levels. However, transcripts and protein levels are not necessarily correlated [298], nor are all transcripts and all proteins necessarily regulated in the same way. For some genes the dominant regulation may occur at transcriptional level, whereas for others it may occur at the post-transcriptional and/or translational level. The challenge remains to be able to decipher the biological significance of the information obtained [136] via data integration from different functional genomics investigations [254]. In this investigation perturbation-specific compensatory mechanisms were detected in the transcriptome and confirmed in the proteome and the metabolome, corroborating the biological significance of OAT and AdoMet synthetase upon PfAdoMetDC/ODC co-inhibition.

CHAPTER 5

CONCLUDING DISCUSSION

At a time when antimalarial drug resistance is critical and the need for compounds with novel modes of action is beyond the point of urgency, cytostatic drugs should be considered in drug screening and development programmes. Cytostatic drugs have proven therapeutic potential in protozoan diseases, e.g. DFMO, which is still the safest alternative in the treatment of West African sleeping sickness [78]. Even the acclaimed antimalarial, artesunate, has a partial cytostatic effect [299]. However, the cytostatic mechanism resulting in growth arrest of treated cells and normal progression of untreated controls requires special consideration for basic comparisons of response in terms of assay methodology used and data analysis. This is particularly important when studying multistage organisms such as *P. falciparum*, which constantly develop during the IDC, such that growth arrest compared to normal progression will result in significant differences merely due to stage. This critical principle was kept in mind throughout the entire investigation presented here, from the drug sensitivity assays up to the functional genomics investigations, and gave rise to the relative t_0 strategy, which was an integral part of the analyses performed.

The global aim of the study was to perform functional genomics analyses of polyamine metabolism (specifically during polyamine depletion resulting in cytostasis) via the co-inhibition of the bifunctional PfAdoMetDC/ODC. This is the first report of such a comprehensive functional genomics approach to the response of the malaria parasite to environmental perturbation. In order to achieve this, the study was preceded with drug sensitivity assays to determine the appropriate inhibitor concentrations (including characterisation of the interaction between the two inhibitors used), radio-labelled substrate assays to ensure complete enzyme inhibition, membrane-integrity assays to ascertain that the high dosages used did not cause chemical cytotoxicity and parasite morphology studies to determine the most appropriate sampling times. The experimental design of the functional genomics investigations was carefully considered to be most informative. A time course experiment was performed in duplicate (two biological replicates) on synchronous parasites, with samples taken at three time points (just before and during cytostasis) such that the expression period of PfAdoMetDC/ODC was spanned. For the transcriptomics investigation, a reference design microarray experiment was conducted to enable normalisation across all the arrays for easy consolidation of replicates and cross sample comparison during differential abundance analysis. The master image compiled during the proteomics data analysis (Fig. 4.1) is analogous to the reference design of the microarray. Three independent functional genomics investigations (transcriptomics, proteomics and metabolomics) were performed. Raw data quality was carefully assessed by visual inspection and diagnostic analyses, where appropriate, to ensure

proper data correction and normalisation. Data quality assurance formed a crucial part of data analysis, since the quality of the data indirectly determines the reproducibility/reliability of the derived differential abundance lists and the validity of the biological conclusions [232].

Global expression profiling after treatment with cytostatic drugs has been performed in cancer [233, 234], but not in multistage organisms such as *P. falciparum*. One of the major finds of this investigation was the demonstration that transcriptional arrest precedes the growth arrest induced by polyamine depletion. It is the first time to our knowledge that this preceding event and mechanism of cytostasis was elucidated, and it could be a more general phenomenon also pertaining to other organisms/systems. The transcriptional arrest was particularly evident due to the multistage nature of *P. falciparum* and the arrest of treated and normal transcriptional progression of untreated parasites were easily visualised when the microarray data were ordered according to gene peak expression times within the IDC. In addition, the approximate time of the transcriptional arrest was estimated to occur at about 15 - 16 hpi of the IDC, thus late ring/early trophozoite stage, which correlates with the start of PfAdoMetDC/ODC expression. At the dosages used, complete enzyme inhibition occurred soon after protein expression, which further underscored the enzyme-specific inhibitory effects of DFMO and MDL73811 [153, 154]. The exact mechanism by which polyamine depletion results in transcriptional arrest is currently not clear, but the importance of this in macromolecular synthesis (including RNA and proteins e.g. transcription factors) [88], optimal ribosome function [236] and the association of the main fraction of polyamines with RNA [64] is well established. On the transcript level, differential abundance and GO analysis indicated the increase of transcription factors and ribosomal components and on the protein level the increase of proteins involved with protein synthesis was observed. These could indicate a physiological attempt by the parasite to induce transcription and translation to overcome the transcriptional arrest, as opposed to other processes, such as DNA replication and energy metabolism, which were clearly suppressed.

Despite the cytostasis and generalised transcriptional arrest, the abundance of 10.1% (538/5332) transcripts, 10.6% (53/500) protein spots and 26% (24/92) metabolites were differentially affected as a result of the perturbation compared to the relative t_0 . However, many metabolites in the untreated controls were similarly affected. The transcriptomics fold changes range between maximum 3.2-fold up and 5-fold down, similar to other transcriptome reports of perturbed *Plasmodium* where relatively small amplitude transcriptional responses were detected [189, 196]. Yet, in contrast with several other studies [194, 196, 197] perturbation-specific, compensatory responses could be detected in the plasmodial transcriptome after PfAdoMetDC/ODC co-inhibition with the increase in the transcripts for LDC and OAT and the decrease in that for AdoMet synthetase. The additional differential co-regulation of transcripts located adjacently on the chromosomal level after polyamine depletion (e.g. chromosome 10, PF10_0014 to PF10_0025), reiterates the perturbation-specific effect of polyamine-depletion on the transcriptome. The confirmation of the compensatory

transcriptional induction of OAT and suppression of AdoMet synthetase on the protein and metabolite level is quite remarkable compared to other studies of *Plasmodium* [194, 196, 197] where such perturbation-specific transcriptional responses could not be demonstrated. However, in most of these reports the use of unsynchronised cultures and parallel time point comparison could have masked the generally small transcriptional changes seen in *Plasmodium* upon perturbation, compared to the >3-fold transcriptional changes commonly detected during perturbations of *M. tuberculosis* [138]. The limited evidence of compensatory feedback and small amplitude of transcriptional responses have been attributed to the dominant role of post-transcriptional mechanisms of gene regulation in *Plasmodium* [128, 194, 195]. However, the coordinated compensatory responses specific to polyamine and methionine metabolism as detected in the transcriptome, proteome and metabolome in this investigation support the role of transcriptional control in response to environmental perturbation (specifically polyamine depletion) in the parasite. Furthermore, current evidence from other plasmodial perturbations [179, 189, 190, 198, 199], the recent discovery of various *cis*-regulatory motifs [118] and experimental evidence for an expanded family of DNA-binding proteins [122, 123] demands re-assessment of the role of transcriptional control in *Plasmodium* [118].

Moreover, the results obtained illustrate the potential of microarray transcriptional profiling in investigations of the physiological response of *Plasmodium* to environmental perturbation. Despite previous reports [194, 196, 197], generalised stress (host-parasite interaction transcripts e.g. surface antigens), as well as perturbation-specific compensatory responses, could be detected in the transcriptome, but it required careful experimental design, as discussed above. However, in this investigation the exact drug target was known and specific inhibitors of the bifunctional complex were applied, in contrast to several other reported environmental perturbations of *P. falciparum* (e.g. glucose deprivation [189], heat-shock [190] and even chloroquine treatment [179, 196]) for which the exact target was not known. Therefore, whether microarray technology has the ability to reveal the mode of action of novel antimalarial compounds, as demonstrated for *M. tuberculosis* [138], remains to be seen, but it will most certainly be influenced by the specificity of such compounds for single targets, as well as the proper functional annotation of the genes/transcripts within the biochemical pathways involved.

Future experiments to confirm the proposed transcriptional control on the expression of LDC, OAT and AdoMet synthetase could include promoter studies, i.e. the upstream sequences of these genes could be tested for their ability to drive expression of reporter genes (e.g. luciferase) [300, 301] upon polyamine depletion. If true regulation at the level of transcription initiation and not due to alteration of mRNA stability or other post-transcriptional means [302, 303] exists for these genes, then PfAdoMetDC/ODC co-inhibition should cause the reporter gene expression to increase with the LDC and OAT promoters and to decrease with the AdoMet synthetase promoter.

It appears as if distinct biological processes in *Plasmodium* involve specific combinations of regulatory mechanisms. Some cellular processes may be predominantly controlled by transcription factor binding and recruitment or by post-transcriptional regulation, whereas others may require the additional involvement of epigenetic regulatory processes, e.g. *var* gene expression and switching [118]. In this investigation some genes (OAT and AdoMet synthetase) showed coordinated levels in the transcriptome and the proteome and appear to be regulated at the transcriptional level, whereas another showed translational delay (LDH) and others (e.g. falcipain-2 and pdx1) resulted in incremental changes at the transcriptional level compared to significant changes on the protein level, which could be attributed to post-transcriptional regulation of these particular enzymes. The transcript for PfAdoMetDC/ODC was decreased ~2-fold with DFMO/MDL73811-treatment in accordance with the transcripts for the proteins DHFR/TS and DHPS/PPPK when targeted by pyrimethamine and sulphadoxine [197]. DHFR/TS expression is regulated by the binding of the protein to its own mRNA, thus acting as a negative feedback to control its own translation [242]. A similar mechanism could apply to PfAdoMetDC/ODC, but this needs to be elucidated, since the protein was too large to penetrate the 2D-gels and protein levels could not be assessed in this study. This potential protein-RNA interaction could be investigated by ChIP (chromatin immunoprecipitation)-chip analysis or electrophoretic mobility shift assays. Alternatively, polyamines may also be required to stabilise the transcript of PfAdoMetDC/ODC, resulting in its instability and degradation upon polyamine depletion.

LDC induction as compensatory mechanism for polyamine depletion in *Plasmodium* could not be confirmed, since the protein could not be detected by 2D-GE or cadaverine with LC-MS/MS or protein activity with radio-labelled substrate assays. The possible inhibition of the induced LDC via DFMO as in *S. ruminantum* [73] cannot be excluded at the current time, but demonstration of an increased protein concentration via Western blot analysis will indisputably confirm or reject the compensatory role of LDC during polyamine depletion of *P. falciparum*. The simultaneous expression of the transcripts for LDC and PfAdoMetDC/ODC at 24 – 25 hpi is indicative of this and although parasite growth was not restored at the treatment dosage the increased transcript abundance of LDC may indicate a potential resistance mechanism, should PfAdoMetDC/ODC be clinically targeted in the future. Additional experiments to confirm the compensatory role of LDC could include PfAdoMetDC/ODC co-inhibition of stable or transient LDC overexpressing parasites, followed by IC₅₀ determination. If LDC indeed has the capacity to restore polyamine depletion to some extent, the IC₅₀s of DFMO and MDL73811 are expected to increase under conditions of LDC overexpression.

This study presented the first description of a comprehensive metabolite analysis (92 metabolites with reliable data) of perturbed *Plasmodium*. However, due to the large number of metabolites simultaneously analysed, global metabolomics do not take into account basic enzyme kinetics or metabolic flux, which are fundamental to any study of metabolism [304]. Interpretation of global metabolomics data in isolation without supporting evidence (e.g. from the transcriptome and proteome) is extremely difficult and can easily result in inaccurate

conclusions [304]. Therefore, biological interpretation of the metabolomics data in this investigation was cautiously limited to confirmation of transcriptional and proteomic responses, yet interesting results were obtained. Metabolic homeostasis was maintained despite the transcriptional arrest and corresponding decreased proteome. The most compelling differences between the metabolomes of treated and untreated parasites were downstream of the co-inhibited PfAdoMetDC/ODC with the perturbation-specific decrease of putrescine, spermidine and 5-methylthioinosine, indicating a halt of metabolism downstream of the enzymatic blockade. Yet, upstream of PfAdoMetDC/ODC, metabolic homeostasis was preserved and ornithine and AdoMet levels were maintained despite the complete inhibition of PfAdoMetDC/ODC. Thus, on a biochemical level, regulatory mechanisms were demonstrated in this study. This includes the role of OAT in the maintenance of ornithine concentration in *P. falciparum*. Moreover, we propose feedback inhibition of AdoMet on the AdoMet synthetase transcript and protein levels, in contrast to the poorly-regulated trypanosomal enzyme [157, 198]. The proposed difference in the regulation of AdoMet synthetase between Trypanosoma and Plasmodia could be the reason for the efficacy of MDL73811 in *T. brucei rhodesiense*-infected mice [184] and failure of MDL73811 in *P. berghei*-infected mice [153], resulting in hypermethylation with polyamine depletion in the first case and possibly only polyamine depletion in the second. This requires further investigation in these animal models, but AdoMet synthetase promoter studies in the presence of high levels of AdoMet, as discussed above, could be particularly useful to confirm true transcriptional regulation of this enzyme.

Methylation assays as performed here indicated that MDL73811 does not result in hypermethylation of *P. falciparum* gDNA, but histone-methylation can also result in transcriptional repression [125] and was not investigated. However, in contrast to other reports [124, 126, 127], the presence of 5mC was detected in both treated and untreated *P. falciparum* gDNA via South-Western immunoblotting, despite the low GC content of the genome [96]. 5mC-Methylation appeared to increase during development independent of PfAdoMetDC/ODC co-inhibition, which may be explained by the expression of the putative DNA(cytosine-5)-methyltransferase (MAL7P1.151) early in the trophozoite stage. The proposed stage-dependent gDNA methylation (as opposed to perturbation-dependent methylation) was further substantiated by the fact that AdoMet levels in both treated and untreated parasites were maintained during the time course.

The ultimate objective of the investigation was to validate PfAdoMetDC/ODC as a potential drug target for antimalarial therapeutic intervention. In *S. cerevisiae* it was shown that the transcriptional changes associated with target deletion or under-expression theoretically mimic the effect of chemically inhibiting that target [188]. Since genetic manipulation of *P. falciparum* is technically challenging [130] and essential gene knock-out mutants are not viable [including ODC knock-out and silent mutants (C. Wrenger, unpublished data)] and can therefore not be studied, the functional genomics approach was followed. The induction of perturbation-specific compensatory responses to circumvent the detrimental effects of polyamine depletion corroborates

the importance of this pathway to the malaria parasite. In the absence of polyamines transcriptional arrest and cytostasis occurs, which interrupts the IDC and prevents schizogony and parasite proliferation. Therefore, polyamines are essential molecules for parasite survival and PfAdoMetDC/ODC can be regarded as a valid drug target for antimalarial drug development.

There is often scepticism about the clinical significance of polyamine metabolism as drug target in the treatment of malaria, since even upon complete inhibition of biosynthesis and success of treatment *in vitro*, the parasite is still able to salvage and thus maintain its polyamines when it resides *in vivo* [145]. However, our laboratory is currently involved in an active search for the protein responsible for polyamine transport within the parasite. Once it is elucidated and both polyamine biosynthesis and transport can be rationally inhibited, as demonstrated with the combination of DFMO and the bis(benzyl)polyamine, MDL27695 [161], this target may hold promise for antimalarial treatment with a novel mechanism radically different from those currently employed clinically. A follow-up investigation could perhaps aim at designing a single molecule that is able to destabilise the protein as a whole (e.g. by binding to the hinge region, which connects the two catalytic sites), thereby inactivating both the active sites of ODC and AdoMetDC simultaneously. Such a compound, in combination with an inhibitor of the yet evasive polyamine transporter, could form the predecessors of the next generation of antimalarial drugs.

Every day more than 3000 people die of malaria in Africa [13], which is more than the number of people who tragically died in the 9/11 terrorist attacks in the United States. This number is 1.6% of the annual 57 million deaths that occur globally, yet malaria accounts for only 0.4% of the world's biomedical research [305]. Therefore, research on this intriguing parasite should have the overall aim ultimately to relieve the enormous burden of the disease, e.g. by contributing information leading to novel drug targets or leads that can eventually result in clinical treatment, prevention or vector control. The investigation presented here contributed to this long-term goal by indicating the most appropriate drug sensitivity methods to employ in screening efforts to avoid potentially excluding cytostatic drug leads, by shedding light on the basic mechanism resulting in cytostasis (i.e. transcriptional arrest), by providing evidence of compensatory mechanisms in parasite polyamine metabolism, which supports the role of transcriptional regulation and contributes to the validation of PfAdoMetDC/ODC as an antimalarial drug target, and by revealing a potential resistance mechanism (i.e. compensatory LDC induction) against polyamine depletion as a treatment strategy. It is sincerely hoped that this knowledge, even in the smallest possible way, will contribute to eventually finding a solution against this devastating disease.

REFERENCES

- 1 Boyd, M. (1949) Historical review. In *Malaria* (Boyd, M., ed.). pp. 3-25, The W.B. Saunders Co., Philadelphia
- 2 Miller, R., Ikram, S., Armelagos, G., Walker, R., Harer, W., Shiff, C., Baggett, D., Carrigan, M. and Maret, S. (1994) Diagnosis of *Plasmodium falciparum* infections in mummies using the rapid manual *ParaSight*-F test. *Trans. R. Soc. Trop. Med. Hyg.* **88**, 31-32
- 3 Bruce-Chwatt, L. (1988) History of malaria from prehistory to eradication. In *Malaria. Principles and practice of malariology* (Wernsdorfer, W. and McGregor, I., eds.). pp. 1-59, Churchill Livingstone, Edinburgh
- 4 Kean, B., Mott, K. and Russell, A. (1978) *Tropical medicine and parasitology*, vol. 1. Classic investigations. (Kean, B., Mott, K. and Russell, A., eds.). pp. 23-44, Cornell University Press, New York
- 5 Sherman, I. (1998) A brief history of malaria and discovery of the parasite's life cycle. In *Malaria. Parasite biology, pathogenesis and protection* (Sherman, I., ed.). pp. 3-10, ASM Press, Washington D.C.
- 6 Ross, R. (1923) *Memoirs - with a full account of the great malaria problem and its solution*. Murray, London
- 7 Harrison, G. (1978) *Mosquitoes, malaria and man: a history of the hostilities since 1880*. Dutton, New York
- 8 Harrison, G. (1978) *Mosquitoes, malaria and man: a history of the hostilities since 1980*. Dutton, New York
- 9 Garnham, P. (1966) *Malaria parasites and other haemosporidia*. Blackwell Scientific, Oxford
- 10 Greenwood, B. and Mutabingwa, T. (2002) Malaria in 2002. *Nature*. **415**, 670-672
- 11 Organisation, W. H. (1973) Chemotherapy of malaria and resistance to antimalarials: report of a WHO Scientific Group. In *W.H.O. Tech. Rep. Ser. ed.)^eds.* pp. 30-35
- 12 Noedl, H., Wongsrichanalai, C. and Wernsdorfer, W. (2003) Malaria drug-sensitivity testing: new assays, new perspectives. *Trends Parasitol.* **19**, 175-181
- 13 Greenwood, B., Bojang, K., Whitty, C. and Targett, G. (2005) Malaria. *Lancet*. **365**, 1487-1498
- 14 Snow, R., Guerra, C., Noor, A., Myint, H. and Hay, S. (2005) The global distribution of clinical episodes of *Plasmodium falciparum* malaria. *Nature*. **434**, 214-217
- 15 Bremen, J. (2001) The ears of the hippopotamus: manifestations, determinants, and estimates of the malaria burden. *Am. J. Trop. Med. Hyg.* **64**, 1-11
- 16 Hay, S., Cox, J., Rogers, D., Randolph, S., Stern, D., Shanks, G., Myers, M. and Snow, R. (2002) Climate change and the resurgence of malaria in the East African highlands. *Nature*. **415**, 905-909
- 17 Kuhn, K., Campbell-Lendrum, D., Armstrong, B. and Davies, C. (2003) Malaria in Britain: Past, present, and future. *Proc. Natl. Acad. Sci. USA*. **100**, 9997-10001
- 18 Hemmer, C., Frimmel, S., Kinzelbach, R., Gürtler, L. and Reisinger, E. (2008) Global warming: trailblazer for tropical infections in Germany? *Dtsch. Med. Wochenschr.* **132**, 2583-2589
- 19 McCarthy, J., Canziani, O., Leary, N., Dokken, D. and White, K. (2001) *Impacts, Adaptation and Vulnerability - Contribution of Working Group II to the Third Assessment Report of the Intergovernmental Panel on Climate Change*. Cambridge Univ. Press, Cambridge
- 20 Sachs, J. and Malaney, P. (2002) The economic and social burden of malaria. *Nature*. **415**, 680-685
- 21 Mathers, C., Ezzati, M. and Lopez, A. (2007) Measuring the burden of neglected tropical diseases: The global burden of disease framework. *PLoS Negl. Trop. Dis.* **1**, e114
- 22 Williams, T. (2006) Red blood cell defects and malaria. *Mol. Biochem. Parasitol.* **149**, 121-127
- 23 Schuster, F. (2002) Cultivation of *Plasmodium* spp. *Clin. Microbiol. Rev.* **15**, 355-364
- 24 Tracy, J. and Webster, L. (2001) Drugs used in the chemotherapy of protozoal infections: Malaria. In *Goodman and Gilman's The Pharmacological Basis of Therapeutics* (Hardman, J. and Limbird, L., eds.). pp. 1069-1095, The McGraw-Hill Companies, New York

- 25 Lagerberg, R. (2008) Malaria in pregnancy: a literature review. *J. Midwifery Women's Health*. **53**, 209-215
- 26 Liu, J., Istvan, E., Gluzman, I., Gross, J. and Goldberg, D. (2006) *Plasmodium falciparum* ensures its amino acid supply with multiple acquisition pathways and redundant proteolytic enzyme systems. *PNAS*. **103**, 8840-8845
- 27 Krugliak, M., Zhang, J. and Ginsburg, H. (2002) Intraerythrocytic *Plasmodium falciparum* utilizes only a fraction of the amino acids derived from the digestion of host cell cytosol for the biosynthesis of its proteins. *Mol. Biochem. Parasitol.* **119**, 249-256
- 28 Egan, T. (2008) Recent advances in understanding the mechanism of hemozoin (malaria pigment) formation. *J. Inorg. Biochem.* **102**, 1288-1299
- 29 Bozdech, Z., Llinás, M., Pulliam, B., Wong, E., Zhu, J. and DeRisi, J. (2003) The transcriptome of the intraerythrocytic developmental cycle of *Plasmodium falciparum*. *PLoS Biology*. **1**, E5
- 30 Hall, N. and Carlton, J. (2005) Comparative genomics of malaria parasites. *Curr. Opin. Genet. Develop.* **15**, 609-613
- 31 Golenda, C., Li, J. and Rosenberg, R. (1997) Continuous in vitro propagation of the malaria parasite *Plasmodium vivax*. *Proc. Natl. Acad. Sci. USA*. **94**, 6786-6791
- 32 Heddini, A. (2002) Malaria pathogenesis: a jigsaw with an increasing number of pieces. *Int. J. Parasitol.* **32**, 1587-1598
- 33 Miller, L., Good, M. and Milon, G. (1994) Malaria pathogenesis. *Science*. **264**, 1878-1883
- 34 Dzikowski, R., Templeton, T. and Deitsch, K. (2006) Variant antigen gene expression in malaria. *Cell. Microbiol.* **8**
- 35 Mackintosh, C., Beeson, J. and Marsh, K. (2004) Clinical features and pathogenesis of severe malaria. *Trends Parasitol.* **20**, 597-603
- 36 Singh, B., Sung, L., Matusop, A., Radhakrishnan, A., Shamsul, S., Cox-Singh, J., Thomas, A. and Conway, D. (2004) A large focus of naturally acquired *Plasmodium knowlesi* infections in human beings. *Lancet*. **363**, 1017-1024
- 37 Chin, W., Contacos, P., Coatney, G. and Kimball, H. (1965) A naturally acquired quotidian-type malaria in man transferable to monkeys. *Science*. **149**, 865
- 38 Cox-Singh, J. and Singh, B. (2008) Knowlesi malaria: newly emergent and of public health importance? *Trends Parasitol.* **24**, 406-410
- 39 Clark, I. and Cowden, W. (2003) The pathophysiology of falciparum malaria. *Pharmacol. Ther.* **99**, 221-260
- 40 Gramaglia, I., Sobolewski, P., Meays, D., Contreras, R., Nolan, J., Frangos, J., Intaglietta, M. and Van der Heyde, H. (2006) Low nitric oxide bioavailability contributes to the genesis of experimental cerebral malaria. *Nat. Med.* **12**, 1417-1422
- 41 Pamplona, A., Ferreira, A., Balla, J., Jeney, V., Balla, G., Epiphonio, S., Chora, A., Rodrigues, C., Gregoire, I., Cunha-Rodrigues, M., Portugal, S., Soares, M. and Mota, M. (2007) Heme oxygenase-1 and carbon monoxide suppress the pathogenesis of experimental cerebral malaria. *Nat. Med.* **13**, 703-710
- 42 Rasti, N., Wahlgren, M. and Chen, Q. (2004) Molecular aspect of malaria pathogenesis. *FEMS Immunol. Med. Microbiol.* **41**, 9-26
- 43 Spycher, C., Rug, M., Klonis, N., Ferguson, D., Cowman, A., Beck, H.-P. and Tilley, L. (2006) Genesis and trafficking to the Maurer's clefts of *Plasmodium falciparum*-infected erythrocytes. *Mol. Cell. Biol.* **26**, 4074-4085
- 44 Richie, T. and Saul, A. (2002) Progress and challenges for malaria vaccines. *Nature*. **415**, 694-701
- 45 Van de Perre, P. and Dedet, J.-P. (2004) Vaccine efficacy: winning a battle (not war) against malaria. *Lancet*. **364**, 1380-1383
- 46 Bojang, K., Milligan, P., Pinder, M., Vigneron, L., Allouche, A., Kester, K., Ballou, W., Conway, D., Reece, W., Gothard, P., Yamuah, L., Delchambre, M., Voss, G., Greenwood, B., Hill, A., Mcadam, K., Tornieporth, N., Cohen, J. and Doherty, T. (2001) Efficacy of RTS,S/ASO2 malaria vaccine against *P. falciparum* infection in semi-immune adult men in The Gambia: a randomised trial. *Lancet*. **358**, 1927-1934

- 47 Sacarial, J., Aponte, J., Aide, P., Mandomando, I., Bassat, Q., Guinovart, C., Leach, A., Milman, J., Macete, E., Espasa, M., Ofori-Anyinam, O., Thonnard, J., Corachan, S., Dubois, M., Lievens, M., Dubovsky, F., Ballou, W., Cohen, J. and Alonso, P. (2008) Safety of the RTS,S/AS020A malaria vaccine in Mozambican children during a Phase IIb trial. *Vaccine*. **26**, 174-184
- 48 Kester, K., Cummings, J., Ockenhouse, C., Nielsen, R., Hall, B., Gordon, D., Schwenk, R., Krzych, U., Holland, C., Richmond, G., Dowler, M., Williams, J., Wirtz, R., Tornieporth, N., Vigneron, L., Delchambre, M., Demoitie, M.-A., Ballou, W., Cohen, J. and Heppner, D. J. (2008) Phase 2A trial of 0, 1, and 3 month and 0, 7, and 28 day immunization schedules of malaria vaccine RTS, S/AS02 in malaria-naïve adults at the Walter Reed Army Institute of Research. *Vaccine*. **26**, 2191-2202
- 49 White, N. (2002) The assessment of antimalarial drug efficacy. *Trends Parasitol.* **18**, 458-464
- 50 Trouiller, P. and Olliaro, P. (1998) Drug development output from 1975 to 1996: what proportion for tropical diseases? *J. Infect. Dis.* **3**, 61-63
- 51 Ridley, R. (2002) Medical need, scientific opportunity and the drive for antimalarial drugs. *Nature*. **415**, 686-693
- 52 Wongsrichanalai, C. and Meshnick, S. (2008) Declining artesunate-mefloquine efficacy against falciparum malaria on the Cambodia-Thailand border. *EID.* **14**, 716-719
- 53 Egan, T. (2002) Does oxidative stress have a role in the antimalarial activity of chloroquine. *Trends Parasitol.* **18**, 437-438
- 54 Yeh, I. and Altman, R. (2006) Drug targets for *Plasmodium falciparum*: a post-genomic review/survey. *Mini Rev. Med. Chem.* **6**, 177-202
- 55 Wongsrichanalai, C., Pickard, A., Wernsdorfer, W. and Meshnick, S. (2002) Epidemiology of drug-resistant malaria. *Lancet Infect. Dis.* **2**, 209-218
- 56 Martin, R., Lehane, A., Marchetti, R., Hayward, R., Saliba, K., Howitt, S., Bröer, S. and Kirk, K. (2008) The role of PfCRT in chloroquine resistance. *Int. J. Parasitol.* **38**, S17
- 57 Srivastava, I., Morrisey, J., Darrouzet, E., Daldal, F. and Vaidya, A. (1999) Resistance mutations reveal the atovaquone-binding domain of cytochrome b in malaria parasites. *Mol. Microbiol.* **33**, 704-711
- 58 Jambou, R., Legrand, E., Niang, M., Khim, N., Lim, P., Volney, B., Ekala, M., Bouchier, C., Esterre, P., Fandeur, T. and Mercereau-Puijalon, O. (2005) Resistance of *Plasmodium falciparum* field isolates to *in-vitro* artemether and point mutations of the SERCA-type PfATPase6. *Lancet.* **366**, 1960-1963
- 59 Chotivanich, K., Udomsanpetch, R., Dondorp, A., Williams, T., Angus, B., Simpson, J., Pukrittayakamee, S., Looareesuwan, S., Newbold, C. and White, N. (2000) The mechanisms of parasite clearance after antimalarial treatment. *J. Infect. Dis.* **182**, 629-633
- 60 Sibley, C., Hyde, J., Sims, P., Plowe, C., Kublin, J., Mberu, E., Cowman, A., Winstanley, P., Watkins, W. and Nzila, A. (2001) Pyrimethamine-sulfadoxine resistance in *Plasmodium falciparum*: what next? *Trends Parasitol.* **17**, 582-588
- 61 Birkholtz, L.-M., van Brummelen, A., Clark, K., Niemand, J., Maréchal, E., Llinas, M. and Louw, A. (2008) Exploring functional genomics for targets and therapeutics discovery in *Plasmodia*. *Acta Trop.* **105**, 113-123
- 62 Dahl, E., Shock, J., Shenai, B., Gut, J., Derisi, J. and Rosenthal, P. (2006) Tetracyclines specifically target the apicoplast of the malaria parasite *Plasmodium falciparum*. *Antimicrob. Agents Chemother.* **50**, 3124-3131
- 63 Wallace, H., Fraser, A. and Huges, A. (2003) A perspective of polyamine metabolism. *Biochem. J.* **376**, 1-14
- 64 Igarashi, K. and Kashiwagi, K. (2000) Polyamines: mysterious modulators of cellular functions. *Biochem. Biophys. Res. Commun.* **271**, 559-564
- 65 Tadolini, B. (1988) Polyamine inhibition of lipid peroxidation. *Biochem. J.* **249**, 33-36
- 66 Muscari, C., Guarnieri, C., Giaccari, A. and Calderera, C. (1995) Protective effect of spermine on DNA exposed to oxidative stress. *Mol. Cell Biochem.* **144**, 125-129
- 67 Seiler, N. and Raul, F. (2005) Polyamines and apoptosis. *J. Cell. Mol. Med.* **9**, 623-642
- 68 Thomas, T. and Thomas, T. (2001) Polyamines in cell growth and cell death: molecular mechanisms and therapeutic applications. *Cell. Mol. Life Sci.* **58**, 244-258
- 69 Kamio, Y. (1987) Structural specificity of diamines covalently linked to peptidoglycan for cell growth of *Veillonella alcalescens* and *Selenomonas ruminantium*. *J. Bacteriol.* **169**, 4837-4840

- 70 Pösö, H., McCann, P., Tanskanen, R., Bey, P. and Sjoerdsma, A. (1984) Inhibition of growth of *Mycoplasma dispar* by DL- α -difluoromethyllysine, a selective and irreversible inhibitor of lysine decarboxylase, and reversal by cadaverine (1,5-diaminopentane). *J. Biol. Chem.* **267**, 150-158
- 71 Tabor, H., Hafner, E. and Tabor, C. (1980) Construction of an *Escherichia coli* strain unable to synthesize putrescine, spermidine, or cadaverine: characterization of two genes controlling lysine decarboxylase. *J. Bacteriol.* **144**, 952-956
- 72 Cacciapuoti, G., Porcelli, M., Moretti, M., Sorrentino, F., Concilio, L., Zappia, V., Liu, Z.-J., Tempel, W., Schubot, F., Rose, J., Wang, B.-C., Brereton, P., Jenney, F. and Adams, M. (2007) The first agmatine/cadaverine aminopropyl transferase: biochemical and structural characterization of an enzyme involved in polyamine biosynthesis in the hyperthermophilic archaeon *Pyrococcus furiosus*. *J. Bacteriol.* **189**, 6057-6067
- 73 Takatsuka, Y., Yamaguchi, Y., M, O. and Kamio, Y. (2000) Gene cloning and molecular characterization of lysine decarboxylase from *Selenomonas ruminantium* delineate its evolutionary relationship to ornithine decarboxylases from eukaryotes. *J. Bacteriol.* **182**, 6732-6741
- 74 Ickson, I., Bakhanashvili, M. and Apelbaum, A. (1986) Inhibition by ethylene of polyamine biosynthetic enzymes enhanced lysine decarboxylase activity and cadaverine accumulation in pea seedlings. *Plant Physiol.* **82**, 607-609
- 75 Gamarnik, A. and Frydman, R. (1991) Cadaverine, an essential diamine for the normal root development of germinating soybean (*Glycine max*) seeds. *Plant Physiol.* **97**, 778-785
- 76 Kim, J.-S., Choi, S. and Lee, J. (2006) Lysine decarboxylase expression by *Vibrio vulnificus* is induced by SoxR in response to superoxide stress. *J. Bacteriol.* **188**, 8586-8592
- 77 Jiang, Y., Roberts, S., Jardim, A., Carter, N., Shih, S., Ariyanayagam, M., Fairlamb, A. and Ullman, B. (1999) Ornithine decarboxylase gene deletion mutants of *Leishmania donovani*. *J. Biol. Chem.* **274**, 3781-3788
- 78 Shapiro, T. and Goldberg, D. (2006) Chemotherapy of protozoal infections: Amebiasis, Giardiasis, Trichomoniasis, etc. In Goodman and Gilman's The Pharmacological Basis of Therapeutics (Brunton, L., Lazo, J. and Parker, K., eds.). pp. 1053-1055, McGraw-Hill Companies, New York
- 79 Müller, I., Das Gupta, R., Lüersen, K., Wrenger, C. and Walter, R. (2008) Assessing the polyamine metabolism of *Plasmodium falciparum* as chemotherapeutic target. *Mol. Biochem. Parasitol.* **160**, 1-7
- 80 Pegg, A. (1986) Recent advances in biochemistry of polyamines in eukaryotes. *Biochem. J.* **234**, 249-262
- 81 Müller, S., Coombs, G. and Walter, R. (2001) Targeting polyamines of parasitic protozoa in chemotherapy. *Trends Parasitol.* **17**, 242-249
- 82 Müller, S., Da'dara, A., Lüersen, K., Wrenger, C., Gupta, R. D., Madhubala, R. and Walter, R. (2000) In the human malaria parasite *Plasmodium falciparum*, polyamines are synthesized by a bifunctional ornithine decarboxylase, S-adenosylmethionine decarboxylase. *J. Biol. Chem.* **275**, 8097-8102
- 83 Krause, T., Lüersen, K., Wrenger, C., Gilberger, T.-W., Müller, S. and Walter, R. (2000) The ornithine decarboxylase domain of the bifunctional ornithine decarboxylase/S-adenosylmethionine decarboxylase of *Plasmodium falciparum*: recombinant expression and catalytic properties of two different constructs. *Biochem. J.* **352**, 287-292
- 84 Birkholtz, L.-M., Wrenger, C., Joubert, F., Wells, G., Walter, R. and Louw, A. (2004) Parasite-specific inserts in the bifunctional S-adenosylmethionine decarboxylase/ornithine decarboxylase of *Plasmodium falciparum* modulate catalytic activities and domain interactions. *Biochem. J.* **377**, 439-448
- 85 Haider, N., Eschbach, M.-L., De Souza Dias, S., Gilberger, T.-W., Walter, R. and Lüersen, K. (2005) The spermidine synthase of the malaria parasite *Plasmodium falciparum*: Molecular and biochemical characterisation of the polyamine synthesis enzyme. *Mol. Biochem. Parasitol.* **142**, 224-236
- 86 Willert, E. and Phillips, M. (2008) Regulated expression of an essential allosteric activator of polyamine biosynthesis in African trypanosomes. *PLoS Pathogens.* **4**, e1000183
- 87 Wrenger, C., Lüersen, K., Krause, T., Müller, S. and Walter, R. (2001) The *Plasmodium falciparum* bifunctional ornithine decarboxylase, S-adenosyl-L-methionine decarboxylase, enables a well balanced polyamine synthesis without domain-domain interaction. *J. Biol. Chem.* **276**, 29651-29656

- 88 Assaraf, Y., Golenser, J., Spira, D. and Bachrach, U. (1984) Polyamine levels and the activity of their biosynthetic enzymes in human erythrocytes infected with the malarial parasite, *Plasmodium falciparum*. *Biochem. J.* **222**, 815-819
- 89 Geary, T., Divo, A. and Jensen, J. (1983) An *in vitro* assay system for the identification of potential antimalarial drugs. *J. Parasitol.* **69**, 577-583
- 90 Das Gupta, R., Krause-Ihle, T., Bergmann, B., Müller, I., Khomutov, A., Müller, S., Walter, R. and Lüersen, K. (2005) 3-Aminoxy-1-aminopropane and derivatives have an antiproliferative effect on cultured *Plasmodium falciparum* by decreasing intracellular polyamine concentrations. *Antimicrob. Agents Chemother.* **49**, 2857-2864
- 91 Llinás, M., Bozdech, Z., Wong, E., Adai, A. and DeRisi, J. (2006) Comparative whole genome transcriptome analysis of three *Plasmodium falciparum* strains. *Nucleic Acids Res.* **34**, 1166-1173
- 92 Bzik, D., Li, W., Horii, T. and Inselburg, J. (1987) Molecular cloning and sequence analysis of the *Plasmodium falciparum* dihydrofolate reductase-thymidylate synthase gene. *Proc. Natl. Acad. Sci. U.S.A.* **84**, 8360-8364
- 93 Ivanetich, K. and Santi, D. (1990) Bifunctional thymidylate synthase-dihydrofolate reductase in protozoa. *FASEB J.* **4**, 1591-1597
- 94 Triglia, T. and Cowman, F. (1994) Primary structure and expression of the dihydropteroate synthase gene of *Plasmodium falciparum*. *Proc. Natl. Acad. Sci. U.S.A.* **91**, 7149-7153
- 95 Williams, M. (2008) Delineation of functional roles of parasite-specific inserts in the malarial S-adenosylmethionine decarboxylase/ornithine decarboxylase. In Department of Biochemistry ed.)^eds.). p. 139, University of Pretoria, Pretoria
- 96 Gardner, M., Hall, N., Fung, E., White, O., Berriman, M., Hyman, R., Carlton, J., Pain, A., Nelson, K., Bowman, S., Paulsen, I., James, K., Eisen, J., Rutherford, K., Salzberg, S., Craig, A., Kyes, S., Chan, M.-S., Nene, V., Shallom, S., Suh, B., Peterson, J., Angiuoli, S., Pertea, M., Allen, J., Selengut, J., Haft, D., Mather, M., Vaidya, A., Martin, D., Fairlamb, A., Fraunholz, M., Roos, D., Ralph, S., McFadden, G., Cummings, L., Subramanian, G., Mungall, C., Venter, J., Carucci, D., Hoffman, S., Newbold, C., Davis, R., Fraser, C. and Barrell, B. (2002) Genome sequence of the human malaria parasite *Plasmodium falciparum*. *Nature.* **419**, 498-511
- 97 Carlton, J., Angiuoli, S., Suh, B., Kooij, T., Pertea, M., Silva, J., Ermolaeva, M., Allen, J., Selengut, J., Koo, H., Peterson, J., Pop, M., Kosack, D., Shumway, M., Bidwell, S., Shallom, S., Van Aken, S., Riedmuller, S., Fieldblyum, T., Cho, J., Quackenbush, J., Sedegah, M., Shoaibi, A., Cummings, L., Florens, L., Yates III, J., Raine, J., Sinden, R., Harris, M., Cunningham, D., Preiser, P., Bergman, L., Vaidya, A., Van Lin, L., Janse, C., Waters, A., Smith, H., White, O., Salzberg, S., Venter, J., Fraser, C., Hoffman, S., Gardner, M. and Carucci, D. (2002) Genome sequence and comparative analysis of the model rodent malaria parasite *Plasmodium yoelii yoelii*. *Nature.* **419**
- 98 Hall, N., Karras, M., Raine, J., Carlton, J., Kooij, T., Berriman, M., Florens, L., Janssen, C., Pain, A., Christophides, G., James, K., Rutherford, K., Harris, B., Harris, D., Churcher, C., Quail, M., Ormond, D., Dogget, J., Trueman, H., Mendoza, J., Bidwell, S., Rajandream, M.-A., Carucci, D., Yates III, J., Kafatos, F., Janse, C., Barrell, B., Turner, C., Waters, A. and Sinden, R. (2005) A comprehensive survey of the *Plasmodium* life cycle by genomic transcriptomic and proteomics analyses. *Science.* **307**, 82-86
- 99 Pain, A., Böhme, U., Berry, A., Mungall, K., Finn, R., Jackson, A., Mourier, T., Misty, J., Pasini, E., Aslett, M., Balasubramaniam, S., Borgwardt, K., Brooks, K., Carret, C., Carver, T., Cherevach, I., Keane, T., Larke, N., Lapp, S., Marti, M., Moule, S., Meyer, I., Ormond, D., Peters, N., Sanders, M., Sanders, S., Sargeant, T., Simmonds, M., Smith, F., Squares, R., Thurston, S., Tivey, A., Walker, D., White, B., Zuiderwijk, E., Churcher, C., Quail, M., Cowman, A., Turner, C., Rajandram, M., Kocken, C., Thomas, A., Newbold, C., Barrell, B. and Berriman, M. (2008) The genome of the simian and human malaria parasite *Plasmodium knowlesi*. *Nature.* **456**, 799-804
- 100 Carlton, J., Adams, J., Silva, J., Bidwell, S., Lorenzi, H., Caler, E., Crabtree, J., Angiuoli, S., Merino, E., Amedeo, P., Cheng, Q., Roulson, R., Crabb, B., Del Portillo, H., Essien, K., Fieldblyum, T., Fernandez-Becerra, C., Gilson, P., Gueye, A., Guo, X., Kang'a, S., Kooij, T., Korsinczky, M., Meyer, E.-S., Nene, V., Paulsen, I., White, O., Ralph, S., Ren, Q., Sargeant, T., Salzberg, S., Stoeckert, C., Sullivan, S., Yamamoto, M., Hoffman, S., Wortman, J., Gardner, M., Galinski, M., Barnwell, J. and Fraser-Liggett, C.

- (2008) Comparative genomics of neglected human malaria parasite *Plasmodium vivax*. *Nature*. **455**, 757-763
- 101 Carlton, J. (2008) *Plasmodium vivax*: genetics and genomics of a 'neglected' human malaria parasite. *Int. J. Parasitol.* **38** Supplement 1, S27
- 102 Painter, H., Morrissey, J., Mather, M. and Vaidya, A. (2007) Specific role of mitochondrial electron transport in blood-stage *Plasmodium falciparum*. *Nature*. **446**, 88-91
- 103 Strachan, T. and Read, A. (1998) *Human molecular genetics*. BIOS Scientific Publishers Limited, Oxford
- 104 Vaidya, A., Akella, R. and Suplick, K. (1989) Sequences similar to genes for two mitochondrial proteins and portions of ribosomal RNA in tandemly arrayed 6-kilobase-pair DNA of a malaria parasite. *Mol. Biochem. Parasitol.* **1989**, 97-107
- 105 Anderson, S., Bankier, A., Barrell, B., Bruijn, M. D., Coulson, A., Drouin, J., Eperon, I., Nierlich, D., Roe, B., Sanger, F., Shreier, P., Smith, A., Staden, R. and Young, I. (1981) Sequence and organization of the human mitochondrial genome. *Nature*. **290**, 457-465
- 106 Wilson, R., Denny, P., Preiser, P., Rangachari, K., Roberts, K., Roy, A., Whyte, A., Strath, M., Moore, P. and Williamson, D. (1996) Complete gene map of the plastid-like DNA of the malaria parasite *Plasmodium falciparum*. *J. Mol. Biol.* **261**, 155-172
- 107 Waters, A. (1994) The ribosomal RNA genes of *Plasmodium*. *Adv. Parasitol.* **34**, 33-79
- 108 Le Roch, K., Zhou, Y., Blair, P., Grainger, M., Moch, J., Haynes, J., De La Vega, P., Holder, A., Batalov, S., Carucci, D. and Winzeler, E. (2003) Discovery of gene function by expression profiling of the malaria parasite life cycle. *Science*. **301**, 1503-1508
- 109 Tarun, A., Peng, X., Dumpit, R., Ogata, Y., Silva-Rivera, H., Camargo, N., Daly, T., Bergman, L. and Kappe, S. (2008) A combined transcriptome and proteome survey of malaria parasite liver stages. *Proc. Natl. Acad. Sci. USA*. **105**, 305-310
- 110 Bozdech, Z., Mok, S., Guangan, H., Imwong, M., Jaidee, A., Russel, B., Ginsburg, H., Nosten, F., Day, P., White, N., Carlton, J. and Preiser, P. (2008) The transcriptome of *Plasmodium vivax* reveals divergence and diversity of transcriptional regulation in malaria parasites. *PNAS*. **105**, 16290-16295
- 111 Gleeson, M. (2000) The plastid in Apicomplexa: what use is it? *Int. J. Parasitol.* **30**, 1053-1070
- 112 Florens, L., Washburn, M., Dale-Raine, J., Anthony, R., Grainger, M., Haynes, J., Moch, J., Muster, N., Sacci, J., Tabb, D., Witney, A., Wolters, D., Wu, Y., Gardner, M., Holder, A., Sinden, R., Yates, J. and Carucci, D. (2002) A proteomic view of the *Plasmodium falciparum* life cycle. *Nature*. **419**, 520-526
- 113 Date, S. and Stoeckert, C. (2006) Computational modeling of the *Plasmodium falciparum* interactome reveals protein function on a genome-wide scale. *Genome Res.* **16**, 542-549
- 114 Wuchty, S. (2007) Rich-club phenomenon in the interactome of *P. falciparum* - artifact or signature of a parasitic life style. *PLoS One*. **3**, e335
- 115 Wuchty, S. and Ipsaro, J. (2007) A draft of protein interactions in the malaria parasite *P. falciparum*. *J. Proteome Res.* **6**, 1461-1470
- 116 Teng, R., Junankar, P., Bubb, W., Rae, C., Mercier, P. and Kirk, K. (2008) Metabolite profiling of the intraerythrocytic malaria parasite *Plasmodium falciparum* by ¹H NMR spectroscopy. *NMR Biomed.*, In Press
- 117 Ginsburg, H. (2006) Progress in *in silico* functional genomics: the Malaria Metabolic Pathways database. *Trends Parasitol.* **22**, 238-240
- 118 Coleman, B. and Duraisingh, M. (2008) Transcriptional control and gene silencing in *Plasmodium falciparum*. *Cell. Microbiol.* **10**, 1935-1946
- 119 Coulson, M., Hall, N. and Ouzounis, C. (2004) Comparative genomics of transcriptional control in the human malaria parasite *Plasmodium falciparum*. *Genome Res.* **14**, 1548-1554
- 120 Callebaut, I., Prat, K., Meurice, E., Mornon, J. and Tornavo, S. (2005) Prediction of the general transcription factors associated with RNA polymerase II in *Plasmodium falciparum*: conserved features and differences relative to other eukaryotes. *BMC Genomics*. **6**, 100
- 121 Polson, H. and Blackman, M. (2005) A role for poly(dA)poly(dT) tracts in directing activity of the *Plasmodium falciparum* calmodulin gene promoter. *Mol. Biochem. Parasitol.* **141**, 179-189

- 122 Balaji, S., Babu, M., Iyer, L. and Aravind, L. (2005) Discovery of the principal specific transcription factors of Apicomplexa and their implication for the evolution of the AP2-integrase DNA binding domains. *Nucl. Acids Res.* **33**, 3994-4006
- 123 De Silva, E., Gehrke, A., Olszewski, K., León, I., Chahal, J., Bulyk, M. and Llinás, M. (2008) Specific DNA-binding by Apicomplexan AP2 transcription factors. *Proc. Natl. Acad. Sci. USA.* **105**, 8393-8398
- 124 Choi, S., Keyes, M. and Horrocks, P. (2006) LC/ESI-MS demonstrates the absence of 5-methyl-2'-deoxycytosine in *Plasmodium falciparum* genomic DNA. *Mol. Biochem. Parasitol.* **150**, 350-352
- 125 Miao, J., Fan, Q., Cui, L., Li, J., Li, J. and Cui, L. (2006) The malaria parasite *Plasmodium falciparum* histones: Organization, expression, and acetylation. *Gene.* **369**, 53-65
- 126 Pollack, Y., Kogan, N. and Golenser, J. (1991) *Plasmodium falciparum*: Evidence for a DNA methylation pattern. *Exp. Parasitol.* **72**, 339-344
- 127 Neafsey, D., Hartl, D. and Berriman, M. (2005) Evolution of non-coding and silent coding sites in the *Plasmodium falciparum* and *Plasmodium reichenowi* genomes. *Mol. Biol. Evol.* **22**, 1621-1626
- 128 Deitsch, K., Duraisingh, R., Dzikowski, A., Gunaseker, A., Khan, S., Le Roch, K., Llinás, M., Mair, G., McGovern, V., Roos, D., Shock, J., Sims, J., Wiegand, R. and Winzeler, E. (2007) Mechanisms of gene regulation in *Plasmodium*. *Am. J. Trop. Med. Hyg.* **77**, 201-208
- 129 Balu, B., Shoue, D., Fraser, J. and Adams, J. (2005) High-efficiency transformation of *Plasmodium falciparum* by the lepidopteran transposon element *piggyBac*. *Proc. Natl. Acad. Sci. USA.* **102**, 16391-16396
- 130 De Koning-Ward, T., Janse, C. and Waters, A. (2000) The development of genetic tools for dissecting the biology of malaria parasites. *Annu. Rev. Microbiol.* **54**, 157-185
- 131 Fidock, D. and Wellems, T. (1997) Transformation with human dihydrofolate reductase renders malaria parasites insensitive to WR99210 but does not affect the intrinsic activity of proguanil. *Proc. Natl. Acad. Sci. USA.* **94**, 10931-10936
- 132 Wu, Y., Sifri, D., Lei, H.-H., Su, X.-Z. and Wellems, T. (1995) Transfection of *Plasmodium falciparum* within human blood cells. *Proc. Natl. Acad. Sci. USA.* **92**, 973-977
- 133 Brown, A. and Catteruccia, F. (2006) Toward silencing the burden of malaria: progress and prospects for RNAi-based approaches. *Biotechniques.* **40**, S38-44
- 134 Gray, N., Wodicka, A., Thunnissen, A., Norman, T., Kwon, S., Espinoza, F., Morgan, D., Barnes, G., LeClerc, S., Meijer, L., Kim, S., Lockhart, D. and Schultz, P. (1998) Exploiting chemical libraries, structure, and genomics in the search for kinase inhibitors. *Science.* **281**, 533-538
- 135 Sakata, T. and Winzeler, E. (2007) Genomics, systems biology and drug development for infectious diseases. *Mol. BioSyst.* **3**, 841-848
- 136 Boshoff, H. and Manjunatha, U. (2006) The impact of genomics on discovering drugs against infectious diseases. *Microbes Infect.* **8**, 1654-1661
- 137 Wilson, M., DeRisi, J., Kristensen, H., Imboden, P., Rane, S., Brown, P. and Schoolnik, G. (1999) Exploring drug-induced alterations in gene expression in *Mycobacterium tuberculosis* by microarray hybridization. *Proc. Natl. Acad. Sci. USA.* **96**, 12833-12838
- 138 Boshoff, H., Myers, T., Copp, B., McNeil, M., Wilson, M. and Clifton, B. (2004) The transcriptional responses of *Mycobacterium tuberculosis* to inhibitors of metabolism. *J. Biol. Chem.* **279**, 40174-40184
- 139 Marton, M., Derisi, J., Bennett, H., Iyer, V., Meyer, M., Roberts, C., Stoughton, R., Burchard, J., Slade, D., Dai, H., Basset, D., Hartwell, L., Brown, P. and Friend, S. (1998) Drug target validation and identification of secondary drug target effects using DNA microarrays. *Nat. Med.* **4**, 1293-1301
- 140 Freiberg, C. and Brotz-Oesterhelt, H. (2005) Functional genomics in antibacterial drug discovery. *Drug Disc. Today.* **10**, 927-935
- 141 Ohlstein, E. H., Ruffolo Jr., R. R. and Elliot, J. D. (2000) Drug discovery in the next millennium. *Annu. Rev. Pharmacol. Toxicol.* **40**, 177-191
- 142 Wang, S., Sim, T. B., Kim, Y.-S. and Chang, Y.-T. (2004) Tools for target identification and validation. *Curr. Opin. Chem. Biol.* **8**, 371-377
- 143 Paolini, G. V., Shapland, R. H., van Hoorn, W. P., Mason, J. S. and Hopkins, A. L. (2006) Global mapping of pharmacological space. *Nature Biotechnol.* **24**, 805-815
- 144 Sawyer, T. K. (2006) Smart drug discovery leveraging innovative technologies and predictive knowledge. *Nature Chem. Biol.* **2**, 646-648

- 145 Reguera, R., Tekwani, B. and Balaña-Fouce, R. (2005) Polyamine transport in parasites: A potential target for new antiparasitic drug development. *Comp. Biochem. Physiol. C.* **140**, 151-164
- 146 Metcalf, B., Bey, P., Danzin, C., Jung, M., Casara, P. and Vevert, J. (1978) Catalytic irreversible inhibition of mammalian ornithine decarboxylase by substrate and product analogues. *J. Am. Chem. Soc.* **100**, 2551-2553
- 147 Seiler, N. (2003) Thirty years of polyamine-related approaches to cancer therapy. Retrospect and prospect. Part 1. Selective enzyme inhibitors. *Curr. Drug Targets.* **4**, 537-564
- 148 Sporn, M. and Hong, W. (2008) Concomitant DFMO and sulindac chemoprevention of colorectal cancer: a major clinical advance. *Nat. Clin. Pract. Oncol.* **In Press**
- 149 Simoneau, A., Gerner, E., Nagle, R., Ziogas, A., Fujikawa-Brooks, S., Yerushalmi, H., Ahlering, T., Lieberman, R., McLaren, C., Anton-Culver, H. and Meyskens, F. (2008) The effect of difluoromethylornithine on decreasing prostate size and polyamines in men: results of a year-long phase IIb randomized placebo-controlled chemoprevention trial. *Cancer Epidemiol. Biomarkers Prev.* **17**, 292-299
- 150 VanNieuwenhove, S., Schechter, P., Declercq, J., Bone, G., Burke, J. and Sjoerdsma, A. (1985) Treatment of gambiense sleeping sickness in the Sudan with oral DFMO (DL-a-difluoromethylornithine), an inhibitor of ornithine decarboxylase; first field trial. *Trans. R. Soc. Trop. Med. Hyg.* **79**, 692-698
- 151 Iten, M., Mett, H., Evans, A., Enyaru, J., Brun, R. and Kaminsky, R. (1997) Alterations in ornithine decarboxylase characteristics account for tolerance of *Trypanosoma brucei rhodesiense* to D,L-alpha-difluoromethylornithine. *Antimicrob. Agents Chemother.* **41**, 1922-1925
- 152 McCann, P., Bacchi, C., Hanson, W., Cain, G., Nathan, H., Hutner, S. and Sjoerdsma, A. (1981) Effect on parasitic protozoa of a-difluoromethylornithine, an inhibitor of ornithine decarboxylase. *Adv. Polyamine Res.* **3**, 97-110
- 153 Wright, P., Byers, T., Cross-Doersen, D., McCann, P. and Bitonti, A. (1991) Irreversible inhibition of S-adenosylmethionine decarboxylase in *Plasmodium falciparum*-infected erythrocytes: growth inhibition *in vitro*. *Biochem. Pharmacol.* **41**, 1713-1718
- 154 Assaraf, Y., Golenser, J., Spira, D., Messer, G. and Bachrach, U. (1987) Cytostatic effect of DL-a-difluoromethylornithine against *Plasmodium falciparum* and its reversal by diamines and spermidine. *Parasitol. Res.* **73**, 313-318
- 155 Bitonti, A., McCann, P. and Sjoerdsma, A. (1987) *Plasmodium falciparum* and *Plasmodium berghei*: Effects of ornithine decarboxylase inhibitors on erythrocytic schizogony. *Exp. Parasitol.* **64**, 237-243
- 156 Casar, P., Marchal, P., Wagner, J. and Danzin, C. (1989) 5'-[[Z]-4-Amino-2-butenyl]methylamino-5'-deoxyadenosine: a [potent enzyme-activated irreversible inhibitor of S-adenosyl-L-methionine decarboxylase from *Escherichia coli*. *J. Am. Chem. Soc.* **111**, 9111-9113
- 157 Byers, T., Bush, T., McCann, P. and Bitonti, A. (1991) Antitrypanosomal effect of polyamine biosynthesis inhibitors correlate with increases in *Trypanosoma brucei brucei* S-adenosyl-L-methionine. *Biochem. J.* **274**, 527-533
- 158 Secrist III, J. (1987) New substrate analogues as inhibitors of S-adenosylmethionine decarboxylase. *Nucleosides Nucleotides Nucleic Acids.* **6**, 78-83
- 159 Tekwani, B., Bacchi, C., Secrist, J. and Pegg, A. (1992) Irreversible inhibition of S-adenosylmethionine decarboxylase of *Trypanosoma brucei brucei* by S-adenosylmethionine analogues. *Biochem. Pharmacol.* **44**, 905-911
- 160 Pegg, A., Jones, D. and Secrist, J. (1988) Effect of S-Adenosylmethionine decarboxylase on polyamine content and growth of L1210 cells. *Biochemistry.* **27**, 1408-1415
- 161 Bitonti, A., Dumont, J., Bush, T., Edwards, M., Stemerick, D., McCann, P. and Sjoerdsma, A. (1989) Bis(benzyl)polyamine analogs inhibit the growth of chloroquine-resistant human malaria parasites (*Plasmodium falciparum*) *in vitro* and in combination with a-difluoromethylornithine cure murine malaria. *Proc. Natl. Acad. Sci. USA.* **86**, 651-655
- 162 Bitonti, A., Bush, T. and McCann, P. (1989) Regulation of polyamine biosynthesis in rat hepatoma (HTC) cells by a bisbenzyl polyamine analogue. *Biochem. J.* **257**, 769-774
- 163 Mukhopadhyay, R. and Madhubala, R. (1995) Effects of bis(benzyl)polyamine analogs on *Leishmania donovani* promastigotes. *Exp. Parasitol.* **81**, 39-46

- 164 Rieckmann, K., Campbell, G., Sax, L. and Mrema, J. (1978) Drug sensitivity of *Plasmodium falciparum*: An *in vitro* microtechnique. *Lancet*. **1**, 22-23
- 165 Desjardins, R., Canfield, C., Haynes, J. and Chulay, J. (1979) Quantitative assesment of antimalarial activity *in vitro* by a semiautomated microdilution technique. *Antimicrob. Agents Chemother.* **16**, 710-718
- 166 Makler, M., Ries, J., Williams, J., Bancroft, J., Piper, R., Gibbins, B. and Hinrichs, D. (1993) Parasite lactate dehydrogenase as an assay for *Plasmodium falciparum* drug sensitivity. *Am. J. Trop. Med. Hyg.* **48**, 739-741
- 167 Druilhe, P., Moreno, A., Blanc, C., Brasseur, P. and Jacquier, P. (2001) A colorimetric *in vitro* drug sensitivity assay for *Plasmodium falciparum* based on highly sensitive double-site lactate dehydrogenase antigen capture enzyme-linked immunosorbent assay. *Am. J. Trop. Med. Hyg.* **64**, 233-241
- 168 Noedl, H., Wernsdorfer, W., Miller, R. and Wongsrichanalai, C. (2002) Histidine-rich protein II: a novel approach to malaria drug sensitivity testing. *Antimicrob. Agents Chemother.* **46**, 1658-1664
- 169 Trager, W. and Jensen, J. (1976) Human malaria parasites in continuous culture. *Science*. **193**, 673-675
- 170 Brecher, G. and Schneiderman, M. (1950) A time saving device for the counting of reticulocytes. *Am. J. Clin. Pathol.* **20**, 1079-1083
- 171 Lambros, C. and Vanderberg, J. (1979) Synchronisation of *Plasmodium falciparum* erythrocytic stages in culture. *J. Parasitol.* **65**, 418-420
- 172 Schulze, D., Makgatho, E., Coetzer, T., Louw, A., VanRensburg, C. and Visser, L. (1997) Development and application of a modified flow cytometric procedure for rapid *in vitro* quantitation of malaria parasitaemia. *S. Afr. J. Sci.* **93**, 156-158
- 173 Bianco, A., Battye, F. and Brown, G. (1986) *Plasmodium falciparum*: Rapid quantification of parasitemia in fixed malaria cultures by flow cytometry. *Exp. Parasitol.* **62**, 275-282
- 174 Tarcha, P., Chu, V. and Whittern, D. (1987) 2,3-Diaminophenazine is the product from the horseradish peroxidase catalyzed oxidation of o-penylenediamine. *Anal. Biochem.* **165**, 230-233
- 175 Makler, M., Lee, L. and Recktenwald, D. (1987) Thiazole orange: A new dye for *Plasmodium* species analysis. *Cytometry*. **8**, 568-570
- 176 Motulsky, H. and Christopoulos, A. (2003) Fitting models to biological data using linear and nonlinear regression. A practical guide to curve fitting. GraphPad Software Inc., San Diego
- 177 Wouters, P., Bos, A. and Ueckert, J. (2001) Membrane permeabilization in relation to inactivation kinetics of *Lactobacillus* species due to pulsed electric fields. *Appl. Environ. Microbiol.* **67**, 3092-3101
- 178 Cho, M.-H., Niles, A., Huang, R., Inglese, J., Austin, C., Riss, T. and Xia, M. (2008) A bioluminescent cytotoxicity assay for assessment of membrane integrity using a proteolytic biomarker. *Toxicol. in Vitro.* **22**, 1099-1106
- 179 Gunasekera, A., Patankar, S., Schug, J., Eisen, G. and Wirth, D. (2003) Drug-induced alterations in gene expression of the asexual blood forms of *Plasmodium falciparum*. *Mol. Microbiol.* **50**, 1229-1239
- 180 Desakorn, V., Silamut, K., Angus, B., Sahassananda, D., Chotivanich, K., Suntharasamai, P., Simpson, J. and White, N. (1997) Semi-quantitative measurement of *Plasmodium falciparum* antigen PfHRP2 in blood and plasma. *Trans. R. Soc. Trop. Med. Hyg.* **91**, 479-483
- 181 Fivelman, Q., Adagu, I. and Warhurst, D. (2004) Modified fixed-ratio isobologram method for studying *in vitro* interactions between atovaquone and proguanil or dihydroartemisinin against drug-resistant strains of *Plasmodium falciparum*. *Antimicrob. Agents Chemother.* **48**, 4097-4102
- 182 Russel, B., Chalfein, F., Prasetyorini, B., Kenangalem, E., Piera, K., Suwanarusk, R., Brockman, A., Proayoga, P., Sugiarto, P., Cheng, Q., Tjitra, E., Anstey, N. and Price, R. (2008) Determinants of *in vitro* drug susceptibility testing of *Plasmodium vivax*. *Antimicrob. Agents Chemother.* **52**, 1040-1045
- 183 Caillard, V., Beaute-Lafitte, A., Chabaud, A., Ginsburg, H. and Landau, I. (1995) Stage sensitivity of *Plasmodium vinckei petteri* to quinine, mefloquine and pyrimethamine. *J. Parasitol.* **81**, 295-301
- 184 Bitonti, A., Byers, T., Bush, T., Casara, P., Bacchi, C., Clarkson, A., McCann, P. and Sjoerdsma, A. (1990) Cure of *Trypanosoma brucei brucei* and *Trypanosoma brucei rhodesiense* infections in mice with an irreversible inhibitor of S-adenosylmethionine decarboxylase. *Antimicrob. Agents Chemother.* **34**, 1485-1490

- 185 Bacchi, C., Nathan, H., Yarlett, N., Goldberg, B., McCann, P., Bitonti, A. and Sjoerdsma, A. (1992) Cure of murine *Trypanosoma brucei rhodesiense* infections with an S-adenosylmethionine decarboxylase inhibitor. *Antimicrob. Agents Chemother.* **36**, 2736-2740
- 186 Wells, G., Birkholtz, L.-M., Joubert, F., Walter, R. and Louw, A. (2006) Novel properties of malarial S-adenosylmethionine decarboxylase as revealed by structural modelling. *J. Mol. Graph. Model.* **24**, 307-318
- 187 Birkholtz, L.-M., van Brummelen, A., Clark, K., Niemand, J., Maréchal, E., Llinas, M. and Louw, A. (2007) Exploring functional genomics for targets and therapeutics discovery in *Plasmodia*. *Acta Trop.* **105**, 113-123
- 188 Shaw, K. and Morrow, B. (2003) Transcriptional profiling and drug discovery. *Curr. Opin. Pharmacol.* **3**, 508-512
- 189 Fang, J., Zhou, H., Rathore, D., Sullivan, M., Su, X.-Z. and McCutchan, T. (2003) Ambient glucose concentration and gene expression in *Plasmodium falciparum*. *Mol. Biochem. Parasitol.* **133**, 125-129
- 190 Oakley, M., Kumar, S., Anantharaman, V., Zheng, H., Mahajan, B., Haynes, J., Moch, J., Fairhurst, R., McCutchan, T. and Aravind, L. (2007) Molecular factors and biochemical pathways induced by febrile temperature in intraerythrocytic *Plasmodium falciparum* parasites. *Infect. Immun.* **75**, 2012-2025
- 191 Cui, L., Miao, J., Furuya, T., Fan, Q., Li, X., Rathod, P., Su, X.-Z. and Cui, L. (2008) The histone acetyltransferase inhibitor anacardic acid leads to changes in global gene expression during *in vitro Plasmodium falciparum* development. *Eukaryot. Cell.* **7**, 1200-1210
- 192 Mair, G., Braks, J., Garver, L., Dimopoulos, G., Hall, N., Wiegant, J., Dirks, R., Khan, S., Janse, C. and Waters, A. (2006) Translational repression is essential for *Plasmodium* sexual development and mediated by DDX6-type RNA helicase. *Science.* **313**, 667-669
- 193 Shock, J., Fischer, K. and DeRisi, J. (2007) Whole genome analysis of mRNA decay in *Plasmodium falciparum* reveals a global lengthening of mRNA half-life during the intraerythrocytic development cycle. *Genome Biol.* **8**, R134
- 194 Le Roch, K. and Winzeler, E. (2005) The transcriptome of the malaria parasite *Plasmodium falciparum*. In *Molecular approaches to malaria* (Sherman, I., ed.). pp. 68-84, ASM Press, Washington, D.C.
- 195 Young, J. and Winzeler, E. (2005) Using expression information to discover new drug and vaccine targets in the malaria parasite *Plasmodium falciparum*. *Pharmacogenomics.* **6**, 1-26
- 196 Gunasekera, A., Myrick, A., Le Roch, K., Winzeler, E. and Wirth, D. (2007) *Plasmodium falciparum*: Genome wide perturbations in transcript profiles among mixed stage cultures after chloroquine treatment. *Exp. Parasitol.* **117**, 87-92
- 197 Nirmalan, N., Wang, P., Sims, P. and Hyde, J. (2002) Transcriptional analysis of genes encoding enzymes of the folate pathway in the human malaria parasite *Plasmodium falciparum*. *Mol. Microbiol.* **46**, 179-190
- 198 Natalang, O., Bischoff, E., Deplaine, G., Proux, C., Dillies, M.-A., Sismeiro, O., Guigon, C., Bonnefoy, S., Patarapotikul, J., Mercereau-Puijalon, O., Coppee, J.-Y. and David, P. (2008) Dynamic RNA profiling in *Plasmodium falciparum* synchronized blood stages exposed to lethal doses of artesunate. *BMC Genomics.* **9**, 388
- 199 Tamez, P., Bhattacharjee, S., Van Ooij, C., Hiller, N., Llinás, M., Balu, B., Adams, J. and Haldar, K. (2008) An erythrocyte vesicle protein exported by the malaria parasite promotes tubovesicular lipid import from the host cell surface. *PLoS Pathogens.* **4**, e10000118
- 200 Quackenbush, J. (2001) Computational analysis of microarray data. *Nat. Rev. Genet.* **2**, 418-427
- 201 Velculescu, V. (1999) SAGE and its use in global gene expression analysis. *Science.* **286**, 1491-1492
- 202 Lisitsyn, N., Lisitsyn, N. and Wigler, M. (1993) Cloning the differences between two complex genomes. *Science.* **259**, 5640-5648
- 203 Yang, Y. and Speed, T. (2002) Design issues for cDNA microarray experiments. *Nat. Rev. Genet.* **3**, 670-688
- 204 Hardiman, G. (2004) Microarray platforms - comparisons and contrasts. *Pharmacogenomics.* **5**, 487-502
- 205 Leung, Y. and Cavalieri, D. (2003) Fundamentals of cDNA microarray data analysis. *Trends Genet.* **19**, 649-659

- 206 Smyth, G. (2005) Limma: linear models for microarray data In Bioinformatics and computational biology solutions using R and bioconductor (Gentleman, R., Carey, V., Dudoit, S., Irizarry, R. and Huber, W., eds.). pp. 397-420, Springer, New York
- 207 Brazma, A., Hingamp, P., Quackenbush, J., Sherlock, G., Spellman, P., Stoeckert, C., Aach, J., Ansorge, W., Ball, C., Causton, H., Gaasterland, T., Glenisson, P., Holstege, F., Kim, I., Markowitz, V., Matese, J., Parkinson, H., Robinson, A., Sarkans, U., Schulze-Kremer, S., Stewart, J., Taylor, R., Vilo, J. and Vingron, M. (2001) Minimum information about a microarray experiment (MIAME) - toward standards for microarray data. *Nat. Genet.* **29**, 365-371
- 208 Chomczynski, P. and Sacchi, N. (1987) Single-step method of RNA isolation by acid guanidinium thiocyanate-phenol-chloroform extraction. *Anal. Biochem.* **162**, 156-159
- 209 Sambrook, J. and Russel, D. (2001) Molecular cloning, a laboratory manual. Cold Spring Harbor Laboratory Press, New York
- 210 Bozdech, Z., Zhu, J., Joachimiak, M., Cohen, F., Pulliam, B. and DeRisi, J. (2003) Expression profiling of the schizont and trophozoite stages of *Plasmodium falciparum* with a long-oligonucleotide microarray. *Genome Biol.* **4**, R9
- 211 Marko, M., Chipperfield, R. and Bimboim, H. (1982) A procedure for the large-scale isolation of highly purified plasmid DNA using alkaline extraction and binding to glass powder. *Anal. Biochem.* **121**, 382-387
- 212 Eisen, M., Spellman, P., Brown, P. and Botstein, D. (1998) Cluster analysis and display of genome-wide expression patterns. *Proc. Natl. Acad. Sci. USA.* **95**, 14863-14868
- 213 Yang, Y. and Paquet, A. (2005) Preprocessing two-color spotted arrays. In Bioinformatics and computational biology solutions using R and bioconductor (Gentleman, R., Carey, V., Huber, W., Irizarry, R. and Dudoit, S., eds.). pp. 49-69, Springer, New York
- 214 Smyth, G. (2004) Linear models and empirical Bayes methods for assessing differential expression in microarray experiments. *Stat Appl Genet Mol Biol.* **3**, Article 3
- 215 Storey, J., Xiao, W., Leek, J., Tompkins, R. and Davis, R. (2005) Significance analysis of time course microarray experiments. *Proc. Natl. Acad. Sci. USA.* **102**, 12837-12842
- 216 Dennis, G. J., Sherman, B., Hosack, D., Yang, J., Gao, W., Lane, H. and Lempicki, R. (2003) DAVID: Database for annotation, visualization, and integrated discovery. *Genome Biol.* **4**, P3
- 217 Stoeckert, C., Fischer, S., Kissinger, J., Heiges, M., Aurrecochea, C., Gajria, B. and Roos, D. (2006) PlasmoDB v5: new looks, new genomes. *Trends Parasitol.* **22**, 543-546
- 218 Rychlik, W., Spencer, W. and Rhoads, R. (1990) Optimisation of the annealing temperature for DNA amplification *in vitro*. *Nucl. Acids Res.* **18**, 6409-6412
- 219 Clark, K., Dhoogra, M., Louw, A. and Birkholtz, L.-M. (2008) Transcriptional responses of *Plasmodium falciparum* to α -difluoromethylornithine-induced polyamine depletion. *Biol. Chem.* **389**, 111-125
- 220 Hoppe, H., Verschoor, J. and Louw, A. (1991) *Plasmodium falciparum*: A comparison of synchronisation methods for *in vitro* cultures. *Exp. Parasitol.* **72**, 464-467
- 221 Gutteridge, W. and Trigg, P. (1972) Periodicity of nuclear DNA synthesis in the intraerythrocytic cycle of *Plasmodium knowlesi*. *J. Protozool.* **19**, 378-381
- 222 Bozdech, Z. and Ginsburg, H. (2004) Antioxidant defense in *Plasmodium falciparum* - data mining of the transcriptome. *Malaria Journal.* **3**, 23-33
- 223 Bozdech, Z. and Ginsburg, H. (2005) Data mining of the transcriptome of *Plasmodium falciparum*: the pentose phosphate pathway and ancillary processes. *Malaria Journal.* **4**, 17-29
- 224 Alm, K., Berntsson, A. and Oredsson, S. (1999) Topoisomerase II is non-functional in polyamine-depleted cells. *J. Cell. Biochem.* **75**, 46-55
- 225 Tkachenko, A. and Nesterova, L. (2002) Polyamines as modulators of gene expression under oxidative stress in *Escherichia coli*. *Biochemistry (Moscow).* **68**, 850-856
- 226 Yoshida, M., Kashiwagi, K., Shigemasa, A., Taniguchi, S., Yamamoto, K., Makinoshima, H., Ishihama, A. and Igarashi, K. (2004) A unifying model for the role of polyamines in bacterial cell growth, the polyamine modulon. *J. Biol. Chem.* **279**, 46008-46013
- 227 Morgan, D. (1990) Polyamines and cellular regulation: perspectives. *Biochem. Soc. Trans.* **18**, 1080-1084

- 228 Frostesjo, L. and Heby, O. (1999) Polyamine depletion up-regulates c-Myc expression yet induces G1 arrest and terminal differentiation of teratocarcinoma stem cells. *J. Cell. Biochem.* **76**, 143-152
- 229 Kumar, N., Cha, G., Pineda, F., Maciel, J., Haddad, D., Bhattacharyya, M. and Nagayasu, E. (2004) Molecular complexity of sexual development and gene regulation in *Plasmodium falciparum*. *Int. J. Parasitol.* **34**, 1451-1458
- 230 Morgan, D., Blankenship, J. and Mathews, H. (1991) Polyamines and acetylpolyamines increase the stability and alter the conformation of nucleosome core particles. *Biochemistry.* **26**, 3643-3649
- 231 Volkman, S., Barry, A., Lyons, E., Nielsen, K., Thomas, S., Choi, M., Thakore, S., Day, K., Wirth, D. and Hartl, D. (2001) Recent origin of *Plasmodium falciparum* from a single progenitor. *Science.* **293**, 482-484
- 232 Shi, L., Perkins, R., Fang, H. and Tong, W. (2008) Reproducible and reliable microarray results through quality control: good laboratory proficiency and appropriate data analysis practices are essential. *Curr. Opin. Biotech.* **19**, 10-18
- 233 Efferth, T., Gillet, J., Sauerbrey, A., Zintl, F., Bertholet, V., De Longueville, F., Remacle, J. and Steinbach, D. (2006) Expression profiling of ATP-binding cassette transporters in childhood T-cell acute lymphoblastic leukemia. *Mol. Cancer Ther.* **5**, 1986-1994
- 234 Johnsson, A., Vallon-Christensson, J., Strand, C., Litman, T. and Eriksen, J. (2005) Gene expression profiling in chemoresistant variants of three cell lines of different origin. *Anticancer Res.* **25**, 2661-2668
- 235 Nemoto, T., Kamel, S., Seyama, Y. and Kubota, S. (2001) p53 Independent G1arrest induced by DL-a-difluoromethylornithine. *Biochem. Biophys. Res. Commun.* **280**, 848-854
- 236 Tabor, C. and Tabor, H. (1985) Polyamines in microorganisms. *Microbiol. Rev.* **49**, 81-99
- 237 Childs, A., Mehta, D. and Gerner, E. (2003) Polyamine-dependent gene expression. *Cell. Mol. Life Sci.* **60**, 1394-1406
- 238 Brehelin, L., Dufayard, J. and Gacuel, O. (2008) PlasmoDraft: a database of *Plasmodium falciparum* gene function predictions based on post-genomic data. *BMC Bioinformatics.* **9**, 440
- 239 Reguera, R., Redondo, C., Pérez-Pertejo, Y. and Balaña-Fouce, R. (2007) S-adenosylmethionine in protozoan parasites: Functions, synthesis and regulation. *Mol. Biochem. Parasitol.* **152**, 1-10
- 240 Oden, K. and Clarke, S. (1983) S-Adenosyl-L-methionine synthetase from human erythrocytes: role in the regulation of cellular S-adenosylmethionine levels. *Biochemistry.* **22**, 2978-2986
- 241 Kloor, D. and Osswald, H. (2004) S-adenosylhomocysteine hydrolase as a target for intracellular adenosine action. *Trends. Pharmacol. Sci.* **25**, 294-297
- 242 Nirmalan, N., Sims, J. and Hyde, J. (2004) Translational up-regulation of antifolate drug targets in the human malaria parasite *Plasmodium falciparum* upon challenge with inhibitors. *Mol. Biochem. Parasitol.* **136**, 63-70
- 243 Cochet, C. and Chambaz, E. (1983) Polyamine-mediated protein phosphorylations: a possible target for intracellular polyamine action. *Mol. Cell Endocrinol.* **30**, 247-266
- 244 Gissot, M., Briquet, S., Refour, P., Boschet, C. and Vauqero, C. (2005) PfMyb1, a *Plasmodium falciparum* transcription factor, is required for intra-erythrocytic growth and controls key genes for cell cycle regulation. *J. Mol. Biol.* **346**, 29-42
- 245 Fukuchi, J., Hiipakka, R., Kokontis, J., Nishimura, K., Igarashi, K. and Liao, S. (2004) TATA-binding protein-associated factor 7 regulates polyamine transport activity and polyamine analog-induced apoptosis. *J. Biol. Chem.* **279**, 29921-29929
- 246 Le Roch, K., Johnson, J., Florens, L., Zhou, Y., Santrosyan, A., Grainger, M., Yan, S., Williamson, K., Holder, A., Carucci, D., Yates III, J. and Winzeler, E. (2004) Global analysis of transcript and protein levels across the *Plasmodium falciparum* life cycle. *Genome Res.* **14**, 2308-2318
- 247 Ueda, M., Masu, Y., Ando, A., Maeda, H., Del Monte, M., Uyama, M. and Ito, S. (1998) Prevention of ornithine cytotoxicity by proline in human retinal pigment epithelial cells. *Invest. Ophthalmol. Vis. Sci.* **39**, 820-827
- 248 Wu, G. and Morris, S. J. (1998) Arginine metabolism: nitric oxide and beyond. *Biochem. J.* **336**, 1-17
- 249 Kidron, H., Repo, S., Johnson, M. and Salminen, T. (2007) Functional classification of aminoacid decarboxylases form the alanine racemase structural family by phylogenetic studies. *Mol. Biol. Evol.* **24**, 79-89

- 250 Edgar, R., Domrachev, M. and Lash, A. (2002) Gene expression omnibus: NCBI gene expression and hybridization array data repository. *Nucl. Acids Res.* **30**, 207-210
- 251 Makanga, M., Bray, P., Horrocks, P. and Ward, S. (2005) Towards a proteomic definition of CoArtem action in *Plasmodium falciparum* malaria. *Proteomics.* **5**, 1849-1858
- 252 Le Roch, K. G., Johnson, J. R., Ahiboh, H., Plouffe, D., Henson, K., Zhou, Y., Mamoun, C., Yates, J. R. r., Vial, H. and Winzeler, E. A. (2006) Genomic profiling of the malaria parasite response to the choline analogue reveals drug mechanism of action. In *Keystone Symposia: Malaria Functional Genomics to Biology to Medicine ed.)*^eds.)
- 253 Fraunholz, M. J. (2005) Systems biology in malaria research. *Trends Parasitol.* **21**, 393-395
- 254 Pir, P., Kirdar, B., Hayes, A., Ylsen Onsan, Z., Ulgen, K. and Oliver, S. G. (2006) Integrative investigation of metabolic and transcriptomic data. *BMC Bioinformatics.* **7**, 203
- 255 Carrette, O., Burkhard, P., Sanchez, J.-C. and Hochstrasser, D. (2006) State-of-the-art two-dimensional gel electrophoresis: a key tool of proteomics research. *Nat. Protocols.* **1**, 812-823
- 256 Schratzenholz, A. (2004) Proteomics: how to control highly dynamic patterns of millions of molecules and interpret changes correctly. *Drug Discov. Today.* **1**, 1-8
- 257 Barret, J., Brophy, P. and Hamilton, J. (2005) Analysing proteomic data. *Int. J. Parasitol.* **35**, 543-553
- 258 Wu, W., Wang, G., Baek, S. and Shen, R.-F. (2006) Comparative study of three proteomic quantitative methods, DIGE, cICAT, and iTRAQ, using 2D gel- or MALDI TOF/TOF. *J. Proteome Res.* **5**, 651-658
- 259 Nirmalan, N., Sims, P. and Hyde, J. (2004) Quantitative proteomics of the human malaria parasite *Plasmodium falciparum* and its application to studies of development and inhibition. *Mol. Microbiol.* **52**, 1187-1199
- 260 Wolters, D., Washburn, M. and Yates III, J. (2001) An automated multidimensional protein identification technology for shotgun proteomics. *Anal. Chem.* **73**, 5683-5690
- 261 Wu, Y. and Craig, A. (2006) Comparative proteomic analysis of metabolically labelled proteins from *Plasmodium falciparum* isolates with different adhesion properties. *Malaria J.* **5:67**
- 262 Wysocki, V., Resing, K., Zhang, Q. and Cheng, G. (2005) Mass spectrometry of peptides and proteins. *Methods.* **35**, 211-222
- 263 Lu, W., Kimball, E. and Rabinowitz, J. (2006) A high-performance liquid chromatography-tandem mass spectrometry method for quantitation of nitrogen-containing intracellular metabolites. *J. Am. Soc. Mass Spectrom.* **17**, 37-50
- 264 Tweeddale, H., Notley-Mcrobbs, L. and Ferenci, T. (1998) Effect of slow growth on metabolism of *Escherichia coli*, as revealed by global metabolite pool ("metabolome") analysis. *J. Bacteriol.* **180**, 5109-5116
- 265 Wittmann, C., Krömer, J., Kiefer, P., Binz, T. and Heinzle, E. (2004) Impact of the cold shock phenomenon on quantification of intracellular metabolites in bacteria. *Anal. Biochem.* **327**, 135-139
- 266 Bajad, S., Kimball, E., Yuan, J., Peterson, C. and Rabinowitz, J. (2006) Separation and quantitation of water soluble cellular metabolites by hydrophilic interaction chromatography-tandem mass spectrometry. *J. Chromatogr. A.* **1125**, 76-88
- 267 Munger, J., Bajad, S., Collier, H., Shenk, T. and Rabinowitz, J. (2006) Dynamics of the cellular metabolome during human cytomegalovirus infection. *PLOS Pathogens.* **2**, e132
- 268 Alwood, J., Ellis, D. and Goodacre, R. (2008) Metabolomic technologies and their application to the study of plants and plant-host interactions. *Physiol. Plant.* **132**, 117-135
- 269 Goodacre, R., Vaidyanathan, S., Dunn, W., Harrigan, G. and Kell, D. (2004) Metabolomics by numbers: acquiring and understanding global metabolite data. *Trends Biotech.* **22**, 245-252
- 270 Nielsen, J. and Oliver, S. (2005) The next wave in metabolome analysis. *Trends Biotech.* **23**, 544-546
- 271 Fernie, A., Trethewey, R., Krotzky, A. and Willmitzer, L. (2004) Metabolite profiling: from diagnostics to systems biology. *Nat. Rev. Mol. Cell Biol.* **5**, 1-7
- 272 Hall, R. (2005) Plant metabolomics: from holistic hope to hype, to hot topic. *New Phytologist.* **169**, 453-468
- 273 Bradford, M. (1976) A rapid and sensitive method for the quantitation of microgram quantities of protein utilizing the principle of protein-dye binding. *Anal. Biochem.* **72**, 248-254

- 274 Chang, W., Huang, L., Shen, M., Webster, C., Burlingame, A. and Roberts, J. (2000) Patterns of protein synthesis and tolerance of anoxia in root tips of maize seedling acclimated to a low-oxygen environment, and identification of proteins by mass spectrometry. *Plant Physiol.* **122**, 295-317
- 275 Lemonnier, M. and Lane, D. (1998) Expression of the second lysine decarboxylase gene of *Escherichia coli*. *Microbiology.* **144**, 751-760
- 276 Kikuchi, Y., Kojima, H., Tanaka, T., Takatsuka, Y. and Kamio, Y. (1997) Characterization of a second lysine decarboxylase isolated from *Escherichia coli*. *J. Bacteriol.* **179**, 4486-4492
- 277 Fisher, O., Siman-Tov, R. and Ankri, S. (2004) Characterization of cytosine methylated regions and 5-cytosine DNA methyltransferase (EhMeth) in the protozoan parasite. *Nucleic Acids Res.* **32**, 287-297
- 278 Thiede, B., Höhenwarter, W., Krah, A., Mattow, J., Schmid, M., Schmidt, F. and Jungblut, P. (2005) Peptide mass fingerprinting. *Methods.* **35**, 237-247
- 279 Sandmeier, E., Hale, T. and Christen, P. (1994) Multiple evolutionary origin of pyridoxal-5-phosphate-dependent amino acid decarboxylases. *Eur. J. Biochem.* **221**, 997-1002
- 280 Shenai, B., Sijwali, P., Singh, S. and Rosenthal, P. (2000) Characterization of native and recombinant falcipain-2, a principal trophozoite cysteine protease and essential hemoglobinase of *Plasmodium falciparum*. *J. Biol. Chem.* **275**, 29000-29010
- 281 Pei, X., An, X., Guo, X., Tarnawski, M., Coppel, R. and Mohandas, N. (2005) Structural and functional studies of interaction between *Plasmodium falciparum* knob-associated histidine-rich protein (KAHRP) and erythrocyte spectrin. *J. Biol. Chem.* **280**, 31166-31171
- 282 Assaraf, Y., Abu-Elheiga, L., Spira, D., Desser, H. and Bachrach, U. (1987) Effect of polyamine depletion on macromolecular synthesis of the malarial parasite, *Plasmodium falciparum*, cultured in human erythrocytes. *Biochem. J.* **242**, 221-226
- 283 Kim, H., Kim, B. and Cho, Y. (1998) Purification and characterization of monomeric lysine decarboxylase from soybean (*Glycine max*) axes. *Arch. Biochem. Biophys.* **354**, 40-46
- 284 Wingler, A., Walker, R., Chen, Z.-H. and Leegood, R. (1999) Phosphoenolpyruvate carboxykinase is involved in the decarboxylation of aspartate in the bundle sheath of maize. *Plant Physiol.*, 539-545
- 285 Diefenbach, R. and Duggleby, R. (1991) Pyruvate decarboxylase from *Zymomonas mobilis*. Structure and re-activation of apoenzyme by the cofactors thiamine diphosphate and magnesium ion. *Biochem. J.* **276**, 439-445
- 286 Tanner, A., Bowater, L., Fairhurst, S. and Bornemann, S. (2001) Oxalate decarboxylase requires manganese and dioxygen for activity. *J. Biol. Chem.* **276**, 43627-43634
- 287 Gower, H., Leismann, O. and Jeltsch, A. (2000) DNA of *Drosophila melanogaster* contains 5-methylcytosine. *EMBO J.* **19**, 6918-6923
- 288 Dahl, C. and Guldberg, P. (2003) DNA methylation analysis techniques. *Biogerontology.* **4**, 233-250
- 289 Becker, M., Yen, R. and Itkin, P. (1979) Methylation of mouse liver DNA studied by means of the restriction enzymes *MspI* and *HpaII*. *Science.* **203**, 1019-1021
- 290 Achwal, C., Iyer, C. and Chandra, H. (1983) Immunochemical evidence for the presence of 5mC, 6mA and 7mG in human, *Drosophila* and mealybug DNA. *FEBS Journal.* **158**, 353-358
- 291 Hattman, S. (2005) DNA-[Adenine] methylation in lower eukaryotes. *Biochemistry (Moscow).* **70**, 550-558
- 292 Görg, A., Weiss, W. and Dunn, M. (2005) Current two-dimensional electrophoresis technology for proteomics. *Proteomics.* **4**, 3665-3685
- 293 Panpumthong, P. and Vattnaviboon, P. (2006) Improvement of proteomic profile of *Plasmodium falciparum* by two-step protein extraction in two-dimensional gel electrophoresis. *Thammasat Int. J. Sc. Tech.* **11**, 61-68
- 294 Souza, R., Henriques, C., Alves-Ferreira, M., Mendonça-Lima, L. and Degraeve, W. (2007) Investigation of a protein expression profile by high-resolution bidimensional electrophoresis of *Trypanosoma cruzi* epimastigotes. *Anal. Biochem.* **365**, 144-146
- 295 Sims, P. and Hyde, J. (2006) Proteomics of the human malaria parasite *Plasmodium falciparum*. *Expert Rev. Proteomics.* **3**, 87-95
- 296 Steuer, R. (2006) On the analysis and interpretation of correlations in metabolomic data. *Brief. Bioinform.* **7**, 151-158

- 297 Wertheimer, S. and Leifer, Z. (1983) Putrescine and spermidine sensitivity of lysine decarboxylase in *Escherichia coli*: evidence for a constitutive enzyme and its mode of regulation. *Biochem. Biophys. Res. Commun.* **114**, 882-888
- 298 Gygi, S., Rochon, Y., Franza, B. and Aebersold, R. (1999) Correlation between protein and mRNA abundance in yeast. *Mol. Cell Biol.* **19**, 1720-1730
- 299 Hoshen, M., Na-Bangchang, K., Stein, W. and Ginsburg, H. (2000) Mathematical modelling of the chemotherapy of *Plasmodium falciparum* with artesunate: postulation of 'dormancy', a partial cytostatic effect of the drug, and its implication for treatment regimens. *Parasitology.* **121**, 237-246
- 300 Horrocks, P. and Lanzer, M. (1999) Mutational analysis identifies a five base-pair *cis*-acting sequence essential for GBP130 promoter activity in *Plasmodium falciparum*. *Mol. Biochem. Parasitol.* **99**, 77-87
- 301 Osta, M., Gannoun-Zaki, L., Bonnefoy, S., Roy, C. and Vial, H. (2002) A 24 bp *cis*-acting element essential for the transcriptional activity of *Plasmodium falciparum* CDP-diacylglycerol synthase gene promoter. *Mol. Biochem. Parasitol.* **121**, 87-98
- 302 Kyes, S., Christodoulou, Z., Pinches, R., Kriek, N., Horrocks, P. and Newbold, C. (2007) *Plasmodium falciparum* *var* gene expression is developmentally controlled at the level of RNA II-mediated transcription initiation. *Mol. Microbiol.* **63**, 1234-1247
- 303 Schieck, E., Pfahler, J., Sanchez, C. and Lanzer, M. (2007) Nuclear run-on analysis of *var* gene expression in *Plasmodium falciparum*. *Mol. Biochem. Parasitol.* **153**, 207-212
- 304 Stipanuk, M. and Dominy, J. (2006) Surprising insights that aren't so surprising in the modeling of sulfur amino acid metabolism. *Amino Acids.* **30**, 251-256
- 305 Lewison, G. and Srivastava, D. (2008) Malaria research, 1980-2004, and the burden of disease. *Acta Trop.* **106**, 96-103



APPENDIX A

DIFFERENTIAL TRANSCRIPT ABUNDANCE DATASET (LIMMA)

| # | FUNCTIONAL CLASSIFICATION | PLASMID ID | OLIGO | ANNOTATION | GO ID | FUNCTIONAL ANNOTATION | FOLD CHANGE TO RELATIVE IS WITH F-VALUES ADJUSTED FOR MDR | | | | | | | | |
|----|---------------------------|------------|---|---|----------------------------|---|---|-------------------|--------------|------------------------------------|-------------------|--------------|------------------------------------|-------------------|--------------|
| | | | | | | | T ₀ log ₂ FC | T ₁ FC | adj. p value | T ₀ log ₂ FC | T ₁ FC | adj. p value | T ₀ log ₂ FC | T ₁ FC | adj. p value |
| 1 | CYTOKINESIS/CELL CYCLE | PF10_0094 | J73_4 | tubulin beta chain, putative: PF10_0094 (J73_4) | GO:000226 | microtubule cytoskeleton organization and organization center | -0.877117856 | 0.544454029 | 1.73E-06 | -0.695815503 | 0.621654329 | 1.51E-06 | -0.386724309 | 0.764864296 | 0.000462446 |
| 2 | | PF11_0056 | K879_2 | putative: PF11_0056 (K879_2) | GO:000707 | mitosis | -0.615929357 | 0.562839424 | 4.00E-05 | -0.820345517 | 0.57293941 | 1.79E-06 | | | |
| 3 | | PF13_0328 | M9264_1 | origon: PF13_0328 (M9264_1) | GO:000275 | regulation of DNA replication (cyclic signature) | -1.706908296 | 0.306315803 | 7.54E-07 | -1.241521596 | 0.422809121 | 1.19E-05 | -0.8904367 | 0.53736832 | 3.01E-05 |
| 4 | | PF14_0443 | N151_64 | centrin, putative: PF14_0443 (N151_64) | GO:0008150 | biological_process | -0.848623885 | 0.595007834 | 0.000471307 | -0.848623885 | 0.595007834 | 0.000471307 | -0.893345456 | 0.52142093 | 0.002198876 |
| 5 | | PF14_0504 | N136_76 | hypothetical protein: PF14_0504 (N136_76) | DAVID | cyclic-related protein | -0.820976269 | 0.741760183 | 0.002057867 | -0.820976269 | 0.741760183 | 0.002057867 | -0.791235864 | 0.577648934 | 7.11E-06 |
| 6 | | PFAD190c | AG010_16 | actin: PFAD190c (AG010_16) | GO:001628 | actin cytoskeleton | -0.999594919 | 0.501042587 | 0.012324662 | -0.999594919 | 0.501042587 | 0.012324662 | -0.797480159 | 0.575383224 | 0.021713375 |
| 7 | | PFAD520c | A13725_9 | domain, putative: PFAD520c (A13725_9) | GO:0006334 | nucleosome assembly | -1.048414161 | 0.483164334 | 2.83E-06 | -0.87768062 | 0.544239637 | 1.39E-05 | -0.684803092 | 0.522093728 | 1.70E-05 |
| 8 | | PFCE060w | C569 | kinase, putative: PFCE060w (C569) | GO:0007016 | microtubule-based movement | -0.558289134 | 0.679130564 | 0.009316004 | -0.774708401 | 0.584050753 | 0.000121797 | -0.38676511 | 0.764864296 | 0.000462446 |
| 9 | | PFEB165w | E13013_1 | actin: PFEB165w (E13013_1) | GO:0030042 | actin filament depolymerization | -0.832326233 | 0.561612662 | 2.15E-06 | -1.189394342 | 0.438399966 | 2.13E-09 | -0.987152039 | 0.50447265 | 8.31E-09 |
| 10 | | PFEB175c | OPFBL08060 | unconventional myosin IIb: PFEB175c (OPFBL08060) | GO:0016459 | myosin complex | -0.826336897 | 0.563959358 | 4.34E-05 | -0.826336897 | 0.563959358 | 4.34E-05 | -0.810386212 | 0.570224443 | 4.30E-05 |
| 11 | | PFEB175c | E1E509_5 | unconventional myosin IIb: PFEB175c (E1E509_5) | GO:0016459 | myosin complex | -1.188434644 | 0.438778587 | 7.94E-05 | -1.188434644 | 0.438778587 | 7.94E-05 | -0.704370306 | 0.474878286 | 1.48E-05 |
| 12 | | PFEP1320c | PMAL6P1_156_432 | trypsin c-like protein, putative: PFEP1320c (PMAL6P1_156_432) | GO:0005639 | calcium ion binding | -0.924538687 | 0.526848962 | 1.48E-06 | -0.785617967 | 0.580103421 | 4.48E-07 | -0.752079108 | 0.593742726 | 0.038916505 |
| 11 | | PFEP180w | OPF17633 | alpha tubulin: PFEP180w (OPF17633) | GO:0007017 | microtubule-based process | -1.142784503 | 0.452814496 | 2.19E-05 | -0.996079589 | 0.515481489 | 1.04E-05 | -0.72089311 | 0.606717371 | 0.000167754 |
| 13 | | PFEP180w | I16830_2 | alpha tubulin: PFEP180w (I16830_2) | GO:0007017 | microtubule-based process | -1.142784503 | 0.452814496 | 2.19E-05 | -0.996079589 | 0.515481489 | 1.04E-05 | -0.72089311 | 0.606717371 | 0.000167754 |
| 14 | PFEP180w | I16830_1 | hypothetical protein: PFEP180w (I16830_1) | GO:0007016 | microtubule-based movement | -1.142784503 | 0.452814496 | 2.19E-05 | -0.996079589 | 0.515481489 | 1.04E-05 | -0.72089311 | 0.606717371 | 0.000167754 | |
| 15 | PFEP180w | I16830_1 | hypothetical protein: PFEP180w (I16830_1) | GO:0007016 | microtubule-based movement | -1.142784503 | 0.452814496 | 2.19E-05 | -0.996079589 | 0.515481489 | 1.04E-05 | -0.72089311 | 0.606717371 | 0.000167754 | |
| 14 | PFEP180w | I16830_1 | hypothetical protein: PFEP180w (I16830_1) | GO:0007016 | microtubule-based movement | -1.142784503 | 0.452814496 | 2.19E-05 | -0.996079589 | 0.515481489 | 1.04E-05 | -0.72089311 | 0.606717371 | 0.000167754 | |
| 15 | PFEP180w | I16830_1 | hypothetical protein: PFEP180w (I16830_1) | GO:0007016 | microtubule-based movement | -1.142784503 | 0.452814496 | 2.19E-05 | -0.996079589 | 0.515481489 | 1.04E-05 | -0.72089311 | 0.606717371 | 0.000167754 | |
| 14 | PFEP180w | I16830_1 | hypothetical protein: PFEP180w (I16830_1) | GO:0007016 | microtubule-based movement | -1.142784503 | 0.452814496 | 2.19E-05 | -0.996079589 | 0.515481489 | 1.04E-05 | -0.72089311 | 0.606717371 | 0.000167754 | |
| 15 | PFEP180w | I16830_1 | hypothetical protein: PFEP180w (I16830_1) | GO:0007016 | microtubule-based movement | -1.142784503 | 0.452814496 | 2.19E-05 | -0.996079589 | 0.515481489 | 1.04E-05 | -0.72089311 | 0.606717371 | 0.000167754 | |
| 14 | PFEP180w | I16830_1 | hypothetical protein: PFEP180w (I16830_1) | GO:0007016 | microtubule-based movement | -1.142784503 | 0.452814496 | 2.19E-05 | -0.996079589 | 0.515481489 | 1.04E-05 | -0.72089311 | 0.606717371 | 0.000167754 | |
| 15 | PFEP180w | I16830_1 | hypothetical protein: PFEP180w (I16830_1) | GO:0007016 | microtubule-based movement | -1.142784503 | 0.452814496 | 2.19E-05 | -0.996079589 | 0.515481489 | 1.04E-05 | -0.72089311 | 0.606717371 | 0.000167754 | |
| 14 | PFEP180w | I16830_1 | hypothetical protein: PFEP180w (I16830_1) | GO:0007016 | microtubule-based movement | -1.142784503 | 0.452814496 | 2.19E-05 | -0.996079589 | 0.515481489 | 1.04E-05 | -0.72089311 | 0.606717371 | 0.000167754 | |
| 15 | PFEP180w | I16830_1 | hypothetical protein: PFEP180w (I16830_1) | GO:0007016 | microtubule-based movement | -1.142784503 | 0.452814496 | 2.19E-05 | -0.996079589 | 0.515481489 | 1.04E-05 | -0.72089311 | 0.606717371 | 0.000167754 | |
| 14 | PFEP180w | I16830_1 | hypothetical protein: PFEP180w (I16830_1) | GO:0007016 | microtubule-based movement | -1.142784503 | 0.452814496 | 2.19E-05 | -0.996079589 | 0.515481489 | 1.04E-05 | -0.72089311 | 0.606717371 | 0.000167754 | |
| 15 | PFEP180w | I16830_1 | hypothetical protein: PFEP180w (I16830_1) | GO:0007016 | microtubule-based movement | -1.142784503 | 0.452814496 | 2.19E-05 | -0.996079589 | 0.515481489 | 1.04E-05 | -0.72089311 | 0.606717371 | 0.000167754 | |
| 14 | PFEP180w | I16830_1 | hypothetical protein: PFEP180w (I16830_1) | GO:0007016 | microtubule-based movement | -1.142784503 | 0.452814496 | 2.19E-05 | -0.996079589 | 0.515481489 | 1.04E-05 | -0.72089311 | 0.606717371 | 0.000167754 | |
| 15 | PFEP180w | I16830_1 | hypothetical protein: PFEP180w (I16830_1) | GO:0007016 | microtubule-based movement | -1.142784503 | 0.452814496 | 2.19E-05 | -0.996079589 | 0.515481489 | 1.04E-05 | -0.72089311 | 0.606717371 | 0.000167754 | |
| 14 | PFEP180w | I16830_1 | hypothetical protein: PFEP180w (I16830_1) | GO:0007016 | microtubule-based movement | -1.142784503 | 0.452814496 | 2.19E-05 | -0.996079589 | 0.515481489 | 1.04E-05 | -0.72089311 | 0.606717371 | 0.000167754 | |
| 15 | PFEP180w | I16830_1 | hypothetical protein: PFEP180w (I16830_1) | GO:0007016 | microtubule-based movement | -1.142784503 | 0.452814496 | 2.19E-05 | -0.996079589 | 0.515481489 | 1.04E-05 | -0.72089311 | 0.606717371 | 0.000167754 | |
| 14 | PFEP180w | I16830_1 | hypothetical protein: PFEP180w (I16830_1) | GO:0007016 | microtubule-based movement | -1.142784503 | 0.452814496 | 2.19E-05 | -0.996079589 | 0.515481489 | 1.04E-05 | -0.72089311 | 0.606717371 | 0.000167754 | |
| 15 | PFEP180w | I16830_1 | hypothetical protein: PFEP180w (I16830_1) | GO:0007016 | microtubule-based movement | -1.142784503 | 0.452814496 | 2.19E-05 | -0.996079589 | 0.515481489 | 1.04E-05 | -0.72089311 | 0.606717371 | 0.000167754 | |
| 14 | PFEP180w | I16830_1 | hypothetical protein: PFEP180w (I16830_1) | GO:0007016 | microtubule-based movement | -1.142784503 | 0.452814496 | 2.19E-05 | -0.996079589 | 0.515481489 | 1.04E-05 | -0.72089311 | 0.606717371 | 0.000167754 | |
| 15 | PFEP180w | I16830_1 | hypothetical protein: PFEP180w (I16830_1) | GO:0007016 | microtubule-based movement | -1.142784503 | 0.452814496 | 2.19E-05 | -0.996079589 | 0.515481489 | 1.04E-05 | -0.72089311 | 0.606717371 | 0.000167754 | |
| 14 | PFEP180w | I16830_1 | hypothetical protein: PFEP180w (I16830_1) | GO:0007016 | microtubule-based movement | -1.142784503 | 0.452814496 | 2.19E-05 | -0.996079589 | 0.515481489 | 1.04E-05 | -0.72089311 | 0.606717371 | 0.000167754 | |
| 15 | PFEP180w | I16830_1 | hypothetical protein: PFEP180w (I16830_1) | GO:0007016 | microtubule-based movement | -1.142784503 | 0.452814496 | 2.19E-05 | -0.996079589 | 0.515481489 | 1.04E-05 | -0.72089311 | 0.606717371 | 0.000167754 | |
| 14 | PFEP180w | I16830_1 | hypothetical protein: PFEP180w (I16830_1) | GO:0007016 | microtubule-based movement | -1.142784503 | 0.452814496 | 2.19E-05 | -0.996079589 | 0.515481489 | 1.04E-05 | -0.72089311 | 0.606717371 | 0.000167754 | |
| 15 | PFEP180w | I16830_1 | hypothetical protein: PFEP180w (I16830_1) | GO:0007016 | microtubule-based movement | -1.142784503 | 0.452814496 | 2.19E-05 | -0.996079589 | 0.515481489 | 1.04E-05 | -0.72089311 | 0.606717371 | 0.000167754 | |
| 14 | PFEP180w | I16830_1 | hypothetical protein: PFEP180w (I16830_1) | GO:0007016 | microtubule-based movement | -1.142784503 | 0.452814496 | 2.19E-05 | -0.996079589 | 0.515481489 | 1.04E-05 | -0.72089311 | 0.606717371 | 0.000167754 | |
| 15 | PFEP180w | I16830_1 | hypothetical protein: PFEP180w (I16830_1) | GO:0007016 | microtubule-based movement | -1.142784503 | 0.452814496 | 2.19E-05 | -0.996079589 | 0.515481489 | 1.04E-05 | -0.72089311 | 0.606717371 | 0.000167754 | |
| 14 | PFEP180w | I16830_1 | hypothetical protein: PFEP180w (I16830_1) | GO:0007016 | microtubule-based movement | -1.142784503 | 0.452814496 | 2.19E-05 | -0.996079589 | 0.515481489 | 1.04E-05 | -0.72089311 | 0.606717371 | 0.000167754 | |
| 15 | PFEP180w | I16830_1 | hypothetical protein: PFEP180w (I16830_1) | GO:0007016 | microtubule-based movement | -1.142784503 | 0.452814496 | 2.19E-05 | -0.996079589 | 0.515481489 | 1.04E-05 | -0.72089311 | 0.606717371 | 0.000167754 | |
| 14 | PFEP180w | I16830_1 | hypothetical protein: PFEP180w (I16830_1) | GO:0007016 | microtubule-based movement | -1.142784503 | 0.452814496 | 2.19E-05 | -0.996079589 | 0.515481489 | 1.04E-05 | -0.72089311 | 0.606717371 | 0.000167754 | |
| 15 | PFEP180w | I16830_1 | hypothetical protein: PFEP180w (I16830_1) | GO:0007016 | microtubule-based movement | -1.142784503 | 0.452814496 | 2.19E-05 | -0.996079589 | 0.515481489 | 1.04E-05 | -0.72089311 | 0.606717371 | 0.000167754 | |
| 14 | PFEP180w | I16830_1 | hypothetical protein: PFEP180w (I16830_1) | GO:0007016 | microtubule-based movement | -1.142784503 | 0.452814496 | 2.19E-05 | -0.996079589 | 0.515481489 | 1.04E-05 | -0.72089311 | 0.606717371 | 0.000167754 | |
| 15 | PFEP180w | I16830_1 | hypothetical protein: PFEP180w (I16830_1) | GO:0007016 | microtubule-based movement | -1.142784503 | 0.452814496 | 2.19E-05 | -0.996079589 | 0.515481489 | 1.04E-05 | -0.72089311 | 0.606717371 | 0.000167754 | |
| 14 | PFEP180w | I16830_1 | hypothetical protein: PFEP180w (I16830_1) | GO:0007016 | microtubule-based movement | -1.142784503 | 0.452814496 | 2.19E-05 | -0.996079589 | 0.515481489 | 1.04E-05 | -0.72089311 | 0.606717371 | 0.000167754 | |
| 15 | PFEP180w | I16830_1 | hypothetical protein: PFEP180w (I16830_1) | GO:0007016 | microtubule-based movement | -1.142784503 | 0.452814496 | 2.19E-05 | -0.996079589 | 0.515481489 | 1.04E-05 | -0.72089311 | 0.606717371 | 0.000167754 | |
| 14 | PFEP180w | I16830_1 | hypothetical protein: PFEP180w (I16830_1) | GO:0007016 | microtubule-based movement | -1.142784503 | 0.452814496 | 2.19E-05 | -0.996079589 | 0.515481489 | 1.04E-05 | -0.72089311 | 0.606717371 | 0.000167754 | |
| 15 | PFEP180w | I16830_1 | hypothetical protein: PFEP180w (I16830_1) | GO:0007016 | microtubule-based movement | -1.142784503 | 0.452814496 | 2.19E-05 | -0.996079589 | 0.515481489 | 1.04E-05 | -0. | | | |



| # | FUNCTIONAL CLASSIFICATION | FLASMOOB ID | OLIGO | ANNOTATION | GO ID | FUNCTIONAL ANNOTATION | FOLD CHANGE TO RELATIVE 16 WITH P-VALUES ADJUSTED FOR MDR DATA WITH P<0.05 ARE PRESENTED | | | | | | | | |
|----|---------------------------|-------------|----------|--|------------|-------------------------------------|--|--------------------|--------------|-------------------------------------|--------------------|--------------|-------------------------------------|--------------------|--------------|
| | | | | | | | T ₁₆ log ₂ FC | T ₁₆ FC | adj. p value | T ₁₆ log ₂ FC | T ₁₆ FC | adj. p value | T ₁₆ log ₂ FC | T ₁₆ FC | adj. p value |
| | | PF00830w | OPFD6954 | bifunctional dihydroxyacetone reductase/thymidylate synthase:PF00830w:(OPFD6954) | GO:0006231 | dTMP biosynthetic process | -0.905177893 | 0.53396687 | 0.0004105 | -0.77419848 | 0.584713384 | 0.001109119 | -0.722171625 | 0.506184293 | 0.000184442 |
| 46 | | PF00950w | D1263_36 | ran binding protein 1:PF00950w:(D1263_36) | GO:0006260 | DNA replication | 1.001957896 | 2.002160899 | 0.011627336 | 0.881620395 | 1.842898572 | 0.00547603 | | | |
| 47 | | PF00975c | OPFD0352 | deoxythymidylate synthase (phosphotransferase domain):PF00975c:(OPFD0352) | GO:0006261 | DNA replication | -0.848048988 | 0.55630617 | 2.73E-05 | -0.72350359 | 0.605622475 | 1.38E-05 | -0.62607405 | 0.547607947 | 4.14E-05 |
| 48 | | PF00975c | F1745L_1 | deoxythymidylate synthase (phosphotransferase domain):PF00975c:(F1745L_1) | GO:0006261 | DNA replication | -1.507194144 | 0.351794748 | 4.81E-06 | -0.80941946 | 0.570913211 | 0.000397407 | | | |
| 49 | | PF0235w | OPFI1721 | DNA polymerase epsilon, catalytic subunit a, putative:PF0235w:(OPFI1721) | GO:0006260 | DNA replication | -0.88862636 | 0.55147396 | 2.63E-06 | -0.82144625 | 0.787298179 | 0.00070861 | | | |
| 50 | | PF0235w | F18417_1 | DNA polymerase epsilon, catalytic subunit a, putative:PF0235w:(F18417_1) | GO:0006260 | DNA replication | -1.201008797 | 0.434870723 | 1.13E-06 | -0.931971996 | 0.69180052 | 0.00020647 | -0.27186648 | 0.838261139 | 0.03229814 |
| 51 | HOST PARASITE INTERACTION | PF0330c | I11401_2 | DNA primase large subunit 1:PF0330c:(I11401_2) | GO:0006568 | apna DNA polymerase primase complex | -0.833283283 | 0.56142384 | 0.00252301 | -0.652976762 | 0.83969731 | 2.81E-05 | -0.28526569 | 0.8206952 | 0.01828900 |
| | | PF0330c | M8971_2 | hyphal protein:PF0330c:(M8971_2) | GO:0006260 | DNA replication | -1.10795808 | 0.46308874 | 0.00146886 | | | | | | |
| 52 | | MAL13P1.176 | I895L_1 | Plasmodium falciparum reticulocyte binding protein 2 homolog b:MAL13P1.176:(I895L_1) | GO:0003260 | entry into host cell | 1.06461678 | 2.077022407 | 0.00358752 | | | | | | |
| 53 | | MAL7P1.176 | I1487L_1 | erythrocyte binding antigen:MAL7P1.176:(I1487L_1) | GO:0009405 | pathogenesis | 0.698664488 | 1.514513552 | 0.00180674 | -0.19937014 | 0.566466873 | 4.97E-07 | -0.874807625 | 0.548439111 | 1.53E-07 |
| 54 | | MAL7P1.176 | F739_1 | erythrocyte membrane protein 1 (PEMP1) precursor:MAL7P1.176:(F739_1) | GO:0009405 | pathogenesis | 0.645728884 | 1.564229524 | 0.00180674 | -1.041773487 | 0.485732005 | 7.30E-08 | -1.195475396 | 0.439374974 | 8.31E-05 |
| 55 | | MAL7P1.176 | F1754L_3 | erythrocyte membrane protein 1 (PEMP1) precursor:MAL7P1.176:(F1754L_3) | GO:0009405 | pathogenesis | 0.68472128 | 1.70346479 | 0.01209336 | | | | | | |
| 56 | | PF07_049 | F244L_1 | erythrocyte membrane protein 1 (PEMP1):PF07_049:(F244L_1) | GO:0009405 | pathogenesis | 0.836793372 | 1.78607878 | 0.02896874 | -0.49918905 | 0.707504363 | 0.00218747 | -1.21066365 | 0.432062915 | 2.11E-05 |
| 57 | | PF10_019 | J33_16 | early transcribed membrane protein:PF10_019:(J33_16) | GO:0008150 | biological process | 0.439593215 | 1.407947184 | 0.02416421 | | | | -1.45480077 | 0.45203401 | 2.29E-06 |
| 58 | | PF10_028 | J17C_10 | | | | | | | | | | | | |



| # | FUNCTIONAL CLASSIFICATION | PLASMID ID | OLIGO | ANNOTATION | GO ID | FUNCTIONAL ANNOTATION | FOLD CHANGE TO RELATIVE 6 WITH P-VALUES ADJUSTED FOR MDR DATA WITH P<0.05 ARE PRESENTED | | | | | | | | | | | | |
|-----|---------------------------|------------|--------------|---|------------|-----------------------|---|------------|--------------|------------------------|-------|--------------|------------------------|-------|--------------|--|--|--|--|
| | | | | | | | Tn log ₂ FC | Tn FC | adj. p value | Tn log ₂ FC | Tn FC | adj. p value | Tn log ₂ FC | Tn FC | adj. p value | | | | |
| 291 | | MALBP1_122 | F5489_1 | hypothetical protein: MALBP1_122 (F5489_1) | | | 1.270616236 | 2.10033314 | 0.00782554 | | | | | | | | | | |
| 292 | | MALBP1_158 | F5489_1 | hypothetical protein: MALBP1_158 (F5489_1) | | | | | | | | | | | | | | | |
| 293 | | MALBP1_38 | F2455_6 | hypothetical protein: MALBP1_38 (F2455_6) | | | | | | | | | | | | | | | |
| 294 | | MALBP1_43 | E1097_2 | hypothetical protein: MALBP1_43 (E1097_2) | | | | | | | | | | | | | | | |
| 295 | | MALBP1_53 | F5489_1 | hypothetical protein: MALBP1_53 (F5489_1) | | | | | | | | | | | | | | | |
| 296 | | MALBP1_63 | F7076_3 | hypothetical protein: MALBP1_63 (F7076_3) | GO:0016020 | membrane | | | | | | | | | | | | | |
| 297 | | MALBP1_82 | F1074_1 | hypothetical protein: MALBP1_82 (F1074_1) | | | | | | | | | | | | | | | |
| 298 | | MALBP1_86 | F2455_6 | hypothetical protein: MALBP1_86 (F2455_6) | GO:0020111 | actinopod | | | | | | | | | | | | | |
| 299 | | MALBP1_89 | F482_1 | hypothetical protein: MALBP1_89 (F482_1) | GO:0005822 | intracellular | | | | | | | | | | | | | |
| 300 | | PF02_001 | F55_1 | hypothetical protein: PF02_001 (F55_1) | | | | | | | | | | | | | | | |
| 301 | | PF02_006 | PF02_006 | hypothetical protein: PF02_006 (PF02_006) | | | | | | | | | | | | | | | |
| 302 | | PF02_009 | PF02_009 | hypothetical protein: PF02_009 (PF02_009) | | | | | | | | | | | | | | | |
| 303 | | PF02_012 | F482_1 | hypothetical protein: PF02_012 (F482_1) | GO:0016020 | membrane | | | | | | | | | | | | | |
| 304 | | PF02_037 | F482_1 | hypothetical protein: PF02_037 (F482_1) | | | | | | | | | | | | | | | |
| 305 | | PF02_107 | F6670_1 | hypothetical protein: PF02_107 (F6670_1) | | | | | | | | | | | | | | | |
| 306 | | PF02_001 | PF02_001_281 | hypothetical protein: PF02_001_281 (PF02_001_281) | GO:0020111 | actinopod | | | | | | | | | | | | | |
| 307 | | PF02_003 | PF02_003 | hypothetical protein: PF02_003 (PF02_003) | | | | | | | | | | | | | | | |
| 308 | | PF02_005 | F2455_6 | hypothetical protein: PF02_005 (F2455_6) | | | | | | | | | | | | | | | |
| 309 | | PF02_011 | F2455_6 | hypothetical protein: PF02_011 (F2455_6) | | | | | | | | | | | | | | | |
| 310 | | PF02_030 | PF02_030 | hypothetical protein: PF02_030 (PF02_030) | GO:0008150 | biological_process | | | | | | | | | | | | | |
| 311 | | PF02_030 | F720_2 | hypothetical protein: PF02_030 (F720_2) | GO:0008150 | biological_process | | | | | | | | | | | | | |
| 312 | | PF02_030 | F720_2 | hypothetical protein: PF02_030 (F720_2) | GO:0008150 | biological_process | | | | | | | | | | | | | |
| 313 | | PF02_030 | F1484_2 | hypothetical protein: PF02_030 (F1484_2) | GO:0008150 | biological_process | | | | | | | | | | | | | |
| 314 | | PF02_030 | F1484_2 | hypothetical protein: PF02_030 (F1484_2) | GO:0008150 | biological_process | | | | | | | | | | | | | |
| 315 | | PF02_030 | F2814_1 | hypothetical protein: PF02_030 (F2814_1) | GO:0008150 | biological_process | | | | | | | | | | | | | |
| 316 | | PF02_030 | F2814_1 | hypothetical protein: PF02_030 (F2814_1) | GO:0008150 | biological_process | | | | | | | | | | | | | |
| 317 | | PF02_030 | F2814_1 | hypothetical protein: PF02_030 (F2814_1) | GO:0008150 | biological_process | | | | | | | | | | | | | |
| 318 | | PF02_030 | F2814_1 | hypothetical protein: PF02_030 (F2814_1) | GO:0008150 | biological_process | | | | | | | | | | | | | |
| 319 | | PF02_030 | F2814_1 | hypothetical protein: PF02_030 (F2814_1) | GO:0008150 | biological_process | | | | | | | | | | | | | |
| 320 | | PF02_030 | F2814_1 | hypothetical protein: PF02_030 (F2814_1) | GO:0008150 | biological_process | | | | | | | | | | | | | |
| 321 | | PF02_030 | F2814_1 | hypothetical protein: PF02_030 (F2814_1) | GO:0008150 | biological_process | | | | | | | | | | | | | |
| 322 | | PF02_030 | F2814_1 | hypothetical protein: PF02_030 (F2814_1) | GO:0008150 | biological_process | | | | | | | | | | | | | |
| 323 | | PF02_030 | F2814_1 | hypothetical protein: PF02_030 (F2814_1) | GO:0008150 | biological_process | | | | | | | | | | | | | |
| 324 | | PF02_030 | F2814_1 | hypothetical protein: PF02_030 (F2814_1) | GO:0008150 | biological_process | | | | | | | | | | | | | |
| 325 | | PF02_030 | F2814_1 | hypothetical protein: PF02_030 (F2814_1) | GO:0008150 | biological_process | | | | | | | | | | | | | |
| 326 | | PF02_030 | F2814_1 | hypothetical protein: PF02_030 (F2814_1) | GO:0008150 | biological_process | | | | | | | | | | | | | |
| 327 | | PF02_030 | F2814_1 | hypothetical protein: PF02_030 (F2814_1) | GO:0008150 | biological_process | | | | | | | | | | | | | |
| 328 | | PF02_030 | F2814_1 | hypothetical protein: PF02_030 (F2814_1) | GO:0008150 | biological_process | | | | | | | | | | | | | |
| 329 | | PF02_030 | F2814_1 | hypothetical protein: PF02_030 (F2814_1) | GO:0008150 | biological_process | | | | | | | | | | | | | |
| 330 | | PF02_030 | F2814_1 | hypothetical protein: PF02_030 (F2814_1) | GO:0008150 | biological_process | | | | | | | | | | | | | |
| 331 | | PF02_030 | F2814_1 | hypothetical protein: PF02_030 (F2814_1) | GO:0008150 | biological_process | | | | | | | | | | | | | |
| 332 | | PF02_030 | F2814_1 | hypothetical protein: PF02_030 (F2814_1) | GO:0008150 | biological_process | | | | | | | | | | | | | |
| 333 | | PF02_030 | F2814_1 | hypothetical protein: PF02_030 (F2814_1) | GO:0008150 | biological_process | | | | | | | | | | | | | |
| 334 | | PF02_030 | F2814_1 | hypothetical protein: PF02_030 (F2814_1) | GO:0008150 | biological_process | | | | | | | | | | | | | |
| 335 | | PF02_030 | F2814_1 | hypothetical protein: PF02_030 (F2814_1) | GO:0008150 | biological_process | | | | | | | | | | | | | |
| 336 | | PF02_030 | F2814_1 | hypothetical protein: PF02_030 (F2814_1) | GO:0008150 | biological_process | | | | | | | | | | | | | |
| 337 | | PF02_030 | F2814_1 | hypothetical protein: PF02_030 (F2814_1) | GO:0008150 | biological_process | | | | | | | | | | | | | |
| 338 | | PF02_030 | F2814_1 | hypothetical protein: PF02_030 (F2814_1) | GO:0008150 | biological_process | | | | | | | | | | | | | |
| 339 | | PF02_030 | F2814_1 | hypothetical protein: PF02_030 (F2814_1) | GO:0008150 | biological_process | | | | | | | | | | | | | |
| 340 | | PF02_030 | F2814_1 | hypothetical protein: PF02_030 (F2814_1) | GO:0008150 | biological_process | | | | | | | | | | | | | |
| 341 | | PF02_030 | F2814_1 | hypothetical protein: PF02_030 (F2814_1) | GO:0008150 | biological_process | | | | | | | | | | | | | |
| 342 | | PF02_030 | F2814_1 | hypothetical protein: PF02_030 (F2814_1) | GO:0008150 | biological_process | | | | | | | | | | | | | |
| 343 | | PF02_030 | F2814_1 | hypothetical protein: PF02_030 (F2814_1) | GO:0008150 | biological_process | | | | | | | | | | | | | |
| 344 | | PF02_030 | F2814_1 | hypothetical protein: PF02_030 (F2814_1) | GO:0008150 | biological_process | | | | | | | | | | | | | |
| 345 | | PF02_030 | F2814_1 | hypothetical protein: PF02_030 (F2814_1) | GO:0008150 | biological_process | | | | | | | | | | | | | |
| 346 | | PF02_030 | F2814_1 | hypothetical protein: PF02_030 (F2814_1) | GO:0008150 | biological_process | | | | | | | | | | | | | |
| 347 | | PF02_030 | F2814_1 | hypothetical protein: PF02_030 (F2814_1) | GO:0008150 | biological_process | | | | | | | | | | | | | |
| 348 | | PF02_030 | F2814_1 | hypothetical protein: PF02_030 (F2814_1) | GO:0008150 | biological_process | | | | | | | | | | | | | |
| 349 | | PF02_030 | F2814_1 | hypothetical protein: PF02_030 (F2814_1) | GO:0008150 | biological_process | | | | | | | | | | | | | |
| 350 | | PF02_030 | F2814_1 | hypothetical protein: PF02_030 (F2814_1) | GO:0008150 | biological_process | | | | | | | | | | | | | |
| 351 | | PF02_030 | F2814_1 | hypothetical protein: PF02_030 (F2814_1) | GO:0008150 | biological_process | | | | | | | | | | | | | |
| 352 | | PF02_030 | F2814_1 | hypothetical protein: PF02_030 (F2814_1) | GO:0008150 | biological_process | | | | | | | | | | | | | |
| 353 | | PF02_030 | F2814_1 | hypothetical protein: PF02_030 (F2814_1) | GO:0008150 | biological_process | | | | | | | | | | | | | |
| 354 | | PF02_030 | F2814_1 | hypothetical protein: PF02_030 (F2814_1) | GO:0008150 | biological_process | | | | | | | | | | | | | |
| 355 | | PF02_030 | F2814_1 | hypothetical protein: PF02_030 (F2814_1) | GO:0008150 | biological_process | | | | | | | | | | | | | |
| 356 | | PF02_030 | F2814_1 | hypothetical protein: PF02_030 (F2814_1) | GO:0008150 | biological_process | | | | | | | | | | | | | |
| 357 | | PF02_030 | F2814_1 | hypothetical protein: PF02_030 (F2814_1) | GO:0008150 | biological_process | | | | | | | | | | | | | |
| 358 | | PF02_030 | F2814_1 | hypothetical protein: PF02_030 (F2814_1) | GO:0008150 | biological_process | | | | | | | | | | | | | |
| 359 | | PF02_030 | F2814_1 | hypothetical protein: PF02_030 (F2814_1) | GO:0008150 | biological_process | | | | | | | | | | | | | |
| 360 | | PF02_030 | F2814_1 | hypothetical protein: PF02_030 (F2814_1) | GO:0008150 | biological_process | | | | | | | | | | | | | |
| 361 | | PF02_030 | F2814_1 | hypothetical protein: PF02_030 (F2814_1) | GO:0008150 | biological_process | | | | | | | | | | | | | |
| 362 | | PF02_030 | F2814_1 | hypothetical protein: PF02_030 (F2814_1) | GO:0008150 | biological_process | | | | | | | | | | | | | |
| 363 | | PF02_030 | F2814_1 | hypothetical protein: PF02_030 (F2814_1) | GO:0008150 | biological_process | | | | | | | | | | | | | |
| 364 | | PF02_030 | F2814_1 | hypothetical protein: PF02_030 (F2814_1) | GO:0008150 | biological_process | | | | | | | | | | | | | |
| 365 | | PF02_030 | F2814_1 | hypothetical protein: PF02_030 (F2814_1) | GO:0008150 | biological_process | | | | | | | | | | | | | |
| 366 | | PF02_030 | F2814_1 | hypothetical protein: PF02_030 (F2814_1) | GO:0008150 | biological_process | | | | | | | | | | | | | |



| # | FUNCTIONAL CLASSIFICATION | PLASMID ID | OLIGO | ANNOTATION | GO ID | FUNCTIONAL ANNOTATION | FOLD CHANGE TO RELATIVE WITH P-VALUES ADJUSTED FOR MDR DATA WITH P<0.05 ARE PRESENTED | | | | | | | | | | | | |
|-----|---------------------------|------------|---------------|---|------------|----------------------------|---|-------------------|--------------|------------------------------------|-------------------|--------------|------------------------------------|-------------------|--------------|------------------------------------|-------------------|--------------|--|
| | | | | | | | T ₀ log ₂ FC | T ₀ FC | adj. p value | T ₀ log ₂ FC | T ₀ FC | adj. p value | T ₀ log ₂ FC | T ₀ FC | adj. p value | T ₀ log ₂ FC | T ₀ FC | adj. p value | |
| 414 | | PF14_0570 | N130_6 | hypothetical protein, conserved:PF14_0570(-N130_6) | GO:0008150 | biological_process | -1.12359847 | 0.46615635 | 0.00181255 | -0.75504789 | 0.93262241 | 0.001091389 | | | | | | | |
| 415 | | PF14_0582 | OPFN2027 | hypothetical protein:PF14_0582(+OPFN2027) | | | -0.82711730 | 0.64748583 | 0.00514401 | -0.73413650 | 0.90177739 | 0.00493361 | -0.76299404 | 0.58927318 | 0.000317596 | | | | |
| 416 | | PF14_0582 | N134_126 | hypothetical protein:PF14_0582(-N134_126) | | | -0.72088090 | 0.58868890 | 0.00238323 | -0.62921506 | 0.94629975 | 0.00262363 | -0.46843345 | 0.72724821 | 0.00232623 | | | | |
| 417 | | PF14_0582 | N134_23 | hypothetical protein:PF14_0582(-N134_23) | | | -0.78102408 | 0.58841295 | 0.00211705 | | | | | | | | | | |
| 418 | | PF14_0582 | N137_4 | hypothetical protein:PF14_0582(-N137_4) | GO:0008150 | biological_process | -0.42872038 | 0.74291909 | 0.02374527 | 0.15647692 | 1.68818946 | 3.81E-07 | 0.89582491 | 1.84762362 | 3.27E-08 | | | | |
| 419 | | PF14_0586 | N137_23 | hypothetical protein:PF14_0586(-N137_23) | | | -0.80202381 | 0.47863313 | 5.60E-07 | -0.73179777 | 0.90232779 | 5.24E-06 | -0.72113914 | 0.902663879 | 2.38E-06 | | | | |
| 420 | | PF14_0586 | N137_21 | hypothetical protein:PF14_0586(-N137_21) | | | -0.80666178 | 0.47863313 | 5.60E-07 | -0.73651169 | 0.93923995 | 7.75E-07 | -0.63419161 | 0.64411978 | 3.27E-06 | | | | |
| 421 | | PF14_0590 | PF14_0590_16 | hypothetical protein:PF14_0590(+PF14_0590_16) | GO:0008150 | biological_process | -1.00755219 | 0.49739026 | 2.36E-06 | -0.60951955 | 0.95899037 | 3.99E-05 | -0.39924214 | 0.73222399 | 0.00199932 | | | | |
| 422 | | PF14_0730 | PF14_0730_170 | hypothetical protein:PF14_0730(+PF14_0730_170) | GO:0008150 | biological_process | -0.44989767 | 1.38942050 | 0.00309669 | -0.69702662 | 0.16484952 | 3.20E-04 | -0.04437414 | 0.494789233 | 2.97E-07 | | | | |
| 423 | | PF14_0732 | N125_33 | hypothetical protein:PF14_0732(-N125_33) | GO:0008150 | biological_process | -0.874504145 | 0.828340573 | 1.073E-06 | -1.17370147 | 0.43008263 | 0.0201073 | -0.41348199 | 0.12659477 | 0.00056519 | | | | |
| 424 | | PFAD18w | PFAD18w_278 | hypothetical protein:PFAD18w(+PFAD18w_278) | GO:0020111 | apoptosis | -1.18959362 | 0.20378987 | 7.48E-07 | -1.61816967 | 0.34965247 | 1.06E-08 | -1.46318985 | 0.36973993 | 2.20E-08 | | | | |
| 425 | | PFAD24w | PFAD24w | hypothetical protein:PFAD24w | | | -0.83027483 | 0.52478399 | 0.00521281 | -0.79310373 | 0.97898221 | 1.32E-05 | -0.60214436 | 0.87060261 | 0.001490036 | | | | |
| 426 | | PFAD25c | A4704_11 | hypothetical protein:PFAD25c(+A4704_11) | | | -0.53136814 | 0.69176935 | 0.01120697 | -0.82028622 | 0.86280260 | 0.00399899 | -0.66330442 | 0.83740591 | 0.00291291 | | | | |
| 427 | | PFAD25c | A8109_21 | hypothetical protein:PFAD25c(+A8109_21) | GO:0010712 | heat shock protein binding | -0.80467073 | 0.87203118 | 3.94E-05 | -0.69517823 | 0.42094973 | 9.85E-05 | -0.63419161 | 0.64411978 | 3.27E-06 | | | | |
| 428 | | PFAD25c | A1462_13 | glutamic acid-rich protein (conserved:PFAD25c(-A1462_13)) | | | -0.81902812 | 0.56802439 | 0.00219024 | -0.91786214 | 0.52326931 | 0.00106212 | -1.14451335 | 0.45146824 | 1.18E-06 | | | | |
| 429 | | PFAD25c | A1480_24 | hypothetical protein:PFAD25c(-A1480_24) | | | -0.45132936 | 0.73168905 | 0.04894320 | -0.82804158 | 0.54232317 | 0.00146520 | | | | | | | |
| 430 | | PFAD70c | PFAD70c_135 | hypothetical protein:PFAD70c(+PFAD70c_135) | GO:0008150 | biological_process | -0.34448464 | 0.73962955 | 0.01307194 | -0.29124223 | 0.46929732 | 6.81E-06 | | | | | | | |
| 431 | | PFAD70c | 880 | hypothetical protein:PFAD70c(-880) | GO:0008150 | biological_process | -0.82049492 | 0.87164154 | 0.02377608 | -0.81167874 | 0.64972738 | 0.0010742 | | | | | | | |
| 432 | | PFAD70c | 884 | hypothetical protein:PFAD70c(-884) | GO:0008150 | biological_process | -0.73012972 | 0.80280389 | 0.00107013 | -1.37183111 | 0.34637118 | 1.68E-06 | | | | | | | |
| 433 | | PFAD70c | 889 | hypothetical protein:PFAD70c(-889) | | | 0.751992029 | 1.584114478 | 0.00342123 | 1.34247867 | 0.32646474 | 7.23E-05 | 1.72928097 | 3.31613989 | 4.82E-06 | | | | |
| 434 | | PFAD70c | 891 | hypothetical protein:PFAD70c(-891) | | | 0.10413101 | 2.00198189 | 0.00032607 | 0.64511076 | 1.56933895 | 0.04830731 | | | | | | | |
| 435 | | PFAD70c | 8310 | hypothetical protein:PFAD70c(-8310) | GO:0008150 | biological_process | 0.00808026 | 1.75175475 | 0.00194246 | 0.46854406 | 1.38105036 | 0.01907497 | | | | | | | |
| 436 | | PFAD70c | 8310 | hypothetical protein:PFAD70c(-8310) | | | -0.54610478 | 0.54681843 | 0.00116629 | -0.71642876 | 0.94409059 | 0.00296333 | -0.68642674 | 0.90273686 | 0.00072629 | | | | |
| 437 | | PFAD70c | 8370 | hypothetical protein:PFAD70c(-8370) | GO:0008150 | biological_process | -0.78464728 | 0.80489386 | 0.00170273 | -0.84428252 | 0.91864261 | 4.42E-06 | -1.01944479 | 0.430308179 | 3.43E-06 | | | | |
| 438 | | PFAD70c | 8389 | hypothetical protein:PFAD70c(-8389) | | | -0.70732846 | 0.57533047 | 0.00507626 | -0.67021929 | 0.52341118 | 0.02436181 | -0.95415699 | 0.51412036 | 0.000711061 | | | | |
| 439 | | PFAD70c | 8392 | hypothetical protein:PFAD70c(-8392) | GO:0008150 | biological_process | -1.549378 | 0.34166907 | 0.01192077 | -1.09775266 | 0.46724793 | 0.00540599 | -1.0808103 | 0.47038663 | 0.02116748 | | | | |
| 440 | | PFAD70c | 8392 | hypothetical protein:PFAD70c(-8392) | | | -0.42841430 | 1.72056637 | 0.00179893 | -1.04507076 | 0.48421127 | 1.67E-07 | -1.03420964 | 0.31788109 | 2.32E-07 | | | | |
| 441 | | PFAD70c | 8393 | hypothetical protein:PFAD70c(-8393) | GO:0008150 | biological_process | -0.489991161 | 0.70701415 | 0.02476458 | -0.7744997 | 0.98924315 | 7.22E-04 | -1.07349071 | 0.47516790 | 1.22E-07 | | | | |
| 442 | | PFAD70c | 8665 | hypothetical protein:PFAD70c(-8665) | GO:0008150 | biological_process | 0.50159197 | 1.415774965 | 0.006684194 | 0.324874059 | 0.88619094 | 2.93E-04 | 1.03929294 | 2.05612696 | 6.51E-07 | | | | |
| 443 | | PFAD70c | 8772 | liver stage antigen 3-PFAD70c(+8772) | GO:0008150 | biological_process | -0.93104874 | 0.52447325 | 0.00147202 | -0.82961251 | 0.84634962 | 0.00360533 | -0.41914749 | 0.74623119 | 0.01274929 | | | | |
| 444 | | PFAD70c | 8577 | hypothetical protein:PFAD70c(-8577) | GO:0008150 | biological_process | -1.30022294 | 0.47859746 | 1.740E-07 | -0.40088129 | 0.31574036 | 7.98E-06 | -0.20315117 | 0.73495977 | 8.42E-07 | | | | |
| 445 | | PFAD70c | 8623 | hypothetical protein:PFAD70c(-8623) | | | 0.39302629 | 1.91708265 | 0.04848691 | 0.78364578 | 0.48486959 | 0.00072629 | | | | | | | |
| 446 | | PFAD70c | C49 | hypothetical protein:PFAD70c(-C49) | | | 0.89241622 | 0.52397901 | 0.00101128 | 1.06716718 | 0.47073442 | 0.0012036 | | | | | | | |
| 447 | | PFAD70c | C54 | hypothetical protein:PFAD70c(-C54) | GO:0020111 | apoptosis | 0.759146964 | 1.60251184 | 0.00311416 | | | | | | | | | | |
| 448 | | PFAD70c | C33 | hypothetical protein:PFAD70c(-C33) | GO:005622 | intracellular | 1.17489507 | 2.28789302 | 0.004134871 | | | | | | | | | | |
| 449 | | PFAD70c | C239 | hypothetical protein:PFAD70c(-C239) | GO:0020111 | apoptosis | | | | 0.89190489 | 1.85630352 | 0.00042142 | 0.70930089 | 1.63572924 | 0.00489696 | | | | |
| 450 | | PFAD70c | C385 | hypothetical protein:PFAD70c(-C385) | | | -0.81216493 | 0.56930915 | 0.00427062 | -0.76277611 | 0.58930932 | 0.00170722 | -0.61178474 | 0.55411776 | 5.00E-05 | | | | |
| 451 | | PFAD70c | C385 | hypothetical protein:PFAD70c(-C385) | | | -0.54554561 | 0.63439547 | 0.02354817 | -0.51589103 | 0.63295852 | 0.00251455 | | | | | | | |
| 452 | | PFAD70c | C419 | hypothetical protein:PFAD70c(-C419) | GO:0020111 | apoptosis | -0.51449599 | 0.70037911 | 0.00114114 | -0.8147615 | 0.56801023 | 1.82E-05 | -0.54073445 | 0.81058343 | 0.00073953 | | | | |
| 453 | | PFAD70c | C419 | hypothetical protein:PFAD70c(-C419) | GO:0020111 | apoptosis | -0.65895952 | 0.62339894 | 0.01192858 | -0.65895952 | 0.62339894 | 0.01192858 | -0.72373751 | 0.554668105 | 0.00407294 | | | | |
| 454 | | PFAD70c | D4798_1 | hypothetical protein:PFAD70c(+D4798_1) | GO:0008150 | biological_process | -0.60214468 | 0.68976472 | 3.78E-05 | -0.80491849 | 0.57263044 | 4.20E-06 | | | | | | | |
| 455 | | PFAD70c | C488 | hypothetical protein:PFAD70c(-C488) | GO:0008150 | biological_process | -0.66232801 | 0.61367029 | 2.45E-05 | -0.62524801 | 0.56437078 | 1.77E-06 | | | | | | | |
| 456 | | PFAD70c | C541 | hepatocyte stage antigen:PFAD70c(+C541) | | | -0.73964324 | 0.59931827 | 0.00114264 | -1.20074229 | 0.42078349 | 4.83E-06 | | | | | | | |
| 457 | | PFAD70c | C62 | hypothetical protein:PFAD70c(-C62) | | | -0.786761297 | 0.576643874 | 0.0499594 | | | | | | | | | | |
| 458 | | PFAD70c | C62 | hypothetical protein:PFAD70c(-C62) | | | -1.08709938 | 0.47279617 | 9.52E-05 | -1.15532829 | 0.90977897 | 0.00242234 | -0.64662389 | 0.58405271 | 0.00219934 | | | | |
| 459 | | PFAD70c | C64 | hypothetical protein:PFAD70c(-C64) | | | -0.82701166 | 0.52593948 | 0.00179158 | -0.48169219 | 0.71123461 | 0.00397629 | -0.40724613 | 0.75414646 | 0.02851519 | | | | |
| 460 | | PFAD70c | C239 | hypothetical protein:PFAD70c(-C239) | | | -0.74441702 | 0.58920912 | 0.02061813 | -0.74441702 | 0.58920912 | 0.02061813 | -0.66956671 | 0.55146426 | 0.00023712 | | | | |
| 461 | | PFAD70c | C243_42 | hypothetical protein:PFAD70c(+C243_42) | | | -0.74423238 | 0.58920948 | 0.02042841 | -1.0734617 | 0.48416654 | 1.51E-06 | -0.72443108 | 0.62618974 | 5.02E-05 | | | | |
| 462 | | PFAD70c | D6281_31 | hypothetical protein:PFAD70c(+D6281_31) | | | -0.82246643 | 0.66528619 | 0.02623661 | -0.83425041 | 0.53797345 | 0.00262949 | | | | | | | |
| 463 | | PFAD70c | D4917_61 | hypothetical protein:PFAD70c(+D4917_61) | | | 0.33749348 | 1.2639933 | 0.01193642 | -0.4428684 | 0.8403766 | 6.01E-05 | -0.81346163 | 0.569139361 | 3.26E-07 | | | | |
| 464 | | PFAD70c | C1715_124 | hypothetical protein:PFAD70c(+C1715_124) | | | 0.76384156 | 1.69620504 | 0.00043163 | 0.40945237 | 1.32221021 | 0.00393673 | | | | | | | |
| 465 | | PFAD70c | C2158_20 | hypothetical protein:PFAD70c(-C2158_20) | | | -1.34121682 | 0.39487933 | 4.79E-07 | -0.83516203 | 0.56052157 | 4.09E-06 | -0.60041265 | 0.524147413 | 3.19E-05 | | | | |
| 466 | | PFAD70c | C2316_45 | hypothetical protein:PFAD70c(-C2316_45) | GO:0020111 | apoptosis | -0.76593928 | 0.59238272 | 0.00097292 | | | | 0.369712909 | 1.29120381 | 0.04071644 | | | | |

APPENDIX B

DIFFERENTIAL TRANSCRIPT ABUNDANCE DATASET (EDGE)

| PlasmoDB IDs | NAME |
|-------------------------|--|
| chr13-tRNA-Thr-1 | chr13-tRNA-Thr-1::chr13-tRNA-Thr-1::(PCHR13-TRNA-THR-1_2) |
| chr14.gen_473_MND1 | chr14.gen_473_MND1::chr14.gen_473_MND1::(PCHR14.GEN_473_MND1_168) |
| chr7.rRNA-1-ITS1 | chr7.rRNA-1-ITS1, putative::chr7.rRNA-1-ITS1::(PCHR7.RRNA-1-ITS1_17) |
| chr8.rRNA-1-5.8s-pseudo | chr8.rRNA-1-5.8s, pseudo::chr8.rRNA-1-5.8s-pseudo::(PCHR8.RRNA-1-5.8S-PSEUDO_90) |
| MAL13P1.103 | hypothetical protein::MAL13P1.103::(M10202_2) |
| MAL13P1.109 | conserved hypothetical protein, conserved in <i>P. falciparum</i> ::MAL13P1.109::(OPFM60490) |
| MAL13P1.118 | cAMP-specific 3',5'-cyclic phosphodiesterase 4D, putative::MAL13P1.118::(M16622_2) |
| MAL13P1.131 | hypothetical protein::MAL13P1.131::(M33739_10) |
| MAL13P1.141 | hypothetical protein::MAL13P1.141::(M24561_22) |
| MAL13P1.142 | hypothetical protein::MAL13P1.142::(M24561_19) |
| MAL13P1.15 | hypothetical protein::MAL13P1.15::(PMAL13P1.15_12) |
| MAL13P1.150 | hypothetical protein::MAL13P1.150::(PMAL13P1.150_1377) |
| MAL13P1.158 | hypothetical protein::MAL13P1.158::(J4848_2) |
| MAL13P1.162 | DNAJ-like protein, putative::MAL13P1.162::(PMAL13P1.162_176) |
| MAL13P1.164 | elongation factor tu, putative::MAL13P1.164::(M8032_4) |
| MAL13P1.167 | signal peptidase, putative::MAL13P1.167::(M18924_16) |
| MAL13P1.168 | hypothetical protein::MAL13P1.168::(PMAL13P1.168_448) |
| MAL13P1.182 | hypothetical protein, conserved::MAL13P1.182::(PMAL13P1.182_635) |
| MAL13P1.183 | hypothetical protein::MAL13P1.183::(PMAL13P1.183_168) |
| MAL13P1.184 | endopeptidase, putative::MAL13P1.184::(M32813_2) |
| MAL13P1.19 | hypothetical protein::MAL13P1.19::(I4256_1) |
| MAL13P1.190 | proteasome regulatory component, putative::MAL13P1.190::(M54626_1) |
| MAL13P1.194 | hypothetical protein::MAL13P1.194::(M37794_2) |
| MAL13P1.217 | hypothetical protein::MAL13P1.217::(J8570_1) |
| MAL13P1.218 | UDP-N-acetylglucosamine pyrophosphorylase, putative::MAL13P1.218::(M55888_8) |
| MAL13P1.227 | ubiquitin-conjugating enzyme, putative::MAL13P1.227::(M35930_10) |
| MAL13P1.232 | hypothetical protein::MAL13P1.232::(KN1115_2) |
| MAL13P1.234 | hypothetical protein::MAL13P1.234::(I4738_1) |
| MAL13P1.238 | hypothetical protein::MAL13P1.238::(M15752_2) |
| MAL13P1.24 | hypothetical protein::MAL13P1.24::(M29079_4) |
| MAL13P1.243 | elongation factor Tu, putative::MAL13P1.243::(M45339_1) |
| MAL13P1.248 | nucleoside diphosphate hydrolase::MAL13P1.248::(M24933_5) |
| MAL13P1.250 | hypothetical protein::MAL13P1.250::(PMAL13P1.250_736) |
| MAL13P1.254 | hypothetical protein::MAL13P1.254::(PMAL13P1.254_185) |
| MAL13P1.255 | hypothetical protein::MAL13P1.255::(OPFM60555) |
| MAL13P1.256 | phosphatidylinositol transfer protein, putative::MAL13P1.256::(PMAL13P1.256_3773) |
| MAL13P1.261 | hypothetical protein::MAL13P1.261::(M24315_1) |
| MAL13P1.277 | DnaJ-like protein, putative::MAL13P1.277::(PMAL13P1.277_207) |
| MAL13P1.28 | hypothetical protein::MAL13P1.28::(M16281_2) |
| MAL13P1.281 | glutamate--tRNA ligase, putative::MAL13P1.281::(M21508_6) |
| MAL13P1.292 | riboflavin kinase / FAD synthase family protein, putative::MAL13P1.292::(PMAL13P1.292_332) |
| MAL13P1.299 | hypothetical protein, conserved::MAL13P1.299::(M26245_8) |
| MAL13P1.300 | hypothetical protein::MAL13P1.300::(M26245_9) |
| MAL13P1.303 | polyadenylate binding protein, putative::MAL13P1.303::(M2931_3) |
| MAL13P1.308 | hypothetical protein, conserved::MAL13P1.308::(M36754_2) |
| MAL13P1.318 | hypothetical protein::MAL13P1.318::(OPFM60527) |
| MAL13P1.323 | hypothetical protein::MAL13P1.323::(M1222_1) |
| MAL13P1.332 | hypothetical protein::MAL13P1.332::(M3696_3) |
| MAL13P1.341 | hypothetical protein, conserved::MAL13P1.341::(M38913_6) |
| MAL13P1.343 | proteasome regulatory subunit, putative::MAL13P1.343::(M33419_1) |
| MAL13P1.354 | erythrocyte membrane protein 1 (PEMP1), pseudogene::MAL13P1.354::(L1_21) |
| MAL13P1.40 | hypothetical protein::MAL13P1.40::(OPFM60513) |
| MAL13P1.45 | hypothetical protein, conserved::MAL13P1.45::(M25032_3) |
| MAL13P1.48 | hypothetical protein::MAL13P1.48::(M3590_1) |
| MAL13P1.480 | Histidine Rich protein III (HRPIII)::MAL13P1.480::(PHRPIII_502) |
| MAL13P1.54 | hypothetical protein, conserved::MAL13P1.54::(M2511_2) |
| MAL13P1.61 | hypothetical protein::MAL13P1.61::(M26214_1) |
| MAL13P1.65 | hypothetical protein::MAL13P1.65::(PMAL13P1.65_103) |
| MAL13P1.74 | hypothetical protein::MAL13P1.74::(M364_1) |
| MAL13P1.82 | phosphatidylinositol synthase, putative::MAL13P1.82::(PMAL13P1.82_71) |
| MAL13P1.89 | hypothetical protein::MAL13P1.89::(M5172_2) |
| MAL7P1.110 | hypothetical protein, conserved::MAL7P1.110::(PMAL7P1.110_303) |
| MAL7P1.119 | hypothetical protein::MAL7P1.119::(F53897_2) |
| MAL7P1.138 | hypothetical protein::MAL7P1.138::(F35197_1) |
| MAL7P1.141 | hypothetical protein::MAL7P1.141::(PMAL7P1.141_100) |
| MAL7P1.145 | DNA mismatch repair protein pms1 homologue, putative::MAL7P1.145::(D52830_1) |
| MAL7P1.149 | hypothetical protein::MAL7P1.149::(PMAL7P1.149_1727) |
| MAL7P1.170 | ring stage expressed protein::MAL7P1.170::(OPFBLOB0026) |
| MAL7P1.25 | hypothetical protein::MAL7P1.25::(F42062_1) |
| MAL7P1.27 | chloroquine resistance transporter, putative::MAL7P1.27::(F35774_1) |
| MAL7P1.29 | hypothetical protein::MAL7P1.29::(E12238_1) |
| MAL7P1.6 | hypothetical protein::MAL7P1.6::(PMAL7P1.6_11) |
| MAL7P1.61 | erythrocyte membrane protein 1 (PEMP1) pseudogene::MAL7P1.61::(F17545_3) |
| MAL7P1.76 | hypothetical protein::MAL7P1.76::(F403_1) |
| MAL7P1.77 | hypothetical protein::MAL7P1.77::(F25543_1) |



MAL7P1.83 hypothetical protein::MAL7P1.83::(F66828_2)
MAL7P1.88 thioredoxin-like protein::MAL7P1.88::(F71224_1)
MAL7P1.93 mitochondrial ribosomal protein S8, putative::MAL7P1.93::(F68670_1)
MAL8P1.101 hypothetical protein::MAL8P1.101::(E22273_1)
MAL8P1.108 protein phosphatase, putative::MAL8P1.108::(PMAL8P1.108_541)
MAL8P1.109 hypothetical protein, conserved::MAL8P1.109::(F26666_3)
MAL8P1.113 hypothetical protein::MAL8P1.113::(E4387_1)
MAL8P1.114 hypothetical protein::MAL8P1.114::(F55001_5)
MAL8P1.145 hypothetical protein, conserved::MAL8P1.145::(PMAL8P1.145_328)
MAL8P1.146 hypothetical protein::MAL8P1.146::(F4732_2)
MAL8P1.157 hypothetical protein::MAL8P1.157::(F27536_1)
MAL8P1.17 disulfide isomerase precursor, putative::MAL8P1.17::(F53081_1)
MAL8P1.21 hypothetical protein::MAL8P1.21::(F19190_1)
MAL8P1.3 integral membrane protein, conserved in *P. falciparum*::MAL8P1.3::(OPFBLOB0144)
MAL8P1.30 hypothetical protein::MAL8P1.30::(PMAL8P1.30_1158)
MAL8P1.32 nucleoside transporter, putative::MAL8P1.32::(F4541_1)
MAL8P1.34 hypothetical protein::MAL8P1.34::(F31053_2)
MAL8P1.51 protein-transport protein sec61 beta 1 subunit, putative::MAL8P1.51::(PMAL8P1.51_168)
MAL8P1.53 hypothetical protein::MAL8P1.53::(PMAL8P1.53_1127)
MAL8P1.55 hypothetical protein::MAL8P1.55::(F20870_2)
MAL8P1.62 hypothetical protein, conserved in other *Plasmodium* species::MAL8P1.62::(F70676_1)
MAL8P1.79 hypothetical protein::MAL8P1.79::(KN2562_1)
MAL8P1.99 hypothetical protein::MAL8P1.99::(F4481_1)
PF00_0001 hypothetical protein::PF00_0001::(F5510_1)
PF00_0003 hypothetical protein::PF00_0003::(F39902_1)
PF07_0006 starp antigen::PF07_0006::(OPFG0007)
PF07_0010 hypothetical protein::PF07_0010::(F20792_1)
PF07_0011 hypothetical protein, conserved::PF07_0011::(OPFG0025)
PF07_0023 DNA replication licensing factor mcm7 homologue, putative::PF07_0023::(OPFG0035)
PF07_0032 Cg8 protein::PF07_0032::(D35303_1)
PF07_0034 Cg3 protein::PF07_0034::(OPFG0001)
PF07_0039 hypothetical protein::PF07_0039::(F47864_1)
PF07_0042 hypothetical protein::PF07_0042::(F17836_1)
PF07_0052 hypothetical protein::PF07_0052::(PPF07_0052_366)
PF07_0059 4-nitrophenylphosphatase, putative::PF07_0059::(F7288_1)
PF07_0062 GTP-binding translation elongation factor tu family protein, putative::PF07_0062::(F11707_1)
PF07_0064 hypothetical protein::PF07_0064::(F69212_1)
PF07_0075 hypothetical protein, expressed::PF07_0075::(F56229_4)
PF07_0112 proteasome subunit alpha type 5, putative::PF07_0112::(F960_4)
PF07_0113 hypothetical protein::PF07_0113::(F71022_1)
PF07_0118 hypothetical protein::PF07_0118::(E18957_1)
PF07_0121 hypothetical protein, conserved::PF07_0121::(E14340_1)
PF08_0003 tryptophan/threonine-rich antigen::PF08_0003::(OPFBLOB0065)
PF08_0006 prohibitin, putative::PF08_0006::(OPFH0005)
PF08_0010 hypothetical protein::PF08_0010::(F5206_2)
PF08_0021 hypothetical protein::PF08_0021::(F36803_1)
PF08_0029 hypothetical protein::PF08_0029::(OPFH0035)
PF08_0032 hypothetical protein::PF08_0032::(F1761_1)
PF08_0041 ribosome biogenesis protein nep1 homologue, putative::PF08_0041::(OPFBLOB0134)
PF08_0045 2-oxoglutarate dehydrogenase e1 component::PF08_0045::(F10318_1)
PF08_0053 hypothetical protein::PF08_0053::(PPF08_0053_743)
PF08_0056 zinc finger protein, putative::PF08_0056::(F65493_3)
PF08_0063 hypothetical protein::PF08_0063::(F39343_3)
PF08_0075 60S ribosomal protein L13, putative::PF08_0075::(F21981_2)
PF08_0080 hypothetical protein::PF08_0080::(F17989_1)
PF08_0083 hypothetical protein::PF08_0083::(OPFH0037)
PF08_0091 hypothetical protein::PF08_0091::(F28313_1)
PF08_0097 hypothetical protein::PF08_0097::(PPF08_0097_1500)
PF08_0098 abc transporter, putative::PF08_0098::(F61881_1)
PF08_0112 hypothetical protein::PF08_0112::(PPF08_0112_708)
PF08_0116 hypothetical protein::PF08_0116::(F53446_1)
PF08_0119 hypothetical protein::PF08_0119::(PPF08_0119_76)
PF08_0125 tubulin gamma chain::PF08_0125::(F20448_4)
PF08_0131 1-cys peroxidoxin::PF08_0131::(F46816_2)
PF10_0014 hypothetical protein::PF10_0014::(PPF10_0014_381)
PF10_0015 acyl CoA binding protein, putative::PF10_0015::(OPFJ12802)
PF10_0016 acyl CoA binding protein, putative::PF10_0016::(J33_21)
PF10_0017 hypothetical protein::PF10_0017::(J33_20)
PF10_0019 early transcribed membrane protein::PF10_0019::(J33_16)
PF10_0021 hypothetical protein::PF10_0021::(J33_12)
PF10_0022 hypothetical protein::PF10_0022::(J33_11)
PF10_0025 PF70 protein::PF10_0025::(F67629_1)
PF10_0033 hypothetical protein::PF10_0033::(J120_2)
PF10_0034 hypothetical protein::PF10_0034::(J120_6)
PF10_0036 N-acetyltransferase, putative::PF10_0036::(J120_11)
PF10_0047 hypothetical protein::PF10_0047::(KS2508_1)
PF10_0051 ADP/ATP carrier protein, putative::PF10_0051::(J43_12)
PF10_0052 hypothetical protein::PF10_0052::(J43_15)
PF10_0053 tRNA ligase, putative::PF10_0053::(J43_16)
PF10_0065 hypothetical protein::PF10_0065::(J163_7)
PF10_0066 hypothetical protein::PF10_0066::(J163_6)
PF10_0068 hypothetical protein::PF10_0068::(J634_1)
PF10_0079 hypothetical protein::PF10_0079::(J73_15)
PF10_0084 tubulin beta chain, putative::PF10_0084::(J73_4)
PF10_0092 hypothetical protein::PF10_0092::(PPF10_0092_84)
PF10_0093 hypothetical protein::PF10_0093::(J267_2)
PF10_0097 hypothetical protein::PF10_0097::(J647_6)
PF10_0100 hypothetical protein::PF10_0100::(J1417_2)
PF10_0101 hypothetical protein::PF10_0101::(J920_3)
PF10_0108 hypothetical protein::PF10_0108::(J252_1)
PF10_0116 hypothetical protein::PF10_0116::(J293_1)
PF10_0120 hypothetical protein::PF10_0120::(KM827_4)



PF10_0132 phospholipase C-like, putative::PF10_0132::(J53_7)
PF10_0134 hypothetical protein::PF10_0134::(PPF10_0134_457)
PF10_0152 hypothetical protein::PF10_0152::(J53_42)
PF10_0153 hsp60::PF10_0153::(J53_43)
PF10_0158 hypothetical protein::PF10_0158::(J53_52)
PF10_0163 hypothetical protein::PF10_0163::(J425_2)
PF10_0168 hypothetical protein::PF10_0168::(J248_4)
PF10_0174 26s proteasome subunit p55, putative::PF10_0174::(J110_4)
PF10_0181 hypothetical protein::PF10_0181::(J109_2)
PF10_0200 hypothetical protein, conserved::PF10_0200::(J26_1)
PF10_0222 hypothetical protein::PF10_0222::(PPF10_0222_11)
PF10_0227 hypothetical protein, conserved::PF10_0227::(PPF10_0227_403)
PF10_0235 hypothetical protein::PF10_0235::(J245_5)
PF10_0238 hypothetical protein::PF10_0238::(J245_10)
PF10_0246 hypothetical protein::PF10_0246::(J212_1)
PF10_0259 hypothetical protein::PF10_0259::(J232_6)
PF10_0262 hypothetical protein::PF10_0262::(J121_1)
PF10_0275 protoporphyrinogen oxidase, putative::PF10_0275::(J504_4)
PF10_0286 hypothetical protein::PF10_0286::(J151_5)
PF10_0295 hypothetical protein::PF10_0295::(J564_3)
PF10_0301 calmodulin, putative::PF10_0301::(J461_5)
PF10_0311 hypothetical protein, conserved::PF10_0311::(J352_5)
PF10_0313 hypothetical protein::PF10_0313::(D38761_3)
PF10_0317 hypothetical protein::PF10_0317::(J153_2)
PF10_0330 ubiquitin-conjugating enzyme, putative::PF10_0330::(J1011_2)
PF10_0331 hypothetical protein, conserved::PF10_0331::(J141_1)
PF10_0334 flavoprotein subunit of succinate dehydrogenase::PF10_0334::(J167_8)
PF10_0345 merozoite Surface Protein 3, MSP3::PF10_0345::(J116_9)
PF10_0346 merozoite Surface protein 6, MSP6::PF10_0346::(J116_7)
PF10_0359 hypothetical protein::PF10_0359::(J21_27)
PF10_0360 hypothetical protein::PF10_0360::(J21_24)
PF10_0363 pyruvate kinase, putative::PF10_0363::(J21_14)
PF11_0036 hypothetical protein, conserved::PF11_0036::(KS54_4)
PF11_0039 early transcribed membrane protein 11.1::PF11_0039::(KS75_16)
PF11_0040 early transcribed membrane protein 11.2::PF11_0040::(KS75_15)
PF11_0047 hypothetical protein::PF11_0047::(KS75_1)
PF11_0048 casein kinase II beta chain, putative::PF11_0048::(KS375_3)
PF11_0084 hypothetical protein::PF11_0084::(PPF11_0084_251)
PF11_0087 Rad51 homolog, putative::PF11_0087::(KS42_6)
PF11_0105 hypothetical protein::PF11_0105::(KS2345_1)
PF11_0123 hypothetical protein::PF11_0123::(KS26_1)
PF11_0130 hypothetical protein::PF11_0130::(KS1022_8)
PF11_0140 hypothetical protein::PF11_0140::(KS306_2)
PF11_0142 hypothetical protein, conserved::PF11_0142::(KS178_2)
PF11_0149 hypothetical protein::PF11_0149::(PPF11_0149_206)
PF11_0152 hypothetical protein::PF11_0152::(PPF11_0152_17)
PF11_0154 hypothetical protein::PF11_0154::(KS152_1)
PF11_0159 hypothetical protein::PF11_0159::(PPF11_0159_288)
PF11_0164 peptidyl-prolyl cis-trans isomerase::PF11_0164::(KS2_14)
PF11_0165 falcipain 2 precursor::PF11_0165::(KS826_1)
PF11_0166 hypothetical protein::PF11_0166::(KS826_2)
PF11_0177 ubiquitin C-terminal hydrolase, family 1, putative::PF11_0177::(KS113_1)
PF11_0179 hypothetical protein::PF11_0179::(KS509_7)
PF11_0198 hypothetical protein, conserved::PF11_0198::(KS97_20)
PF11_0212 hypothetical protein::PF11_0212::(KS12_11)
PF11_0223 hypothetical protein::PF11_0223::(KS91_4)
PF11_0228 hypothetical protein::PF11_0228::(KS244_8)
PF11_0249 hypothetical protein::PF11_0249::(KS168_5)
PF11_0276 hypothetical protein::PF11_0276::(KS266_16)
PF11_0301 spermidine synthase::PF11_0301::(KS488_1)
PF11_0306 A/G-specific adenine glycosylase, putative::PF11_0306::(KS101_1)
PF11_0332 hypothetical protein::PF11_0332::(KS135_4)
PF11_0347 hypothetical protein::PF11_0347::(KS44_10)
PF11_0363 hypothetical protein::PF11_0363::(KS586_5)
PF11_0366 hypothetical protein::PF11_0366::(KS85_6)
PF11_0393 hypothetical protein, conserved::PF11_0393::(KS125_6)
PF11_0396 Protein phosphatase 2C::PF11_0396::(KS81_2)
PF11_0409 hypothetical protein, conserved::PF11_0409::(KS316_19)
PF11_0412 Vacuolar ATP synthase subunit F, putative::PF11_0412::(KS667_1)
PF11_0414 hypothetical protein::PF11_0414::(KS1030_4)
PF11_0419 hypothetical protein::PF11_0419::(KS694_2)
PF11_0429 hypothetical protein::PF11_0429::(KS545_1)
PF11_0460 hypothetical protein::PF11_0460::(KS127_17)
PF11_0469 hypothetical protein::PF11_0469::(KS225_10)
PF11_0485 hypothetical protein::PF11_0485::(KS56_24)
PF11_0488 hypothetical protein::PF11_0488::(KS56_33)
PF11_0489 hypothetical protein::PF11_0489::(KS222_1)
PF11_0504 hypothetical protein::PF11_0504::(KS157_19)
PF11_0505 hypothetical protein::PF11_0505::(KS157_18)
PF11_0507 antigen 332, putative::PF11_0507::(F40797_1)
PF11_0509 ring-infected erythrocyte surface antigen, putative::PF11_0509::(KS157_11)
PF11_0512 ring-infected erythrocyte surface antigen 2, RESA-2 - malaria parasite (Plasmodium falciparum)-related::PF11_0512::(KS157_1)
PF11_0513 hypothetical protein::PF11_0513::(KS48_18)
PF11_0521 erythrocyte membrane protein 1 (PfEMP1)::PF11_0521::(E686_1)
PF11_0524 U6 snRNA associated Sm-like protein Ls; U6 snRNA associated Sm-like protein LsM4, putative::PF11_0524::(KS25_17)
PF13_0011 plasmodium falciparum gamete antigen 27/25::PF13_0011::(M32775_1)
PF13_0029 hypothetical protein::PF13_0029::(M27404_1)
PF13_0036 DNAJ protein, putative::PF13_0036::(M45727_11)
PF13_0043 CCAAT-binding transcription factor, putative::PF13_0043::(M58024_1)
PF13_0045 40S ribosomal protein S27, putative::PF13_0045::(M3816_2)
PF13_0051 snornc protein gar1 homologue, putative::PF13_0051::(M12190_2)
PF13_0058 hypothetical protein::PF13_0058::(M2610_1)

PF13_0059 ribosomal protein S15, mitochondrial precursor, putative::PF13_0059::(M38127_1)
 PF13_0061 ATP synthase gamma chain, mitochondrial precursor, putative::PF13_0061::(M2511_7)
 PF13_0076 hypothetical protein::PF13_0076::(M1595_2)
 PF13_0095 DNA replication licensing factor mcm4-related::PF13_0095::(M4927_3)
 PF13_0096 Ubiquitin Carboxyl-terminal Hydrolase-like zinc finger protein::PF13_0096::(M4927_1)
 PF13_0101 hypothetical protein::PF13_0101::(I4500_1)
 PF13_0128 beta-hydroxyacyl-ACP dehydratase precursor::PF13_0128::(M44397_17)
 PF13_0129 ribosomal protein L6 homologue, putative::PF13_0129::(M44397_14)
 PF13_0132 60S ribosomal protein L23a, putative::PF13_0132::(M44397_10)
 PF13_0134 hypothetical protein::PF13_0134::(M44397_1)
 PF13_0138 hypothetical protein, conserved::PF13_0138::(M43799_11)
 PF13_0139 hypothetical protein::PF13_0139::(M43799_1)
 PF13_0141 L-lactate dehydrogenase::PF13_0141::(M12812_7)
 PF13_0148 hypothetical protein::PF13_0148::(M49680_3)
 PF13_0158 hypothetical protein::PF13_0158::(OPFM60543)
 PF13_0162 hypothetical protein::PF13_0162::(M56256_2)
 PF13_0169 hypothetical protein::PF13_0169::(OPFM60551)
 PF13_0173 hypothetical protein::PF13_0173::(J1010_1)
 PF13_0182 hypothetical protein::PF13_0182::(KN945_3)
 PF13_0192 hypothetical protein::PF13_0192::(J541_4)
 PF13_0193 MSP7-like protein::PF13_0193::(I11584_1)
 PF13_0199 hypothetical protein::PF13_0199::(I5698_1)
 PF13_0217 hypothetical protein::PF13_0217::(M48963_5)
 PF13_0220 hypothetical protein::PF13_0220::(M28331_2)
 PF13_0221 hypothetical protein::PF13_0221::(J12778_2)
 PF13_0222 RNA lariat debranching enzyme, putative::PF13_0222::(M951_1)
 PF13_0260 hypothetical protein, conserved::PF13_0260::(M5968_1)
 PF13_0268 ribosomal protein L17, putative::PF13_0268::(M59170_2)
 PF13_0271 ABC transporter, putative::PF13_0271::(M26914_8)
 PF13_0276 hypothetical protein::PF13_0276::(PPF13_0276_110)
 PF13_0281 hypothetical protein::PF13_0281::(M56059_1)
 PF13_0291 replication licensing factor, putative::PF13_0291::(M446_3)
 PF13_0296 hypothetical protein, conserved::PF13_0296::(PPF13_0296_50)
 PF13_0303 hypothetical protein::PF13_0303::(M43376_3)
 PF13_0304 elongation factor 1 alpha::PF13_0304::(M40872_8)
 PF13_0315 RNA binding protein, putative::PF13_0315::(M49010_1)
 PF13_0319 hypothetical protein::PF13_0319::(PPF13_0319_120)
 PF13_0323 binding protein, putative::PF13_0323::(M1774_1)
 PF13_0328 proliferating cell nuclear antigen::PF13_0328::(M36754_1)
 PF13_0330 ATP-dependent DNA helicase, putative::PF13_0330::(M22193_8)
 PF13_0331 hypothetical protein, conserved::PF13_0331::(M22193_10)
 PF13_0344 UBA/THIF-type NAD/FAD binding protein, putative::PF13_0344::(M34743_8)
 PF13_0349 nucleoside diphosphate kinase b, putative::PF13_0349::(M38941_10)
 PF14_0015 aminopeptidase, putative::PF14_0015::(N145_28)
 PF14_0016 hypothetical protein::PF14_0016::(N145_23)
 PF14_0038 cytochrome c, putative::PF14_0038::(N165_2)
 PF14_0047 hypothetical protein::PF14_0047::(N159_4)
 PF14_0051 hypothetical protein, conserved::PF14_0051::(N159_13)
 PF14_0053 ribonucleotide reductase small subunit::PF14_0053::(N159_20)
 PF14_0054 hypothetical protein, conserved::PF14_0054::(N159_23)
 PF14_0064 vacuolar protein sorting 29, putative::PF14_0064::(N159_39)
 PF14_0068 fibrillarin, putative::PF14_0068::(N159_46)
 PF14_0072 hypothetical protein, conserved::PF14_0072::(N171_4)
 PF14_0077 plasmepsin 2 precursor::PF14_0077::(N150_91)
 PF14_0096 hypothetical protein::PF14_0096::(N150_60)
 PF14_0105 hypothetical protein::PF14_0105::(N150_44)
 PF14_0107 hypothetical protein, conserved::PF14_0107::(PPF14_0107_497)
 PF14_0108 hypothetical protein::PF14_0108::(N150_33)
 PF14_0109 hypothetical protein::PF14_0109::(PPF14_0109_47)
 PF14_0122 nuclear transport factor 2, putative::PF14_0122::(N150_3)
 PF14_0146 ribonucleoprotein, putative::PF14_0146::(N175_12)
 PF14_0150 RNA polymerase small subunit, putative::PF14_0150::(N127_54)
 PF14_0170 hypothetical protein::PF14_0170::(N127_12)
 PF14_0176 hypothetical protein::PF14_0176::(N143_71)
 PF14_0192 glutathione reductase::PF14_0192::(N143_29)
 PF14_0200 hypothetical protein::PF14_0200::(M18376_1)
 PF14_0208 hypothetical protein, conserved::PF14_0208::(N141_57)
 PF14_0217 hypothetical protein::PF14_0217::(N141_41)
 PF14_0232 hypothetical protein, conserved::PF14_0232::(N189_1)
 PF14_0251 hypothetical protein::PF14_0251::(N136_12)
 PF14_0253 hypothetical protein::PF14_0253::(N157_1)
 PF14_0255 hypothetical protein::PF14_0255::(N157_7)
 PF14_0257 hypothetical protein, conserved::PF14_0257::(N157_10)
 PF14_0270 ribosomal protein L15, putative::PF14_0270::(N166_3)
 PF14_0279 hypothetical protein::PF14_0279::(N138_13)
 PF14_0285 exodeoxyribonuclease III, putative::PF14_0285::(N138_30)
 PF14_0288 cytochrome c oxidase subunit II precursor, putative::PF14_0288::(N138_34)
 PF14_0300 syntaxin, putative::PF14_0300::(N138_61)
 PF14_0310 hypothetical protein::PF14_0310::(N138_94)
 PF14_0314 chromatin assembly factor 1 p55 subunit, putative::PF14_0314::(N138_102)
 PF14_0316 DNA topoisomerase II, putative::PF14_0316::(N172_3)
 PF14_0321 ABC transporter, putative::PF14_0321::(N132_184)
 PF14_0327 methionine aminopeptidase, type II, putative::PF14_0327::(N132_172)
 PF14_0329 hypothetical protein, conserved::PF14_0329::(M41547_1)
 PF14_0369 hypothetical protein::PF14_0369::(N132_66)
 PF14_0380 hypothetical protein::PF14_0380::(N132_37)
 PF14_0381 delta-aminolevulinic acid dehydratase::PF14_0381::(N132_27)
 PF14_0382 metalloendopeptidase, putative::PF14_0382::(N132_24)
 PF14_0387 hypothetical protein::PF14_0387::(N132_11)
 PF14_0392 Ser/Thr protein kinase, putative::PF14_0392::(I9716_1)
 PF14_0395 hypothetical protein, conserved::PF14_0395::(N128_94)
 PF14_0401 methionine -- tRNA ligase, putative::PF14_0401::(N128_85)



PF14_0403 protein prenyltransferase alpha subunit, putative::PF14_0403::(N128_76)
PF14_0411 small nuclear ribonucleic protein, putative::PF14_0411::(PPF14_0411_230)
PF14_0413 hypothetical protein::PF14_0413::(N128_62)
PF14_0417 heat shock protein, putative::PF14_0417::(N128_56)
PF14_0421 hypothetical protein, conserved::PF14_0421::(OPFN0277)
PF14_0432 hypothetical protein::PF14_0432::(N128_23)
PF14_0444 hypothetical protein::PF14_0444::(N151_60)
PF14_0464 hypothetical protein::PF14_0464::(N151_11)
PF14_0475 hypothetical protein::PF14_0475::(N185_7)
PF14_0488 hypothetical protein::PF14_0488::(N149_13)
PF14_0493 sortilin, putative::PF14_0493::(N149_30)
PF14_0495 hypothetical protein::PF14_0495::(M52375_1)
PF14_0502 hypothetical protein::PF14_0502::(N140_10)
PF14_0518 nifU protein, putative::PF14_0518::(N168_34)
PF14_0519 ribosomal protein S11, putative::PF14_0519::(N168_32)
PF14_0524 hypothetical protein::PF14_0524::(PPF14_0524_219)
PF14_0525 hypothetical protein::PF14_0525::(N168_21)
PF14_0529 gamma-adaptin, putative::PF14_0529::(N168_3)
PF14_0535 hypothetical protein::PF14_0535::(N153_9)
PF14_0538 hypothetical protein::PF14_0538::(N153_15)
PF14_0571 hypothetical protein::PF14_0571::(N130_4)
PF14_0574 hypothetical protein::PF14_0574::(N134_142)
PF14_0583 hypothetical protein::PF14_0583::(N134_120)
PF14_0584 ribosomal protein S4, putative::PF14_0584::(N134_119)
PF14_0591 hypothetical protein::PF14_0591::(N134_103)
PF14_0592 hypothetical protein::PF14_0592::(N134_102)
PF14_0601 replication factor C3::PF14_0601::(N134_82)
PF14_0604 hypothetical protein::PF14_0604::(N134_76)
PF14_0607 hypothetical protein::PF14_0607::(N134_73)
PF14_0615 ATP synthase (C/AC39) subunit, putative::PF14_0615::(N134_44)
PF14_0621 hypothetical protein::PF14_0621::(N134_29)
PF14_0630 protein serine/threonine phosphatase::PF14_0630::(N134_2)
PF14_0632 26S proteasome subunit, putative::PF14_0632::(N135_24)
PF14_0637 rhoGTPase, putative::PF14_0637::(N135_14)
PF14_0665 hypothetical protein::PF14_0665::(KN5123_1)
PF14_0673 hypothetical protein::PF14_0673::(N137_43)
PF14_0677 RNA 3'-Terminal Phosphate Cyclase-like protein, putative::PF14_0677::(N187_5)
PF14_0680 hypothetical protein::PF14_0680::(PPF14_0680_16)
PF14_0681 diacylglycerol kinase, putative::PF14_0681::(N133_58)
PF14_0691 hypothetical protein::PF14_0691::(N133_36)
PF14_0694 protein disulfide isomerase, putative::PF14_0694::(N133_19)
PF14_0697 dihydroorotase, putative::PF14_0697::(N133_9)
PF14_0713 hypothetical protein::PF14_0713::(N147_18)
PF14_0716 Proteasome subunit alpha type 1, putative::PF14_0716::(N147_25)
PF14_0717 hypothetical protein::PF14_0717::(N148_12)
PF14_0730 hypothetical protein::PF14_0730::(PPF14_0730_170)
PF14_0731 hypothetical protein::PF14_0731::(N129_36)
PF14_0738 lysophospholipase, putative::PF14_0738::(N129_14)
PFA0110w ring-infected erythrocyte surface antigen precursor::PFA0110w::(A10325_29)
PFA0140c hypothetical protein::PFA0140c::(A23157_1)
PFA0180w hypothetical protein::PFA0180w::(A8010_10)
PFA0210c hypothetical protein::PFA0210c::(A8010_31)
PFA0300c vacuolar ATP synthase, putative::PFA0300c::(A8109_6)
PFA0335w P. falciparum GTP binding protein RAB5::PFA0335w::(PPFA0335W_427)
PFA0345w centrin, putative::PFA0345w::(A12797_1)
PFA0395c hypothetical protein::PFA0395c::(PPFA0395C_496)
PFA0400c beta3 proteasome subunit, putative::PFA0400c::(A14680_4)
PFA0405w hypothetical protein::PFA0405w::(A9766_1)
PFA0415c hypothetical protein::PFA0415c::(A21885_5)
PFA0420w hypothetical protein::PFA0420w::(A12706_1)
PFA0450c mRNA cleavage factor-like protein, putative::PFA0450c::(A31914_8)
PFA0485w hypothetical protein::PFA0485w::(A3310_11)
PFA0510w hypothetical protein::PFA0510w::(A3310_1)
PFA0525w transcription initiation factor TFIIIB, putative::PFA0525w::(A13725_6)
PFA0545c replication factor c protein, putative::PFA0545c::(A1718_1)
PFA0565c hypothetical protein::PFA0565c::(PPFA0565C_278)
PFA0570w hypothetical protein::PFA0570w::(A13231_2)
PFA0670c hypothetical protein::PFA0670c::(PPFA0670C_135)
PFB0010w erythrocyte membrane protein 1 (PfEMP1)::PFB0010w::(B11)
PFB0085c hypothetical protein::PFB0085c::(B50)
PFB0100c knob associated histidine-rich protein::PFB0100c::(A11546_1)
PFB0110w hypothetical protein::PFB0110w::(B68)
PFB0120w early transcribed membrane protein, putative::PFB0120w::(B70)
PFB0160w ERCC1 nucleotide excision repair protein, putative::PFB0160w::(B95)
PFB0190c hypothetical protein::PFB0190c::(B114)
PFB0250w hypothetical protein::PFB0250w::(B149)
PFB0315w 41 kDa antigen::PFB0315w::(B197)
PFB0365w hypothetical protein, conserved::PFB0365w::(B251)
PFB0385w acyl carrier protein, putative::PFB0385w::(B270)
PFB0390w ribosome releasing factor, putative::PFB0390w::(B272)
PFB0475c hypothetical protein, conserved::PFB0475c::(B326)
PFB0575c hypothetical protein::PFB0575c::(B388)
PFB0580w hypothetical protein::PFB0580w::(B389)
PFB0595w heat shock 40 kDa protein, putative::PFB0595w::(B396)
PFB0600c hypothetical protein::PFB0600c::(B397)
PFB0605w Ser/Thr protein kinase, putative::PFB0605w::(B403)
PFB0620w hypothetical protein::PFB0620w::(B424)
PFB0635w T-complex protein 1, putative::PFB0635w::(B432)
PFB0705w hypothetical protein::PFB0705w::(B467)
PFB0810w hypothetical protein::PFB0810w::(B513)
PFB0865w small nuclear ribonucleoprotein, putative::PFB0865w::(B549)
PFB0900c hypothetical protein::PFB0900c::(B565)

PFB0915w liver stage antigen 3::PFB0915w::(B572)
PFB0953w hypothetical protein::PFB0953w::(B603)
PFC0090w hypothetical protein, conserved::PFC0090w::(C54)
PFC0115c erythrocyte membrane protein 1 (PfEMP1) pseudogene::PFC0115c::(C67)
PFC0145c hypothetical protein, conserved::PFC0145c::(C97)
PFC0165w hypothetical protein, conserved::PFC0165w::(C114)
PFC0170c dihydrolipoamide acyltransferase, putative::PFC0170c::(C116)
PFC0220w hypothetical protein::PFC0220w::(C141)
PFC0255c ubiquitin-conjugating enzyme E2, putative::PFC0255c::(C161)
PFC0325c hypothetical protein::PFC0325c::(C223)
PFC0350c T-complex protein eta subunit, putative::PFC0350c::(C234)
PFC0405c hypothetical protein::PFC0405c::(C258)
PFC0440c helicase, putative::PFC0440c::(C281)
PFC0445w hypothetical protein::PFC0445w::(PPFC0445W_93)
PFC0540w hypothetical protein::PFC0540w::(C365)
PFC0571c hypothetical protein::PFC0571c::(C386)
PFC0581w hypothetical protein::PFC0581w::(C416)
PFC0670c hypothetical protein::PFC0670c::(C441)
PFC0705c hypothetical protein::PFC0705c::(C458)
PFC0715c hypothetical protein::PFC0715c::(C470)
PFC0745c proteasome component C8, putative::PFC0745c::(C497)
PFC0765c hypothetical protein::PFC0765c::(C507)
PFC0800w band 7-related protein::PFC0800w::(C526)
PFC0830w trophozoite stage antigen::PFC0830w::(C541)
PFC0845c ubiquitin-protein ligase, putative::PFC0845c::(C559)
PFC0890w vesicle transport protein, putative::PFC0890w::(C591)
PFC0910w hypothetical protein::PFC0910w::(C600)
PFC0911c hypothetical protein::PFC0911c::(C602)
PFC0912w hypothetical protein::PFC0912w::(C604)
PFC0935c N-acetylglucosamine-1-phosphate transferase, putative::PFC0935c::(PPFC0935C_329)
PFC1025w F49C12.11-like protein::PFC1025w::(C681)
PFD0010w unknown::PFD0010w::(OPFD66971)
PFD0165w ubiquitin-specific protease, putative::PFD0165w::(D6287_29)
PFD0175c hypothetical protein::PFD0175c::(D6287_31)
PFD0225w hypothetical protein::PFD0225w::(D49176_1)
PFD0230c protease, putative::PFD0230c::(D49176_6)
PFD0235c hypothetical protein::PFD0235c::(D49176_8)
PFD0285c lysine decarboxylase, putative::PFD0285c::(D49176_36)
PFD0320c hypothetical protein::PFD0320c::(D49176_61)
PFD0330w hypothetical protein::PFD0330w::(D17715_136)
PFD0360w hypothetical protein::PFD0360w::(D17715_110)
PFD0365c hypothetical protein::PFD0365c::(D17715_109)
PFD0440w hypothetical protein::PFD0440w::(D17715_64)
PFD0465c hypothetical protein, conserved::PFD0465c::(D17715_51)
PFD0595w hypothetical protein::PFD0595w::(D17715_12)
PFD0670c hypothetical protein, conserved::PFD0670c::(D23156_20)
PFD0685c chromosome associated protein, putative::PFD0685c::(D23156_27)
PFD0690c hypothetical protein::PFD0690c::(D23156_45)
PFD0755c adenylate kinase 1::PFD0755c::(D33539_32)
PFD0760c hypothetical protein::PFD0760c::(D33539_33)
PFD0795w hypothetical protein::PFD0795w::(D33539_55)
PFD0830w bifunctional dihydrofolate reductase-thymidylate synthase::PFD0830w::(D33539_76)
PFD0845w hypothetical protein::PFD0845w::(D33539_85)
PFD0850c hypothetical protein, conserved::PFD0850c::(OPFH0015)
PFD0930w CGI-141 protein homolog, putative::PFD0930w::(D12635_22)
PFD0945c hypothetical protein::PFD0945c::(D12635_33)
PFD1015c erythrocyte membrane protein 1 (PfEMP1)::PFD1015c::(D53677_1)
PFD1090c clathrin assembly protein, putative::PFD1090c::(D16785_10)
PFD1135c hypothetical protein::PFD1135c::(D15909_4)
PFD1140w hypothetical protein::PFD1140w::(D15909_8)
PFD1165w protein kinase, conserved in P. falciparum::PFD1165w::(D34948_3)
PFE0045c kinase, putative::PFE0045c::(E20800_1)
PFE0065w skeleton binding protein::PFE0065w::(E598_1)
PFE0070w interspersed repeat antigen, putative::PFE0070w::(E12394_2)
PFE0090w hypothetical protein::PFE0090w::(E17057_1)
PFE0110w hypothetical protein::PFE0110w::(F15289_3)
PFE0140c hypothetical protein::PFE0140c::(E13140_2)
PFE0150c 4-diphosphocytidyl-2c-methyl-D-erythritol kinase (CMK), putative::PFE0150c::(E14176_1)
PFE0165w actin depolymerizing factor, putative::PFE0165w::(E13013_1)
PFE0175c unconventional myosin pfm-b::PFE0175c::(E15509_11)
PFE0215w ATP-dependent helicase, putative::PFE0215w::(E714_9)
PFE0265c hypothetical protein::PFE0265c::(E20827_1)
PFE0420c guanidine nucleotide exchange factor, putative::PFE0420c::(E21208_5)
PFE0435c single-strand binding protein, putative::PFE0435c::(E30064_1)
PFE0445c SNAP protein (soluble N-ethylmaleimide-sensitive factor Attachment Protein), putative::PFE0445c::(D13568_1)
PFE0730c ribose 5-phosphate epimerase, putative::PFE0730c::(E27247_7)
PFE0795c nif-like protein, putative::PFE0795c::(E3215_6)
PFE0800w hypothetical protein::PFE0800w::(E3215_4)
PFE0810c 40S ribosomal subunit protein S14, putative::PFE0810c::(E3215_1)
PFE0855c hypothetical protein::PFE0855c::(E26351_1)
PFE0955w hypothetical protein::PFE0955w::(E13038_9)
PFE1025c hypothetical protein::PFE1025c::(E26771_4)
PFE1040c hypothetical protein::PFE1040c::(E17542_1)
PFE1045c hypothetical protein::PFE1045c::(E18031_10)
PFE1170w hypothetical protein::PFE1170w::(E6125_5)
PFE1175w hypothetical protein::PFE1175w::(E27173_1)
PFE1190c hypothetical protein::PFE1190c::(PPFE1190C_105)
PFE1230c hypothetical protein, conserved::PFE1230c::(F52907_2)
PFE1250w long-chain fatty acid CoA ligase, putative::PFE1250w::(E13599_1)
PFE1255w hypothetical protein::PFE1255w::(E24637_1)
PFE1280w hypothetical protein::PFE1280w::(E5415_6)
PFE1325w hypothetical protein::PFE1325w::(PPFE1325W_13374)

PFE1340w transmembrane protein, putative::PFE1340w::(F35756_2)
PFE1405c eukaryotic translation initiation factor 3, subunit 6, putative::PFE1405c::(E248_3)
PFE1425c hypothetical protein::PFE1425c::(D65681_1)
PFE1430c cyclophilin, putative::PFE1430c::(E20260_8)
PFE1450c hypothetical protein, conserved::PFE1450c::(F53383_11)
PFE1595c hypothetical protein::PFE1595c::(E19695_2)
PFE1615c hypothetical protein::PFE1615c::(D57574_1)
PFF0115c elongation factor G, putative::PFF0115c::(E6534_1)
PFF0205w hypothetical protein, conserved::PFF0205w::(PMAL6P1.45_104)
PFF0210w hypothetical protein::PFF0210w::(PMAL6P1.46_2093)
PFF0230c glyoxalase I, putative::PFF0230c::(PMAL6P1.50_552)
PFF0235c hypothetical protein::PFF0235c::(PMAL6P1.51_1594)
PFF0290w long chain polyunsaturated fatty acid elongation enzyme, putative::PFF0290w::(PMAL6P1.62_738)
PFF0365c conserved hypothetical protein, EXS family::PFF0365c::(OPFF72474)
PFF0435w ornithine aminotransferase::PFF0435w::(OPFF72412)
PFF0490w hypothetical protein::PFF0490w::(PMAL6P1.102_2416)
PFF0500c step II splicing factor, putative::PFF0500c::(F38861_1)
PFF0570c hypothetical protein::PFF0570c::(PMAL6P1.308_619)
PFF0580w hypothetical protein::PFF0580w::(OPFF72489)
PFF0595c hypothetical protein::PFF0595c::(PMAL6P1.303_4968)
PFF0620c hypothetical protein::PFF0620c::(OPFF72480)
PFF0670w hypothetical protein::PFF0670w::(E9475_1)
PFF0695w hypothetical protein, conserved::PFF0695w::(OPFF72512)
PFF0775w pyridoxal kinase-like protein, putative::PFF0775w::(OPFF72459)
PFF0785w hypothetical protein, conserved::PFF0785w::(PMAL6P1.264_388)
PFF0825c mitochondrial import receptor subunit tom40::PFF0825c::(PMAL6P1.256_494)
PFF0885w 60S ribosomal protein L27a, putative::PFF0885w::(OPFF72427)
PFF0905w hypothetical protein::PFF0905w::(PMAL6P1.240_748)
PFF0925w hypothetical protein::PFF0925w::(PMAL6P1.236_640)
PFF0940c cell division cycle protein 48 homologue, putative::PFF0940c::(F4425_1)
PFF0955c hypothetical protein::PFF0955c::(OPFF72446)
PFF1030w hypothetical protein, conserved::PFF1030w::(F30774_1)
PFF1065c hypothetical protein::PFF1065c::(PMAL6P1.207_638)
PFF1080w hypothetical protein, conserved::PFF1080w::(PMAL6P1.204_137)
PFF1260c hypothetical protein::PFF1260c::(D5782_1)
PFF1270c hypothetical protein::PFF1270c::(OPFF72513)
PFF1280w hypothetical protein::PFF1280w::(E18868_1)
PFF1355w hypothetical protein::PFF1355w::(OPFF72509)
PFF1365c hypothetical protein::PFF1365c::(D27403_1)
PFF1375c ethanalaminephosphotransferase, putative::PFF1375c::(OPFF72461)
PFF1425w RNA binding protein, putative::PFF1425w::(E18025_1)
PFI0085c hypothetical protein::PFI0085c::(I3470_1)
PFI0130c hypothetical protein::PFI0130c::(I15913_1)
PFI0135c papain family cysteine protease, putative::PFI0135c::(I587_1)
PFI0145w hypothetical protein::PFI0145w::(PFI0145W_292)
PFI0155c ras family GTP-ase, putative::PFI0155c::(I17263_1)
PFI0160w hypothetical protein::PFI0160w::(E25749_1)
PFI0180w alpha tubulin::PFI0180w::(I16837_2)
PFI0215c signal peptidase, putative::PFI0215c::(OPFI17697)
PFI0235w replication factor A-related protein, putative::PFI0235w::(F18417_1)
PFI0280c hypothetical protein, conserved::PFI0280c::(I4355_3)
PFI0335w hypothetical protein::PFI0335w::(I15927_5)
PFI0380c formylmethionine deformylase, putative::PFI0380c::(I9302_2)
PFI0475w small nuclear ribonucleoprotein (snRNP), putative::PFI0475w::(I5180_1)
PFI0505c selenophosphate synthetase, putative::PFI0505c::(I3489_1)
PFI0540w hypothetical protein::PFI0540w::(E25593_1)
PFI0570w GTP-binding protein, putative::PFI0570w::(F5048_1)
PFI0575c hypothetical protein::PFI0575c::(KN1713_1)
PFI0590c hypothetical protein::PFI0590c::(OPFI17707)
PFI0610w hypothetical protein::PFI0610w::(OPFI17724)
PFI0645w EF-1B::PFI0645w::(F19787_1)
PFI0670w hypothetical protein, conserved::PFI0670w::(I6724_2)
PFI0675w hypothetical protein::PFI0675w::(F67796_1)
PFI0725c hypothetical protein::PFI0725c::(I4179_1)
PFI0730w hypothetical protein::PFI0730w::(F48839_1)
PFI0750c hypothetical protein::PFI0750c::(I884_1)
PFI0760w hypothetical protein::PFI0760w::(I17631_1)
PFI0820c RNA-binding protein, putative::PFI0820c::(I16748_1)
PFI0860c ATP-dependant RNA helicase, putative::PFI0860c::(F51170_1)
PFI0870w hypothetical protein::PFI0870w::(E11286_1)
PFI0890c large ribosomal subunit protein L3, prokaryotic (50S)-like, putative::PFI0890c::(I6033_4)
PFI0895c hypothetical protein, conserved::PFI0895c::(I15861_1)
PFI0910w DNA helicase, putative::PFI0910w::(I3002_1)
PFI0925w gamma-glutamylcysteine synthetase::PFI0925w::(F46067_3)
PFI0975c hypothetical protein::PFI0975c::(F37098_2)
PFI1000w hypothetical protein::PFI1000w::(I4780_1)
PFI1005w ADP-ribosylation factor-like protein, putative::PFI1005w::(I3555_1)
PFI1070c hypothetical protein::PFI1070c::(I4487_1)
PFI1075w hypothetical protein::PFI1075w::(F61293_1)
PFI1110w glutamate-ammonia ligase (glutamine synthetase), putative::PFI1110w::(I4989_2)
PFI1155w hypothetical protein::PFI1155w::(OPFI17661)
PFI1160w hypothetical protein::PFI1160w::(I17587_1)
PFI1170c Thioredoxin reductase::PFI1170c::(F64095_4)
PFI1240c prolyl-t-RNA synthase, putative::PFI1240c::(I1781_2)
PFI1245c Protein phosphatase-beta::PFI1245c::(I5252_1)
PFI1295c membrane transporter, putative::PFI1295c::(OPFI17700)
PFI1320c hypothetical protein::PFI1320c::(I13466_1)
PFI1325w hypothetical protein::PFI1325w::(OPFI17667)
PFI1405c hypothetical protein::PFI1405c::(KN5081_1)
PFI1420w guanylate kinase, putative::PFI1420w::(OPFI17660)
PFI1445w hypothetical protein::PFI1445w::(F5910_2)
PFI1470c hypothetical protein::PFI1470c::(I12692_1)



PFI1475w merozoite surface protein 1, precursor::PFI1475w::(F8511_1)
PFI1515w hypothetical protein::PFI1515w::(PPFI1515W_82)
PFI1520w hypothetical protein::PFI1520w::(D56470_1)
PFI1575c peptide release factor, putative::PFI1575c::(F27464_2)
PFI1610c hypothetical protein::PFI1610c::(PPFI1610C_208)
PFI1625c organelle processing peptidase, putative::PFI1625c::(F26774_1)
PFI1720w hypothetical protein::PFI1720w::(F68282_1)
PFI1735c hypothetical protein::PFI1735c::(F37100_2)
PFI1740c hypothetical protein::PFI1740c::(OPFI17638)
PFI1745c hypothetical protein::PFI1745c::(PPFI1745C_158)
PFI1755c hypothetical protein::PFI1755c::(I12552_2)
PFI1760w hypothetical protein::PFI1760w::(PPFI1760W_133)
PFI1780w hypothetical protein::PFI1780w::(OPFI17716)
PFL0035c octapeptide-repeat antigen, putative::PFL0035c::(L1_28)
PFL0110c PfmpC::PFL0110c::(L1_63)
PFL0140w hypothetical protein::PFL0140w::(PPFL0140W_120)
PFL0225c hypothetical protein::PFL0225c::(L2_10)
PFL0280c hypothetical protein::PFL0280c::(L2_31)
PFL0355c hypothetical protein::PFL0355c::(L2_72)
PFL0400w 50S ribosomal protein L29, putative::PFL0400w::(L2_101)
PFL0415w acyl carrier protein, mitochondrial precursor, putative::PFL0415w::(KN46_3)
PFL0430w tim10 homologue, putative::PFL0430w::(L2_114)
PFL0465c Zinc finger transcription factor (krox1)::PFL0465c::(PPFL0465C_3366)
PFL0485w hypothetical protein::PFL0485w::(L2_139)
PFL0500w 50S ribosomal protein L1, putative::PFL0500w::(L2_146)
PFL0505c hypothetical protein::PFL0505c::(L2_147)
PFL0585w PfpUB Plasmodium falciparum polyubiquitin::PFL0585w::(L2_187)
PFL0610w hypothetical protein::PFL0610w::(L2_194)
PFL0615w hypothetical protein::PFL0615w::(L2_199)
PFL0660w dynein light chain 1, putative::PFL0660w::(L2_212)
PFL0720w hypothetical protein::PFL0720w::(L2_246)
PFL0765w hypothetical protein::PFL0765w::(L2_265)
PFL0785c signal recognition particle 19 kd protein, putative::PFL0785c::(L2_276)
PFL0825c hypothetical protein::PFL0825c::(L3_3)
PFL0940c erythrocyte membrane protein 1 (PfEMP-1) pseudogene::PFL0940c::(J1058_1)
PFL0960w D-ribulose-5-phosphate 3-epimerase, putative::PFL0960w::(OPFL0048)
PFL0970w pre-mRNA splicing factor, putative::PFL0970w::(J938_1)
PFL1010c hypothetical protein conserved::PFL1010c::(KN267_1)
PFL1025c hypothetical protein::PFL1025c::(J2541_2)
PFL1075w hypothetical protein::PFL1075w::(KN2497_2)
PFL1140w hypothetical protein, conserved::PFL1140w::(OPFL0109)
PFL1180w Chromatin assembly protein (ASF1), putative::PFL1180w::(KN5186_1)
PFL1350w RNA pseudouridylate synthase, putative::PFL1350w::(OPFL0122)
PFL1390w hypothetical protein::PFL1390w::(KN3690_1)
PFL1405w hypothetical protein::PFL1405w::(F22280_1)
PFL1415w hypothetical protein::PFL1415w::(PPFL1415W_1260)
PFL1465c heat shock protein hslv, putative::PFL1465c::(OPFL0038)
PFL1520w dim1 protein homolog, putative::PFL1520w::(OPFL0027)
PFL1545c chaperonin cpn60::PFL1545c::(OPFL0016)
PFL1585c hypothetical protein::PFL1585c::(KN5414_1)
PFL1605w hypothetical protein::PFL1605w::(J3424_1)
PFL1650w hypothetical protein::PFL1650w::(KN1007_1)
PFL1655c hypothetical protein::PFL1655c::(KN973_2)
PFL1665c hypothetical protein::PFL1665c::(I13218_1)
PFL1685w hypothetical protein, conserved::PFL1685w::(OPFL0102)
PFL1740w hypothetical protein::PFL1740w::(OPFL0147)
PFL1790w ubiquitin activating enzyme, putative::PFL1790w::(KN1056_2)
PFL1830w ubiquitin-like protein, putative::PFL1830w::(PPFL1830W_6)
PFL1845c calyculin binding protein, putative::PFL1845c::(OPFL0091)
PFL1865w hypothetical protein::PFL1865w::(PPFL1865W_5205)
PFL1890c hypothetical protein, conserved::PFL1890c::(OPFL0112)
PFL1900w hypothetical protein::PFL1900w::(E25972_1)
PFL1905w hypothetical protein::PFL1905w::(PPFL1905W_140)
PFL1920c hydroxyethylthiazole kinase, putative::PFL1920c::(OPFL0087)
PFL1945c hypothetical protein::PFL1945c::(OPFL0045)
PFL1960w erythrocyte membrane protein 1 (PfEMP1)::PFL1960w::(KM1590_2)
PFL1980c hypothetical protein::PFL1980c::(PPFL1980C_68)
PFL2095w Translation initiation factor SUI1, putative::PFL2095w::(PPFL2095W_60)
PFL2180w 50S ribosomal protein L3, putative::PFL2180w::(OPFL0098)
PFL2195w hypothetical protein::PFL2195w::(A14263_1)
PFL2205w hypothetical protein::PFL2205w::(KN400_1)
PFL2245w hypothetical protein::PFL2245w::(KN1106_5)
PFL2260w hypothetical protein::PFL2260w::(KN5610_3)
PFL2280w cyclin g-associated kinase, putative::PFL2280w::(KN672_1)
PFL2415w Hbeta58/Vps26 protein homolog, putative::PFL2415w::(KN8928_1)
PFL2445c hypothetical protein::PFL2445c::(OPFL0145)
PFL2460w coronin::PFL2460w::(OPFL0013)
PFL2485c tryptophanyl-tRNA synthetase, putative::PFL2485c::(PPFL2485C_117)
PFL2530w hypothetical protein::PFL2530w::(OPFL0121)
PFL2540w hypothetical protein::PFL2540w::(PPFL2540W_151)
PFL2560c hypothetical protein::PFL2560c::(PPFL2560C_2)
PFL2565w hypothetical protein::PFL2565w::(M30262_1)
pla_rpl14 plastid ribosomal protein 14, large subunit::pla_rpl14::(PRPL14)
pla_rpl16 plastid ribosomal protein 16, large subunit::pla_rpl16::(PRPL16)
pla_rpl4 plastid ribosomal protein 4, large subunit::pla_rpl4::(PRPL4)
pla_rps3 plastid ribosomal protein 3, small subunit::pla_rps3::(PRPS3)
pla_rps5 plastid ribosomal protein 5, small subunit::pla_rps5::(PRPS5)
pla_tRNA-Gly plastid tRNA-Gly::pla_tRNA-Gly::(PTRNA-GLY)
pla_tRNA-Gly2 plastid tRNA-Gly2::pla_tRNA-Gly2::(PTRNA-GLY2)
pla_tRNA-Pro plastid tRNA-Pro::pla_tRNA-Pro::(PTRNA-PRO)
pla_tRNA-Trp plastid tRNA-Trp::pla_tRNA-Trp::(PTRNA-TRP)

APPENDIX C

INTERACTOME DATA COMPARISON

Interactome data obtained from <http://www.cbil.upenn.edu/plasmoMAP/index-v1.html#log> and used with permission from S. Date

| Strain selected: 3D7 | | | |
|---|------------|---|---|
| Query: PF10_0322 S-adenosylmethionine decarboxylase-ornithine decarboxylase | | | |
| Score | Protein ID | Description | Present in PFA0MetDC/ODC co-inhibition differential abundance dataset |
| 9.53 | PF11_0317 | structural maintenance of chromosome protein, putative | |
| 8.31 | PFE0195w | P-type ATPase, putative | |
| 7.98 | PFA0390w | DNA repair exonuclease, putative | |
| 6.62 | MAL8P1.99 | hypothetical protein | Yes |
| 6.62 | PF11_0427 | dolichyl-phosphate b-D-mannosyltransferase, putative | |
| 6.62 | PF07_0129 | ATP-dept. acyl-coa synthetase | Yes |
| 6.62 | PFA0590w | ABC transporter, putative | Yes |
| 5.9 | PF10_0260 | hypothetical protein | |
| 5.9 | PF13_0348 | hypothetical protein | |
| 5.7 | PF14_0053 | ribonucleotide reductase small subunit | Yes |
| 4.71 | PFD0685c | chromosome associated protein, putative | Yes |
| 4.71 | PFC0125w | ABC transporter, putative | Yes |
| 4.71 | PF14_0709 | ribosomal protein L20, putative | Yes |
| 4.71 | PF08_0131 | 1-cys peroxidoxin | Yes |
| 4.71 | PF11_0117 | replication factor C subunit 5, putative | Yes |
| 4.71 | PF11_0181 | tyrosine --tRNA ligase, putative | Yes |
| 4.71 | PFB0180w | 5'-3' exonuclease, N-terminal resolvase-like domain, putative | Yes |
| 4.71 | PFL2180w | 50S ribosomal protein L3, putative | |
| 4.71 | PF14_0097 | cytidine diphosphate-diacylglycerol synthase | |
| 4.71 | PF14_0081 | DNA repair helicase, putative | Yes |
| 4.71 | PF11_0044 | hypothetical protein | |
| 4.71 | PF11_0197 | hypothetical protein | |
| 4.52 | PF14_0338 | hypothetical protein | |
| 4.52 | PF14_0397 | hypothetical protein, conserved | |
| 4.52 | PF10_0362 | DNA polymerase zeta catalytic subunit, putative | |
| 4.52 | PFB0605w | Ser/Thr protein kinase, putative | Yes |
| 4.52 | PF08_0034 | histone acetyltransferase Gcn5 | |
| 4.52 | PF10_0132 | phospholipase C-like, putative | |
| 4.52 | PFI1310w | NAD synthase, putative | |
| 4.52 | PF13_0016 | methyl transferase-like protein, putative | |
| 4.52 | PFB0520w | protein kinase, putative | |
| 4.52 | PF11_0049 | hypothetical protein, conserved | |
| 4.52 | PF11_0074 | hypothetical protein | |
| 4.52 | PF14_0161 | hypothetical protein, conserved | |
| 4.52 | PF14_0441 | pyruvate dehydrogenase E1 beta subunit, putative | |
| 4.52 | PFE0040c | PFEMP2 | Yes |
| 4.52 | MAL13P1.95 | ferredoxin | |
| 4.52 | PFE0585c | myo-inositol 1-phosphate synthase, putative | Yes |
| 4.52 | PF13_0021 | small heat shock protein, putative | |
| 4.52 | PFC0915w | ATP-dependent RNA helicase, putative | |



| Strain selected: 3D7 | | | |
|---|-------------|--|--|
| Query: PF10_0322 S-adenosylmethionine decarboxylase-ornithine decarboxylase | | | |
| Score | Protein ID | Description | Present in PfAdoMetDC/ODC co-inhibition differential abundance dataset |
| 4.52 | PFA0520c | chromatin assembly factor 1 protein WD40 domain, putative | Yes |
| 4.52 | PF08_0031 | oxoglutarate/malate translocator protein, putative | |
| 4.52 | PFI0910w | DNA helicase, putative | |
| 4.52 | PF14_0200 | hypothetical protein | |
| 4.39 | PFL1545c | chaperonin cpn60, mitochondrial precursor | Yes |
| 3.96 | PF11_0077 | hypothetical protein | |
| 3.96 | MAL8P1.17 | disulfide isomerase precursor, putative | |
| 3.96 | PF14_0570 | hypothetical protein, conserved | Yes |
| 3.68 | PFE1155c | mitochondrial processing peptidase alpha subunit, putative | |
| 3.68 | PF14_0309 | protein-L-isospartate O-methyltransferase beta-aspartate methyltransferase, putative | Yes |
| 3.38 | PFC0955w | ATP-dependent RNA helicase | |
| 3.38 | PFI0490c | hypothetical protein | Yes |
| 3.38 | MAL8P1.157 | hypothetical protein | |
| 3.38 | MAL13P1.138 | hypothetical protein | |
| 3.38 | PF14_0255 | hypothetical protein | |
| 3.38 | PF13_0242 | isocitrate dehydrogenase (NADP), mitochondrial precursor | |
| 3.38 | PFE1320w | hypothetical protein | |
| 3.38 | PFL2245w | hypothetical protein | |
| 3.38 | PFI0670w | hypothetical protein, conserved | |
| 3.38 | PF14_0354 | hypothetical protein | Yes |
| 3.38 | PFB0215c | 3'-5' exonuclease, putative | |
| 3.38 | PF14_0101 | hypothetical protein | |
| 3.38 | PFL0660w | dynein light chain 1, putative | Yes |
| 3.38 | PF14_0112 | POM1, putative | Yes |
| 3.38 | PF14_0348 | ATP-dependent Clp protease proteolytic subunit, putative | Yes |
| 3.38 | PF13_0322 | falcilysin | |
| 3.38 | PF14_0192 | glutathione reductase | Yes |
| 3.38 | PF10_0235 | hypothetical protein | |
| 3.38 | PFE0675c | deoxyriboflavin photolyase (photoreactivating enzyme, DNA photolyase), putative | Yes |
| 3.38 | PFL1070c | endoplasmic homolog precursor, putative | |
| 3.38 | PFC0165w | hypothetical protein | |
| 3.38 | PF13_0117 | hypothetical protein, conserved | |
| 3.34 | PF14_0318 | hypothetical protein | |
| 3.34 | PFE0645w | hypothetical protein | |
| 3.34 | PFI1120c | hypothetical protein | |
| 3.34 | PF08_0010 | hypothetical protein | |
| 3.34 | PF10_0234 | hypothetical protein | |
| 3.34 | MAL13P1.107 | hypothetical protein | Yes |
| 3.34 | PF13_0077 | DEAD box helicase, putative | |
| 3.34 | MAL13P1.180 | hypothetical protein | |



| Strain selected: 3D7 | | | |
|---|-------------|--|--|
| Query: PF10_0322 S-adenosylmethionine decarboxylase-ornithine decarboxylase | | | |
| Score | Protein ID | Description | Present in PFAdoMetDC/ODC co-inhibition differential abundance dataset |
| 3.34 | PF11_0365 | hypothetical protein | Yes |
| 3.34 | PF14_0394 | hypothetical protein | |
| 3.34 | MAL13P1.295 | hypothetical protein | |
| 3.34 | PF14_0014 | hypothetical protein | |
| 3.34 | PF14_0471 | hypothetical protein | |
| 3.34 | MAL13P1.90 | hypothetical protein | |
| 3.34 | PF11_0219 | hypothetical protein | |
| 3.34 | PFA0615w | hypothetical protein | |
| 3.34 | PFF0115c | | |
| 3.34 | PFA0195w | hypothetical protein | |
| 3.34 | PFA0175w | hypothetical protein | |
| 3.34 | PFL0485w | hypothetical protein | |
| 3.34 | PF14_0310 | hypothetical protein | |
| 3.34 | PFI0610w | hypothetical protein | |
| 3.34 | MAL7P1.111 | hypothetical protein | |
| 3.34 | PF11_0054 | hypothetical protein | |
| 3.34 | PFE0310c | hypothetical protein | |
| 3.34 | PF10_0226 | hypothetical protein, conserved | |
| 3.34 | PF08_0046 | hypothetical protein | |
| 3.34 | PFL0965c | hypothetical protein | |
| 3.34 | MAL13P1.332 | hypothetical protein | |
| 3.34 | PFF0655c | | Yes |
| 3.34 | PF14_0176 | hypothetical protein | |
| 3.34 | MAL8P1.55 | hypothetical protein | |
| 3.34 | MAL13P1.127 | hypothetical protein | |
| 3.34 | PFF0555w | | |
| 3.34 | MAL8P1.11 | hypothetical protein | |
| 3.34 | MAL8P1.86 | hypothetical protein | Yes |
| 3.34 | MAL13P1.266 | hypothetical protein | |
| 3.34 | PFL0605c | hypothetical protein | |
| 3.34 | PF13_0192 | hypothetical protein | Yes |
| 3.34 | PF11_0248 | hypothetical protein | Yes |
| 3.34 | PFB0185w | hypothetical protein | |
| 3.34 | MAL13P1.325 | hypothetical protein | |
| 3.34 | PF08_0067 | hypothetical protein | |
| 3.34 | PFL1675c | hypothetical protein | |
| 3.34 | PFC0230c | hypothetical protein | |
| 3.34 | PFA0460c | tubulin-specific chaperone a, putative | |
| 3.34 | PF14_0306 | hypothetical protein | |
| 3.34 | PF13_0134 | hypothetical protein | |
| 3.34 | MAL7P1.114 | T gondii P36-like protein; | |

| Strain selected: 3D7 | | | |
|---|-------------|-----------------------------|--|
| Query: PF10_0322 S-adenosylmethionine decarboxylase-ornithine decarboxylase | | | |
| Score | Protein ID | Description | Present in PFAdoMetDC/ODC co-inhibition differential abundance dataset |
| 3.34 | PFI0585c | hypothetical protein | |
| 3.34 | PF14_0253 | hypothetical protein | |
| 3.34 | PF13_0080 | hypothetical protein | |
| 3.34 | PFF0225w | | |
| 3.34 | PFL1275c | hypothetical protein | |
| 3.34 | PF14_0498 | hypothetical protein | |
| 3.34 | PFF1175c | | |
| 3.34 | PFF0770c | | |
| 3.34 | PFF1395c | | |
| 3.34 | MAL7P1.157 | hypothetical protein | |
| 3.34 | PFF0935c | | Yes |
| 3.34 | PFF0400w | | |
| 3.34 | PF14_0356 | hypothetical protein | |
| 3.34 | PF14_0300 | syntaxin, putative | |
| 3.34 | MAL7P1.74 | hypothetical protein | |
| 3.34 | MAL13P1.390 | | |
| 3.34 | PFF1140c | | |
| 3.34 | PF10_0032 | hypothetical protein | |
| 3.34 | PF14_0186 | hypothetical protein | |
| 3.34 | PF14_0430 | hypothetical protein | Yes |
| 3.34 | PFL0095c | hypothetical protein | |
| 3.34 | PF08_0080 | hypothetical protein | |
| 3.34 | PFB0600c | hypothetical protein | |
| 3.34 | PF13_0241 | hypothetical protein | |
| 3 | PF11_0258 | co-chaperone GrpE, putative | |
| 3 | PFB0685c | acyl-CoA synthetase | |



Interactome data obtained from <http://www.cbil.upenn.edu/plasmoMAP/index-v1.html#log> and used with permission from S. Date

| Strain selected: 3D7 | | | |
|---|-------------|--|--|
| Query: PF08_0095 dihydropteroate synthase/dihydroxymethylpterin pyrophosphokinase | | | |
| Score | Protein ID | Description | Present in PFAdoMetDC/ODC co-inhibition differential abundance dataset |
| 10.32 | PF13_0140 | dihydrofolate synthase/folypolyglutamate synthase | |
| 8.31 | PFL0740c | 10 kd chaperonin, putative | |
| 8.31 | PF11_0258 | co-chaperone GrpE, putative | |
| 8.31 | PF13_0180 | chaperonin, putative | |
| 7.98 | PF08_0006 | prohibitin, putative | |
| 7.98 | PFL1475w | sun-family protein, putative | |
| 5.96 | PF13_0234 | phosphoenolpyruvate carboxykinase | |
| 5.96 | PF11_0188 | heat shock protein 90, putative | |
| 5.96 | PF14_0656 | U2 snRNP auxiliary factor, putative | |
| 5.96 | PF14_0242 | arginine n-methyltransferase, putative | |
| 5.9 | PFB0953w | hypothetical protein | Yes |
| 5.9 | MAL7P1.209 | | |
| 5.9 | PFF0945c | | |
| 5.9 | PFE0060w | hypothetical protein | |
| 5.9 | PF11_0076 | hypothetical protein | |
| 5.9 | PFF0775w | | |
| 5.9 | PF10_0013 | hypothetical protein | |
| 5.9 | MAL8P1.124 | hypothetical protein | |
| 5.9 | PF14_0705 | hypothetical protein | |
| 5.9 | PFE1230c | hypothetical protein, conserved | |
| 5.9 | PF13_0300 | mitochondrial inner membrane translocase, putative | |
| 5.9 | MAL8P1.15 | hypothetical protein | |
| 5.9 | PFE1245w | zinc finger protein, putative | Yes |
| 5.9 | PF11_0511 | hypothetical protein | |
| 5.9 | PFC0790w | hypothetical protein | |
| 5.9 | PF13_0015 | hypothetical protein | |
| 5.9 | PFA0160c | integral membrane protein | |
| 5.9 | MAL13P1.73 | hypothetical protein | |
| 5.9 | PF14_0674 | hypothetical protein | |
| 5.9 | MAL13P1.318 | hypothetical protein | |
| 4.71 | PFB0525w | asparagine -- tRNA ligase, putative | |
| 4.71 | PFL1210w | hypothetical protein | |
| 4.71 | PF07_0079 | 60S ribosomal protein L11a, putative | |
| 4.71 | PFL1425w | t-complex protein 1, gamma subunit, putative | |
| 4.71 | MAL13P1.284 | pyrroline carboxylate reductase | |
| 4.71 | PF11100w | Para-aminobenzoic acid synthetase | |
| 4.71 | PFE0475w | asparagine -- t RNA ligase, putative | |



| Strain selected: 3D7 | | | |
|---|------------|---|--|
| Query: PF08_0095 dihydropteroate synthase/dihydroxymethylpterin pyrophosphokinase | | | |
| Score | Protein ID | Description | Present in PFAdoMetDC/ODC co-inhibition differential abundance dataset |
| 4.71 | PF14_0370 | RNA helicase, putative | |
| 4.71 | PFC0285c | T-complex protein beta subunit, putative | |
| 4.52 | PFL0705c | adrenodoxin-type ferredoxin, putative | |
| 4.52 | PFB0545c | ribosomal protein L7/L12, putative | |
| 4.52 | PF14_0023 | hypothetical protein, conserved | |
| 4.52 | PF11_0339 | hypothetical protein | |
| 4.52 | PFA0145c | aspartyl-tRNA synthetase | |
| 4.52 | PF14_0517 | peptidase, putative | |
| 4.52 | PF14_0230 | Ribosomal protein family L5, putative | |
| 4.52 | PF13_0345 | aminomethyltransferase, mitochondrial precursor | |
| 4.52 | PFB0595w | heat shock 40 kDa protein, putative | |
| 4.52 | PFD0755c | adenylate kinase 1 | |
| 4.52 | PF11_0077 | hypothetical protein | |
| 4.52 | PF08_0018 | Translation initiation factor like protein | |
| 4.52 | PFL2395c | dimethyladenosine transferase, putative | |
| 4.52 | PFL1150c | ribosomal protein L24, putative | |
| 4.52 | PF10_0121 | hypoxanthine phosphoribosyltransferase | |
| 4.52 | PF10_0325 | hypothetical protein, conserved | |
| 4.39 | PF14_0668 | hypothetical protein | |
| 4.39 | PF14_0036 | acid phosphatase, putative | |
| 4.39 | PFB0115w | hypothetical protein | Yes |
| 4.39 | PF14_0297 | putative | Yes |
| 4.39 | PFE0605c | glutathione synthetase | |
| 4.39 | PFL0255c | putative | |
| 4.39 | PFL1310c | ATP-dependent RNA helicase, putative | |
| 4.39 | PF11_0264 | DNA-dependent RNA polymerase | |
| 4.39 | PF11_0351 | heat shock protein hsp70 homologue | |
| 4.39 | PF13_0243 | hypothetical protein | |
| 4.39 | PF11570c | aminopeptidase, putative | |
| 4.39 | PF14_0022 | exopolyphosphatase, putative | |
| 3.38 | PFE0630c | orotate phosphoribosyltransferase, putative | |
| 3.38 | MAL13P1.54 | hypothetical protein, conserved | |
| 3.38 | PF14_0378 | triose-phosphate isomerase | Yes |
| 3.38 | PF10_0153 | hsp60 | Yes |
| 3.38 | PFC0271c | glutaredoxin, putative | |
| 3.38 | PF11_0165 | falcipain 2 precursor | |
| 3.38 | PFD0980w | holo-(acyl-carrier protein) synthase, putative | |
| 3.38 | PFB0200c | aspartate aminotransferase, putative | |



| Strain selected: 3D7 | | | |
|---|-------------|--|--|
| Query: PF08_0095 dihydropteroate synthase/dihydroxymethylpterin pyrophosphokinase | | | |
| Score | Protein ID | Description | Present in PFAdoMetDC/ODC co-inhibition differential abundance dataset |
| 3.38 | PFE1080w | putative | |
| 3.38 | PF14_0381 | delta-aminolevulinic acid dehydratase | |
| 3.38 | PF11_0507 | antigen 332, putative | |
| 3.38 | PF14_0147 | ATP-dependent protease, putative | |
| 3.38 | PFC0550w | hypothetical protein | |
| 3.38 | PF14_0166 | lysine -- tRNA ligase, putative | |
| 3.38 | PF13_0141 | L-lactate dehydrogenase | Yes |
| 3.38 | PFD0555c | hypothetical protein | |
| 3.38 | PF11_0301 | spermidine synthase | |
| 3.38 | PFC0205c | PfGLP-1, 1-cys-glutaredoxin-like protein-1 | |
| 3.38 | PFL1710c | tetQ family GTPase, putative | |
| 3.38 | PF10_0152 | hypothetical protein | |
| 3.38 | PFL0690c | hypothetical protein | |
| 3.38 | PF07_0100 | hypothetical protein | |
| 3.38 | PF14_0341 | glucose-6-phosphate isomerase | |
| 3.38 | PF14_0096 | hypothetical protein | Yes |
| 3.34 | PF14_0209 | hypothetical protein | |
| 3.34 | PF10_0064 | hypothetical protein | |
| 3.34 | MAL13P1.221 | | |
| 3.34 | PF11750c | hypothetical protein | |
| 3.34 | PFF0105w | | |
| 3.34 | PF13_0029 | hypothetical protein | |
| 3.34 | PFF1330c | | |
| 3.34 | PF08_0029 | hypothetical protein | |
| 3.34 | PFD0365c | hypothetical protein | |
| 3.34 | PF14_0410 | hypothetical protein | |
| 3.34 | PFE0295w | hypothetical protein | |
| 3.34 | PF11_0319 | hypothetical protein | |
| 3.34 | PF13_0183 | hypothetical protein | Yes |
| 3.34 | PFB0470w | hypothetical protein | |
| 3.34 | PF14_0037 | hypothetical protein | |
| 3.34 | PFA0630c | hypothetical protein | |
| 3.34 | PFF0820w | | |
| 3.34 | PFL2355w | hypothetical protein | |
| 3.34 | PFB0620w | hypothetical protein | |
| 3.34 | PFB0560w | hypothetical protein | |
| 3.34 | PFF0120w | | |
| 3.34 | PF11_0404 | malaria antigen | |



| Strain selected: 3D7 | | | |
|---|-------------|---|--|
| Query: PF08_0095 dihydropteroate synthase/dihydroxymethylpterin pyrophosphokinase | | | |
| Score | Protein ID | Description | Present in PFAdoMetDC/ODC co-inhibition differential abundance dataset |
| 3.34 | PFE1605w | protein with DNAJ domain | |
| 3.34 | PF13_0098 | hypothetical protein | |
| 3.34 | PF14_0312 | hypothetical protein | |
| 3.34 | PF08_0051 | hypothetical protein | Yes |
| 3.34 | PFE0670w | hypothetical protein | |
| 3.34 | MAL8P1.32 | nucleoside transporter, putative | Yes |
| 3.34 | PFI1415w | Serine/Threonine protein kinase, putative | |
| 3.34 | PF13_0191 | hypothetical protein | |
| 3.34 | MAL13P1.46 | hypothetical protein | |
| 3.34 | PFI1615c | | |
| 3.34 | PF14_0180 | hypothetical protein | |
| 3.34 | PFB0921c | hypothetical protein | |
| 3.34 | PF14_0687 | hypothetical protein | |
| 3.34 | PFF1335c | | |
| 3.34 | PFI0430c | hypothetical protein | |
| 3.34 | PFA0100c | hypothetical protein | |
| 3.34 | MAL13P1.333 | hypothetical protein | |
| 3.34 | PFE0800w | hypothetical protein | |
| 3.34 | PFB0110w | hypothetical protein | |
| 3.34 | PF13_0281 | hypothetical protein | |
| 3.34 | PFC0166w | | |
| 3.34 | PF13_0101 | hypothetical protein | |
| 3.34 | PFF0590c | | |
| 3.34 | PF13_0252 | nucleoside transporter 1 | |
| 3.34 | PF11_0247 | hypothetical protein | |
| 3.34 | PFC0085c | hypothetical protein | Yes |
| 3.34 | PF11_0254 | hypothetical protein | |
| 3.34 | PF10_0324 | hypothetical protein | |
| 3.34 | MAL7P1.225 | | |
| 3.34 | PFF0435w | | Yes |
| 3.34 | PFL0640w | hypothetical protein | |
| 3.34 | PF13_0097 | hypothetical protein | |
| 3.34 | PFB0930w | hypothetical protein | |
| 3.34 | MAL13P1.352 | hypothetical protein | |
| 3.34 | PFF1400w | | |
| 3.34 | PF07_0075 | hypothetical protein | |
| 3.34 | PF11_0508 | hypothetical protein | Yes |
| 3.34 | PF11_0506 | hypothetical protein | |

| Strain selected: 3D7 | | | |
|---|-------------|----------------------|--|
| Query: PF08_0095 dihydropteroate synthase/dihydroxymethylpterin pyrophosphokinase | | | |
| Score | Protein ID | Description | Present in PFAdoMetDC/ODC co-inhibition differential abundance dataset |
| 3.34 | MAL7P1.31 | hypothetical protein | |
| 3.34 | PF13_0071 | hypothetical protein | |
| 3.34 | PF13_0099 | hypothetical protein | |
| 3.34 | MAL7P1.201 | | |
| 3.34 | PF10_0265 | hypothetical protein | |
| 3.34 | PF10_0029 | hypothetical protein | |
| 3.34 | PF13_0112 | hypothetical protein | |
| 3.34 | PFE0595w | hypothetical protein | |
| 3.34 | PFA0255c | hypothetical protein | Yes |
| 3.34 | MAL13P1.274 | | |
| 3.34 | PFI1385c | hypothetical protein | |
| 3.34 | PF14_0308 | hypothetical protein | |
| 3.34 | PFE1615c | hypothetical protein | Yes |

APPENDIX D

PROTEOMICS 2D-GE SPOT EXCISION LIST

| SSP | Annotation | Spot densities and ratios compared to UT _{T1} (relative t ₀) | | | | | | | |
|------|---|---|-------|-----------------|-------|-----------------|-------|-----------------|-------|
| | | UT _{T1} | Ratio | T _{T1} | Ratio | T _{T2} | Ratio | T _{T3} | Ratio |
| 213 | | 2869318 | 1 | 4508792 | 1.57 | 704448.6 | 0.25 | 1620015 | 0.56 |
| 215 | | 2190291 | 1 | 1211539 | 0.55 | 2648142 | 1.21 | 6412805 | 2.93 |
| 1102 | Falcpain-2 (PF11_0165) | 894643.1 | 1 | 867554.4 | 0.97 | 1054486 | 1.18 | 2591236 | 2.9 |
| 1707 | | 1336849 | 1 | 1334699 | 1 | 2516244 | 1.88 | 3913316 | 2.93 |
| 1722 | | 523218.4 | 1 | 759024.9 | 1.45 | 1902331 | 3.64 | 1688286 | 3.23 |
| 1828 | Human erythroid alpha-spectrin | 3680704 | 1 | 6395287 | 1.74 | 17274236 | 4.69 | 6387526 | 1.74 |
| 2006 | | 2906660 | 1 | 2399245 | 0.83 | 703373.1 | 0.24 | 1071395 | 0.37 |
| 2105 | | 68055.3 | 1 | 259310 | 3.81 | 206534.4 | 3.03 | 117665.2 | 1.73 |
| 2407 | Human beta-actin (fragment) | 3364660 | 1 | 4195220 | 1.25 | 4597818 | 1.37 | 9063727 | 2.69 |
| 2903 | Human erythroid alpha-spectrin | 4843321 | 1 | 4921287 | 1.02 | 14176775 | 2.93 | 16156811 | 3.34 |
| 2904 | Human erythroid alpha-spectrin | 1050788 | 1 | 6207556 | 5.91 | 3713321 | 3.53 | 4896287 | 4.66 |
| 2908 | Human erythroid alpha-spectrin | 2718422 | 1 | 2733009 | 1.01 | 7295902 | 2.68 | 4799249 | 1.77 |
| 4102 | | 708179.6 | 1 | 1431409 | 2.02 | 212995.4 | 0.3 | 353271.8 | 0.5 |
| 4109 | | 192948.1 | 1 | 248409.8 | 1.29 | 399896.7 | 2.07 | 509413.5 | 2.64 |
| 4110 | | 87676.6 | 1 | 73404 | 0.84 | 228144 | 2.6 | 335853.4 | 3.83 |
| 4302 | | 498470.5 | 1 | 604199.6 | 1.21 | 198448.3 | 0.4 | 258172.3 | 0.52 |
| 5106 | | 1254317 | 1 | 1421460 | 1.13 | 843056.3 | 0.67 | 472447.8 | 0.38 |
| 5201 | | 837381.3 | 1 | 281030.6 | 0.34 | 204343.8 | 0.24 | 274797 | 0.33 |
| 5207 | | 1261177 | 1 | 336372.6 | 0.27 | 435374.7 | 0.35 | 482240.5 | 0.38 |
| 5314 | | 396261.8 | 1 | 419522.3 | 1.06 | 1267443 | 3.2 | 1447255 | 3.65 |
| 6005 | | 527602.3 | 1 | 200273.7 | 0.38 | 147416.9 | 0.28 | 161523 | 0.31 |
| 6104 | | 770410.6 | 1 | 1071500 | 1.39 | 234813.4 | 0.3 | 187354.2 | 0.24 |
| 6105 | | 2009352 | 1 | 2198885 | 1.09 | 666891.9 | 0.33 | | 0 |
| 6505 | S-adenosylmethionine synthetase (PF11090w) ^a | 2509872 | 1 | 2592248 | 1.03 | 1781118 | 0.71 | 1200317 | 0.48 |
| 6506 | Ornithine aminotransferase (PFF0435w) ^b | 1042238 | 1 | 1420503 | 1.36 | 1489907 | 1.43 | 2313307 | 2.22 |
| 7103 | | 6916921 | 1 | 2988248 | 0.43 | 4419540 | 0.64 | 1842549 | 0.27 |
| 7104 | | 2328269 | 1 | 877185.6 | 0.38 | 272572 | 0.12 | 358543.8 | 0.15 |
| 7106 | | 1721574 | 1 | 2139107 | 1.24 | 416634.8 | 0.24 | 844223.1 | 0.49 |
| 7718 | | 2544799 | 1 | 588543.2 | 0.23 | 1293771 | 0.51 | 1031303 | 0.41 |
| 7817 | Elongation factor 2 (PF14_0486) | 572182.3 | 1 | 594160.1 | 1.04 | 1607578 | 2.81 | 873754.8 | 1.53 |
| 8001 | | 1304672 | 1 | 978171.5 | 0.75 | 447955.2 | 0.34 | 522991.3 | 0.4 |
| 8002 | | 3035502 | 1 | 980220.3 | 0.32 | 843949.5 | 0.28 | 898411.9 | 0.3 |
| 8004 | | 897505.3 | 1 | 1179157 | 1.31 | 132369.3 | 0.15 | 362044.2 | 0.4 |
| 8018 | | 4875407 | 1 | 812069.3 | 0.17 | 1234645 | 0.25 | 442642.3 | 0.09 |
| 8102 | | 38253012 | 1 | 10144632 | 0.27 | 9096348 | 0.24 | 8096272 | 0.21 |
| 8115 | | 1058422 | 1 | 991311.4 | 0.94 | 58656.1 | 0.06 | 143936.8 | 0.14 |
| 8201 | Pyridoxal-5-phosphate synthase pdx1 (PFF1025c) | 948551.1 | 1 | 943220.3 | 0.99 | 1506122 | 1.59 | 2393723 | 2.52 |
| 8203 | | 4472542 | 1 | 6114925 | 1.37 | 1879056 | 0.42 | 1532572 | 0.34 |
| 8207 | L-lactate dehydrogenase (PF13_0141) | 4834714 | 1 | 13598061 | 2.81 | 7629889 | 1.58 | 5320832 | 1.1 |
| 8301 | | 423341 | 1 | 516469.9 | 1.22 | 173934.7 | 0.41 | 109692.3 | 0.26 |
| 8705 | | 1807778 | 1 | 254621.6 | 0.14 | 848141.9 | 0.47 | 556224.1 | 0.31 |

a. Spot saturated on high intensity scan set, thus SSP number, spot densities and ratios provided obtained from medium intensity scan set.

b. Spot saturated on high intensity scan set, thus SSP number, spot densities and ratios provided obtained from medium intensity scan set.



APPENDIX E

METABOLOMICS DATA

| Metabolomics Data | Metabolite | Mode* | Blank | Relative I ₂ comparison [†] | | | | | | | | | | Parallel time point comparison [†] | | | | | | | | | |
|-------------------------------------|------------|-------|-----------|---|-----------------|-----------------|-----------------|-----------------|-----------------|------------------------|------------------------|------------------------|------------------------|---|------------------------|----------------------------------|----------------------------------|----------------------------------|----------------------------------|----------------------------------|----------------------------------|------|------|
| | | | | UT ₁ | UT ₂ | UT ₃ | T ₁₁ | T ₁₂ | T ₁₅ | UT ₁ -Blank | UT ₂ -Blank | UT ₃ -Blank | T ₁₁ -Blank | T ₁₂ -Blank | T ₁₅ -Blank | UT ₁ /UT ₂ | UT ₁ /UT ₃ | T ₁₁ /UT ₂ | T ₁₁ /UT ₃ | T ₁₂ /UT ₂ | T ₁₂ /UT ₃ | | |
| (2S)-methyldiacylglycerol | 1195.71 | | 6199.25 | 25745.86 | 36214.95 | 9476.89 | 17393.96 | 21955.51 | 5003.54 | 24550.16 | 35019.24 | 6281.18 | 16199.25 | 20769.80 | 1.00 | 4.91 | 7.00 | 1.66 | 2.24 | 4.15 | 1.66 | 0.66 | 0.59 |
| (S)-citrate | 3050.26 | | 22845.53 | 24512.04 | 12743.52 | 18155.29 | 19928.72 | 18840.08 | 19796.27 | 21461.78 | 9893.25 | 15105.03 | 16878.45 | 15589.82 | 1.00 | 0.88 | 0.45 | 0.76 | 0.85 | 0.79 | 0.76 | 0.79 | 0.61 |
| (S)-isoleucine | 231.11 | | 105200.93 | 89921.98 | 93922.06 | 909439.80 | 929360.90 | 869358.44 | 181973.73 | 899992.77 | 939502.96 | 906207.70 | 809193.79 | 869404.33 | 1.00 | 0.86 | 0.86 | 0.76 | 0.82 | 0.86 | 0.86 | 0.86 | 0.86 |
| 1,3-bisphosphoglycerate | 5.34 | | 139712.28 | 154684.31 | 13484.22 | 61756.76 | 118859.45 | 52307.67 | 139706.84 | 154678.97 | 13478.88 | 61751.42 | 118854.11 | 52302.33 | 1.00 | 1.11 | 0.10 | 0.44 | 0.85 | 0.37 | 0.44 | 0.77 | 3.88 |
| 2-dehydro-D-glucuronate | 202.15 | | 14471.40 | 12894.21 | 14393.52 | 16267.69 | 14212.60 | 13686.84 | 14269.25 | 12892.05 | 14191.37 | 16606.54 | 14010.45 | 13363.49 | 1.00 | 0.89 | 0.99 | 1.13 | 0.98 | 0.94 | 1.13 | 1.10 | 0.94 |
| 2-hydroxy-3-methylglutaredioic acid | 35.62 | | 38923.78 | 38517.42 | 44194.85 | 45191.79 | 42087.55 | 47053.73 | 35899.77 | 38492.39 | 44169.33 | 45166.77 | 42082.55 | 47038.71 | 1.00 | 1.07 | 1.23 | 1.25 | 1.12 | 1.31 | 1.26 | 1.05 | 1.06 |
| 2-hydroxyisovalerate | 515.91 | | 1452.12 | 1385.75 | 1918.27 | 2166.50 | 1455.67 | 1683.57 | 932.21 | 856.84 | 1398.16 | 1646.55 | 936.75 | 1163.66 | 1.00 | 0.93 | 1.00 | 1.77 | 1.00 | 1.23 | 1.77 | 1.08 | 0.94 |
| 3-hydroxyglucuronate | 102.98 | | 4221.93 | 32220.88 | 22933.80 | 24645.25 | 35869.23 | 18443.11 | 42109.95 | 32117.80 | 22830.52 | 24642.29 | 35765.25 | 38340.13 | 1.00 | 0.76 | 0.58 | 0.89 | 0.85 | 0.91 | 0.58 | 1.11 | 1.68 |
| 4-aminobutyrate | 3.96 | | 17.29 | 390.22 | 798.44 | 107.07 | 143.24 | 150.25 | 13.34 | 386.07 | 794.49 | 103.11 | 129.29 | 146.20 | 1.00 | 28.55 | 55.58 | 7.73 | 10.44 | 10.97 | 7.73 | 0.36 | 0.18 |
| 5-methylthioinosine | 4.76 | | 11483.09 | 8645.31 | 8451.01 | 254.31 | 137.22 | 295.59 | 1144.33 | 8640.65 | 8455.25 | 249.55 | 132.25 | 291.82 | 1.00 | 5.93 | 7.35 | 0.22 | 0.12 | 0.25 | 0.22 | 0.22 | 0.22 |
| acetylcamitine | 10.35 | | 49957.32 | 42084.15 | 341888.52 | 501773.75 | 382437.57 | 338650.50 | 49946.96 | 420837.80 | 341878.17 | 501763.40 | 382427.22 | 338645.55 | 1.00 | 0.84 | 0.68 | 1.00 | 0.79 | 0.68 | 1.00 | 0.53 | 0.59 |
| acetate | 27.07 | | 2499.17 | 5000.11 | 4787.74 | 2358.50 | 4184.80 | 4235.08 | 2472.10 | 4973.04 | 4760.67 | 2331.44 | 4187.73 | 4207.99 | 1.00 | 2.01 | 1.93 | 0.94 | 1.68 | 1.70 | 0.94 | 0.84 | 0.89 |
| adenosine | 4.16 | | 1358.93 | 2387.72 | 418.80 | 1554.80 | 726.51 | 205.60 | 1354.55 | 2385.55 | 414.33 | 1550.63 | 722.33 | 304.42 | 1.00 | 0.21 | 0.31 | 1.14 | 0.53 | 0.22 | 1.14 | 2.53 | 0.73 |
| ADP | 5.62 | | 16971.78 | 18399.19 | 16570.45 | 16610.10 | 20786.03 | 19005.98 | 16956.18 | 18393.59 | 16654.85 | 16604.50 | 20783.43 | 19004.38 | 1.00 | 0.99 | 0.99 | 0.89 | 1.12 | 1.02 | 0.89 | 1.13 | 1.16 |
| α-ketoglutarate | 1584.26 | | 22539.96 | 95137.44 | 121984.43 | 27856.16 | 62419.87 | 83299.99 | 20955.70 | 93553.18 | 120400.17 | 25971.90 | 60935.51 | 81715.73 | 1.00 | 4.46 | 5.75 | 1.24 | 2.30 | 3.90 | 1.24 | 0.65 | 0.68 |
| AMP | 10.06 | | 849.24 | 722.26 | 818.45 | 1123.51 | 579.56 | 988.45 | 839.19 | 712.20 | 809.39 | 1113.45 | 589.50 | 978.39 | 1.00 | 0.85 | 0.96 | 1.33 | 0.68 | 1.17 | 0.85 | 1.00 | 1.21 |
| asparagine | 4.16 | | 33590.86 | 27633.43 | 18459.56 | 28845.35 | 24090.40 | 23265.55 | 33576.67 | 27529.25 | 18455.57 | 28841.16 | 24092.22 | 23261.26 | 1.00 | 0.82 | 0.65 | 0.86 | 0.74 | 0.69 | 0.82 | 0.50 | 1.26 |
| asparagine | 5.22 | | 25136.41 | 18953.20 | 12823.20 | 21227.15 | 20713.26 | 16412.90 | 25126.18 | 18943.97 | 12823.20 | 21217.93 | 20703.84 | 16403.68 | 1.00 | 0.75 | 0.73 | 0.84 | 0.82 | 0.65 | 0.84 | 1.09 | 0.50 |
| aspartate | 18.70 | | 4716.37 | 3317.43 | 2831.34 | 4160.07 | 4007.29 | 3436.97 | 4697.68 | 3298.73 | 2812.64 | 4141.37 | 3996.59 | 3420.28 | 1.00 | 0.70 | 0.60 | 0.88 | 0.86 | 0.77 | 0.88 | 1.21 | 1.22 |
| ATP | 5.83 | | 16007.53 | 17327.84 | 88521.22 | 122398.50 | 165953.15 | 162020.37 | 160000.70 | 173191.01 | 88511.89 | 122368.67 | 165543.33 | 162022.64 | 1.00 | 1.05 | 0.58 | 0.79 | 1.16 | 0.95 | 0.78 | 1.11 | 1.63 |
| camitine | 6.99 | | 116141.47 | 11074.17 | 10737.03 | 13738.53 | 11578.28 | 8937.89 | 16174.48 | 11067.18 | 10732.04 | 13731.54 | 11588.30 | 8930.50 | 1.00 | 0.68 | 0.66 | 1.07 | 0.70 | 0.55 | 1.07 | 1.03 | 1.22 |
| cholesterol sulfate | 1314.69 | | 109053.99 | 106428.47 | 88812.73 | 102689.77 | 105255.15 | 85230.32 | 106739.30 | 105113.78 | 88498.08 | 102607.08 | 103940.47 | 83916.64 | 1.00 | 0.98 | 0.80 | 1.17 | 0.97 | 0.79 | 1.17 | 0.99 | 0.98 |
| cholesterol | 5072.60 | | 17931.89 | 91035.29 | 89940.49 | 121668.98 | 84781.07 | 80991.82 | 107429.20 | 90322.59 | 84437.88 | 121666.38 | 84747.47 | 80999.22 | 1.00 | 0.84 | 0.80 | 1.13 | 0.78 | 0.82 | 1.13 | 0.93 | 1.03 |
| crutinine | 51.56 | | 9495.90 | 10984.37 | 15293.86 | 11317.28 | 9798.37 | 13504.23 | 9414.85 | 10920.42 | 15241.91 | 11266.33 | 7626.42 | 13552.28 | 1.00 | 1.16 | 1.73 | 1.20 | 0.81 | 1.44 | 1.20 | 0.74 | 0.83 |
| deoxycholic acid | 10.21 | | 829.51 | 523.04 | 940.55 | 619.99 | 588.26 | 667.27 | 819.30 | 512.83 | 930.35 | 609.78 | 578.25 | 657.06 | 1.00 | 0.63 | 1.14 | 0.74 | 0.71 | 0.80 | 0.74 | 1.13 | 0.71 |
| dDIP | 5.48 | | 1469.12 | 1265.07 | 937.30 | 1284.32 | 1431.79 | 1696.84 | 1463.67 | 1250.62 | 931.85 | 1267.77 | 1426.34 | 1691.09 | 1.00 | 0.85 | 0.64 | 0.87 | 0.97 | 1.16 | 0.87 | 1.14 | 1.81 |
| D-glucuronate | 5.47 | | 25411.50 | 17045.62 | 29147.02 | 22644.29 | 23341.95 | 25022.15 | 25421.20 | 17036.35 | 29137.55 | 22634.92 | 23322.22 | 22644.29 | 1.00 | 1.20 | 0.67 | 1.11 | 0.89 | 0.92 | 1.11 | 0.89 | 1.37 |
| D-Glucuro-1-lactone-6-phosphate | 661.07 | | 6923.57 | 6915.42 | 7629.98 | 8670.51 | 8884.50 | 6132.35 | 6923.50 | 6254.35 | 6968.81 | 6005.44 | 6193.42 | 6471.19 | 1.00 | 1.00 | 1.11 | 0.96 | 0.99 | 0.87 | 0.96 | 0.99 | 0.79 |
| D-glyceraldehyde-3-phosphate | 5.74 | | 5178.56 | 6103.55 | 5418.45 | 28897.18 | 7322.24 | 7078.18 | 5178.56 | 6103.55 | 5418.45 | 28897.18 | 7322.24 | 7078.18 | 1.00 | 0.12 | 0.10 | 0.82 | 0.14 | 0.14 | 0.52 | 1.19 | 1.31 |
| D-hydroxyacetone phosphate | 147.49 | | 3993.84 | 4133.21 | 5452.31 | 5234.57 | 4633.55 | 4377.73 | 3948.05 | 3935.73 | 5314.81 | 5087.07 | 4488.05 | 4230.23 | 1.00 | 1.04 | 1.38 | 1.32 | 1.17 | 1.10 | 1.32 | 1.13 | 0.80 |
| D-xylose-5-phosphate | 5.68 | | 5888.15 | 5316.60 | 5804.08 | 30217.67 | 8026.54 | 7404.56 | 5887.40 | 5307.24 | 5482.93 | 30206.51 | 8195.39 | 7383.41 | 1.00 | 0.11 | 0.16 | 0.83 | 0.16 | 0.13 | 0.53 | 1.46 | 1.38 |
| di-phosphonotulose-7-phosphate | 5.24 | | 4479.90 | 1242.97 | 15655.34 | 6778.34 | 9428.10 | 8368.21 | 4474.75 | 1242.97 | 15650.10 | 6773.10 | 8422.86 | 8362.97 | 1.00 | 2.71 | 3.60 | 1.51 | 2.11 | 1.87 | 1.51 | 0.78 | 0.53 |
| fructose-1,6-bisphosphate | 119.60 | | 9405.01 | 7275.35 | 2799.68 | 5647.60 | 7430.19 | 4507.58 | 9286.41 | 7155.75 | 2698.98 | 5528.00 | 7310.59 | 4387.98 | 1.00 | 0.77 | 0.29 | 0.80 | 0.79 | 0.47 | 0.80 | 1.02 | 1.64 |
| fructose-6-phosphate | 5.20 | | 1423.99 | 2951.23 | 2659.68 | 1755.57 | 2003.82 | 2422.21 | 1427.59 | 2975.63 | 2593.49 | 1760.37 | 1995.52 | 2417.01 | 1.00 | 2.28 | 1.82 | 1.23 | 1.40 | 1.59 | 1.23 | 0.67 | 0.53 |
| fumarate | 517.22 | | 2873.97 | 2448.17 | 3485.27 | 1825.67 | 2150.21 | 2298.17 | 1770.75 | 1930.95 | 2699.05 | 1308.45 | 1632.99 | 1780.95 | 1.00 | 1.09 | 1.68 | 0.74 | 0.82 | 1.01 | 1.04 | 0.85 | 0.60 |
| glucuro-1-lactone | 8.61 | | 3264.39 | 3830.51 | 39141.32 | 41897.68 | 37447.98 | 38344.63 | 35275.78 | 38621.91 | 39132.72 | 41889.08 | 37439.37 | 38336.02 | 1.00 | 1.09 | 1.11 | 1.19 | 1.06 | 1.09 | 1.19 | 0.97 | 0.98 |
| glucuro-3-phosphate | 25.28 | | 2318.84 | 3643.35 | 3058.77 | 3117.72 | 2463.94 | 2911.80 | 2318.38 | 3618.10 | 3043.52 | 3052.47 | 2428.69 | 2896.56 | 1.00 | 1.56 | 1.31 | 1.34 | 1.05 | 1.25 | 1.34 | 0.67 | 0.96 |
| glucuro-5-phosphate | 1274.16 | | 22045.45 | 20293.80 | 17534.69 | 20591.75 | 18200.26 | 15173.15 | 20272.28 | 18464.64 | 16250.34 | 19327.60 | 17927.90 | 17899.00 | 1.00 | 0.94 | 0.78 | 0.83 | 0.86 | 0.86 | 0.93 | 0.86 | 0.86 |
| glutamate | 4.60 | | 5038.51 | 44893.06 | 42104.21 | 44189.65 | 43236.77 | 41615.07 | 5038.51 | 44893.06 | 42104.21 | 44189.65 | 43236.77 | 41615.07 | 1.00 | 0.89 | 0.84 | 0.88 | 0.86 | 0.83 | 0.88 | 0.96 | 0.99 |
| glutamine | 7.04 | | 47434.19 | 36390.94 | 294405.70 | 380662.39 | 330674.69 | 343636.73 | 47434.19 | 36390.94 | 294398.65 | 380605.34 | 330667.55 | 343629.69 | 1.00 | 0.77 | 0.62 | 0.80 | 0.70 | 0.72 | 0.80 | 0.91 | 1.17 |
| glutathione | 11.44 | | 101922.15 | 78595.07 | 80365.62 | 222222.22 | 222222.22 | 73761.75 | 742355.95 | 101911.57 | 78597.35 | 80373.97 | 222222.22 | 737674.91 | 1.00 | 0.74 | 1.20 | 0.68 | 0.58 | 0.52 | 0.74 | 1.00 | 0.54 |



“Cytostasis”